Chapter 1:

1.1 Introduction

**1.1.1 Sterically demanding ligands: Generalities**

In recent years sterically demanding ligands have played an instrumental role in many key breakthroughs in lanthanide, transition metal and main group chemistry. Structurally bulky ligands such as β-diketiminates, guanidinates, bis(amine)silyls's and NHC's amongst others have led to numerous landmark discoveries being made across the periodic table. Research activity in this evolving area has been very intense in recent years leading to the publication of several reviews in the use of sterically demanding ligands.[1-4] It is well understood that size has a direct correlation on both the chemical and physical properties of a compound, with pioneers such as Hofmann[5] and Meyer[6] previously describing a relationship between steric effects and reactivity. Changing the steric bulk of ligands by alternating the substituent used, has allowed the possibility to finely tune the steric and electronic properties of ligands. Hence, this has led to important implications in the structure and reactivity of complexes formed when these ligands coordinate to a metal. The use of sterically demanding ligands has allowed the stabilisation of low oxidation states of metals which were previously unknown, low coordination numbers of metal centers to be attained and metal-metal bonding of complexes to be realised which were previously undetermined, as well as many more triumphs. For the sake of brevity, only a handful of the highlights will be discussed hereafter (**Figure 1.1**).

β-diketiminate   bis(amido)silyl   N-heterocyclic carbene
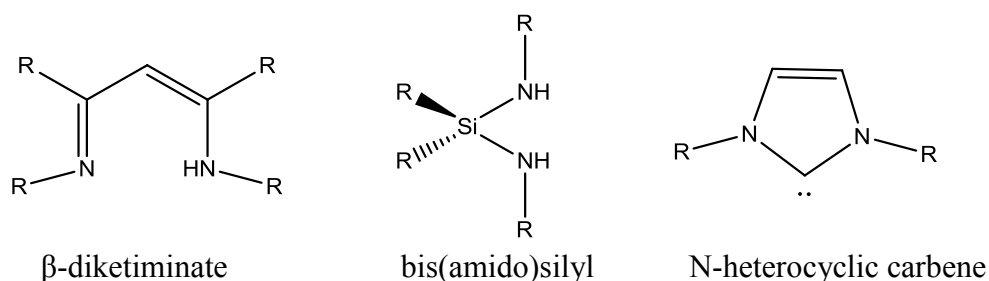
Figure 1.1: Examples of a few of the sterically demanding ligands which will be discussed hereafter.

1.1.2 Sterically demanding bidentate ligands

Using sterically demanding β-diketiminate ligands such as [{(2,6-$Pr^i_2H_3C_6$)N(CH_3)C}$_2$CH]⁻ more commonly known as nacnac, has led to many advances in main group, transition metal and lanthanide chemistry. Their use as ligands is attractive as the electronic and steric properties can be changed by altering the substituent on the nitrogens and, also the diversity of different coordination modes available, either σ alone or σ and π coordination.[3] They form stable six membered chelates when coordinated to a metal and have allowed for the stabilisation of low oxidation states and coordination numbers of metals such as Ti(III)[7], Al(I)[8] and Sn(II),[9] to name a few. Complexes bearing these sterically bulky ligands have displayed diverse reactivity for example, using the lanthanide complex [Sm($η^3$-C_3H_5)$_2$\{HC(MeCNC_6H_3-^iPr-2,6)$_2$\}] shown below in **Figure 1.2**, where each N on the β-diketiminate ligand is bonded to a sterically demanding 2,6-diisopropylphenyl group, Bochmann *et al* have shown that these lanthanide allyl complexes can act as highly effective single site initiators for the ring opening polymerisation of ε-caprolactone and *rac*-lactide,[10] offering better control of the polymerisation in terms of tacticity and stereoselectivity.
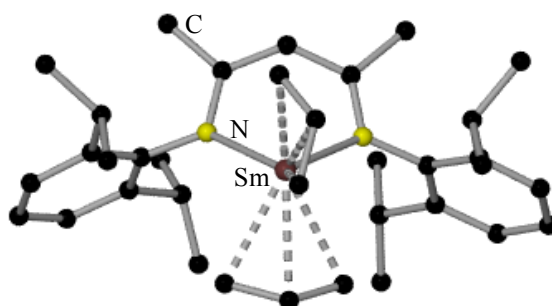
Figure 1.2: Molecular structure of [Sm($η^3$-C_3H_5)$_2$\{HC(MeCNC_6H_3-^iPr-2,6)$_2$\}].

Likewise, it has been shown that the ring opening polymerisation of caprolactone and *rac*-lactide can be carried out by the lanthanide complex displayed below in **Figure 1.3**. The complex [YbL_3], where L is [{N(2-MeC_6H_4)C-(Me)}$_2$CH⁻], also displayed high reactivity, acting as a pre-catalyst in the intramolecular hydroamination reaction

of amines such as aniline and morpholine with diisopropylcarbodiimides producing guanidines in yields of over 90%.[11]
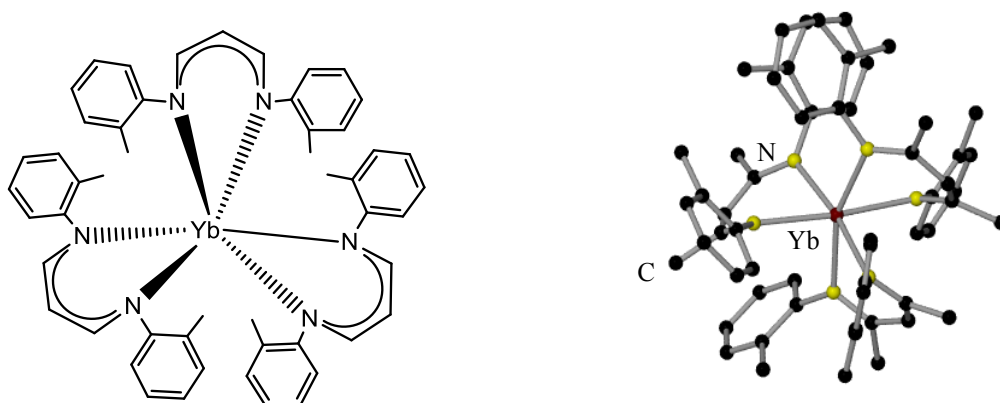
Figure 1.3: Molecular structure and figure of [YbL$_3$], where L is [{N(2-MeC$_6$H$_4$)C-(Me)}$_2$CH$^-$].

Furthermore, recent studies have demonstrated that the use of heavier group two metal complexes containing these bidentate ligands, can promote important synthetic transformations in organic synthesis. Hill *et al* have reported the effective hydroamination reaction of carbodiimides using Ca and Ba amido complexes supported by β-diketiminate ligands to yield the corresponding guanidinate complexes,[12] shown in **Scheme 1.1**. Guanidines have received a lot of interest recently as they are important ancillary ligands in f-block and transition metal chemistry[13] but they also appear as functional groups in many natural products and synthetic pharmaceuticals.[14]
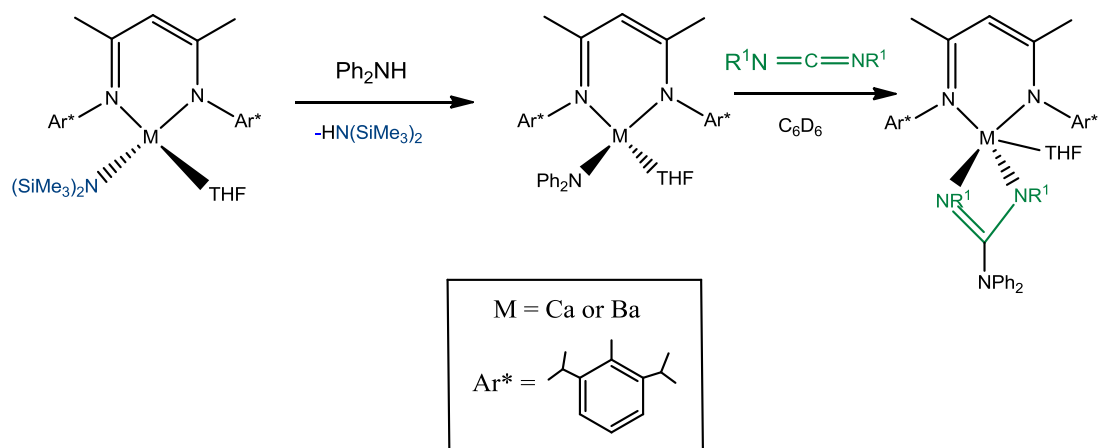
Scheme 1.1: Insertion reaction into carbodiimides.

The bulkiness of the ligands helps to stabilize the heavy alkaline-earth metal. This methodology not only works stoichiometrically[15] but it can also be upgraded to catalytic conditions to generate a range of guanidines,[12] as seen in **Scheme 1.2**. Reactions can be carried out by various 1, 3-dialkylcarbodiimides (^{i}Pr, Cy, and ^{t}Bu) and several amines (2-fluoroaniline, diphenylamine and diisopropylaniline) in relatively mild conditions of 25°C with 2-4 mol % load of pre-catalyst.
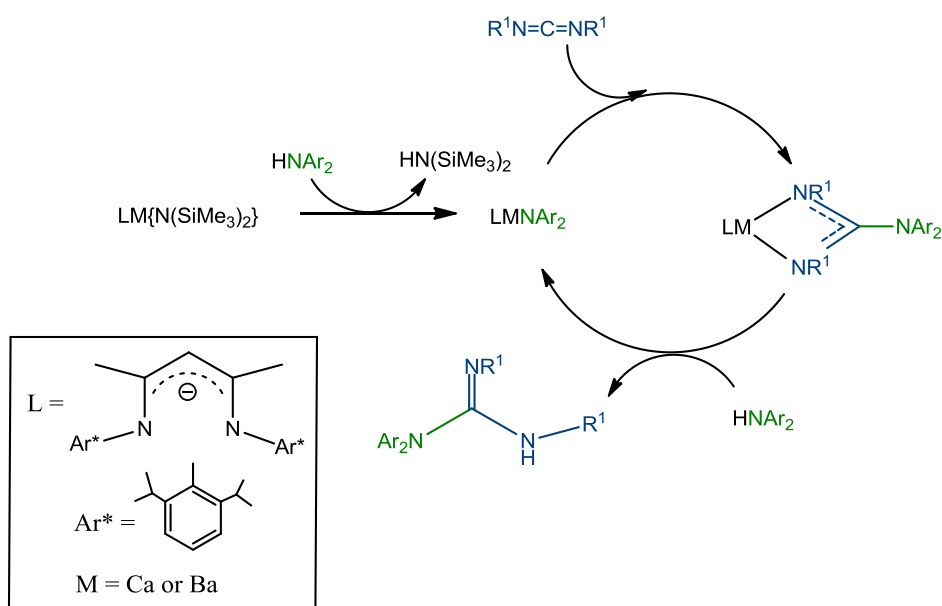
Scheme 1.2: Generalised postulated catalytic cycle for heavy alkaline-metal mediated intramolecular hydroamination of carbodiimides.

In addition, β-diketiminate-stabilised calcium amides have also proven to be efficient pre-catalysts for intramolecular hydroamination/cyclisation of a wide range of aminoalkenes (**Scheme 1.3**). The reactions take place under mild conditions (25-80 ^{o}C) allowing the synthesis of five-, six-, and seven-membered heterocyclic compounds. The sterically demanding β-diketiminate ligand helps in stabilizing the low coordinate and low valent Ca complex whilst also preventing the undesired Schlenk redistribution reaction from taking place.[16]
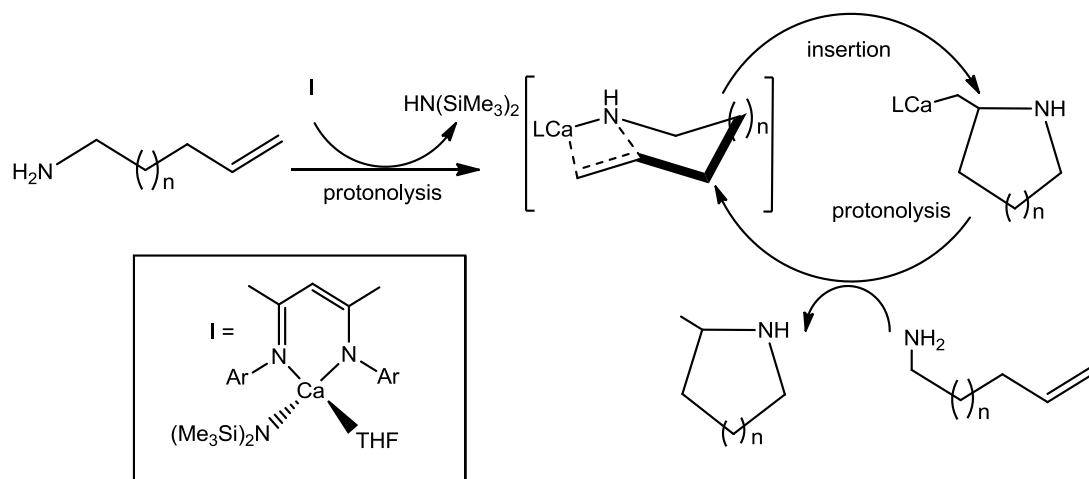
Scheme 1.3: Generalised postulated catalytic cycle for Ca-mediated intramolecular hydroamination.

Moreover, this important family of heavier alkaline-earth metal derivatives have also found use as efficient catalysts for hydrophosphination of alkenes and carbodiimides[17] as well as hydroamination of isocyanates to yield ureas, which have countless applications in synthetic, pharmaceutical and industrial chemistry.[18]

In addition to promoting new synthetic transformations, the use of these highly sterically demanding ligands has been instrumental to unveiling new orders of metal-metal bonding in transition metal and main group chemistry. Using the sterically demanding β-diketiminate ligand, Robinson *et al* has isolated the Zn(I) species, (nacnac)ZnZn(nacnac) (**Figure 1.4**),[19] by reduction of [RZn(μ-I)$_2$Li(OEt$_2$)$_2$] where R = [{(2,6-^{i}Pr$_2$C$_6$H$_3$)N(Me)C}$_2$CH] with K metal.
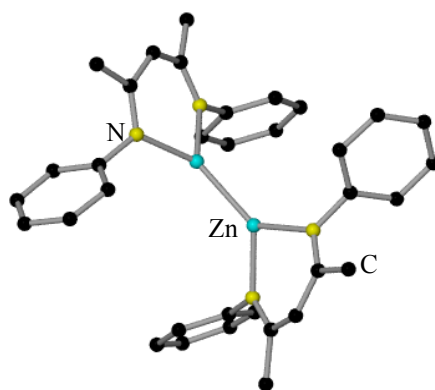
Figure 1.4: Molecular structure of [(nacnac)ZnZn(nacnac)]. Hydrogen and [i]Pr groups on aromatic rings atoms have been omitted for clarity.

Until recently, the chemistry of Zn was considered to be dominated by the +2 oxidation state. However, recent groundbreaking discoveries have revolutionalised this well-established belief. In 2004 Carmona *et al* reported the synthesis of dizincocene Cp*ZnZnCp* (Cp* = η^5-C$_5$Me$_5$), the first stable compound containing a Zn-Zn metal-metal bond (Zn-Zn 2.30(3) Å), by reacting Zn(C$_5$Me$_5$)$_2$ with Zn(C$_2$H$_5$)$_2$ at -10°C in diethylether (**Scheme 1.4**).[20]
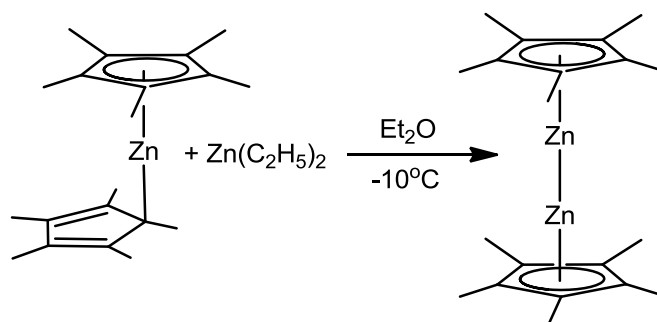
Scheme 1.4: Synthesis of [Zn$_2$(η^5-C$_5$Me$_5$)$_2$].

The only other example of cyclopentadienyl group (Cp') being used as a ligand to support a Zn-Zn bond is [Zn$_2$(η^5-C$_5$Me$_4$Et)$_2$].[21] Surprisingly attempts to form other dizincocenes of the form [Zn$_2$(η^5-Cp')$_2$] (Cp' = C$_5$H$_5$, C$_5$Me$_4$SiMe$_3$ and C$_5$Me$_4$[t]Bu) failed.[20] This highlights the importance of the ligand in stabilising the Zn-Zn bond emphasising the strong impact the different substituents have.
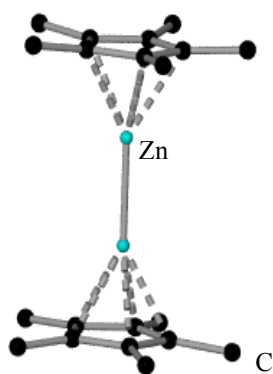
Figure 1.5: Molecular structure of $[Zn_2(\eta^5\text{-}C_5Me_5)_2]$. Hydrogens have been omitted for clarity.

Since this landmark advance, a search in the CSD revealed that there are currently twenty-five compounds containing Zn-Zn metal bonds which have been synthesised and characterised.[22] The general feature in these compounds is that all of them contain highly sterically demanding ligands, for example $[(\eta_2\text{-}Me_2Si(NDipp)_2)ZnZn(\eta_2\text{-}Me_2Si(NDipp)_2)]^{2-}$, which can be prepared by reduction of Zn(II) dimer $[Zn_2(\mu\text{-}\eta_2\text{-}Me_2Si(NDipp)_2)_2]$ with KC_8 (**Scheme 1.5**). The highly sensitive $(Zn\text{-}Zn)^{2+}$ unit is supported on a bulky bis(silyl)amido ligand, which provides steric protective shelter to the highly sensitive metal-metal bond.[23]
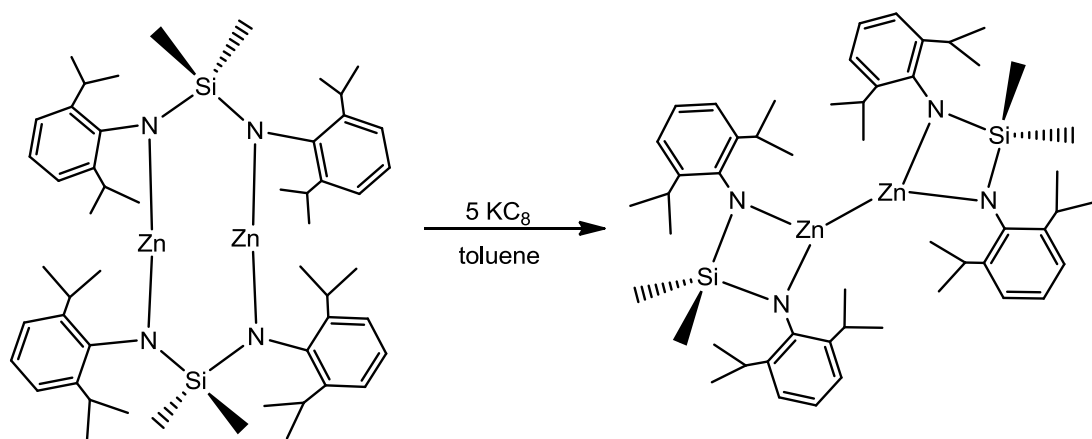
Scheme 1.5: Synthesis of $[(\eta_2\text{-}Me_2Si(NDipp)_2)ZnZn(\eta_2\text{-}Me_2Si(NDipp)_2)]^2$ from the reduction of $[Zn_2(\mu\text{-}\eta_2\text{-}Me_2Si(NDipp)_2)_2]$ with KC_8.

Reactivity studies of Zn(I) species are now beginning to be carried out, with the dizincocene complex $[Zn_2(\eta^5\text{-}C_5Me_5)_2]$ showing promise as a homogeneous catalyst for intra and intermolecular hydroamination reactions of primary and secondary anilines and arylethynes.[24]

Another significant contribution made by the use of sterically demanding (bis)amido ligands has been in the activation of N-heterocycles. Recently Diaconescu *et al* have reported a series of novel f-block metal-mediated N-heterocyclic activation of alkly-imidazoles, pyridine, quinoline and picoline, using a uranium alkyl complex supported on a ferrocene based sterically demanding bis(amide) ligand (**Figure 1.6**).[25]

$(NN^{fc}) = 1,1'\text{-}fc(NSi^tBuMe_2)_2)$
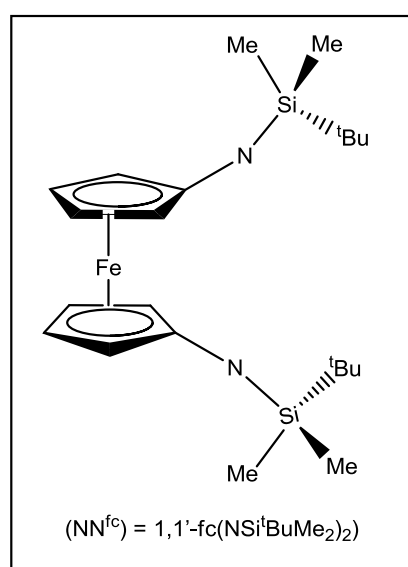
Figure 1.6: Ferrocene based sterically demanding bis(amide) ligand, $(NN^{fc}) = 1,1'\text{-}$fc(NSi^{t}BuMe$_2$)$_2$.

These studies show that the ligand plays an important role in these reactions by stabilising the highly electrophilic uranium center. The 1,1'-disubstituted ferrocene ligand ensures a cis-coordination of the two donors, therefore leaving only one side of the metal center open for attack by any substrate, whilst also having the ability to accommodate changes in the electronic density at the metal center by altering the geometry around iron.[26] Diaconescu *et al* have elegantly shown that using a uranium dibenzyl complex, $[(NN^{fc})U(CH_2Ph)_2]$, (where (NN^{fc}) = 1,1'-fc(NSi^{t}BuMe$_2$)$_2$), the C-H activation of methylimidazole in a cascade of reactions

can been carried out involving deprotonation, (i) C-C coupling, (ii) ring opening and (iii) imidazole migration; a sophisticated mechanism has been proposed (**Scheme 1.6**). In these studies it appears that as well as acting as a stabilising ligand for the U centre, the NN^{fc} ligand plays an instrumental role in facilitating the isolation of the proposed intermediate in these reactions.[25]
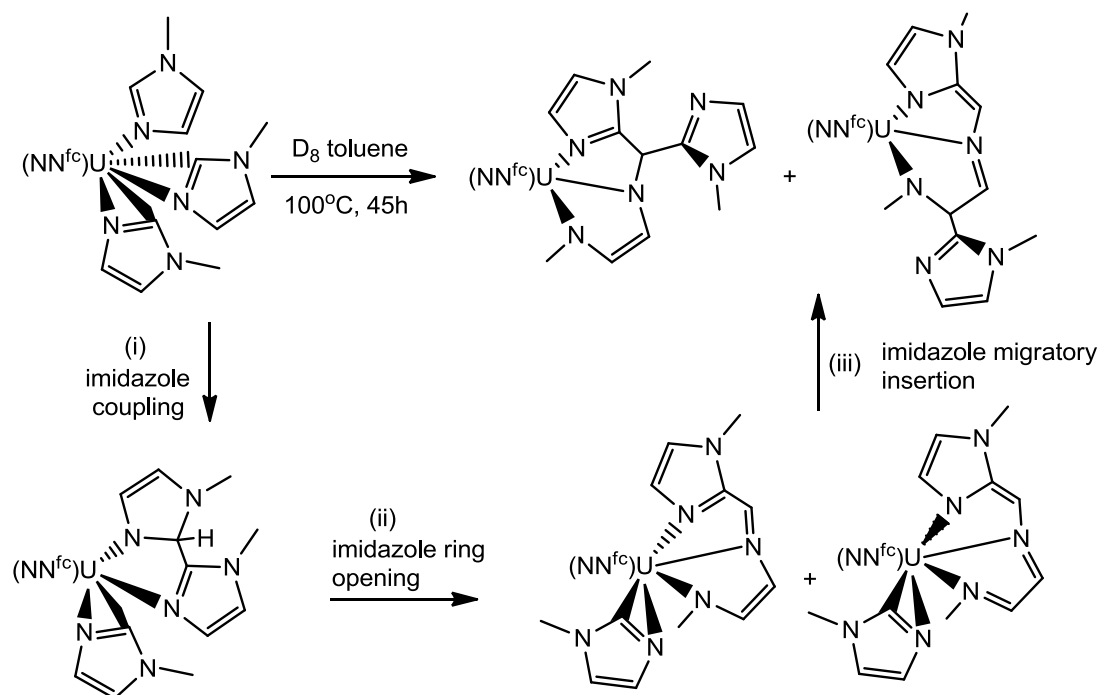
Scheme 1.6: Proposed mechanism for C-H activation of methylimidazole in a cascade reaction by [(NN^{fc})U(CH$_2$Ph)$_2$], (where (NN^{fc}) = 1,1'-fc(NSi^{t}BuMe$_2$)$_2$).

Similarly, Diaconescu has shown that in extending her methodology to group 3 metals (Sc,[27] Y,[28] La[28]), she has prepared a new collection of d^{0}f^n-metal alkyl complexes coordinated to the sterically demanding ferrocene bis(amide) ligand [(NN^{fc})M(CH$_2$Ar)(THF)] (M = Sc, Ar = 3,5-Me$_2$C$_6$H$_3$; M = Y, La, Ar = Ph), which can carry out activations of methylimidazole.[28, 29]

Moreover, another important advance in rare-earth metal chemistry has been made by Arnold *et al* using a sterically demanding macrocyclic ligand coined "Pacman". Arnold *et al* have shown that by mixing a binucleating macrocycle H$_4$L (where L = Schiff base polypyrrolic macrocycle),[30] with excess uranylsilyamide complex she

can successfully achieve unprecedented butterfly shaped U^v oxo dimer complex $[(Me_2SiOUO)_2(L)]$ (**Scheme 1.7**), whereas U compounds are normally linear uranyl dications $[O=U=O]^{2+}$. The steric bulk and rigidity of the ligand are attributed to the formation of the high oxidation state uranium complex and the avoidance of the complexation of two linear uranyl cations instead.[31]
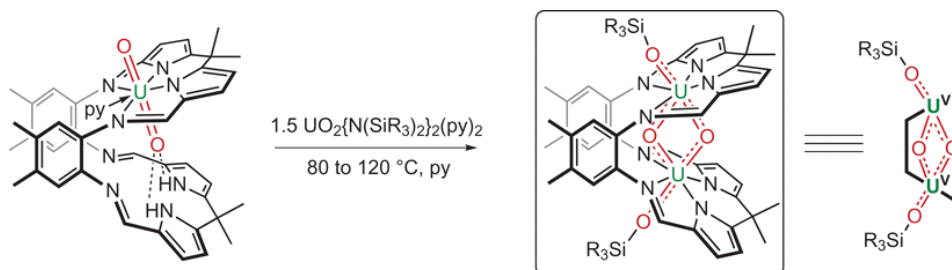
Scheme 1.7: Preparation of $[(Me_2SiOUO)_2(L)]$.

1.1.3 Sterically demanding monodentate ligands

Undoubtedly one of the most important advances in transition metal chemistry has been the progress made in Pd-catalyzed cross coupling reactions to form new C-C bonds, verified by Negishi, Heck and Suzuki being jointly awarded the Nobel prize in 2010 for their efforts. Although the use of phosphine ligands have been at the forefront of this chemistry, recently bulky N-heterocyclic carbene (NHC) ligands have gained increasing interest due to the high thermal stability of the Pd-NHC bond.[32, 33] The use of NHC ligands provides strong binding of the electron rich carbene to the metal centre, helping the metal to remain coordinated to the ligand and hence leading to longer catalyst lifetimes. These ligands also have the advantage that the steric and electronic properties of the N-bound organic group can be finely tuned. Recently it has been shown systematically by Organ *et al* that increasing the steric bulk on the carbene led to an improved activity of the catalyst in cross coupling reactions. Using the ligands shown in **Scheme 1.8** (Pd-PEPPSI-IMes, Pd-PEPPSI-IEt, Pd-PEPPSI-IPr where PEPPSI = pyridine enhanced pre-catalyst preparation, stabilization and initiation),[34] an increase in activity of the catalyst has been displayed as the steric bulk of the NHC was gradually increased.[35]
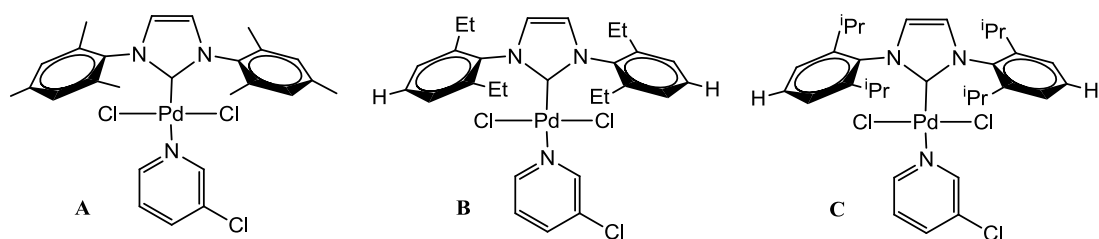
Scheme 1.8: **A** = Pd-PEPPSI-IMes, **B** = Pd-PEPPSI-IEt, **C** = Pd-PEPPSI-IPr.

As the σ-donor abilities of IMes, IEt and IPr are similar;[36] it is thought that the steric factors must be primarily responsible for the increased activity of the catalyst. Current thought is that bulky ligands encourage tri-coordinated Pd intermediates, thereby reducing the overall activation energy in cross coupling reactions.[37]

Pioneered by Arduengo *et al*,[38] NHC ligands have been used extensively in catalysis with transition metals as mentioned above and more recently are making an appearance in main group chemistry. The area is so vast, however, that only a few of the highlights will be discussed here. Recently NHC ligands have been used to catalyse asymmetric allylic alkylation of allyl bromides using Grignard reagents, without the need of a transition metal,[39] whilst also providing the first example of a stable dialane species [{(IPr)(H)$_2$Al}$_2$],[40] a low oxidation state, thermally stable aluminium hydride complex, the stability of which arises from the use of a nucleophilic NHC ligand IPr (IPr = 1,3-bis-(2,2-diisopropylphenyl)imidazol-2-ylidene) (**Figure 1.7**).
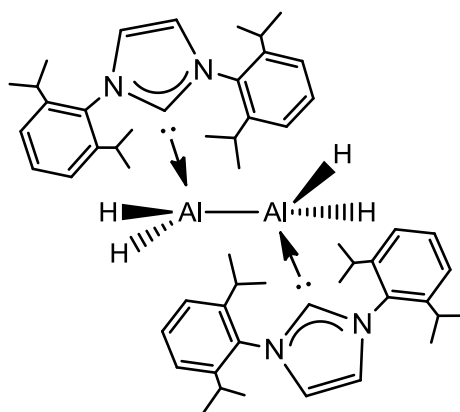
Figure 1.7: [{(IPr)(H)$_2$Al}$_2$] (where IPr = 1,3-bis-(2,2-diisopropylphenyl)imidazol-2-ylidene).

In addition they have also been used to stabilise element-element bonds in main group chemistry, Robinson *et al* have carried out the novel reduction of NHC:SiCl$_4$ with KC$_8$ to form the first Si=Si double bonded complex, where Si is in the formal oxidation state zero[41] shown below in **Scheme 1.9**.
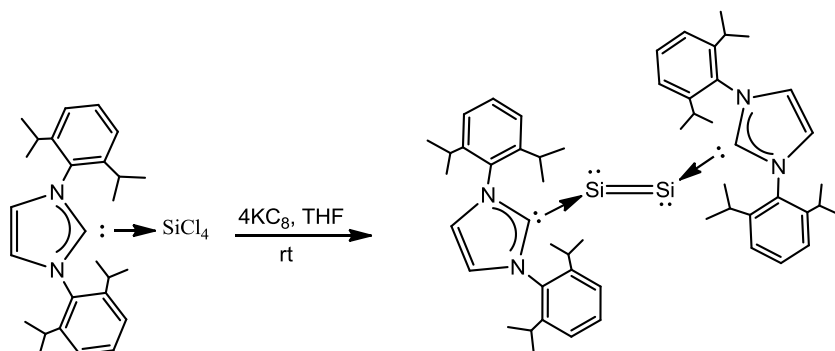
Scheme 1.9: Preparation of first stable Si=Si complex, where Si is in formal oxidation state zero.

Likewise, recently Braunschweig *et al* have remarkably prepared the first stable boron-boron triple bond complex [(NHC)→B≡B←(NHC)] by reduction of a bis(N-heterocyclic carbene) stabilised tetrabromodiborane with four equivalents of sodium napthalenide.[42] Low valent main group centers are normally highly reactive in the absence of extreme steric protection. The steric bulk of the NHC ligand here along with its pronounced donor strength allows the isolation of a stable homoatomic triple bond in this group 13 dimer as depicted in **Scheme 1.10**.
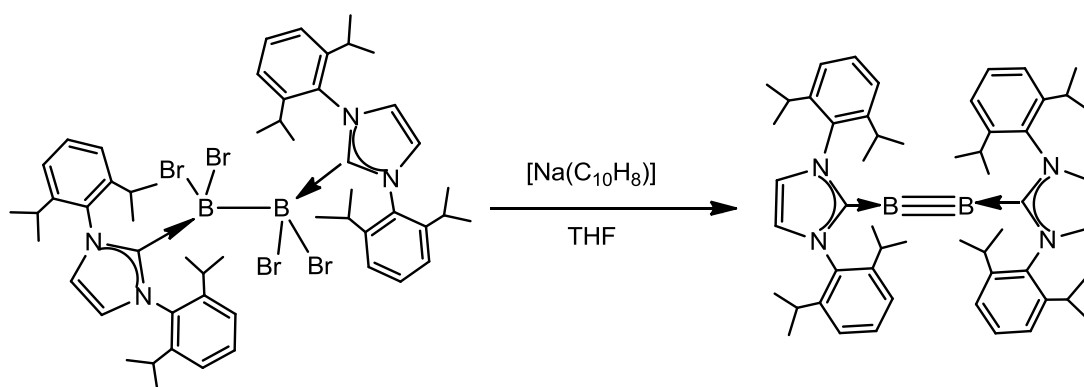
Scheme 1.10: Preparation of [(NHC)→B≡B←(NHC)].

Another important landmark achieved using a bulky monovalent terphenyl ligand was seen in metal-metal bonding of two Cr(I) centers in the formation of a five-fold

bond. Pioneering work carried out by Power *et al* saw the reduction of [Ar'Cr(μ-Cl)]$_2$ with KC$_8$ to form Ar'CrCrAr' (where Ar' = C$_6$H$_3$-2,6(C$_6$H$_3$-2,6-^{i}Pr$_2$)$_2$), with an extremely short Cr-Cr bond distance (1.835(4) Å) between the two Cr(I) centers, which can be attributed to the formation of a quintuple Cr-Cr bond as seen in **Figure 1.8**. In this case the use of the monovalent bulky terphenyl ligand brings both Cr centers into close proximity of each other, allowing stabilisation of the low valent Cr(I) atoms.[43]
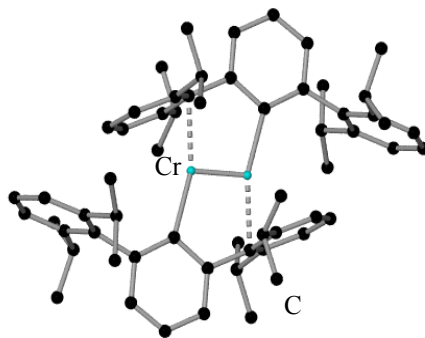
Figure 1.8 Molecular Structure of Ar'CrCrAr' (where Ar' = C$_6$H$_3$-2,6(C$_6$H$_3$-2,6-^{i}Pr$_2$)$_2$). Hydrogens have been omitted for clarity.

1.1.4 Sterically bulky ligands in magnesium chemistry

Focusing on magnesium chemistry, some important breakthroughs in the synthesis and characterisation of compounds with highly sterically demanding ligands include the trapping of high nuclearity {MgH$_2$} clusters as well as the isolation of the first compound exhibiting a stable Mg-Mg metal bond. Thus, recently Hill has shown that by coordinating the bulky NHC carbene [1, 3-bis(2,6-diisopropyl-phenyl)imidazol-2-ylidene] (IPr) to magnesium amide Mg(HMDS)$_2$ followed by the addition of PhSiH$_3$ allows the entrapment of the unprecedented {Mg$_4$H$_6$}$^{2+}$ cluster shown in **Scheme 1.11**. Remarkably, the authors attribute the stabilisation of this cluster to the presence of the NHC ligand, finding that when the same reaction is performed using unsolvated Mg(HMDS)$_2$ an insoluble white solid (presumably MgH$_2$) is formed instead.[44]
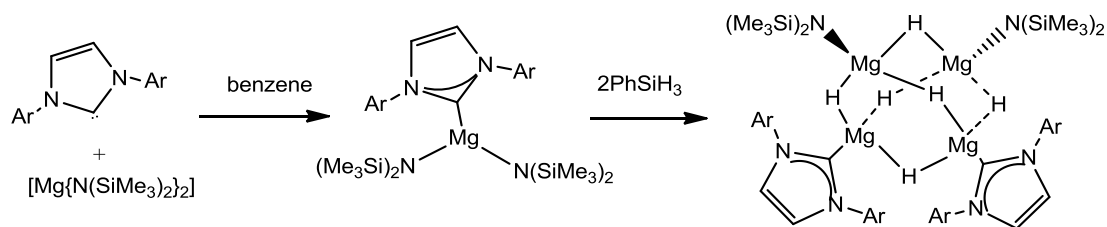
Scheme 1.11: Preparation of Mg$_4$ hydride.

Closely related, recently Harder has reported a record breaking magnesium hydride cluster containing $\{Mg_8H_{10}\}^{6+}$ fragment (**Figure 1.10**) using a modified β-diketiminate ligand para-phenylene which can be employed as a double based nacnac diketiminate (**Figure 1.9**).
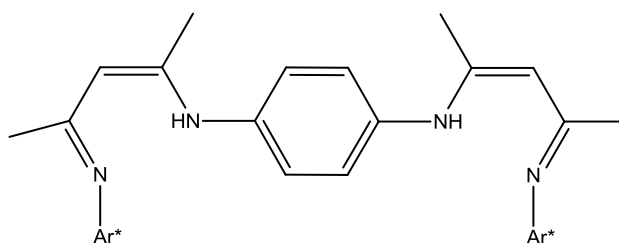
Ar* = 2,6-di-isopropylphenyl

Figure 1.9: paraphenylene ligand employed by Harder *et al* in forming magnesium hydride cluster containing $\{Mg_8H_{10}\}^{6+}$.

Interestingly this newly prepared magnesium hydride cluster releases its H$_2$ completely at 200$^{\text{o}}$C, which has important implications for the development of molecular devices suitable for H$_2$ storage as well as the potential applications of these compounds as chemoselective reducing agents.[45]
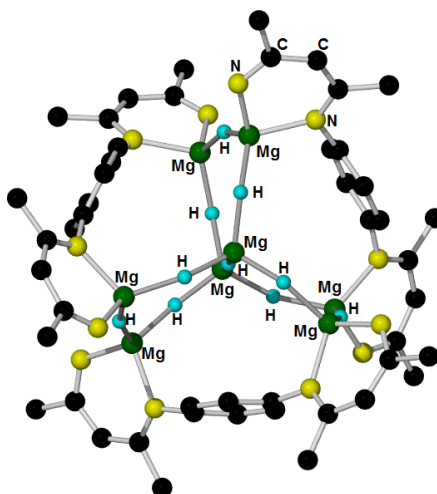
Figure 1.10: Molecular structure of $\{Mg_8H_{10}\}^{6+}$ fragment. Hydrogens have been omitted for clarity.

In addition, following the exceptional discoveries made in metal-metal bonding by Carmona *et al* (Zn-Zn bond), in 2007 Jones and Stasch reported in *Science* the first compound featuring a bond between two Mg centres.[46] In this case the Mg-Mg metal-metal bond is supported by a β-diketiminate ligand which contains the highly sterically demanding aryl group 2,6-diisopropylphenyl (**Figure 1.11**). This compound is prepared by reduction of the relevant magnesium(II) iodide species with potassium metal (**Scheme 1.12**).
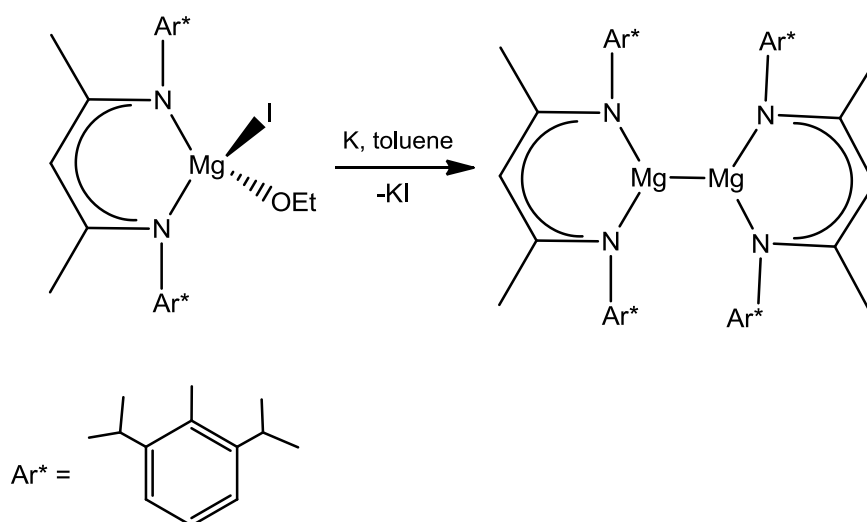
Scheme 1.12: Preparation of [Mg(nacnac)]$_2$.
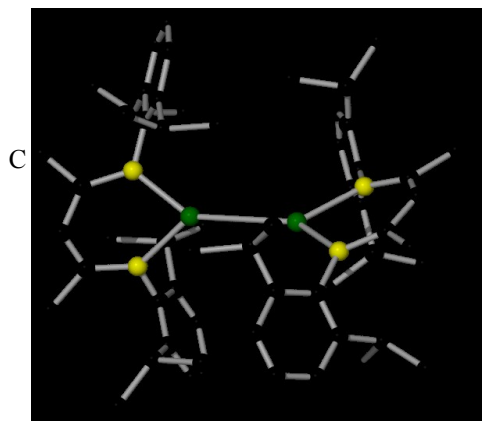
Figure 1.11: Molecular structure of [Mg(nacnac)]₂. Hydrogens have been omitted for clarity.

Since its synthesis, several reactivity studies on this compound have been reported which show it can be reacted with unsaturated electrophiles such as CyN=C=NCy (Cy = cyclohexyl), ^{t}BuN=C=O, AdN₃ (Ad = 1-adamantlyl) and PhN=NPh to yield the reduced product where the electrophile has inserted into the Mg-Mg bond (**Scheme 1.13**).
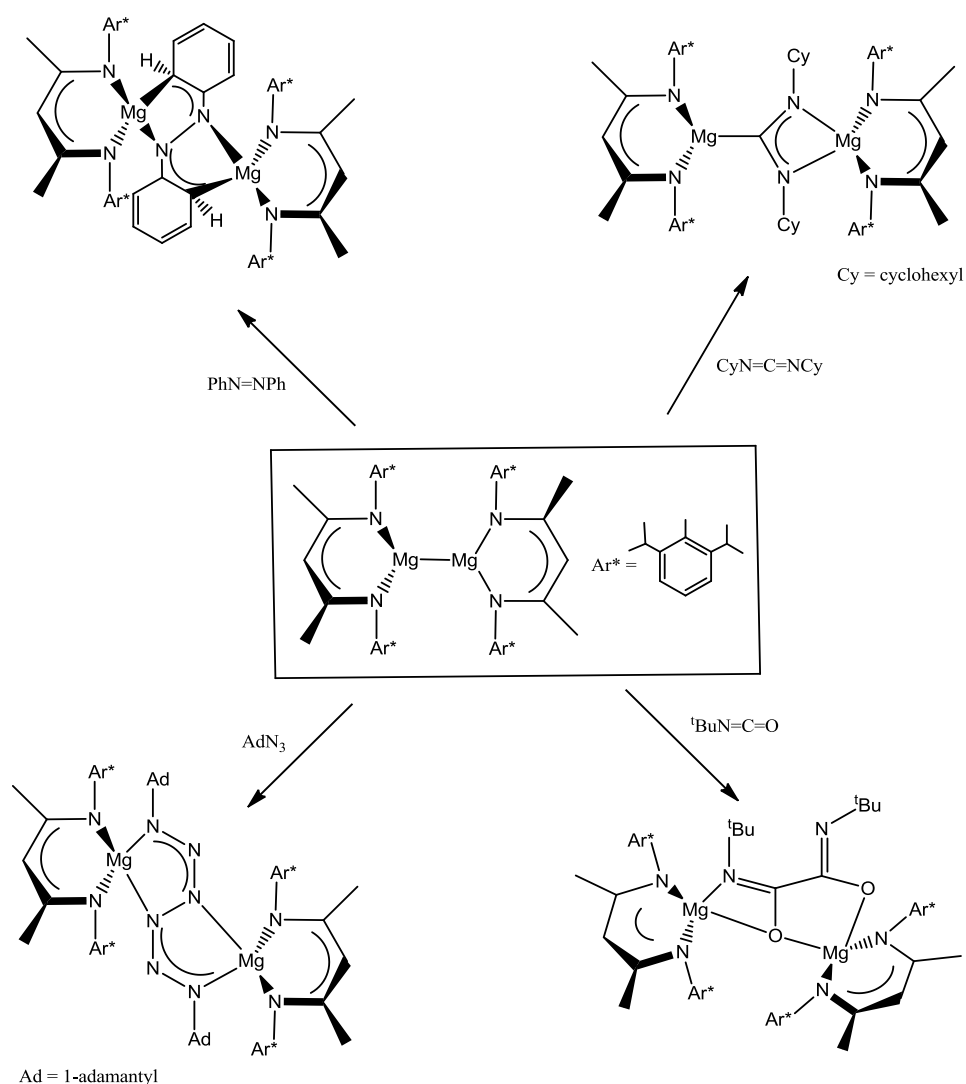
Scheme 1.13: Insertion of various electrophiles into Mg-Mg bond.

Surprisingly, despite these important advances made in magnesium chemistry and considering the wide interest that magnesiate compounds attract from synthetic chemists, there has been very little work reported on the use of these highly sterically demanding ligands to prepare mixed metal magnesium based reagents. A recent example on the use of bis(amido)silyl ligands in bimetallic chemistry has been reported by Zheng for the synthesis of potassium magnesiates via reduction of a relevant magnesium compound with potassium graphite[47] (**Scheme 1.14**). The structure of the potassium-magnesiate solvated by THF is shown in **Figure 1.12**. It constitutes an example of a tetraorganomagnesiate with the molecular structure comprising two K and a Mg center which adopt an almost linear arrangement (K-

Mg-K = 178.02°). This compound exhibits a contacted ion pair structural motif where the central Mg is coordinated to four N atoms of the two bis(amido)silyl ligands, whereas each K center is π-engaging with the two aromatic rings (one from each bis(amido)silyl ligand) in a η^6 fashion and completes its coordination sphere by bonding to two additional molecules of THF.
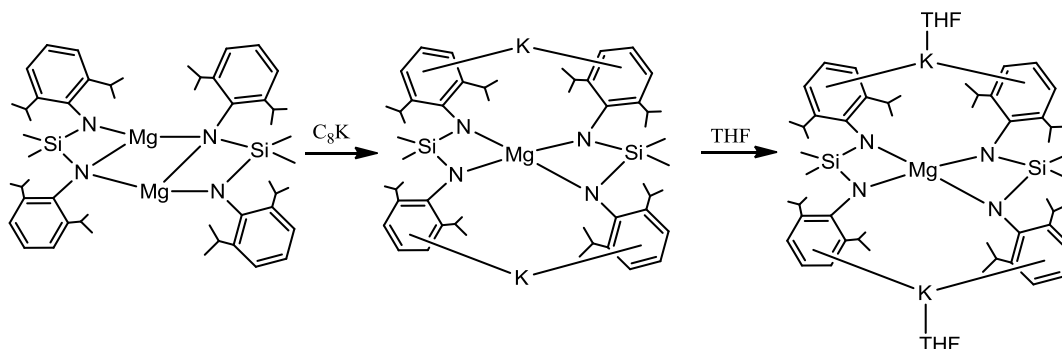
Scheme 1.14: Preparation of potassium-magnesium ate complexes.
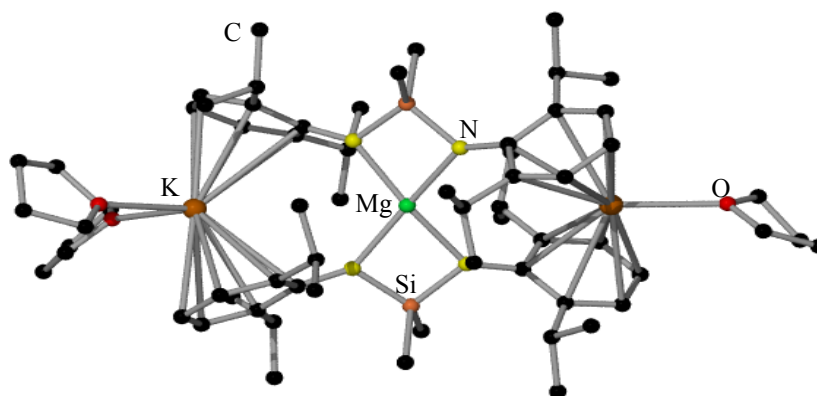
Figure 1.12: Molecular structure of $[(\eta^6:\eta^6\text{-}K(THF))^+][(\eta^6:\eta^6\text{-}K(THF)_2)^+][(\eta_2\text{-}Mg)\{Me_2Si(NDipp)_2\}_2]^{2-}$. Hydrogen atoms omitted for clarity.

1.2 Organomagnesium chemistry

1.2.1 Grignard reagents

Organolithium compounds constitute one of the organometallic reagents most widely used in synthesis, over 95% of pharmaceuticals are made using organolithium reagents at some point in their synthesis;[48-51] however, these highly reactive nucleophiles suffer the drawback of low functional group tolerance, leading to

unwanted side reactions, imposing the use of cryogenic conditions in order to control the selectivity of reactions.[52] Organomagnesium reagents in contrast to their organolithium relatives have a less polar character allowing them to be more chemoselective. They are still strongly basic, but their lower kinetic basicity, allows a greater functional group compatibility and the use of milder reaction conditions.[53] Amongst the different types of organomagnesium reagents available, Grignard reagents (RMgX) are undoubtedly the most extensively used in synthesis. They are relatively easy to prepare and many of them are commercially available, as illustrated by the fact that the company Sigma Aldrich supplies over 150 different Grignard reagents in their catalogue.[54] Grignard reagents were pioneered in 1900 by Victor Grignard,[55] by reacting Mg with an organic halide in ether solution. This discovery coupled with his initial investigations on the applications of these unique organometallic reagents was recognised in 1912 when Victor Grignard was awarded the Nobel Prize in chemistry. On the 100th anniversary of Grignard's Nobel Prize award, the true constitution of RMgX reagents in solution still remains a matter of discussion and study. In general, these compounds exist in equilibrium with the homoleptic species MgX_2 and MgR_2 (Schlenk equilibrium).[56] The natures of the halide group X and the alkyl group R along with the choice of solvent, concentration and temperature has an important effect on the equilibrium position.[57] Recently Imamoto has elegantly proved, using coldspary ionization mass spectroscopy (CSI-MS), that the dominant species present in a THF solution of RMgCl (R = Me, ^tBu, Ph, Bz), is binuclear $RMg_2Cl_3(THF)_x$ (x = 4-6) which can be envisaged as an adduct between $MgCl_2$ and RMgCl.[58]

$$2RMgX \rightleftharpoons R_2Mg + MgX_2$$

Scheme 1.15: Schlenk equilibrium.

Grignard reagents (together with organolithium reagents) are amongst the most commonly used and vitally important reagents in synthesis playing a key role in many fundamental organic transformations. Their relatively easy preparation, good stability and high reactivity make them essential reagents in any research laboratory across the world not only in academic but also in many commercial industrial

environments. Their high reactivity is largely due to the polarization (charge separation) of the metal-carbon bond in these air sensitive compounds. However, this high reactivity also has detrimental effects as it can severely limit the room temperature tolerance of RMgX reagents towards many organic functional groups (e.g. esters, ketones and nitriles). This is a major drawback as these functional groups are extremely common in synthetic chemistry. However, in the last decade the application of Grignard reagents in synthesis has propelled forward due to a great extent to Knochel's innovative "Turbo Grignard" reagents.[53] By adding LiCl to RMgX in THF, Knochel has demonstrated that some of the main drawbacks of conventional Grignard reagents such as poor functional group tolerance or low kinetic reactivity can be overcome. Exhibiting an enhanced "magnesiating" power, these reagents find widespread applications in direct Mg-halogen exchange reactions (**Scheme 1.16**). Thus, reaction with aromatic and heteroaromatic halides, allows access to a wide range of highly functionalised aryl and heteroaryl-magnesium compounds.[59]

FG = F, Cl,Br,CN,CO$_2$R,OMe
E = electrophile
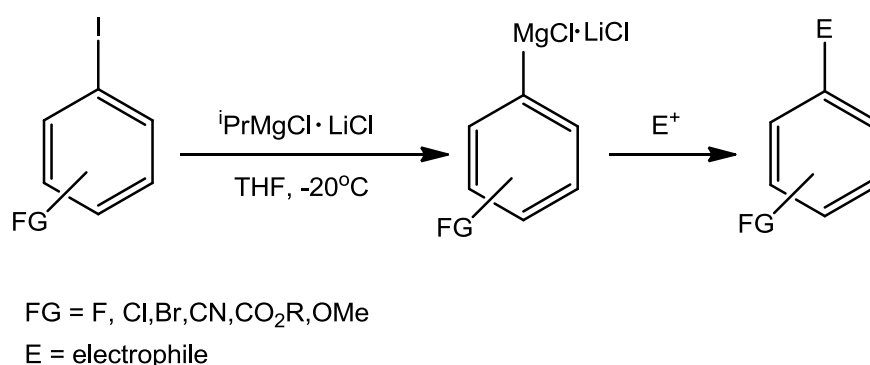
Scheme 1.16: Example of "Turbo Grignard" reagent in metal halogen exchange reaction.

In general Grignard reagents behave as nucleophiles and they have been widely used in nucleophilic addition reactions and substitutions, however their applications as metallating reagents capable of promoting direct Mg-H exchange reactions are still very limited. This is due in a large extent to the lack of kinetic basicity of the Mg-C bond. However, this important drawback can be overcome by using magnesium

compounds which contain amido groups such as, Mg(TMP)$_2$[60] or Hauser bases (TMPMgCl)[61] which contain more kinetically active Mg-N bonds.

1.2.2 Magnesium amides

Introduced in 1903 by Meunier, halomagnesium amides (R$_2$NMgX) are amongst the earliest known organomagnesium compounds.[62] In 1947, Hauser *et al* reported magnesium amides (R$_2$NMgX and (R$_2$N)$_2$Mg) as special Brønstead bases.[61] Eaton *et al* then extended the scope of these reagents to include sterically demanding amides (TMPMgBr).[60] Albeit although magnesium amides display good reactivity in performing metallation reactions they do however have some limitations. They exhibit low solubility in organic solvents and in general a large excess of magnesium amide is needed to obtain high conversions and high reaction rates.[63] Reactions with electrophiles can therefore be difficult[64] and furthermore, some magnesium diamides can act as reducing agents in non-solvating media.[65] Knochel has overcome these setbacks by preparing magnesium amide bases of the form (R$_2$NMgCl·LiCl) which display improved reactivity and have been coined Turbo Hauser bases.[53]
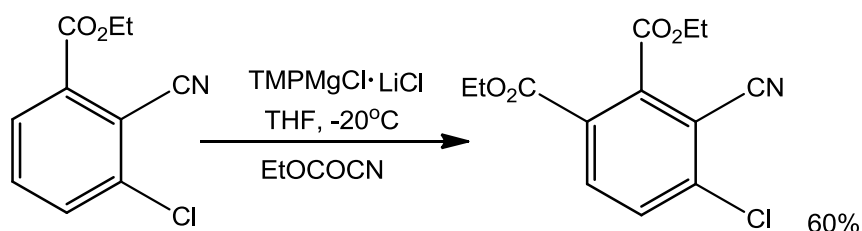
Scheme 1.17: Metallation of substituted benzene by TMPMgCl·LiCl.[53]

Until recently the true constitution of these mixtures was unknown. Spreading new light into this, Mulvey *et al* have revealed the structure of (TMP)MgCl·LiCl, which demonstrates its mixed metal constitution (magnesiate) illustrated in **Figure 1.13**.[66, 67]
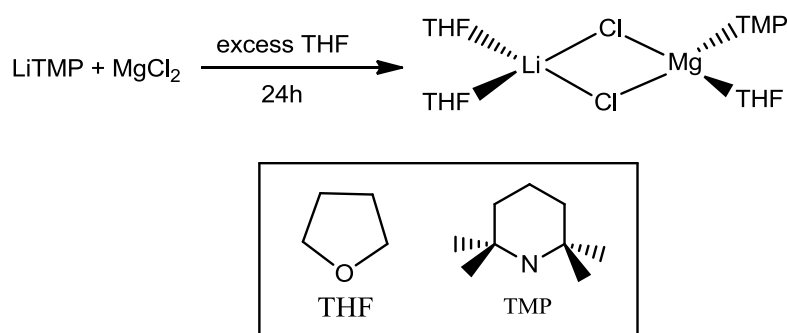
Scheme 1.18: Preparation of TMPMgCl·LiCl.
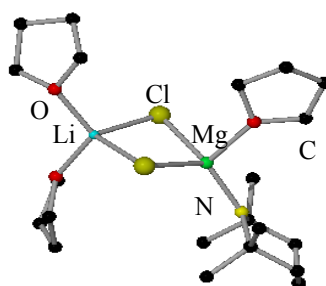
Figure 1.13: Molecular structure of (TMP)MgCl·LiCl. Hydrogen atoms omitted for clarity.

The elucidation of the structure of the "Turbo Hauser" base has shown that (TMP)MgCl·LiCl is a molecular species and not salt like. The active TMP ligand sits in a terminal position and is coordinated to the magnesium, instead of the alkali metal lithium. Finally the THF ligands sitting in a labile position may help in the preco-ordination of the aromatic substrates prior to its magnesiation, which may be influential factors in the increased reactivity of these bimetallic bases.[68]

1.3 Mixed-metal (ate) chemistry

1.3.1 Historic background

In 1858 by reacting $ZnEt_2$ with sodium in a sealed tube, Wanklyn reported the formation $NaZnEt_3$, which constituted the first example of a mixed metal compound combining zinc with an alkali metal in the same molecule (zincate).[69] It would be almost a hundred years later before Wittig would use the term "ate" to describe these types of mixed metal compounds.[70] An "ate" can be described as a bimetallic system in which one metal has a greater Lewis acidity than the other and so it is able

to accept more anionic (Lewis basic) ligands.[71] Wittig reported the synthesis of triphenylzincate LiZnPh$_3$, and also the magnesiate LiMgPh$_3$,[70] and found them to exhibit completely different reactivities and selectivities to those found for the homometallic compounds on their own. For example LiMgPh$_3$ in the reaction with benzalacetophenone forms the product of 1,4-addition whereas LiPh yields mainly 1,2-addition product (**Scheme 1.19**).[70]
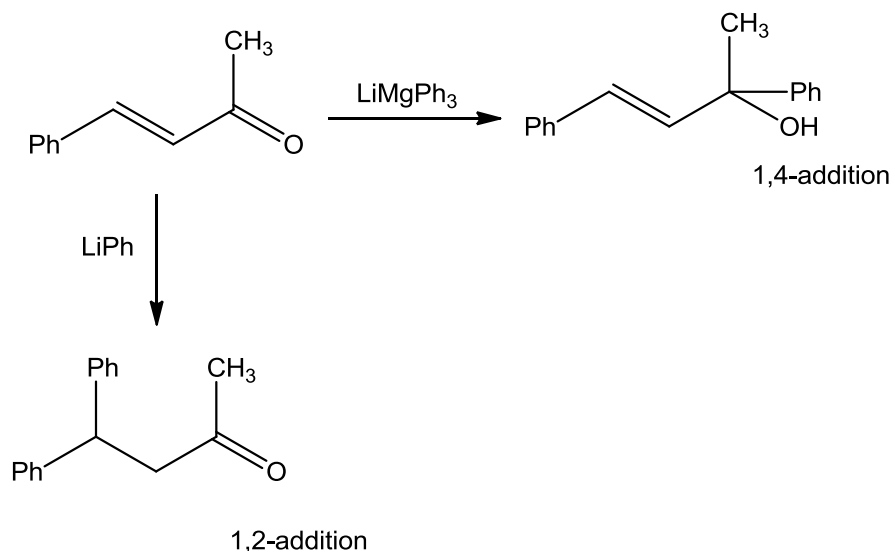
Scheme 1.19: Reaction of benzalacetophenone with LiMgPh$_3$ and LiPh.

Magnesiates have since become extremely useful reagents in organic synthesis, from "turbo Grignard" reagents carrying out functionalisation of aromatic molecules[72] and alkyl-amido magnesiates being used as highly efficient and versatile bases in deprotonative metallation reactions.[50] The unique chemical profiles of alkali-metal magnesiates can be rationalised in terms of cooperative partnership between the two metals present in the magnesiates. This concept is nicely illustrated in **Scheme 1.20** for the synergic deprotonation of toluene using mixed-metal reagent [(TMEDA)NaMg(TMP)$_2$Bu].[73] Toluene can be selectively deprotonated at the *meta* position to yield [(TMEDA)NaMg(Me-C$_6$H$_4$)(TMP)$_2$]. The structural characterisation of this compound demonstrates that the reaction is formally a magnesiation, where the position previously occupied by a hydrogen atom is now filled by a Mg centre.[74] This reaction is truly synergic since the monometallic components Na(TMP) or Mg(TMP)$_2$ are unable to deprotonate toluene on their own.

In fact to the best of our knowledge no organomagnesium reagents known are capable of reacting with toluene. In contrast, BuNa reacts with toluene to form benzylsodium, where the deprotonation occurs exclusively at the CH_3 group to form a benzyl anion which is stabilized by resonance; this regioselectivity has also been reported for other monometallic systems such as [n]BuLi/TMEDA. Here using a sodium magnesiate the methyl group of toluene is left untouched, and the deprotonation (formally a magnesiation) has occurred exclusively at the *meta* position on the ring. This special type of deprotonation reaction has been described as alkali metal mediated magnesiation (*AMMMg*).[75]
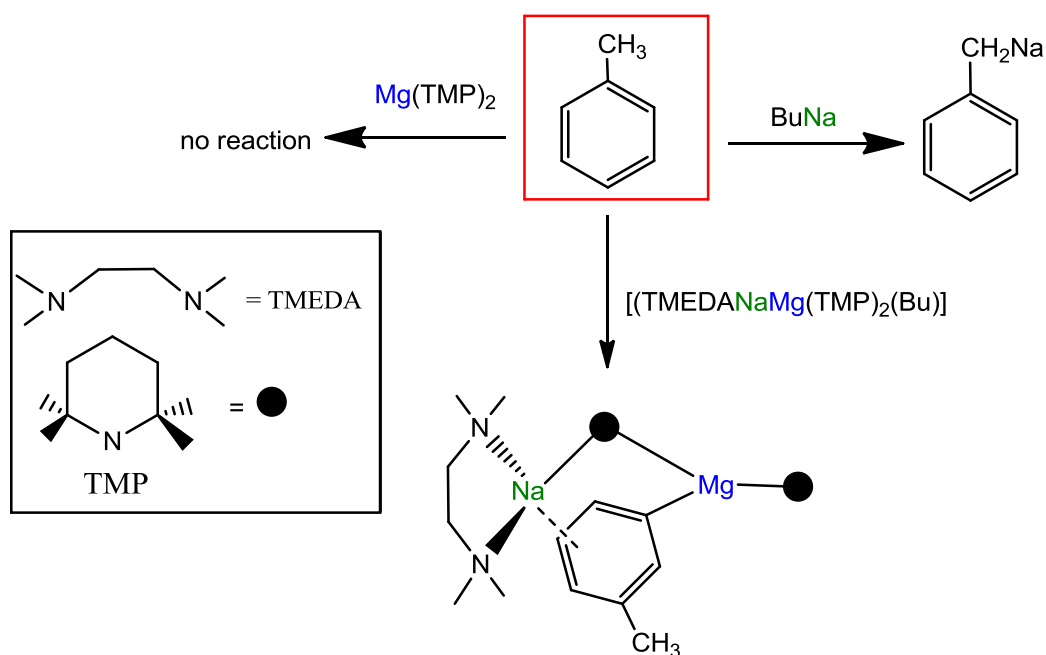
Scheme 1.20: Synergic deprotonation of toluene by the sodium magnesiate [(TMEDA)NaMg(TMP)$_2$(Bu)].

1.3.2 Alkali metal mediated magnesiation (*AMMMg*)

Using the bimetallic approach, Mulvey has reported the selective *ortho*-magnesiation of benzamides and aromatic ethers such as anisole, at room temperature without observing the formation of any side products.[76] Furthermore, the deprotonation of molecules with high pK_a numbers as for example benzene can be achieved. Thus [(TMEDA)NaMg(Bu)(TMP)$_2$] can selectively mono-magnesiate benzene,[73] moreover when the reaction is performed using an unsolvated magnesiate

[NaMg(TMP)$_2$Bu], benzene can be regioselectively two-fold deprotonated at the sterically optimum positions 1 and 4, where the organic dianion is trapped in the core of a dicationic 12-membered ring (**Figure 1.14**).[77] This supramolecular structure where the dianion $\{C_6H_4\}^{2-}$ is trapped in the core of a cationic twelve membered ring [$\{NMgNNa\}_2$] ring can be described as an inverse crown complex.[78]

Figure 1.14: Molecular structure of [Na$_4$Mg$_2$(TMP)$_6$-C$_6$H$_4$]. Hydrogen atoms omitted for clarity.

Likewise, as well as showing the importance of the donor in these mixed metal substrates, Mulvey *et al* have also shown the effect the alkyl group can have on the stereoselectivity of the metallation. Using the alkyl base [Na(Bu)(TMP)Mg(TMP)] Mulvey *et al* observe the 2,5 magnesiation of toluene to form [Na$_4$Mg$_2$(TMP)$_6$-(2,5-C$_6$H$_3$CH$_3$)].[77] However by changing the alkyl group to [Na$_4$Mg$_2$(TMP)$_6$(CH$_2$SiMe$_3$)$_2$], made by reacting a 4:2:6 ratio of BuNa, Mg(CH$_2$SiMe$_3$)$_2$ and TMP(H), they witness the unprecedented 3,5 magnesiation of toluene to form [Na$_4$Mg$_2$(TMP)$_6$(3,5-C$_6$H$_3$CH$_3$)] as seen in **Scheme 1.21**.
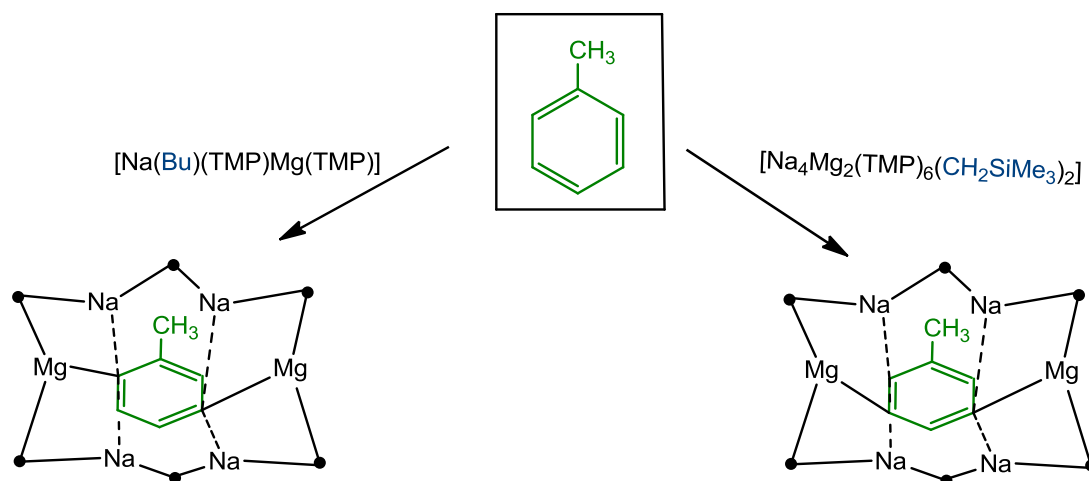
Scheme 1.21: Importance of alkyl group in controlling regioselectivity of metallation.

Macrocyclic compounds of this type have been pioneered by Mulvey *et al* and can be described as inverse crown compounds. These complexes are coined inverse crown compounds as the host ring is Lewis acidic and the guest is Lewis basic in comparison to conventional crown ethers where the host ring is Lewis basic and the guest in Lewis acidic. The concept of alkali metal mediated magnesiation can be extended further to aromatic heterocycles containing heteroatoms such as oxygen and sulfur. Furan undergoes monometallation by [(TMEDA)Na(μ-TMP)(μ-^{n}Bu)Mg(TMP)] to yield the inverse crown complex [{(THF)$_3$Na$_2$}{(TMEDA)Mg$_2$}(C$_4$H$_3$O)$_6$}] resulting from a disproportionation process shown in **Scheme 1.22**.[79]
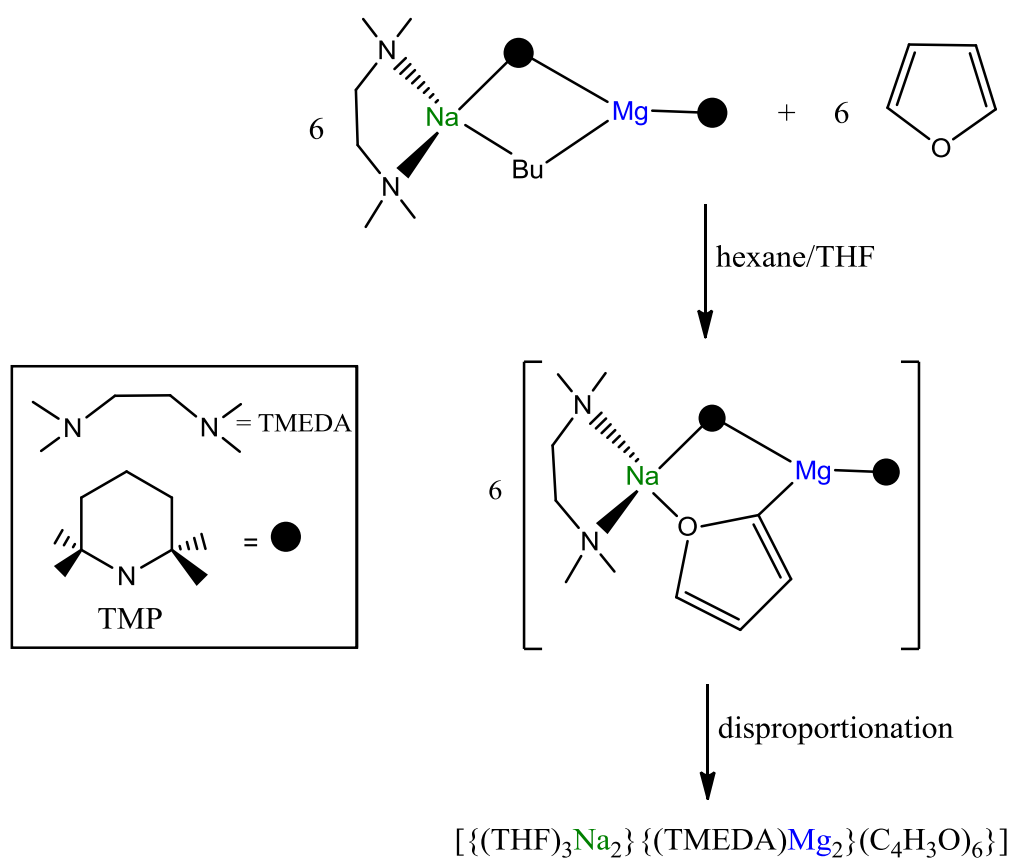
Scheme 1.22: Metallation of furan by [(TMEDA)Na(μ-TMP)(μ-^{n}Bu)Mg(TMP)] to yield the inverse crown complex [{(THF)$_3$Na$_2$}{(TMEDA)Mg$_2$}(C$_4$H$_3$O)$_6$}].
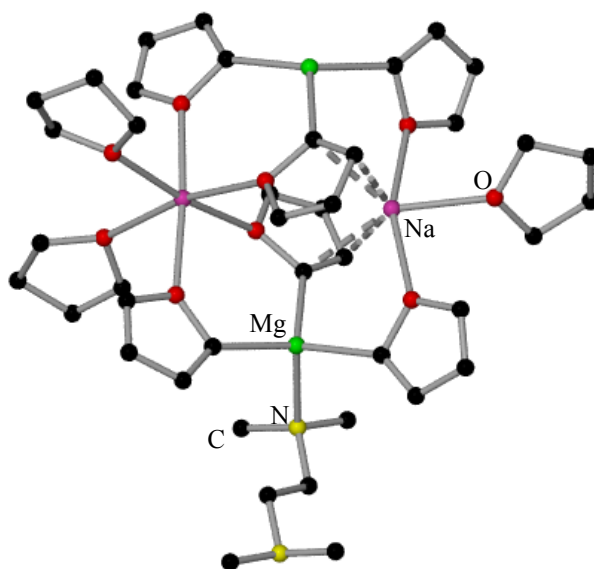
Figure 1.15: Molecular structure of [{(THF)$_3$Na$_2$}{(TMEDA)Mg$_2$}(C$_4$H$_3$O)$_6$}].

Whilst thiophene and tetrahydrothiophene also undergo mono-α-deprotonation by [(TMEDA)Na(TMP)(CH$_2$SiMe$_3$)Mg(TMP)][80] to yield [(TMEDA)Na(C$_4$H$_3$S)$_3$Mg(TMEDA)] and [(TMEDA)Na(μ-C$_4$H$_7$S)Mg(TMP)] in a 53 and 34% yield respectively.[81] But perhaps one of the most spectacular deprotonations performed by these bimetallic bases, is the selective four-fold deprotonation of ferrocene at the 1,1',3,3' positions by tris(amido)magnesiate [NaMg(N^{i}Pr$_2$)$_3$] (**Figure 1.16**).[82]
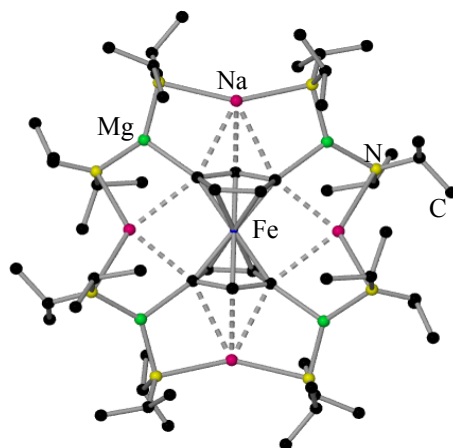
Figure 1.16: Molecular structure of [{Fe-(C$_5$H$_3$)$_2$}Na$_4$Mg$_4$(DPA)$_8$]. Hydrogen atoms omitted for clarity.

This regioselectivity has no precedent in the literature and nicely illustrates the enhanced basicity and magnesiating power of alkali-metal magnesiates as Mg reagents on their own can't metallate ferrocene, whilst BuLi·TMEDA results in dimetallation of ferrocene. Furthermore, the concept has successfully been extended to alkali-metal mediated metallation of other bimetallic pairs which combine an alkali-metal with a low polarity metal such as Zn, Mn, Fe or Cr. However, for brevity, these important contributions to the synthetic applications of ate chemistry will not be discussed in this introduction.

In addition to metallation reactions, alkali-metal magnesiates can also carry out other fundamental organic transformations such as metal-halogen exchange and nucleophilic addition reactions. Metal-halogen exchange involves the activation of a C-X bond (where X is usually I or Br), which is transformed to a more reactive M-C bond, in a single step (**Scheme 1.23**).

$$R-X + R'-M \rightleftharpoons R-M + R'-X$$

Scheme 1.23: General equation showing halogen-metal exchange.

Exchange of a C-X bond for a M-C bond is a kinetic process; as such these reactions are usually carried out at low temperatures to favour this fast exchange over competitive side reactions such as deprotonative metallation and addition reactions. Demonstrated by Knochel *et al* where the metal-halogen exchange reaction of trifluoromethylbromobenzenes can be carried out at 0°C using ^{i}PrMgCl·LiCl and the magnesium-aryl then quenched with an electrophile to give product in high yield of up to 97%.
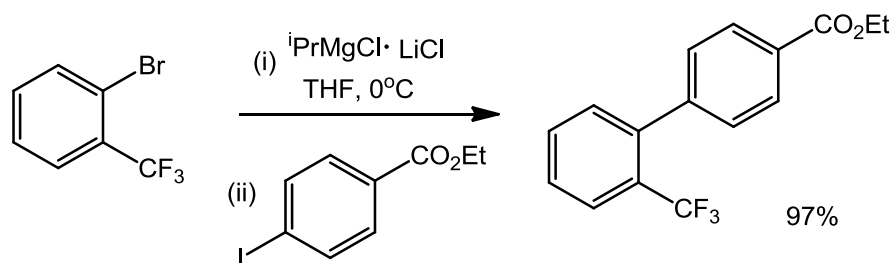
Scheme 1.24: metal-halogen exchange reaction using ^{i}PrMgCl·LiCl.

As mentioned alkali-metal magnesiates are also able to perform nucleophilic addition reactions as for example in, nucleophilic alkylations of ketones and aldehydes. Using conventional reagents such as BuLi and Grignard reagents in 1,2-addition reactions to ketones often results in the unwanted reduction product (through β-hydride elimination) or aldol dimerisation product (if α-hydrogens are present), giving an overall reduction in yield and potential purification problems.

Studies by Ishihara examined the treatment of acetophenone with homometallic BuLi, BuMgCl and MgBu$_2$ and compared these results with the application of mixed-metal lithium magnesiate LiMgBu$_3$ to the same substrate (**Scheme 1.25**). The results can be seen in **Table 1.1**, and show the high selectivity and nucleophilicity of the magnesiate reagent, which gives the desired addition product in a 82% yield with no formation of unwanted side products. Whereas the homometallic reagents display poorer selectivity, with a mixture of products formed in each case, and overall

reduced nucleophilicity, with a maximum yield of the desired product a modest 62% for BuLi, 50% for BuMgCl and 48% for MgBu$_2$.[83]
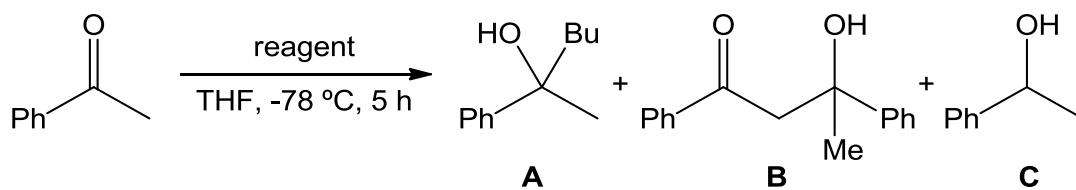
Scheme 1.25: Possible products of reaction of acetophenone with organometallic reagents.

Reagent	A %	B %	C %
BuLi	62	7	0
BuMgCl	50	9	8
MgBu$_2$	48	27	20
LiMgBu$_3$	82	0	0

Table 1.1: Addition to acetophenone by various reagents.

Building on some of these results using organomagnesium and magnesiate reagents to promote direct Mg-H exchange reactions, combined with recent breakthroughs in magnesium chemistry using highly sterically demanding ligands, this report focuses on the development of a new generation of mixed Na/Mg compounds containing the sterically encumbered bis(amido)silyl ligand $\{Ph_2Si(NAr^*)_2\}^{2-}$ ($Ar^* = 2,6\text{-}^iPr_2\text{-}C_6H_3$) and also the preparation of new magnesium complexes bearing the bulky β-diketiminate ligand ^{Dipp}nacnac(H) (^{Dipp}nacnac = $[\{(2,6\text{-}Pr^i_2H_3C_6)N(CH_3)C\}_2CH]^-$). Chapter 2 will introduce a new series of both alkyl and amido sodium magnesiate compounds chelated by bis(amido)silyl ligand $\{Ph_2Si(NAr^*)_2\}^{2-}$ which have been prepared and structurally characterised. Chapter 3 studies the reactivity of these compounds with a series of N-heterocyclic molecules, including thiophene, methylbenzimidazole, benzothiazole, nitron and quinoxaline, disclosing a unique cascade activation for benzothiazole and trapping and characterisation of a novel

quinoxaline radical anion species, as well as reporting the selective magnesiation of thiophene and methylbenzimidazole. Moving to a different type of organomagnesium reagents containing a bulky β-diketiminate ligand (nacnac), Chapter 4 compares the reactivity of alkyl compound [(^{Dipp}nacnac)Mg(Bu)(THF)] with that of TMP-based [(^{Dipp}nacnac)Mg(TMP)] towards 1,3-benzoazoles, showing the first applications of these family of organomagnesium reagents in deprotonative metallation chemistry as well as their capacity to promote sequential C-H, C-C and C-X bond activations of this family of heterocycles. Finally, Chapter 5 will discuss the ability of sodium magnesiate amido complexes supported by bis(amido)silyl ligand $\{Ph_2Si(NAr^*)_2\}^{2-}$ to undergo insertion reactions of unsaturated organic electrophiles such as alkyl and aryl isocyantes and alkyl carbodiimides. Based on our findings in these stoichiometric transformations, this chapter will also study the catalytic hydroamination of these organic heterocumulenes using sodium magnesiate [NaMg(CH$_2$SiMe$_3$)$_3$]. By isolating key organometallic intermediates and monitoring the reactions by ^{1}H NMR spectroscopy, new mechanistic insights have been revealed.

Chapter 2: Results and Discussion

2.1 Synthesis of new sodium magnesiates bearing the bis(amido)silyl ligand $\{Ph_2Si(NAr^*)_2\}^{2-}$

2.1.1 Introduction

One of the main aims of this project was to prepare a series of new sodium magnesiates supported by the highly sterically demanding dianionic bis(amido)silyl ligand $\{Ph_2Si(NAr^*)_2\}^{2-}$ ($Ar^* = 2,6-^iPr_2-C_6H_3$). The precursor of this ligand is the neutral bis(amine)silyl $\{Ph_2Si(NHAr^*)_2\}$ **1**, which was prepared using the synthetic methodology described by Murugavel *et al*,[84] by reacting two equivalents of the lithium amide LiHNAr*, (prepared in situ by deprotonation of H$_2$NAr* with BuLi), with Ph$_2$SiCl$_2$ (**Scheme 2.1**). This bis(amine)silyl ligand was chosen as it is sterically demanding and robust, and as previously mentioned, ligands of this type have already been used in the literature as steric stabilizers which enable the isolation of complexes exhibiting Zn-Zn metal-metal bonds.[23]

purified by recrystallisation
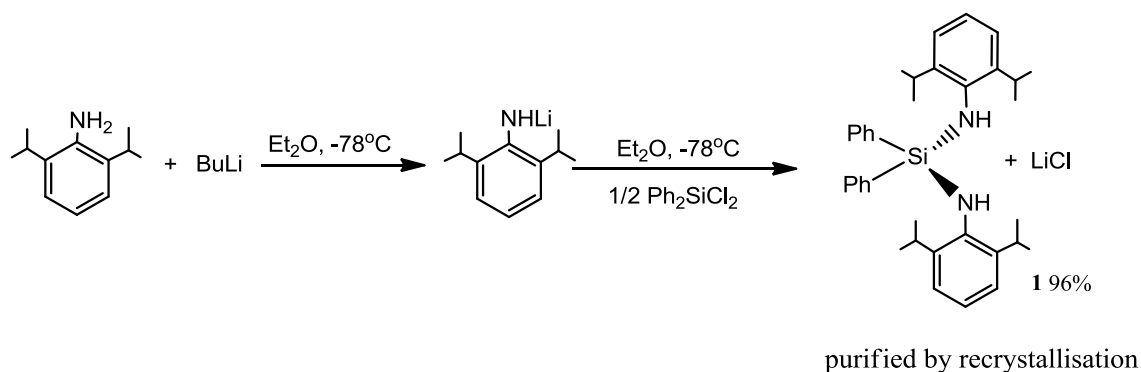
Scheme 2.1: Preparation of $\{Ph_2Si(NHAr^*)_2\}$ **1**.

2.1.2 Synthesis of alkyl complex $[\{Na(THF)_6\}^+\{(Ph_2Si(NAr^*)_2)Mg(Bu)(THF)\}^-]$ **2**

There have been several reports employing bis(amido)silyl ligands in homometallic systems using metals form across the periodic table; in main group chemistry heavier alkaline-earth metal complexes $[\{Me_2Si(NAr^*)_2\}M \cdot nTHF]$ (M= Ca, Sr, Ba, n = 3, 1, 4 respectively) have been prepared by Zheng *et al* by reacting $[M(NSiMe_3)_2(THF)_2]$

(M = Ca, Sr Ba) with an equivalent of {Me$_2$Si(NHAr*)$_2$} in THF.[85] In addition, in transition metal chemistry a Zr complex [Me$_2$Si(NAr*)Zr(Cl)$_2$(THF)$_2$] has been prepared by Hill *et al* by reacting an equivalent of [Me$_2$Si(NAr*Li)$_2$]$_2$ with ZrCl$_4$ in THF,[86] likewise there have been numerous examples in lanthanide chemistry using, Yb, Sm, Nd,[87] to name a few. However, their effect in mixed-metal chemistry is largely unknown, a few exceptions being the potassium magnesiate reported by Zheng *et al*,[47] mentioned beforehand in the introduction. Zheng *et al* were trying to reduce the bis(amido)silyl magnesium complex [(μ-Mg){η^2-Me$_2$Si(NAr*)$_2$}]$_2$ with KC$_8$ to form a Mg-Mg bond, however isolated the potassium magnesiate complex [(η^6-K)$^+$]$_2$[Mg{η^2-Me$_2$Si(NAr*)$_2$}$_2$]$^{2-}$ instead (**Scheme 2.2**).
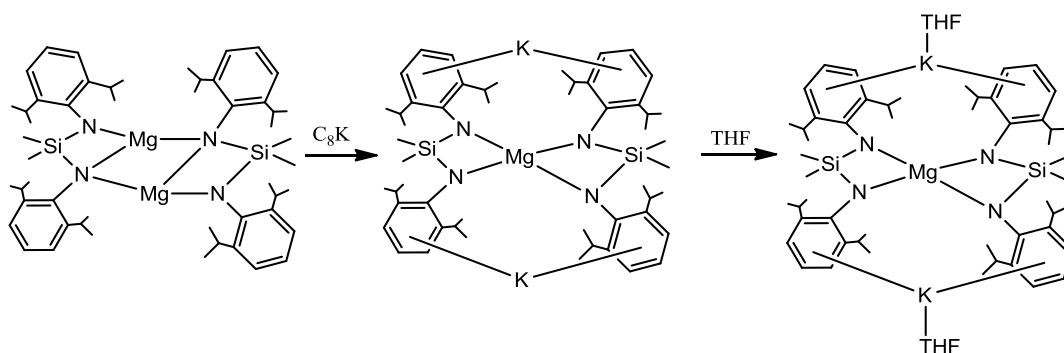
Scheme 2.2: Preparation of potassium-magnesium ate complexes.

Furthermore, as discussed in the introduction by reducing [Zn$_2$(μ-κ^2-Me$_2$Si(NAr*)$_2$)$_2$] with KC$_8$, a stable Zn-Zn metal bond was formed in complex [{κ^2-Me$_2$Si(NAr*)$_2$}Zn-Zn{κ^2-Me$_2$Si(NAr*)$_2$}]$^{2-}$ where the charge is balanced by two K atoms.[23] Likewise a bis(amido)silyl ligand was used in stabilising a Mn-Mn bond by the same group in complex [(THF)$_2$K-18-crown-6]$_2$[Mn{κ^2-MeSi(NAr*)$_2$}$_2$] by reduction of [Mn$_2${κ^2-Me$_2$Si(NAr*)$_2$}$_2$] with KC$_8$.[88]

We initiated our studies by reacting bis(amido)silyl {Ph$_2$Si(NHAr*)$_2$} **1** with NaMgBu$_3$ (which in turn can be prepared in situ by reacting BuNa with Bu$_2$Mg), shown in **Scheme 2.3** below. The resulting white suspension was allowed to stir at room temperature for one hour and THF was then introduced which led to a pale yellow solution which deposited colourless crystals of [{Na(THF)$_6$}$^+${(Ph$_2$Si(NAr*)$_2$)Mg(Bu)(THF)}$^-$] **2** on cooling in a 89% yield.
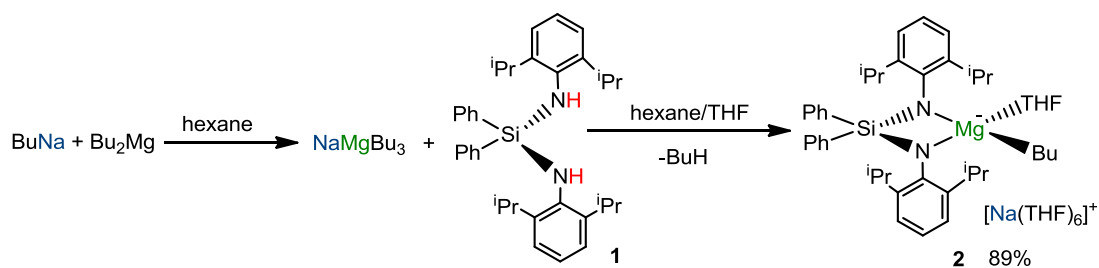
Scheme 2.3: Preparation of complex **2**.

X-ray crystallographic studies confirmed the bimetallic constitution of **2** as well as the incorporation of the bis(amido)silyl ligand $\{Ph_2Si(NAr^*)_2\}^{2-}$ resulting in the di-deprotonation of **1**. Complex **2** exhibits a solvent separated ion pair structure comprising the cation $\{Na(THF)_6\}^+$, with a Na atom in a distorted octahedral environment surrounded by six THF molecules (angles range from 84.26(11)° to 178.10(12)°) **(Figure 2.1)**, and the anion $[\{Ph_2Si(NAr^*)_2\}Mg(Bu)(THF)]^-$ where Mg is in a distorted tetrahedral geometry (angles range from 77.44(10)° to 137.10(12)°; average angle around Mg = 108.68°). The major distortion to this geometry is imposed by the bidentate ligand $\{Ph_2Si(NAr^*)_2\}^{2-}$ which coordinates in a chelating fashion to Mg (bite angle N1-Mg-N2 = 77.44(10)°). Mg completes its coordination sphere bonding to a butyl group and a molecule of THF. The length of the Mg-C bond (2.145(3) Å) is within the range found for other Mg complexes containing terminal butyl groups as for example $(\{^nBuMg(\mu\text{-}TMP)\}_2)$ (2.126(4) Å)[89] and $[(^{tBu}nacnac)Mg(Bu)(THF)]$ (2.122(3) Å).[90] The chelating coordination of the bis(amido) ligand contrasts with that found in related magnesium complex $[\{Me_2Si(NAr^*)\}_2Mg_2]$[47] where the bidentate ligand acts as a bridge between the two magnesium centres (**Scheme 1.14**). Both Mg-N bond lengths in **2** are of the same order (Mg-N1 2.050(3) and Mg-N2 2.081(3) Å).
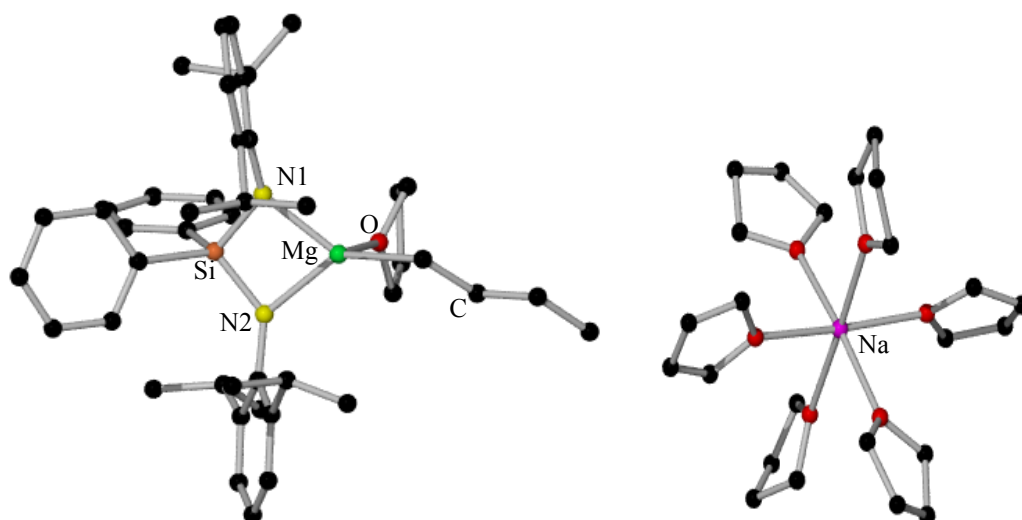
Figure 2.1: Molecular structure of **2**. Hydrogen atoms have been omitted for clarity. Selected bond lengths (Å) and bond angles(º):*Mg-O 2.123(1), Mg-N1 2.050(3) , Mg-N2 2.081(3), Mg-C 2.145(3) , N1-Mg-N2, 77.44(10) , N1-Mg-C 132.14(14) , N2-Mg-C 137.10(12) , N1-Mg-O 106.66(9) , N2-Mg-O 99.97(9), O-Mg-C 98.77(11).*

Previous studies within the group have shown sodium magnesiates to be selective magnesiators in reactions with heterocycles; for example the selective *meta* deprotonation of toluene by [(TMEDA)NaMg(TMP)$_2$(Bu)][73] and the *α*-deprotonation of thiophene and tetrahydrothiophene by [(TMEDA)Na(TMP)(CH$_2$SiMe$_3$)Mg(TMP)].[80] Therefore this new sodium magnesiate will be studied in relation to the metallation of heterocycles. The presence of a molecule of THF on Mg suggests that complex **2** has a labile position, which could be used to coordinate possible substrates (such as aromatic heterocycles), allowing their coordination into close proximity of the Mg-C bond (the predicted reactivity "hot-spot" of **2** which may favour their deprotonation). A direct correlation can be made here to the complex-induced proximity effect (CIPE)[91] in directed *ortho* metallation (D*o*M) reactions. The CIPE suggests that in directed *ortho* metallation, the formation of a prelithiation complex brings reactive groups into close proximity for direct deprotonation[92] (**Scheme 2.4**).
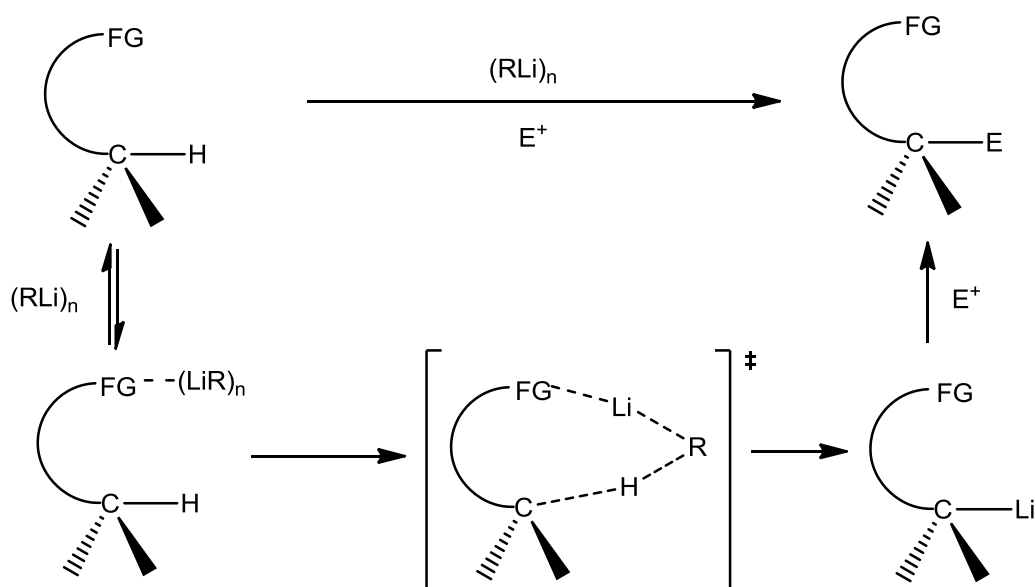
Scheme 2.4: General example of CIPE in D*o*M reactions.

To the best of our knowledge **2** represents the first example of a sodium magnesiate using a bidentate bulky ligand to be structurally defined. The closest precedent in the literature is potassium magnesiate [K$_2$Mg{Me$_2$Si(NAr*)$_2$}] prepared by the reaction of K metal with [Mg$_2${Me$_2$Si(NAr*)$_2$}$_2$], which unlike **2** exhibits a contacted ion pair structure[47] (see **Figure 1.12** in **Chapter 1**).

Complex **2** was also characterised in C$_6$D$_6$ solutions using ^{1}H and ^{13}C NMR spectroscopy with the aid of ^{1}H-^{1}H COSY and ^{1}H-^{13}C HSQC two-dimensional experiments. The most representative signal in the ^{1}H NMR spectrum was a multiplet at -0.34 ppm which can be assigned to the C*H*$_2$ group of the butyl ligand directly bonded to Mg (**Figure 2.2**). The chemical shift is comparable to that found in the related sodium magnesiate [(TMEDA)NaMg(TMP)$_2$(Bu)][73] (-0.78 ppm) and is slightly upfield in relation to the magnesium precursor MgBu$_2$ (0.07 ppm) used in the synthesis of **2**. The ^{1}H NMR spectrum of **2** also demonstrates that the deprotonation of the bis(amine) ligand **1** has occurred. To explain, the relevant signal for the N*H* groups in **1** (3.51 ppm) have disappeared. In addition, the multiplet corresponding to the C*H* group of the [i]Pr substituents is shifted significantly downfield from 3.38 ppm in **1** to 3.98 ppm in **2**.

The ^{13}C NMR spectrum of **2** showed a resonance at 9.38 ppm for Mg-CH_2 group, at a close chemical shift to that observed for MgBu$_2$ (9.12 ppm), as well as ten signals for the carbons of deprotonated bis(amine) **1** (eight of them for aromatic carbons ranging from 154.2 to 116.3 ppm and the remaining two for the CH and CH_3 groups of the ^{i}Pr substituent at 28.1 and 25.1 ppm respectively, (see Experimental Section for full assignment).
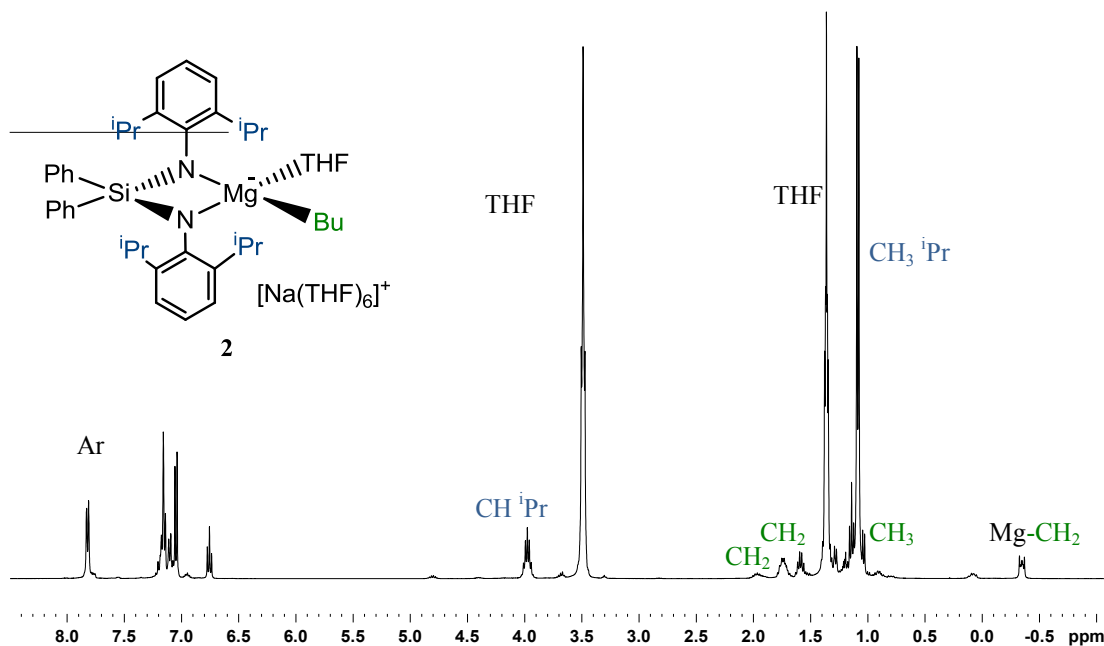
Figure 2.2: ^{1}H NMR spectrum of **2** in C$_6$D$_6$ solution.

Complex **2** could also be prepared using an alternative route by reacting MgBu$_2$ with sodium complex [{Ph$_2$Si(NHAr*)(NAr*)Na}$_2$] **3** which was synthesised and structurally characterised independently in a 33% yield (**Scheme 2.5**), by reacting an equivalent of BuNa with the bis(amine)silyl **1** in a hexane/toluene solution.
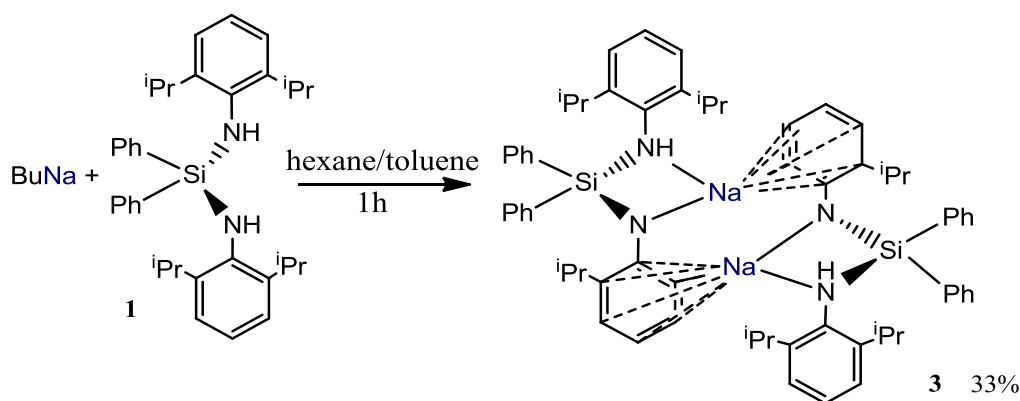
Scheme 2.5: Preparation of [{Ph$_2$Si(NHAr*)(NAr*)Na}$_2$] **3**.

However, by using this alternative route (**Scheme 2.6**), the yield is decreased from 89%, when reacting BuNa with MgBu$_2$ and bis(amine) **1** *in situ* to 69%.
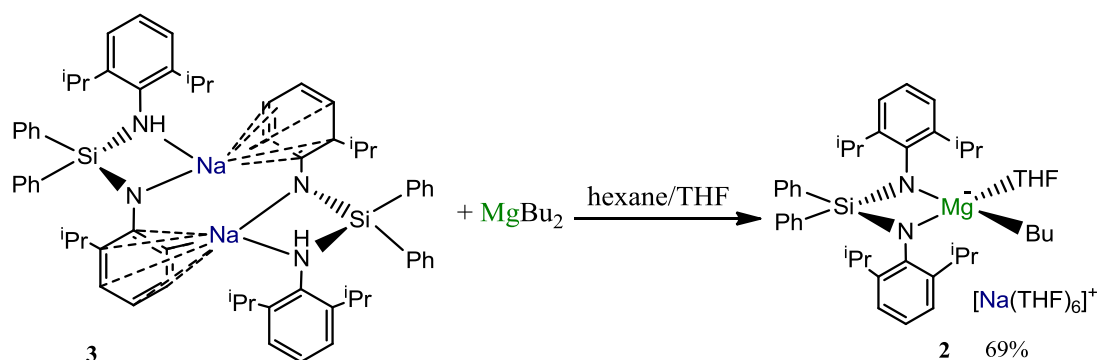
Scheme 2.6: Alternative route to prepare complex **2**, by reacting complex **3** with MgBu$_2$.

Homometallic **3** exhibits a dimeric arrangement in the solid state (**Figure 2.3**). In this case the bis(amine)silyl **1** is only monodeprotonated at one of its amine groups, giving rise to the formation of monanionic [Ph$_2$Si(NHAr*)(NAr*)]$^-$ ligand which coordinates to the Na centre in a chelating fashion. As it would be expected the Na-N$_{amido}$ bond (Na-N1 2.383(3) Å) where the nitrogen has been deprotonated is shorter than the Na-N$_{amine}$ bond where the nitrogen is acting as a Lewis donor (Na-N2 2.488(4) Å). Na completes its coordination sphere by coordinating η^6 to the aryl ring of the amido group of a neighbouring unit, giving rise to a dimeric structure (Na-C distances range from 2.748(4)-2.959(4) Å).
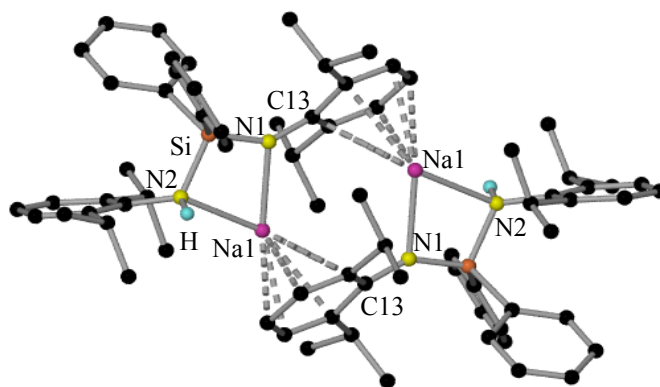
Figure 2.3: Molecular structure of **3**. Hydrogen atoms, a toluene molecule of crystallisation and disorder around the NAr* groups have been omitted for clarity. Selected bond lengths (Å) and bond angles (°): *Na-N1 2.383(3), Na-N2 2.488(4),Na-C13 2.959(4), Na-C14 2.931(4), Na-C15 2.807(4), Na-C16 2.748(4), Na-C17 2.826(5), Na-C18 2.938(4), N1-Na-N2 68.200(11).*

A search in the literature reveals π electrostatic interactions of this type are well known, involving an aromatic ring and an alkali-metal, with several examples structurally defined by X-ray crystallography. These electrostatic interactions between alkali-metal cations and the π-face of neutral aromatic systems are important as a binding force in a range of biological and chemical processes,[93] such as the functioning of ion channels within cell membranes.[94] Closest precedents in the literature to complex **3** are the paramagnetic species [{Na(Ar*NC)$_2$(C$_{12}$H$_6$)}$_2$] prepared by Fedushkin *et al* by the reduction of bis[N-(2,6-diisopropylphenyl)-imino]acenaphthene with Na in ether solution.[95] Na is η^1 coordinated to the aryl ring of a NAr* group with Na-C bond length 2.7330(19) Å in a similar region to the Na-C distances in complex **3**. In addition, [(η^6:η^6-K(THF))$^+$][(η^6:η^6-K(THF)$_2$)$^+$][(η_2-Mg){Me$_2$Si(NAr*)$_2$}$_2$]$^{2-}$ reported by Zheng *et al*[47], as discussed in the introduction K is η^6 coordinated to the aromatic NAr* group, the K-C distances are slightly more elongated than the Na-C distances in complex **3**, presumably due to the larger size of K over Na (K-C distances range from 2.957(3)-3.340(3) Å). Furthermore, Hill *et al* have prepared an alkali-metal complex [Me$_2$Si(NAr*Li)$_2$]$_2$ by metallation of the amine precursor [Me$_2$Si(HNAr*)$_2$] with two equivalents of ^{n}BuLi in hexane.[86] In this instance Li is coordinated to the C$_{ipso}$ atom of a NAr* group, the Li-C bond

distances (average distance 2.318 Å) as would be expected are shorter than the Na-C π electrostatic interaction in complex **3** (Na-C distances range from 2.748(4)-2.959(4) Å).

Complex **3** was also characterised in C_6D_6 solution using ^1H and ^{13}C NMR spectroscopy. As a consequence of lack of symmetry in the monanionic [$Ph_2Si(NHAr^*)(NAr^*)$]$^-$ ligand, now two different sets of signals are observed for its aromatic and ^iPr groups, as well as a singlet at 3.95 ppm for the N*H* which is slightly downfield in comparison to the N*H* resonance found in **1** at 3.51 ppm.

2.1.3 Aluminium contamination: Isolation of [{Na(THF)$_6$}$^+${(Ph$_2$Si(NAr*)$_2$)Al(Bu)$_2$}$^-$] 4

The ^1H NMR spectrum of some of the crystallised samples of **2** showed the presence of another minor product, which also contained the deprotonated bis(amine) **1**, with the most distinct signal being a multiplet at 3.48 ppm for the C*H* of the ^iPr groups. The presence of a Bu group was also apparent from signals at 1.96, 1.78, 1.27 and 0.09 ppm (for the C*H*$_2$, C*H*$_2$, C*H*$_3$ and M-C*H*$_2$ respectively). X-ray crystallographic studies revealed that surprisingly this minor product is a mixed sodium-aluminium complex (**Figure 2.4**). Unfortunately, the Bu groups in this structure are affected by large amounts of motion, which prevents a meaningful discussion of its geometrical parameters. Notwithstanding, the connectivity for this compound is certain, with the Na cation solvated by six THF molecules. The Al anion is in a distorted tetrahedral environment, chelated by the bis(amido)silyl ligand and also coordinated to two butyl groups. The rather unexpected formation of this aluminium complex **4** can be rationalised by taking into consideration that the Bu$_2$Mg, used in this reaction to prepare the relevant sodium-magnesiate, is a commercial solution in hexane supplied by Sigma Aldrich which contains Et$_3$Al in a 1% wt as a viscosity reducer. Although it is present in a very small concentration, sodium-aluminate **4** seems to crystallise and therefore appears as an impurity when complex **2** is isolated as a crystalline solid, ^1H NMR integration of crystalline sample of **2** shows approximately a ~10% contamination with sodium-aluminate **4**. Al contamination in the synthesis of organomagnesium complexes which use commercial Bu$_2$Mg as a precursor has recently been highlighted by Mulvey *et al*, where organoaluminium carbene complex

Bu₃Al·IPr (IPr = 1,3-bis(2,6-diisopropylphenyl)imidazol-2-ylidene) was isolated as the main product of the reaction of the carbene with a commercial solution of Bu$_2$Mg.[96]
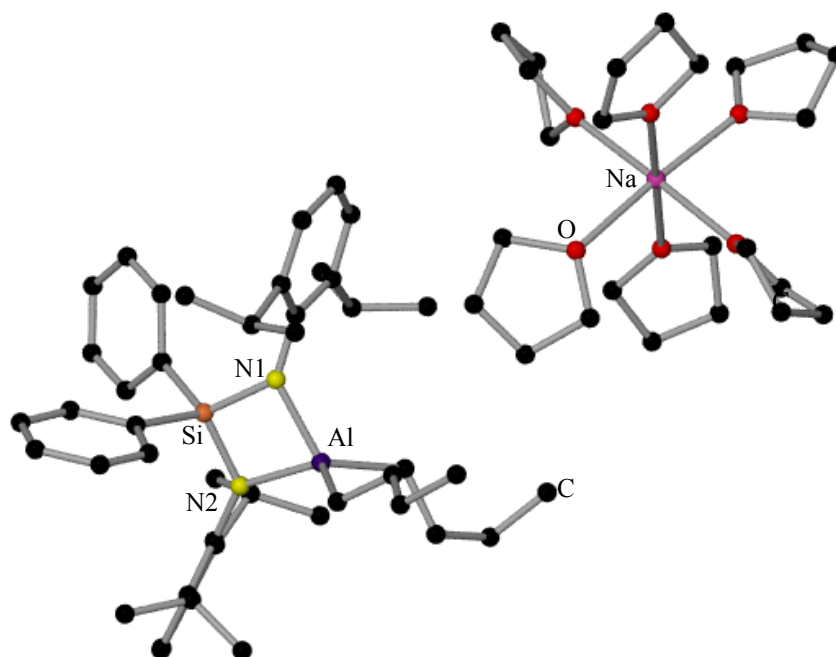
Figure 2.4: Molecular structure of **4**. Hydrogen atoms and disordered THF and Bu groups are omitted for clarity.

For our reactivity studies, in order to prevent the presence of the undesired sodium-aluminate **4**, which could compete with sodium magnesiate **2**, we decided to use dialkyl magnesium Mg(CH$_2$SiMe$_3$)$_2$ as a source for our systems. This magnesium-alkyl compound can easily be prepared by reacting BuLi with trimethylsilylchloride in ether. Precipitated LiCl is then filtered off. All solvent is removed by vacuum and the solid Mg(CH$_2$SiMe$_3$)$_2$ sublimed, the solid can be stored in the glove box for weeks.

2.1.4 Synthesis of alkyl complex [{Na(THF)$_6$}⁺{Ph$_2$Si(NAr*)$_2$)Mg(CH$_2$SiMe$_3$)(THF)}⁻] 5
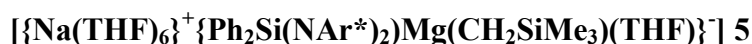
Following the same approach as described for **2**, the reaction of BuNa with Mg(CH$_2$SiMe$_3$)$_2$ along with the bis(amine)silyl {Ph$_2$Si(NHAr*)$_2$} **1**, afforded pure

sodium magnesiate $[\{Na(THF)_6\}^+\{(Ph_2Si(NAr*)_2)Mg(CH_2SiMe_3)(THF)\}^-]$ **5** as a crystalline solid in a 69% yield (**Scheme 2.7**).
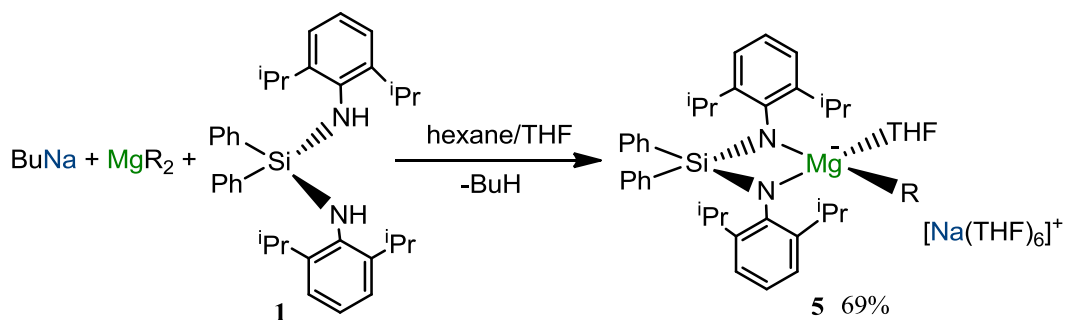
Scheme 2.7: Preparation of $[\{Na(THF)_6\}^+\{(Ph_2Si(NAr*)_2)Mg(CH_2SiMe_3)(THF)\}^-]$ **5**.

Complex **5** was characterised in solution using NMR spectroscopy and its structure in the solid state was established by X-ray crystallographic studies. Its molecular structure (**Figure 2.5**) is identical to that described for butyl derivative **2**, with magnesium centre now bonded to a CH_2SiMe_3 group instead of a butyl group. Alkyl complexes containing silyl substituted methyl groups exhibit enhanced stabilities in comparison to C-based alkyl groups due to the greater steric bulk and lack of β-hydrogens preventing β-hydride elimination from occurring.[97] The Mg-C bond distance in this complex (2.156(4) Å) is comparable to that found in the contacted ion pair sodium magnesiate $[(TMEDA)NaMg(TMP)_2(CH_2SiMe_3)]$ (2.179(2) Å),[98] and it is moderately elongated to that found in butyl derivative **2** (2.124(3) Å) as a consequence of the greater steric hindrance in the CH_2SiMe_3 group.
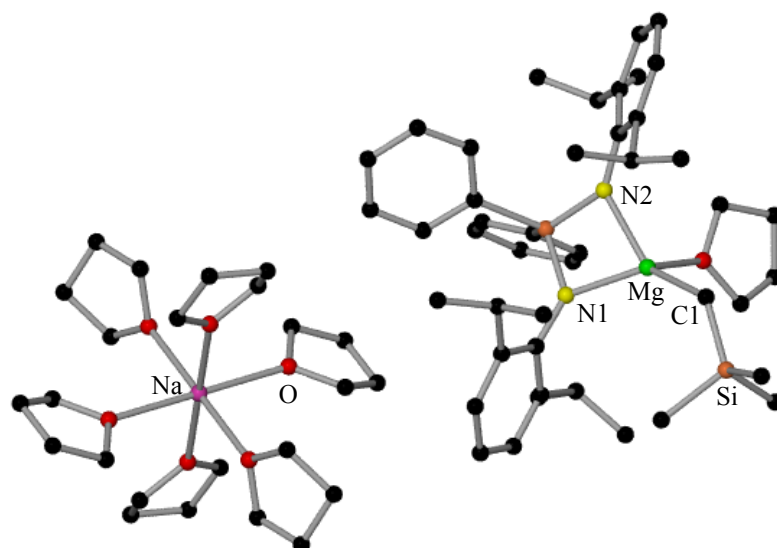
Figure 2.5: Molecular structure in **5**. Hydrogen atoms and disordered THF molecules have been omitted for clarity. Selected bond lengths (Å) and bond angles (º)*: Mg-N1 2.037(3), Mg-N2 2.098(3), Mg-C1 2.156(4), Mg-O 2.104(3), O-Mg-C1 101.52(17), C1-Mg-N1 129.54(16), N1-Mg-N2 77.33(11), N2-Mg-O 92.97(11)*.

Regarding the characterisation of **5** in C_6D_6 solution using NMR spectroscopy, the most indicative resonances which confirm the presence of CH_2SiMe_3 in the ^{1}H NMR spectrum are two singlets at -1.28 and 0.34 ppm which can be assigned to Mg-C*H*$_2$ and Si-*Me*$_3$ groups of the alkyl ligand respectively and two resonances at -0.82 ppm and 4.73 ppm in the ^{13}C NMR for the Mg-C*H*$_2$ and Si-*Me*$_3$ groups respectively. **Table 2.1** compares the most relevant resonances in the ^{1}H NMR spectrum of monosilyl species **5** and butyl derivative **2**.

Complex	δ^1H Mg-CH$_2$ (ppm)	δ^1H CH(^{i}Pr) (ppm)	δ^1H CH$_3$(^{i}Pr) (ppm)	δ^1H SiMe$_3$ (ppm)
2	0.34 (m)	3.98	1.08	____
5	-1.28 (s)	4.22	1.15	0.34

Table 2.1: Selected resonances in the ^{1}H NMR spectra of complexes **2** and **5** in C_6D_6 solution.

For complex **5** the Mg-CH_2 group gives rise to a singlet (-1.28 ppm) significantly more upfield than the multiplet observed for Mg-CH_2 unit in **2** (-0.34 ppm), which can be partly attributed to the negative inductive effect of the SiMe$_3$. Another important resonance that should be mentioned in this discussion for complex **5** is that corresponding to the CH group of the ^{i}Pr unit of the bidentate ligand {(Ph$_2$Si(NAr*)$_2$)}, a multiplet (4.22 ppm) which is significantly different to that observed for the same group in **2** (3.98 ppm) illustrating that the chemical shift of this resonance is highly sensitive to the chemical environment of the magnesium centre.

2.2.1 Synthesis of sodium magnesiate amido complexes [{Na(THF)$_6$}$^+${Ph$_2$Si(NAr*)$_2$Mg(NR$_2$)(THF)}$^-$] (NR$_2$ = HMDS, NPh$_2$, N^{i}Pr$_2$, DMP, TMP).

Magnesium amides including AMMMg amides[50] and "Turbo Hauser" bases[53] have proven to be valuable reagents in metallation reactions in recent years. In addition Hill *et al* have also shown the potential of using magnesium amide complex [{Ar*NC(Me)CHC(Me)NAr*}Mg{N(SiMe$_3$)$_2$}(THF)], where Mg is coordinated to a bulky β-diketiminate ligand to act as a precatalyst in the intramolecular hydroamination of amion-alkenes, although the Ca derivative demonstrates better turnover frequencies.[99] Therefore we next decided to extend our synthetic studies by preparing amido derivatives; using the alkyl complex **5** as a precursor, and investigating its reactivity with a series of amines. For these studies we used the classical utility amines hexamethyldisilazane (HMDS(H)), 2,2,6,6-tetramethylpiperdine (TMP(H)), diisopropylamine (DA(H)) and *cis*-2,6-dimethylpiperidine (*cis*-DMP(H)), which are four of the most widely used amines in synthesis, primarily due to their high Brønstead basicity and low nucleophilicity.[100] We chose achiral *cis*-DMP(H) as it is much cheaper than either of its chiral *trans*-isomers, however if the *trans*-isomer had be used this would allow the potential to introduce chirality to the sodium magnesiates.[101] Similarly to TMP(H), *cis*-DMP(H) is a cyclic amine which is just less sterically demanding and less expensive, therefore can be considered as a cheaper mimic of TMP(H). This study was also extended to diphenylamine (NHPh$_2$), a less hindered amine, but when reacted with a metal such

as Li to form the amide LiNPh$_2$, finds many applications in synthesis including deprotonation reactions[102] and as an initiator in the polymerization of methyl methacrylate.[103] As mentioned in the introduction of this report, in general Mg-N bonds are more kinetically reactive than Mg-C bonds thus in reactivity studies these complexes may prove to be better metallating agents, in fact recent advances in the synthesis of sodium magnesiates containing amido groups have been instrumental for the development of AMMMg.[50]

Alkyl magnesiate species **5** was prepared in situ, then an equivalent of the relevant amine NHR$_2$ was introduced, and the resulting solution left to stir for an hour, affording a colourless solution which deposited crystals of the relevant sodium magnesium amide [{Na(THF)$_6$}$^+${Ph$_2$Si(NAr*)$_2$Mg(NR$_2$)(THF)$_x$}$^-$] (NR$_2$ = HMDS, x=1, **6**; NPh$_2$, x=1, **7**; DA, x=1, **8**; DMP, x=1, **9**, TMP, x=0, **10**) in isolated yields ranging from 26 to 71% (**Scheme 2.8**). All amido complexes were fully characterised in solution using ^{1}H and ^{13}C NMR spectroscopy (see Experimental Section). In addition the structures of **6**, **7**, **9**, and **10** in the solid state were elucidated by X-ray crystallography. Although diisopropyl amido derivative **8** could be obtained as a crystalline solid it appeared to be too unstable to be analysed by crystallography. Thus, several samples have been tried to this date, in all cases crystals seem to decompose after a few minutes in the X-ray diffractometer.
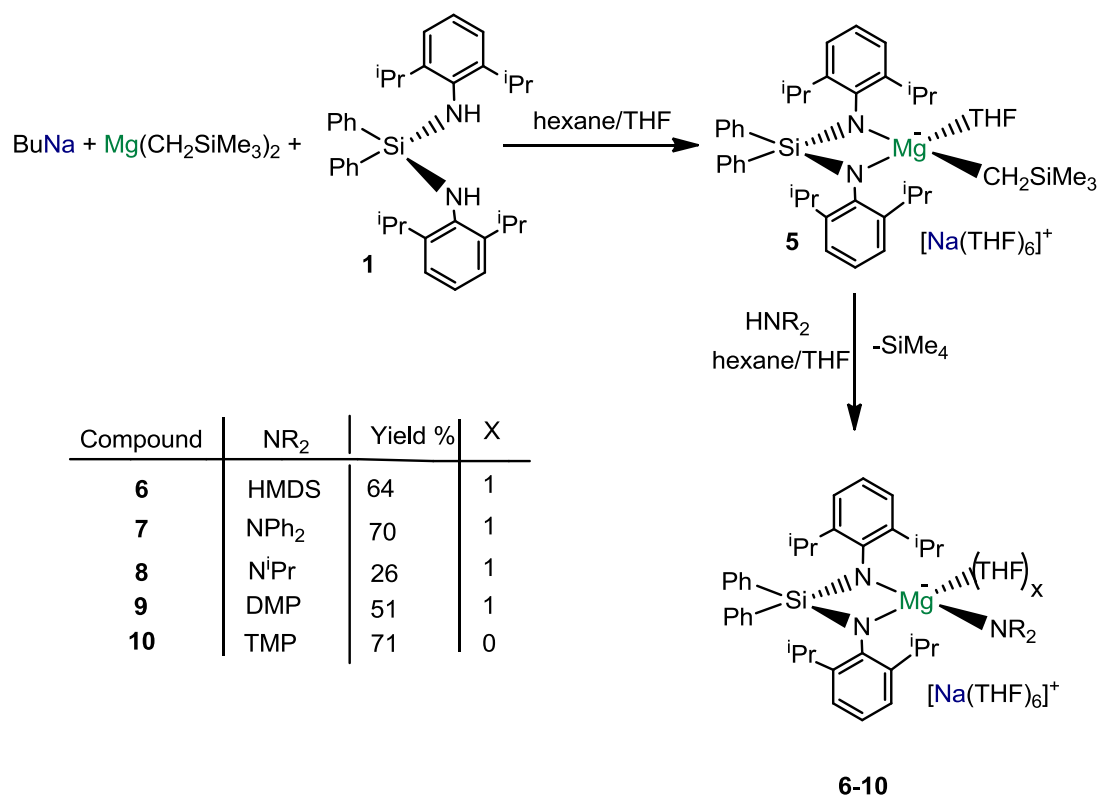
Scheme 2.8: Preparation of sodium magnesiate containing amide ligand **6**, **7**, **8**, **9** and **10**.

Compound	NR_2	Yield %	X
6	HMDS	64	1
7	NPh_2	70	1
8	N^iPr	26	1
9	DMP	51	1
10	TMP	71	0

All complexes **6**, **7**, **9** and **10** exhibit solvent separated ion pair structures with the Na solvated by molecules of THF in an octahedral environment. **Table 2.2** compares all the relevant bond angles and distances. Complex **9** contained two independent molecules in the unit cell, whose parameters differed within experimental error; therefore only one molecule will be discussed here.
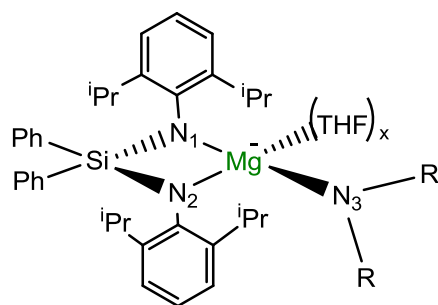
Bond Length (Å) and Angles (º)	6 NR$_2$ = HMDS x = 1	7 NR$_2$ = NPh$_2$ x = 1	9 NR$_2$ = DMP x = 1	10 NR$_2$ = TMP x = 0
Mg-N1	2.076(15)	2.0486(19)	2.110(5)	2.008(6)
Mg-N2	2.049(15)	2.047(19)	2.060(5)	2.026(6)
Mg-N3	2.020(16)	2.021(2)	2.013(6)	1.959(4)
Mg-O1	2.138(13)	2.092(18)	2.106(5)	
N1-Mg-N2	77.85(6)	78.47(7)	76.87(19)	79.31(11)
N2-Mg-N3	134.38(7)	129.40(8)	128.70(3)	138.20(4)
N3-Mg-N1	136.48(7)	135.94(8)	143.70(2)	140.80(4)
O1-Mg-N1	106.58(6)	105.29(8)	92.70(2)	
N2-Mg-O1	103.96(6)	112.72(8)	111.50(2)	
O1-Mg-N3	93.85(6)	94.30(8)	98.50(2)	
Σ around N3	359.4	359.1	352.3	353.7

Table 2.2: Comparison of relative bond lengths and angles of complexes **6**, **7**, **9** and **10**.

The Mg-based anion displays a distorted tetrahedral geometry, with the main distortion resulting from the bulky bidentate ligand $\{Ph_2Si(NAr^*)_2\}^{2-}$ which coordinates in a chelating fashion similar to that described for the alkyl complexes **2** and **5** (N1-Mg-N2 = 77.85(6)º, 78.47(7)º and 76.87(19)º for **6**, **7** and **9** respectively). In all complexes magnesium is coordinated to a terminal amido ligand and a molecule of THF. A comparison of the Mg-O_{THF} bond lengths of all species shows that this distance is slightly elongated for the HMDS derivative **6** (2.138(13) Å) than for **7** (2.092(18) Å) which could be explained in terms of the different steric bulk of the two amido groups. HMDS is considerably more sterically demanding than NPh_2, and therefore must prevent the THF molecule from coordinating to the Mg centre in **7** as closely as in **6** and **9**. Remarkably, this steric effect does not seem to greatly affect the values of the Mg-N_{amide} bonds which are within experimental error for the three complexes (2.027(16) Å for **6**, 2.021(2) Å for **7** and 2.013(6) Å for **9**). These Mg-N_{amide} distances are moderately shorter than those found for the bis(amido) chelating ligand (average Mg-N = 2.063 Å, 2.047 Å and 2.085 Å for **6**, **7** and **9** respectively). Reflecting on the steric constraints of $\{Ph_2SiNAr^*\}^{2-}$ the Mg-N_{amide} distances found in these complexes are elongated when compared with those found in other published complexes containing the same terminal amido groups. Thus, in lithium magnesiate [(THF)Li(HMDS)$_2$Mg(HMDS)] (2.004(3) Å),[104] monomer [(THF)$_2$Mg(NPh$_2$)$_2$] (2.013(3) Å) [105] and [(TMEDA)·Na(*cis*-DMP)$_2$Mg(*cis*-DMP)] (1.984(11) Å).[101] Inspection of the angles around the amido N in these complexes revealed that while in **6** and **7**, the N atom adopts a trigonal planar geometry (Σ<N3 = 359.98º and 359.11º for **6** and **7** respectively), however in **9** it exhibits a slight pyrimidalisation (352.3º). The Mg in complex **9** sits 0.350(2) Å above the plane defined by N$_3$ atoms (see **Figure 2.8**).
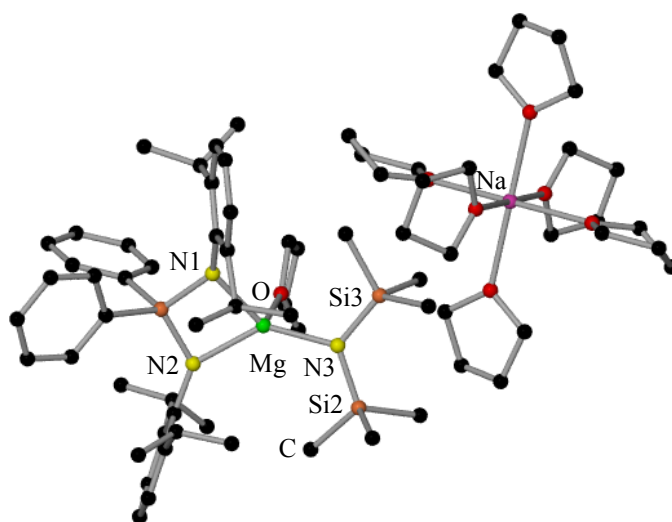
Figure 2.6: Molecular structure of **6**. Hydrogen atoms have been omitted for clarity. Selected bond lengths (Å) and bond angles (º)*: N1-Mg 2.076(15), N2-Mg 2.049(15) , Mg-O 2.138(13), Mg-N3 2.020(16 , N1-Mg-N2 77.85(6), N2-Mg-N3 134.38(7), N3-Mg-O 93.85(6), O-Mg-N1 106.58(6), N2-Mg-O 103.96(6), N1-Mg-N3 136.48(7), Si2-N3-Si3 121.77(9), Si2-N3-Mg 122.00(9), Si3-N3-Mg 115.65(9).*
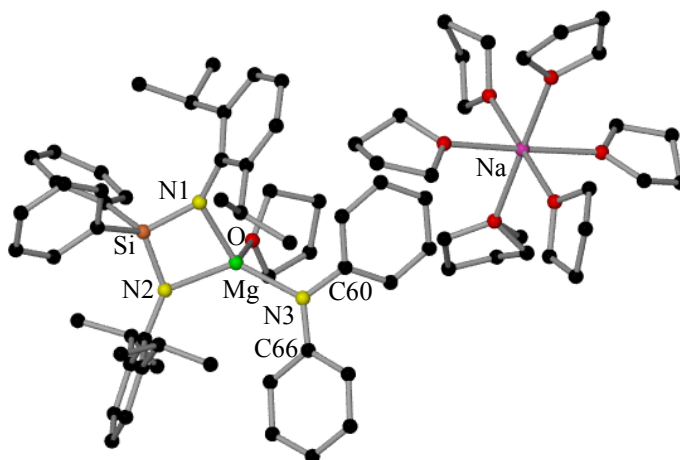
Figure 2.7: Molecular structure of **7**. Hydrogen atoms have been omitted for clarity. Selected bond lengths (Å) and bond angles (º)*: Mg-N1 2.0486(19), Mg-N2 2.047(19), Mg-N3 2.021(2), Mg-O1 2.092(18), N3-Mg-N2 129.40(8), N3-Mg-N1 135.94(8), N2-Mg-N1 78.47(7), N3-Mg-O 94.30(8), N1-Mg-O 105.29(8), N2-Mg-O 112.72(8), C60-N3-C66 120.18(19), C60-N3-Mg 124.23(15), C66-N3-Mg 114.70(15).*

Figure 2.8: Molecular structure of **9**. Hydrogen atoms have been omitted for clarity. Selected bond lengths (Å) and bond angles (º): *Mg1-N1 2.110(5), Mg1-N2 2.060(5), Mg1-N3 2.013(6), Mg-O 2.106(5), N1-Mg1-N3 143.7(2), N1-Mg1-N2 76.87(19), N2-Mg1-N3 128.7(3), N3-Mg-O 98.5(2), O-Mg-N1 92.7(2), N2-Mg-O 111.5(2), C37-N3-Mg1 121.4(7), C41-N3-Mg1 124.6(5), C41-N3-C37 106.3(9).*

TMP derivative **10** also exhibits a solvent seperated ion pair structure but now due to the increased steric bulk of the amide, Mg exhibits a distorted trigonal planar geometry (Σ<Mg = 358.31º) by bonding to three N atoms, two from the chelating bis(amido) ligand and one from the TMP group. The Na cation again displays a distorted octahedral environment coordinated to six THF molecules similar to those reported for **6**, **7** and **9**. The Mg-N3 (1.959(4) Å) bond distance compares well with other Mg-TMP complexes found in the literature such as [(TMEDA)Na(μ-Bu)(μ-TMP)Mg(TMP)] (2.001 Å)[73] and the "Turbo Hauser" base [(THF)$_2$Li(μ-Cl)$_2$Mg(THF)TMP] structurally characterised by Mulvey *et al* (1.981(2) Å).[66] To the best of our knowledge there is only one other solvent separated sodium magnesiate in the CSD containing a terminal Mg-TMP bond, [Na(PMDETA)$_2$Mg(TMP)$_3$] reported by Mulvey *et al*,[106] with the average Mg-N$_{amide}$ bond distance (2.050 Å) in a similar region to complex **10**. In addition the Mg-N3 distance is slightly shorter than those found for the bis(amido) chelating ligand (average Mg-N = 2.017 Å). Furthermore, the N$_{amide}$ exhibits a slight pyrimidalisation (353.70º for **10**) similar to that observed in complex **9**. The Mg in complex **10** sits 0.134(2) Å above the plane defined by N$_3$ atoms (see **Figure 2.9**).
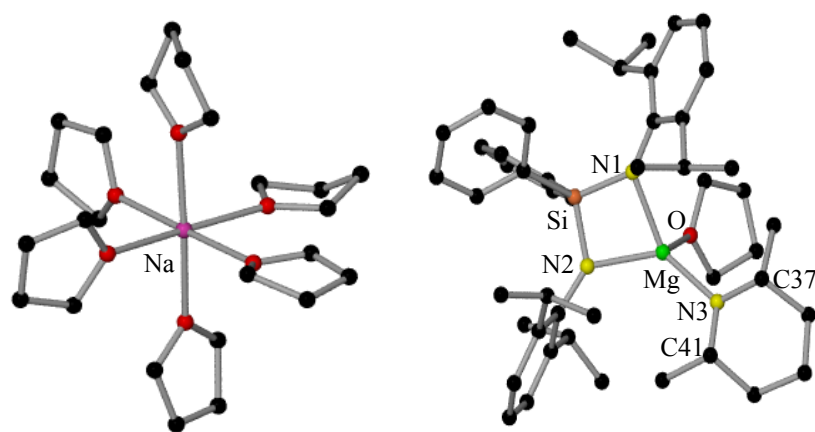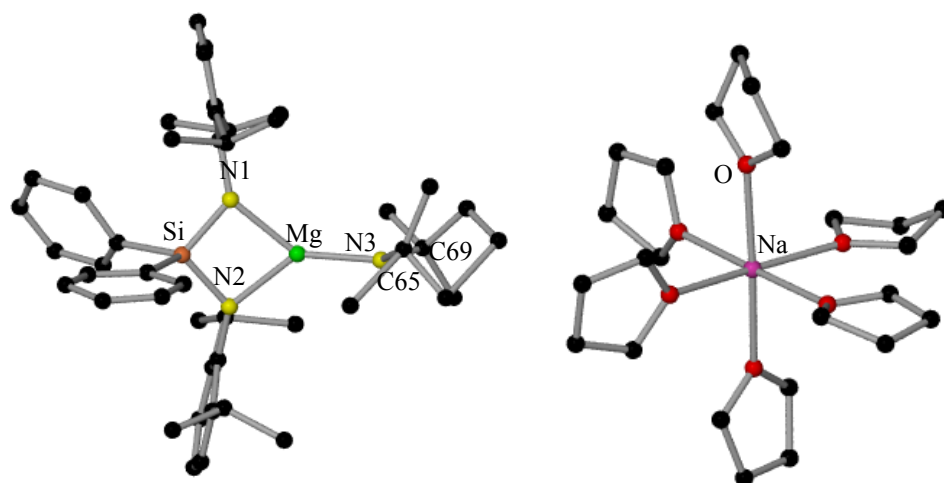
Figure 2.9: Molecular structure of **10**. Hydrogen atoms have been omitted for clarity. Selected bond lengths (Å) and bond angles (º)*: Mg-N1 2.008(6), Mg-N2 2.026(6), Mg-N3 1.959(4), N1-Mg-N3 140.8(4), N1-Mg-N2 79.31(11), N2-Mg-N3 138.2(4), C65-N3–C69 112.6(8), C65-N3-Mg 120.9(3), C69-N3-Mg 120.2(7)*.

The Mg-N$_{amide}$ bond lengths in complex **9** and **10** are in a similar region to each other (2.031(6) and 1.959(4) Å for **9** and **10** respectively). It is presumed this is due to the steric bulk of TMP that labile THF ligand is not able to coordinate to Mg as was seen in **6**, **7** and **9**.

Table 2.3 summarises the most relevant resonances for compound **6-10** in the ^{1}H and ^{13}C NMR spectra (for full details see Experimental Section). As observed for other complexes already reported in this thesis, the chemical shift of the multiplet corresponding to the C*H* unit of the [i]Pr group of the chelating bidentate ligand {Ph$_2$Si(NAr*)}$^{2-}$ is particularly sensitive to the ligands attached to the Mg centre and therefore it varies significantly depending on the NR$_2$ group present in the molecule (e.g. 3.97 ppm for NR$_2$ = NPh$_2$ vs 4.44 ppm for NR$_2$ = TMP). A similar variation is also observed for this C*H* group in the ^{13}C NMR spectra, with the biggest differences found between compounds **7** and **9** (ranging from 21.32 ppm when NR$_2$ = NPh$_2$ to 28.54 ppm when NR$_2$ = *cis*-DMP).

complexes	$\delta^1 H$ NR_2	$\delta^1 H$ $(CH\,^iPr)$	$\delta^{13}C$ NR_2	$\delta^{13}C$ $(CH\,^iPr)$
6	-0.21 (s, CH$_3$)	4.04	5.21 (CH$_3$)	25.92
7	7.62-7.23 (m, Ph)	3.97	156.24-117.92 Ph	21.32
8	3.23 (m, CH, ^iPr) 1.24 (m, CH$_3$, ^iPr)	4.20	49.99 (CH ^iPr) 20.01 (CH$_3$ N^iPr)	28.01
9	1.34 (s, CH$_3$), 1.88 (m, α-H), 1.64 (m, β-H)	4.11	25.98 (CH$_3$) 39.08 (α-C) 26.87 (β-C) 26.35 (γ-C)	28.54
10	1.40 (s, CH$_3$), 1.83 (m, α-H), 1.72 (m, β-H)	4.44	36.78 (CH$_3$) 40.97 (α-C) 51.71 (β-C) 20.02 (γ-C)	27.14

Table 2.3: Selected resonances from the ^{1}H and ^{13}C NMR spectra of compounds **6**, **7, 8, 9** and **10** in C$_6$D$_6$ solutions.

As the molecular structure of complex **8** could not be determined by X-ray crystallography, the ^{1}H NMR in C$_6$D$_6$ is shown in **Figure 2.10**. The C*H* and C*H$_3$* ^{i}Pr groups on the {Ph$_2$Si(NAr*)}$^{2-}$ ligand are displayed at 4.20 and 1.16 ppm respectively. As would be expected integrate to twice the amount for the C*H* and C*H$_3$* ^{i}Pr group of N-^{i}Pr at 3.23 and 1.24 ppm respectively.
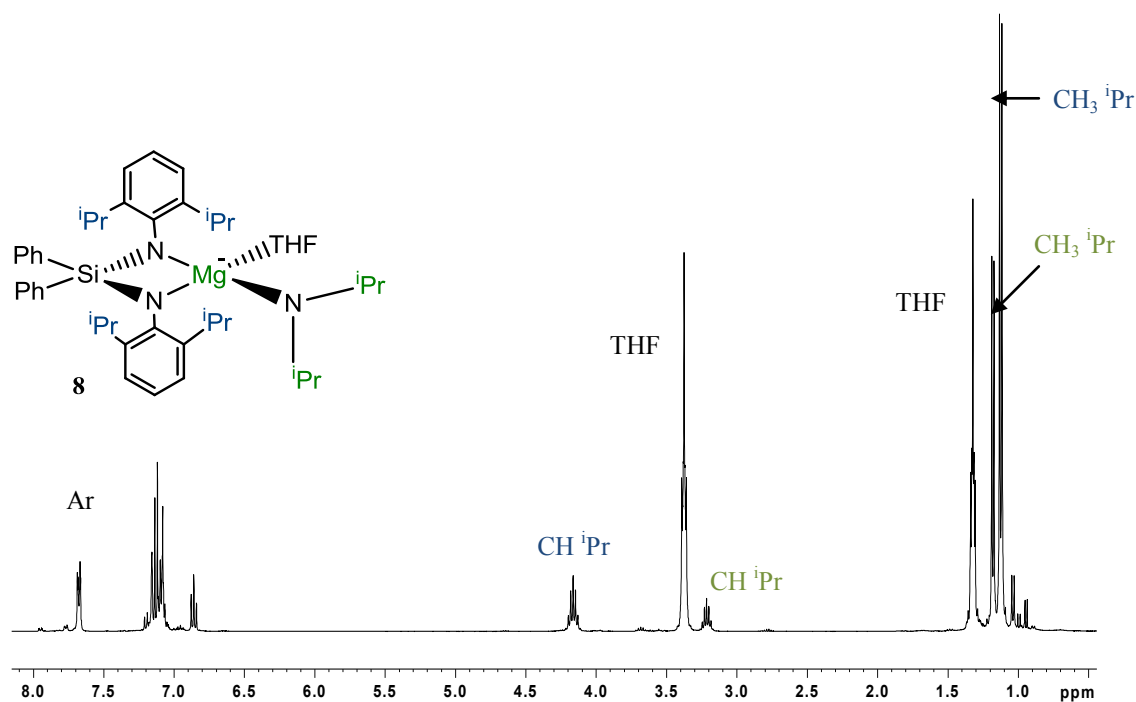
Figure 2.10: ^{1}H NMR in C_6D_6 of complex **8**.

2.2.2 Synthesis of sodium magnesiate amido complex $[\{Na(THF)_6\}^+\{(Ph_2Si(NAr^*)(NHAr^*))Mg(NHAr^*)_2(THF)\}^-]$ 11 and $[\{(Ph_2Si(NAr^*)(NHAr^*))Mg(NC_4H_4)_2(THF)Na(THF)_2\}]$ 12

Building on these results, we next attempted the synthesis of amido complexes derived from primary amine NH$_2$Ar* and the heterocyclic amine pyrrole. Pyrrole is an important molecule in synthesis having exhibited ample applications in agrochemicals,[107] pharmaceuticals[108] and polymer chemistry.[109] Following the same procedure as described for **6-10**, alkyl species **5** was reacted with one molar equivalent of H$_2$NAr* and allowed to stir for one hour, yielding $[\{Na(THF)_6\}^+\{(Ph_2Si(NAr^*)(NHAr^*))Mg(NHAr^*)_2(THF)\}^-]$ **11** in a 15% yield. Likewise, addition of an equivalent of pyrrole to complex **5** and subsequent stirring for one hour resulted in a batch of colourless crystals of $[\{(Ph_2Si(NAr^*)(NHAr^*))Mg(NC_4H_4)_2(THF)Na(THF)_2\}]$ **12** in a 23% yield. As two molecules of the relevant amines had reacted with complex **5** we therefore decided to prepare complexes **11** and **12** rationally by adding two equivalents of the relevant amine to complex **5** resulting in the yields increasing to 28 and 44% for **11** and **12**

respectively, however ^{1}H NMR analysis of the filtrate in both cases shows the reaction to be almost quantitative (**Scheme 2.9**).
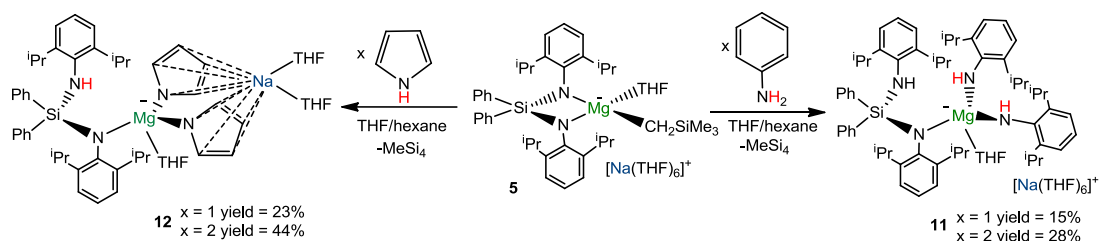
Scheme 2.9: Preparation of sodium magnesiates **11** and **12**.

Both H$_2$NAr* and pyrrole (pK_a 4.58[85] and 23[110] respectively in DMSO) are less basic than the previous amines used such as HNPh$_2$ (pK_a 25, DMSO)[111] due to their ability to delocalize electron density around the aromatic ring, therefore it is not so surprising that even when a shortfall of amine is used the relevant products **11** and **12** are still formed. **Table 2.4** compares some of the relevant bond lengths and angles of complexes **11** and **12**.

Bond length (Å) and angle (º)	11	12
Mg-N2	2.108(3)	2.015(18)
Mg-N3	2.027(4)	2.051(19)
Mg-N4	2.013(4)	2.060(2)
Mg-O1	2.121(3)	2.033(17)
Mean Na-C		2.938
Σ around N2	359.99	353.60

Table 2.4: Comparison of relevant bond lengths and angles for complexes **11** and **12**.

X-ray crystallographic studies revealed that **11** was also a solvent separated structure; the Na cation displays a distorted octahedral environment coordinated to six THF molecules. The Mg anion now displays a different motif to that observed in complexes **6**, **7**, **9** and **10**. Now one equivalent of amine has reacted with one of the basic arms of the bis(amido)silyl ligand to form amido/amine monanionic {$Ph_2Si(NHAr^*)(NAr^*)$}$^-$ ligand which coordinates to Mg through the N_{amide} atom (Mg-N 2.108(3) Å), the Mg-N1 distance, where the N_{amine} atom is not coordinated to Mg is 4.760 Å. Complex **3** also contains this monanionic ligand fragment {$Ph_2Si(NHAr^*)(NAr^*)$}$^-$, however in **3**, Na coordinates to both the N_{amide} and N_{amine} atoms of {$Ph_2Si(NHAr^*)(NAr^*)$}$^-$ ligand. The N_{amide} of {$Ph_2Si(NHAr^*)(NAr^*)$}$^-$ ligand sits in an almost planar geometry (Σ<N2 = 359.99º). Mg completes its coordination sphere by coordinating to two HNAr* groups and finally is solvated by a molecule of THF (Mg-O 2.121(3) Å). The Mg-based anion displays a distorted tetrahedral geometry, with the main distortion resulting from the two bulky NHAr* ligands (angles ranging from 92.34º to 124.54º). As expected the Mg-N distance from the silyl(amido)(amine) ligand (Mg-N 2.108(3) Å) is longer than those for the amide groups NHAr* (2.027(4) and 2.013(4) Å). These Mg-N_{amide} bond values are within the same range of those reported for the related alkyl amido species [BuMgN(H)Ar*·TMEDA] (Mg-N 2.004(17) Å),[112] where the NHAr* group is also coordinated terminally to the Mg centre.
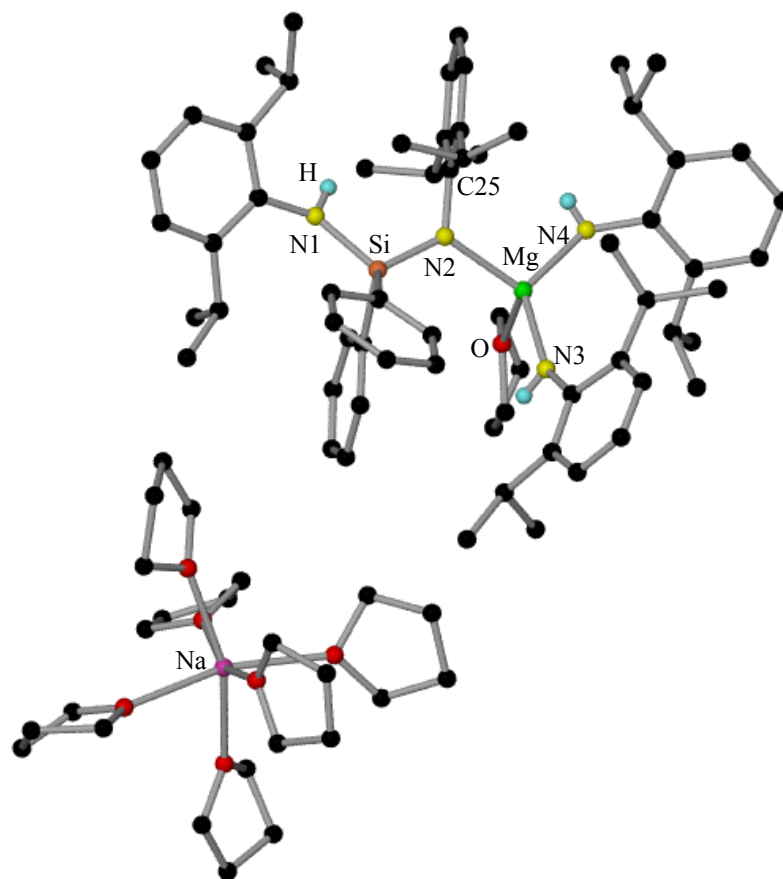
Figure 2.11: Molecular structure of **11**. Hydrogen atoms and disordered THF molecules have been omitted for clarity. Selected bond lengths (Å) and bond angles (°): *Mg-N4 2.013(4), Mg-N3 2.027(4), Mg-N2 2.108(3), Mg-O 2.121(3), N4-Mg-N3 124.54(18), N4-Mg-N3 106.66(16), N3-Mg-N2 118.60(17), N4-Mg-O1 99.23(16), N3-Mg-O1 92.34(16), N2-Mg-O1 111.91(4), C25-N2-Si 119.5(3), C25-N2-Mg 118.3(3), Si-N2-Mg 122.19(18).*

Complex **11** was also characterised in solution by ^{1}H and ^{13}C NMR spectroscopy using C_6D_6 as solvent. The ^{i}Pr signals of the four NAr* groups (two from the {Ph$_2$Si(NHAr*)(NAr*)}$^-$ ligand and two from the amide groups coordinated to Mg) do not give three different signals as would have been expected but instead are represented by only two multiplets at 3.50, 3.36 for the C*H* ^{i}Pr and 1.32 and 0.98 ppm for the C*H$_3$* ^{i}Pr group (**See Figure 2.12**).
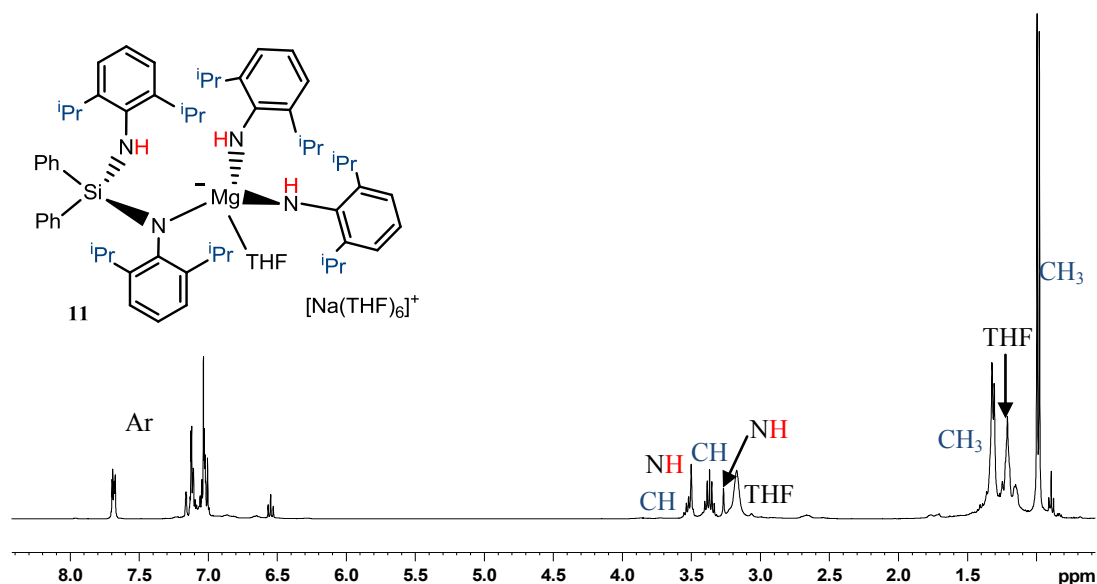
Figure 2.12: ^{1}H NMR spectrum of **11** in C_6D_6 solution.

The three NH groups are represented by two peaks at 3.50 ppm which overlap with one of the CH ^{i}Pr groups of Ar* and at 3.26 ppm. The integration of THF only equates to two molecules, when there should be seven, however the lost THF is thought to have been removed when complex **11** was isolated in vacuo.

X-ray crystallographic studies revealed that unlike the rest of the amido complexes included in this report, **12** exhibits a contacted-ion pair structure, where Mg and Na are connected through two molecules of pyrrolyl anions which are coordinated through N to Mg forming strong Mg-N sigma bonds (Mg-N = 2.051(19) and 2.060(2) Å) and are π-engaged with Na in a η^5-NC$_4$ fashion (Na-C distances range from 2.721(3) to 3.146(13) Å and Na-N distances are 2.635 and 2.796 Å for N3 and N4 respectively). Magnesium is once again in a distorted tetrahedral environment, (bond angles range from 99.46°-123.23°). Similarly to **11** two molecules of the amine have reacted with **5**, protonating one of the basic arms of $\{Ph_2Si(NAr^*)_2\}^{2-}$ and incorporating two pyrrolyl fragments, Mg also coordinates to a molecule of THF. The N$_{amide}$ of the $\{Ph_2Si(NHAr^*)(NAr^*)\}^-$ ligand sits in a much more distorted planar geometry (Σ<N2 = 353.60°) than observed in complex **11** (359.99°). Na completes its coordination sphere bonding to two THF molecules. Complex **12** is similar in structure to complex **11**; however it is thought that probably the presence of a much less sterically demanding amido group favours π coordination of Na over

THF solvation, despite the large amount of THF present in solution. As best as could be ascertained this is the first example where pyrrole has been metallated by Mg. The closest precedent in the literature is where 2,5-bis(dimethylaminomethyl)pyrrole is metallated by $[CpMg(Et_2O)_2]_2$ to form $[CpMg(Et_2O)(Me_2NCH_2(C_4H_2N)CH_2NMe_2)]$, the Mg-N distance (Mg-N = 2.043(16) Å) compares well with the Mg-N distance in **12** (Mg-N = 2.051(19) and 2.060(2) Å).[88]
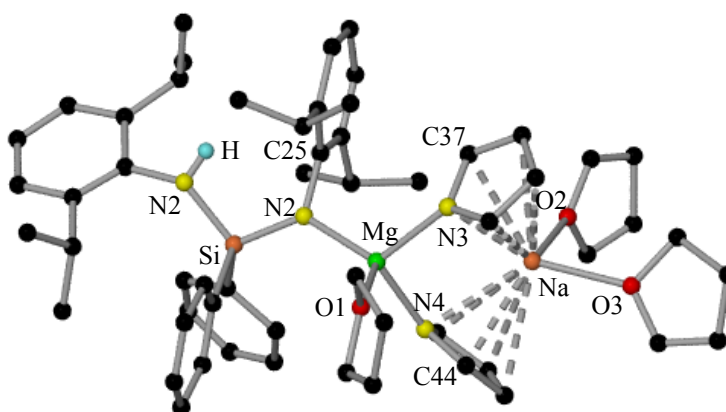
Figure 2.13: Molecular structure of **12**. Hydrogen atoms have been omitted for clarity. Selected bond lengths (Å) and bond angles (º)*: Na-O3 2.265(2), Na-O2 2.294(16),Na-N3 2.635(2), Na-N4 2.796(2), Na-C37 2.721(3), Na-C38 3.002(3), Na-C39 3.066(3), Na-C40 2.837(3), Na-C41 3.0161(3), Na-C42 3.146(13), Na-C43 2.960(3), Na-C44 2.729(3), Mg-O1 2.033(17), Mg-N2 2.015(18), Mg-N3 2.051(19), Mg-N4 2.060(2), N1-Mg-O1 115.23(7), N1-Mg-N3 114.99(8), O1-Mg-N3 99.54(7). N1-Mg-N4 123.27(8), O1-Mg-N4 100.61(8), N3-Mg-N4 99.46(8), C25-N2-S1 135.60(16), C25-N2-H1 109.0(17), Si-N2-H1 109.0(17).*

A comparison can be drawn to a sodium zincate prepared by Mulvey *et al*, $[\{(THF)_2 \cdot NaZn(THF)(NC_4H_4)_3\}_\infty]$,[113] adopting a unique polymeric structure of C_1 symmetry. This sodium zincate $[\{(THF)_2 \cdot NaZn(THF)(NC_4H_4)_3\}_\infty]$, can be considered as a chain of alternating Zn and Na atoms connected via sigma bonding (to Zn) and π-bonding (to Na) ambi-bridging pyrrolyl ligands, with THF completing the coordination sphere of both metal centres. In this case the Na interacts through a η^2-C_2 edge of one pyrrolyl ligand and a much stronger η^5-NC_4 interaction with a second pyrollyl ligand. The Na-C distances range from 2.690(18) to 2.919(15) Å and are in a

similar region to the Na-C distances of **12** ranging from 2.721(3) to 3.146(13) Å. However the Na-N distance is slightly more elongated (Na-N 2.919(15) Å) as the Na lies closer to the back edge of the pyrrolyl ligand (C6-C7 see **Figure 2.14**) than in complex **12** (Na-N3 = 2.635 and Na-N4 2.796 Å) where the Na lies closer to the front edge of the pyrrolyl ligand (C37-C40 and C41-C44).
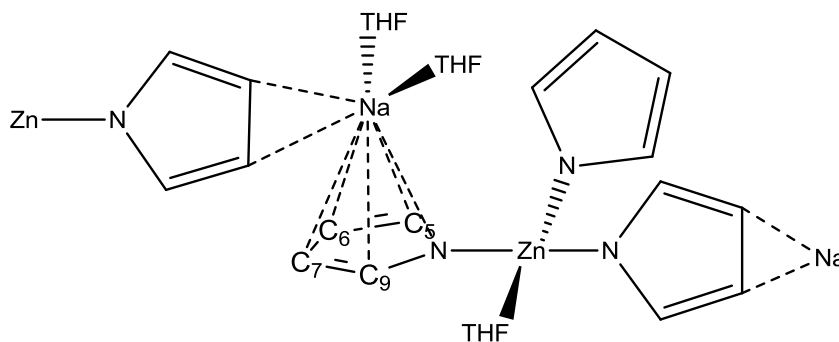
Figure 2.14: $[\{(THF)_2 \cdot NaZn(THF)(NC_4H_4)_3\}_\infty]$ prepared by Mulvey *et al.*[113]

Regarding the solution characterisation of **12** in C_6D_6, two sets of singlets are observed (7.15 and 6.17 ppm) and (7.52 and 6.36 ppm) for the α and β-H of the two deprotonated pyrrole molecules. These are more deshielded than the α and β-H of free pyrrole at (6.37 and 6.31 ppm) due to the greater negative charge on the N centre in **12** caused by the greater polarity of the Mg-N bond over the N-H unit in free pyrrole. Likewise a similar downfield shift is observed in the ^{13}C NMR for the α and β-C of the two pyrrolyl ligands in **12** compared to free pyrrole (127.12 and 107.79 ppm) and (126.76 and 107.45 ppm) for complex **12** and (117.5 and 108.4 ppm) for free pyrrole (see **Table 2.5**). Unfortunately the NH of {Ph_2Si(NHAr*)(NAr*)}⁻ ligand was too broad to be observed by NMR.

Compound	^{1}H α-CH (ppm)	^{1}H β-CH (ppm)	^{13}C α-CH (ppm)	^{13}C β-CH (ppm)
free pyrrole	6.37	6.31	117.5	108.4
12	7.15, 7.52	6.17, 6.36	127.1, 126.8	107.8, 108.4

Table 2.5: Comparison of ^{1}H and ^{13}C chemicals shifts in C_6D_6 of free pyrrole and complex **12**.

2.3.1 Conclusions

Chapter 2 has detailed the preparation and characterisation of a series of new alkyl and amido sodium magnesiates bearing a bulky bis(amido)silyl ligand, which will now be applied in metallation and hydroamination reactions. Alkyl sodium magnesiate **2** was prepared in a 89% yield by reacting BuNa with Bu_2Mg and an equivalent of bis(amine)silyl **1**. A contamination of Et_3Al in Bu_2Mg bottle meant that sodium aluminate **4** crystallised along with complex **2** in roughly a 10% ratio, therefore Bu_2Mg was exchanged for $Mg(CH_2SiMe_3)_2$, resulting in the formation of complex **5** in a 69% yield. The amido derivatives **6**, **7**, **8**, **9** and **10** were formed by preparing complex **5** in situ and adding an equivalent of the relevant amine (HMDS(H), $HNPh_2$, HN^iPr_2, DMP(H) and TMP(H) respectively) in yields ranging from 26-71%. The majority of amido bases displayed the same solvent separated structural motif to the alkyl complexes **2** and **5**, where Na cation is solvated by THF molecules and Mg anion is in a distorted tetrahedral environment chelated by bis(amido)silyl ligand, a molecule of THF and the relevant amide or alkyl group. The exception was the TMP derivative **10** where Mg was only tri-coordinated due the steric bulk of TMP preventing a THF molecule from coordinating. However, when the less basic amines H_2NAr^* and pyrrole were reacted with an equivalent of complex **5**, new sodium magnesiates **11** and **12** were formed respectively. A new structural motif was now observed where the bis(amido)silyl ligand has been protonated to form $\{Ph_2Si(NHAr^*)(NAr^*)\}^-$ ligand which now only coordinates to Mg through the N_{amide}. Complex **11** is solvent separated, with Na solvated by THF molecules and the Mg anion is in a distorted tetrahedral environment coordinated to the $\{Ph_2Si(NHAr^*)(NAr^*)\}^-$ ligand as mentioned, a molecule of THF and two amido Ar^* groups. However, complex **12** displayed our first contact ion pair structure, now Mg and Na are connected through two molecules of pyrrolyl anions which are coordinated through N to Mg forming strong Mg-N sigma bonds and are π-engaged with Na in a η^5-NC_4 fashion. The reactivity of these sodium magnesiates bearing a sterically demanding bis(amido)silyl ligand in metallation and hydroamination reactions will now be studied.

Chapter 3

3.1.1 Metallation reactions

Heterocyclic molecules are common building blocks for the synthesis of a multitude of natural products, pharmaceuticals and biologically active molecules.[114] In fact, the top ten "blockbuster" drugs at the present time all contain a heterocyclic moiety (see **Figure 3.1**), these include Lipitor and Plavix for treatment of cholesterol and heart attack prevention respectively.[97]
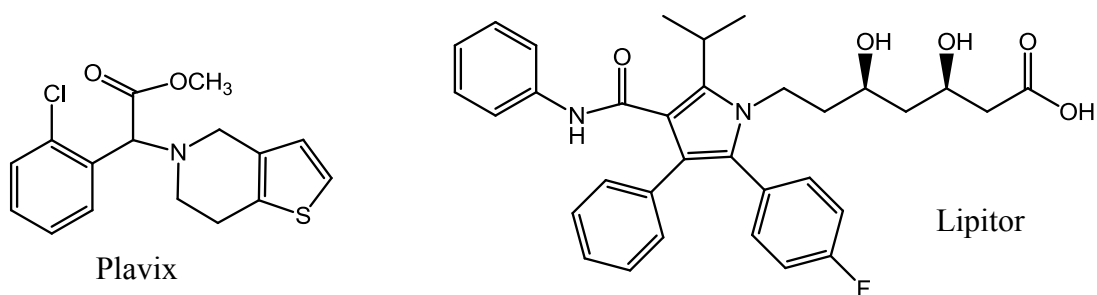
Figure 3.1: Examples from the top ten "blockbuster" drugs on the market.

An invaluable tool which facilitates the incorporation of these heterocyclic rings into more complex organic scaffoldings is deprotonative metallation, by transforming a non-polar C-H bond into a much more reactive M-C bond.[91, 92] Usually the reagents of choice to perform these reactions are polar organolithium complexes, however their application in synthesis can be restricted due to their limited selectivity, poor functional group tolerance and the need for cryogenic conditions (-78°C).[95] As mentioned in the introduction of this report *AMMM* has enabled the activation of low polarity metals Mg, Zn, Al and Mn to perform direct deprotonations, thus alkali-metal magnesiates have proven to be efficient reagents to selectively promote direct Mg-H exchange reactions of substituted aromatic molecules such as anisole and benzamides,[76] as well as molecules with high pK_a numbers such as benzene,[73] under relatively mild conditions (25°C). Building on these studies we decided to probe the metallating ability of our newly generated sodium magnesiates **2** and **10** towards several heterocycles.

3.1.2 Metallation of Thiophene

We commenced our studies by investigating the reactivities of **2** and **10** towards sulfur containing heterocycle thiophene. Thiophenes are used as potent α-glucosidase inhibitors[115] and as selective A_3 agonist and antagonists.[116] Furthermore, in chemical processes they have found applications in catalytic asymmetric epoxidation[117] and recently the adsorption and physical properties of various thiophenes on gold surfaces has come to light as a useful process.[118] Sodium magnesiate **2** was therefore added to an equivalent of thiophene and allowed to stir for two hours at room temperature. The solution remained pale yellow in colour and after a day in the freezer resulted in the formation of colourless crystals. However, ¹H NMR spectroscopic analysis of these crystals proved to be only unreacted complex **2**. Even after the solution had been refluxed for five hours thiophene remained non-metallated by the alkyl derivative **2**. Taking into account the greater kinetic basicity of Mg-N bonds versus Mg-C bonds[119] we next endeavored to try the same reaction using the amido complex [{Na(THF)$_6$}$^+${(Ph$_2$Si(NAr*)$_2$)Mg(TMP)}$^-$] **10**, bearing in mind that TMP-based magnesium reagents such as "Turbo Hauser" base TMPMgCl·LiCl have proved to be good deprotonating reagents. Therefore complex **10** was added to an equivalent of thiophene and allowed to stir for two hours at room temperature (**Scheme 3.1**). The resulting solution deposited colourless crystals of [{Na(THF)$_6$}$^+${(Ph$_2$Si(NAr*)$_2$)Mg(C$_4$H$_3$S)(THF)}$^-$] **13** in a 45% isolated yield, although analysis of the filtrate by ¹H NMR spectroscopy demonstrated the reaction to be nearly quantitative.
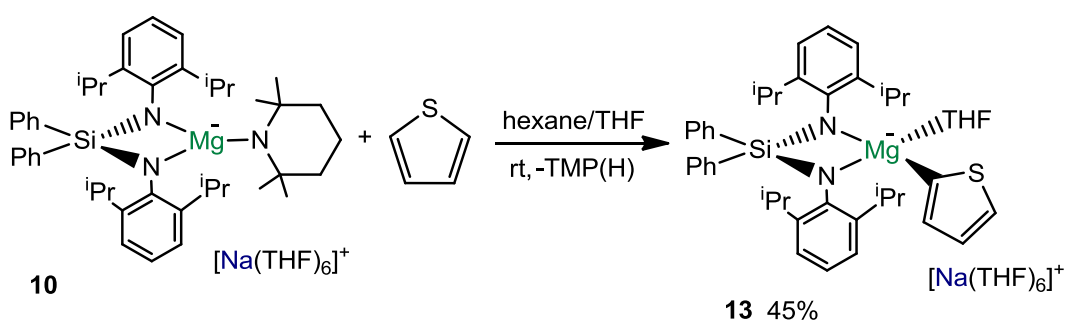
Scheme 3.1: Preparation of [{Na(THF)$_6$}$^+${Ph$_2$Si(NAr*)$_2$Mg(C$_4$H$_3$S)(THF)}$^-$] **13**.

The molecular structure of **13** was established by X-ray crystallographic studies. Displaying a similar solvent separated structural motif to that of its precursor **10**, the Mg centre present in the anionic fragment of **13** exhibits a tetrahedral geometry bonded to the bis(amido) ligand $\{Ph_2Si(NAr^*)_2\}^{2-}$, a solvating molecule of THF and α-deprotonated molecule of thiophene (the α-position being the most acidic $pK_a = 33$, DMSO). Unfortunately, the crystals were of low grade and no refinement could be carried out, preventing any meaningful discussion of its geometrical parameters. Notwithstanding the connectivity is certain, demonstrating that the deprotonation of thiophene by **10** is a genuine example of *AMMMg* (**Figure 3.2**).
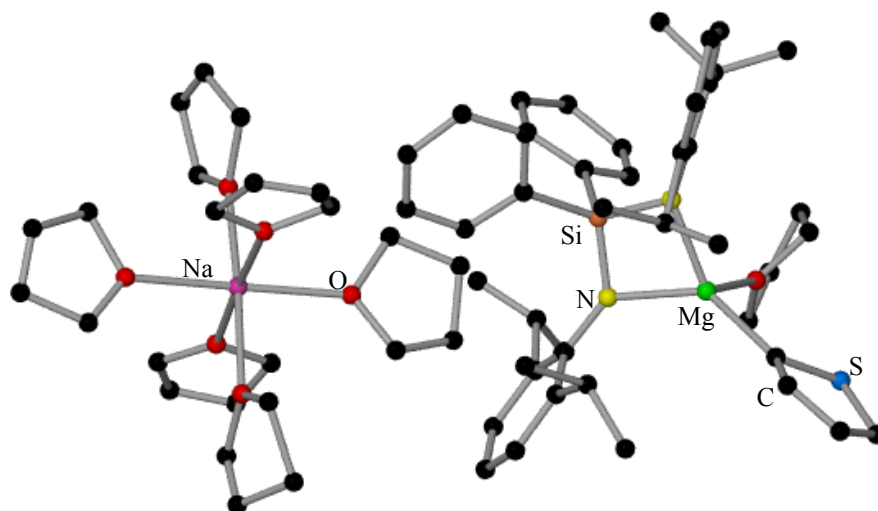
Figure 3.2: Molecular structure present in **13**. Hydrogen atoms have been omitted for clarity.

The α-metallation of thiophene has been known since 1949, and has since been extensively studied.[93] However, most of the metallations are confirmed only indirectly via electrophilic quenching studies and reactions have to be performed at low temperatures. A search in the CSD found only three examples of *α*-magnesiated thiophene structures; $[Mg(C_4H_3S)(THF)_4]$ prepared by Hakansson *et al* by the reaction of Mg turnings with 2-bromothiophene in THF solution, and also reported by the same group $[(C_4H_3S)MgBr(DME)_2]$ synthesised in a similar fashion now using DME as a solvent.[102] More pertinent to our studies however is $[(TMEDA)Na(\mu-C_4H_3S)_3Mg(TMEDA)]$[81] (**Figure 3.3**) prepared by O'Hara *et al* by reacting sodium magnesiate $[(TMEDA)Na(\mu-CH_2SiMe_3)(\mu-TMP)Mg(TMP)]$ with an

equivalent of thiophene. This surprising metallation of not one but three thiophene molecules could also be prepared rationally by reacting three equivalents of thiophene, thus increasing the yield from 26 to 53%. Unlike the solvent separated complex **13**, [(TMEDA)Na(μ-C$_4$H$_3$S)$_3$Mg(TMEDA)][81] is a contacted ion pair structure where Mg σ-bonds to the α-C of thiophene and Na coordinates in π manner to thiophene.
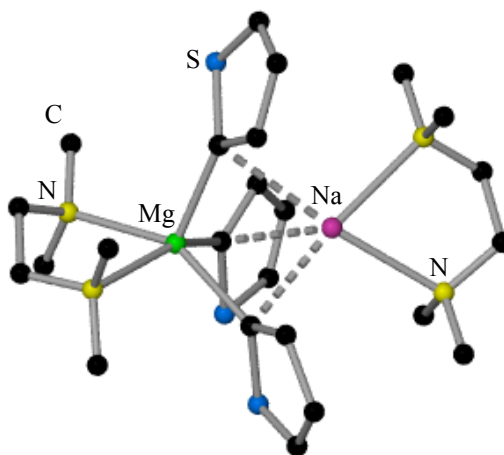
Figure 3.3: Molecular structure of [(TMEDA)Na(μ-C$_4$H$_3$S)$_3$Mg(TMEDA)].[81]

Mongin *et al* have also reported the magnesiation of thiophene at the α-position using lithium magnesiate Bu$_3$MgLi in THF at room temperature, before carrying out quenching reactions using various electrophiles in yields from 48-77%, however no structural information on the constitution of the metallated intermediates has been reported.[103] In addition, Kondo and Sakamoto have shown that the Hauser base ^{i}Pr$_2$MgCl can magnesiate thiophene at the α-position in THF as solvent at room temperature and subsequently carry out the quenching reaction with electrophiles such as I$_2$ in yields of 52-93%, however again no structural information on the metallated intermediates is provided.[99]

Complex **13** displays excellent solubility in C$_6$D$_6$ which allowed its characterisation using ^{1}H and ^{13}C NMR in solutions of this solvent. Regarding the ^{1}H NMR (**Figure 3.4**), signals belonging to the bis(amido) ligand were observed at 4.00 and 1.09 ppm for the C*H* and C*H*$_3$ groups of the ^{i}Pr substituent respectively. However, more importantly is that the signals belonging to TMP in **10** have now disappeared and
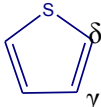
have been replaced by three multiplets at 7.60, 7.57 and 7.29 ppm representing the β, δ and γ protons respectively of a metallated thiophene (α-position being the C which has undergone magnesiation).
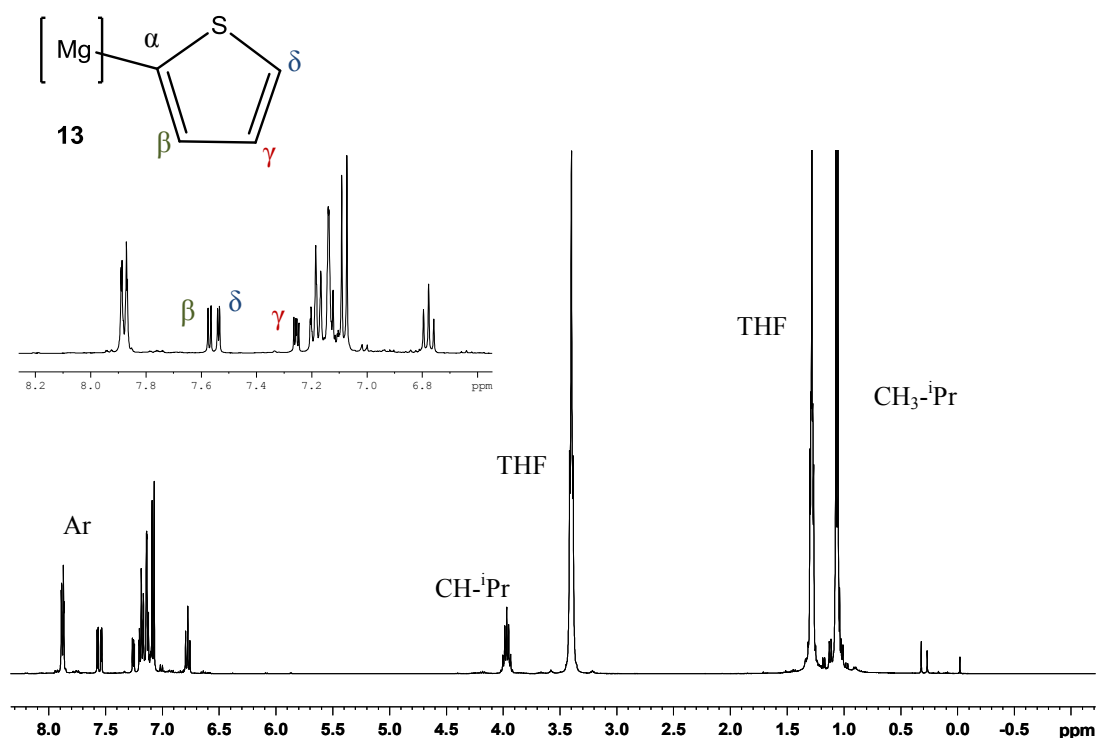
Figure 3.4: ^{1}H NMR spectra of **13** in C_6D_6.

In free thiophene, only two doublets are observed at 6.96 and 7.20 ppm representing the α and β hydrogens which are significantly more shielded than in complex **13**. In comparison to the sodium magnesiate [(TMEDA)Na(μ-C$_4$H$_3$S)$_3$Mg(TMEDA)][81] which displayed three sets of signals for the three different magnesiated thiophenes, complex **13** chemical shifts for the β, δ and γ protons of a metallated thiophene are marginally more upfield (see **Table 3.1** for comparison). In the ^{13}C NMR the resonance for the magnesiated C is displayed at 161.60 ppm whereas those for β, δ and γ carbons appear at 135.94, 135.35 and 130.81 ppm respectively. These shifts also compare well to those reported for [(TMEDA)Na(μ-C$_4$H$_3$S)$_3$Mg(TMEDA)][81] and are remarkably downfield than the resonances for free thiophene at 127.30 and 125.63 ppm.

Sample	δ^1H			$\delta^{13}C$			
	δ	γ	β	δ	γ	β	αC-Mg
[{Na(THF)$_6$}$^+${(Ph$_2$Si(NAr*)$_2$)Mg(C$_4$H$_3$S)(THF)}$^-$]	7.5	7.2	7.6	135.3	130.8	135.4	161.6
[(TMEDA)Na(μ-C$_4$H$_3$S)$_3$Mg(TMEDA)]	7.5	7.5	8.0	136.6	128.5	167.4	196.1
	7.5	7.8	7.9	136.6	128.0	130.9	169.1
	7.4	7.7	7.7	136.6	127.9	130.9	167.4
	7.2	6.9		125.6	127.3		

Table 3.1: Selected chemical shifts from ^{1}H and ^{13}C NMR spectra of **13**, [(TMEDA)Na(μ-C$_4$H$_3$S)$_3$Mg(TMEDA)] and thiophene in C$_6$D$_6$ solutions.

3.2.1 Reactivity studies of 1,3-benzoazoles

To expand our studies on the metallating power of our mixed-metal reagents we next moved onto investigate the reactivity with 1, 3-azoles. Five-membered ring aromatic heterocycles, in particular 1, 3-benzoazoles are common in many natural products, pharmaceuticals and biologically active molecules.[114] As was mentioned in section **3.1.1** an invaluable synthetic tool which facilitates the incorporation of these heterocyclic rings into more complex organic scaffoldings is deprotonative metallation.[120] However the chemoselective metallation of 1,3-benzoazoles is not so straightforward as the competitive ring opening reaction to form the acyclic complex can also occur. Boche *et al* have shown that in the reaction of benzoxazole (Boz) in which the C2 position has a pK_a = 24.8 in DMSO,[121] with organolithium reagents the equilibrium favours the formation of the ring opened complex (**II**). In extension to there studies they have shown that benzothiazole (Btz) which has a less acidic C2 position (pK_a = 27, DMSO),[121] has a lower tendency to undergo ring opening when reacted with an organolithium reagent, likewise methylbenzimidazole (MeBIm) which has the least acidic C2 position (C2, pK_a = 32.5, DMSO),[121] the equilibrium lies midway between the ring remaining closed (**I**) and open (**II**) (**Scheme 3.2**).[122]

X= O (**Boz**), S (**Btz**), NMe (**MeBIm**)
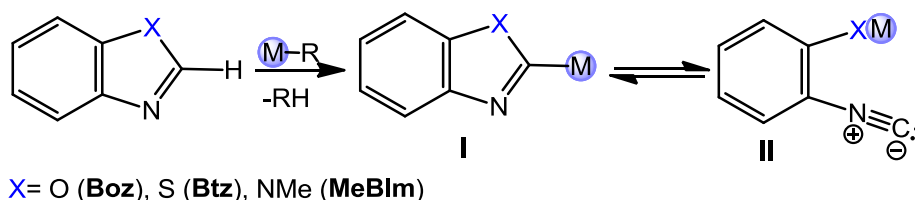
Scheme 3.2: Equilibrium between ring opening to form isonitrile tautomer and ring remaining closed of benzoazoles when metallated using organometallic reagents.

3.2.2 Methylbenzimidazole metallation

Complex **2** was therefore reacted with an equivalent of methylbenzimidazole (MeBIm) in THF at room temperature and allowed to stir for two hours. A pale green solution formed which produced yellow/green crystals of complex $[\{Na(THF)_5\}_2^+\{(Ph_2Si(NAr^*)_2)Mg(MeBIm^*)\}_2^-]$ **14** after two days in the freezer in a 70% yield (**Scheme 3.3**). Contrasting with our previous study, now alkyl base **2** can perform the deprotonation of MeBIm due to the increased activation of the α-H in MeBIm ($pK_a = 32.5$, DMSO) than in thiophene ($pK_a = 33$, DMSO). Amido magnesiate **10** can also perform the selective magnesiation of MeBIm to yield **14** with the yield only increasing marginally to 72%.
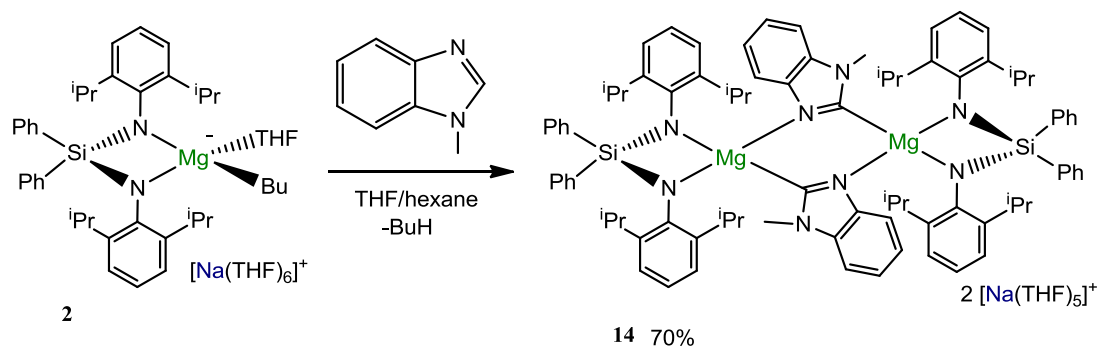
Scheme 3.3: Synthesis of new sodium magnesiate, where MeBIm has been magnesiated at the C2 position $[\{Na(THF)_5\}_2^+\{(Ph_2Si(NAr^*)_2)Mg(MeBIm^*)\}_2^-]$ **14**.

Complex **14** was subject to X-ray crystallographic analysis which evidenced that magnesiation at the C2 position of the heterocycle had taken place giving rise to a solvent separated ion pair complex containing two Na cations each of them solvated by five molecules of THF and a novel dimeric dianion

[{(Ph$_2$Si(NAr*)$_2$)Mg(MeBIm*)}$_2$$^-$] (**Figure 3.5**). The centrosymmetric dinuclear, dianionic Mg anion [{(Ph$_2$Si(NAr*)$_2$)Mg(MeBIm*)}$_2$]$^{2-}$ comprises two Mg centres which are connected by two molecules of MeBIm which have been selectively deprotonated at the C2 position. The dimer results from Mg coordinating to the C2 position of a metallated MeBIm molecule, and also coordinating to the N through its lone pair, to a second molecule of MeBIm. Each magnesium centre is in a distorted tetrahedral environment (angles range from 76.74(4)º to 124.85(9)º; mean = 109.5º). Complex **14** contains two almost planar four membered rings {NSiNMg} (Σ of internal angles = 359.98º), and a central six membered ring. The outer two four membered rings {MgNSiN} are formed by the bis(amido)silyl ligand chelating to Mg, and adopt a perpendicular position to the central six membered ring {MgNCMgNC} formed from the Mg coordinating to both the deprotonated C2 position and the N of a second metallated MeBIm. The Mg-N3 bond length of the bis(amido)silyl ligand (Mg-N3 2.028 Å) is within the same range as those found in complex **2** (Mg-N1 2.050(3) and Mg-N2 2.081(3) Å), however the Mg-N4 bond length of the bis(amido)silyl ligand (Mg-N4 2.160(2) Å) is slightly more elongated which could be attributed to the steric constraints imposed by the dimeric structure of **14**.
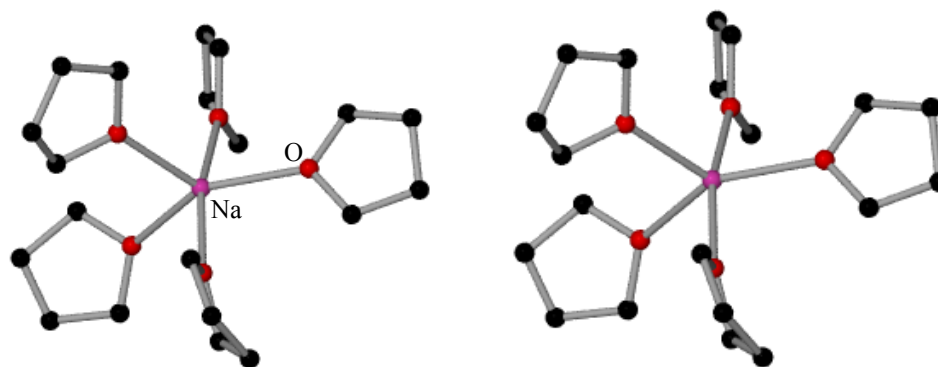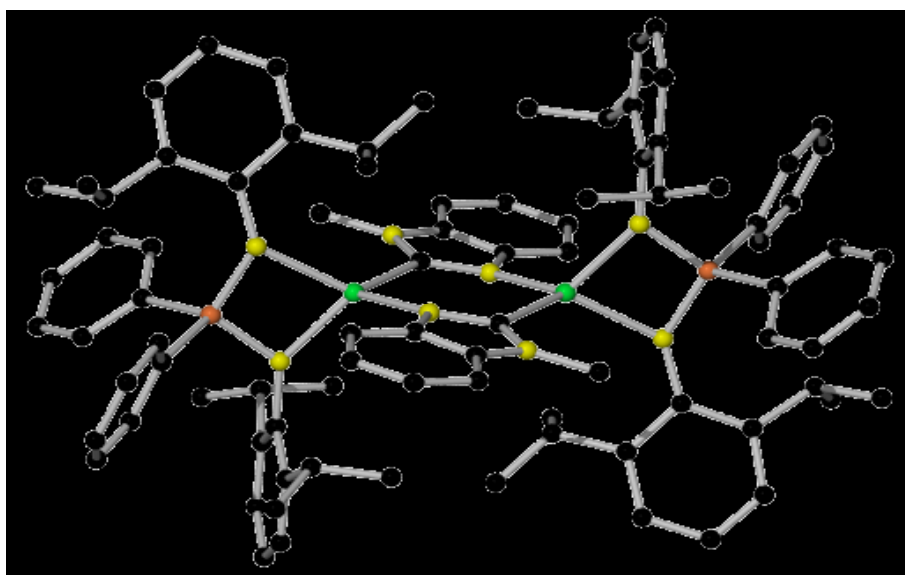
Figure 3.5: Molecular structure of **14**. Hydrogen atoms and disorder in THF molecules have been omitted for clarity. Selected bond lengths (Å) and bond angles (º):*Mg-N1 2.091(2), Mg-C 2.233(3), Mg-N3 2.028(2), Mg-N4 2.160(2), C1-Mg 2.233(3), C1-N1 1.362(3), C1-N2 1.380(3), N3-Mg-N4 76.74(4), N3-Mg-N1 118.00(9), N1-Mg-C 102.91(10), C-Mg-N4 124.85(9), N3-Mg-C 116.18(10), N4-Mg-N1 118.32(9), Si-N4-Mg 89.54(9), N4-Mg-N3 76.74(9), Mg-N3-Si 94.54(10), N3-Si-N4 99.16(11), Mg-C1-N2 123.14(18), Mg-C1-N1 129.24(19), N1-C1-N2 106.9(2)*.

It has been previously reported by Boche *et al* that when imidazoles are metallated at the C2 position by organolithium reagents they can be considered to be Li-imidazole-2-ylidene complexes which display carbene character at the C2 position.[123]
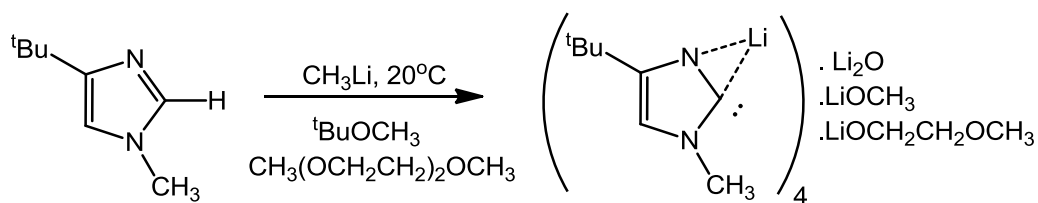
Scheme 3.4: Reaction of *tert*-butyl imidazole with organolithium reagents to form Li-imidazole-2-ylidene complex.

An extensive study by Boche using the bond lengths, angles and ^{13}C NMR data of 1-methyl-4-*tert*-butylimidazole which had been lithiated at the C2 position, whilst also coordinating to the N of the imidazole proved the imidazole to be acting as a carbene, when data was compared to the N-heterocyclic carbene [C{N(Ad)CH}$_2$] (where Ad = adamantyl) prepared by Arduengo *et al.*[38] Similarly in complex **14** the deprotonated MeBIm molecules are acting as bridges between the two Mg atoms. Their coordination can be described by considering two different scenarios (**Figure 3.6**), through the lone pair on the pyridine type N of MeBIm (A) or alternatively through the metallated carbon (B), where now as Boche *et al* had previously shown when lithiating imidazoles, MeBIm could now be acting as a N-metallocarbene. If situation (A) is taking place it would be expected to observe one of the C-N bond distance in the deprotonated MeBIm would be noticeably shorter than the other (C=N versus C-N(Me) single bond), and also the Mg-N1 bond distance should be similar to those found in other Mg-complexes where N is acting as a sigma donor such as pyridine. Alternatively if scenario (B) is occurring a N-metallocarbene would be formed, now both C-N distances within the heterocycles would be expected to be similar and the Mg-N1 distance should be comparable with those for Mg-N$_{amide}$ bonds. Furthermore, if a N-metallocarbene (situation B) is occurring the Mg-C distance in **14** should compare well to other reported N-heterocyclic magnesium compounds found in the literature.
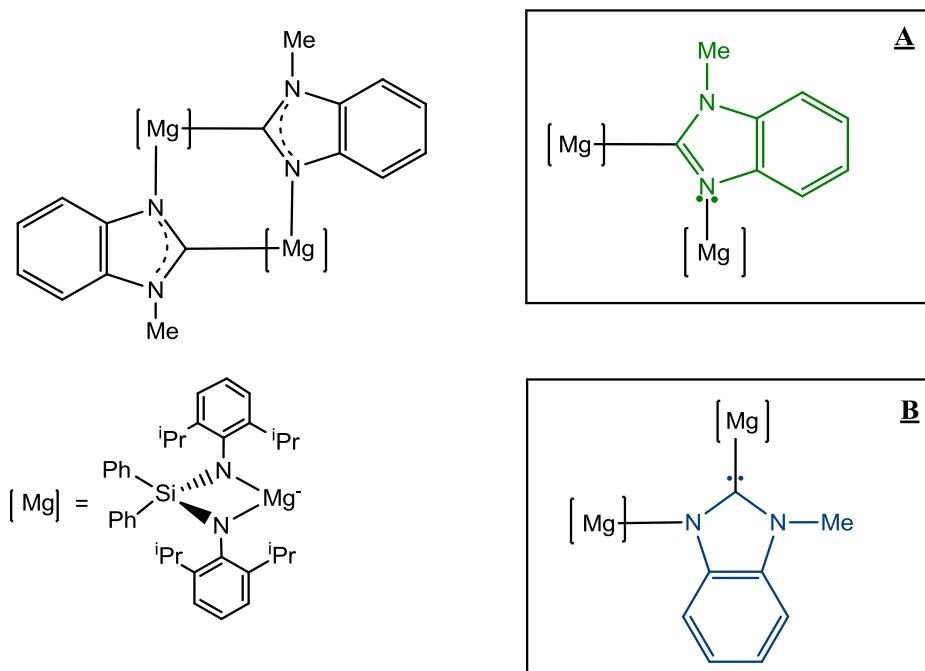
Figure 3.6: Different bonding modes available for **14**.

Taking these variables into consideration, a detailed analysis of the bond lengths within complex **14** was carried out. The N-C bond distances (N1-C, 1.362(3) and N2-C, 1.380(3) Å) are similar in value to each other and compare well to the C-N bond lengths exhibited in the first structurally prepared NHC carbene by Arduengo [C{N(Ad)CH}$_2$] (where Ad = adamantyl) (N-C = 1.373 and N-C = 1.367 Å).[38]

Regarding the Mg-C distance in **14**, a search in the CSD showed that there are currently no other compounds structurally defined containing benzimidazole rings metallated by Mg, however Mulvey *et al* have metallated related N-heterocyclic molecule N-methylindole at the C2 position (**Figure 3.7**), using the sodium magnesiate [(TMEDA)$_2$Na$_2$MgBu$_4$], the Mg-C distance in this compound is (2.216 Å)[124] is in a similar region to the Mg-C distance of complex **14** (Mg-C1 2.233(3) Å).
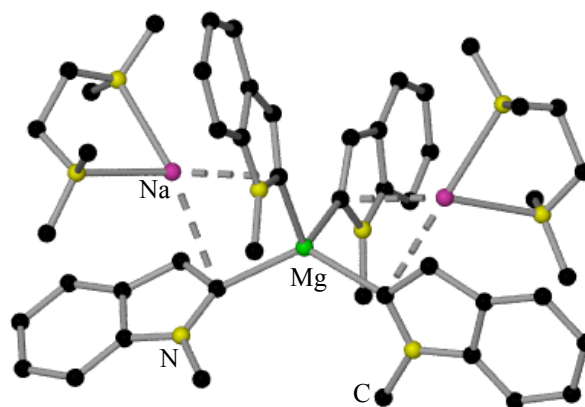
Figure 3.7: Molecular structure of magnesiated N-methylindole.

Furthermore, the Mg-C distance in **14** compares well with other reported N-heterocyclic magnesium compounds found in the literature such as Mg carbene structure [IPr·Mg(NSi(Me$_3$))$_2$] (IPr = 1,3-bis-(2,2-diisopropylphenyl)imidazol-2-ylidene) (**Scheme 1.11**), prepared by Hill *et al* (Mg-C = 2.276(2) Å).[44] The Mg-N1 distance (2.091(2) Å) is significantly shorter than other complexes in the literature where N is acting as a donor such as [Mg{(N^{i}Pr)(SiMe$_3$)}$_2$(DMAP)$_2$] (Mg-N = 2.153(5) Å),[125] and compares much more closely to complexes where N is acting as an amide such as complexes **6** and **7** (Mg-N = 2.020(16) Å **6**, 2.021(2) Å **7**). This solid state data points towards the anion present in **14** being best described as an N-metallocarbene, situation (B), just as Boche *et al* had demonstrated when 1-methyl-4-*tert*-butylimidazole was lithiated at the C2 position.[123] There is precedent already in the literature for N-metallocarbenes being formed from deprotonation of imidazole, such as that displayed by Riera and Perez *et al*, where an alkylimidazole bonded to [Re(CO)$_3$] fragment was shown to be an intermediate to the formation of a rhenium NHC complex. [126]

Complex **14** was also characterised in solution using C$_6$D$_6$ as a solvent by ^{1}H and ^{13}C NMR spectroscopy demonstrating that in solution the structure of complex **14** is retained. In the aliphatic region the indicative multiplet for the C*H* unit of the ^{i}Pr group appears at 4.46 ppm, which is slightly downfield in shift compared to the C*H* unit of the ^{i}Pr group in complex **2** (3.98 ppm). In addition the methyl group of the metallated MeBIm gives rise to a singlet at 3.40 ppm significantly deshielded than

that observed in free methylbenzimidazole at 2.52 ppm. Furthermore the C2-*H* which appears at 8.05 ppm in free methylbenzimidazole is now no longer present in complex **14**. This is in contrast to work carried out by Boche using organolithium reagents to metallate methylbenzimidazole, where he found that in solution there is an equilibrium between the imidazole being ring opened and ring closed.[123]

Regarding the ^{13}C NMR the most indicative resonance that MeBIm has been metallated at the C2 position is the quarternary C at 194.00 ppm, which has moved drastically downfield in shift from that of the C2 position of MeBIm at 142.78 ppm. This high chemical shift also shows a good correlation with chemical shifts reported for the carbenic carbon of several N-heterocyclic carbenes in the literature which are coordinated to Mg such as ^{n}BuMg(HMDS)·IPr prepared by Mulvey *et al* (187 ppm),[127] suggesting that complex **14** is best described as an N-metallocarbene (situation B as described above **Figure 3.6**). For comparison it must be noted that for indole metallated complex mentioned above (**Figure 3.7**), resulting from magnesiation of N-methylindole, the metallated C in this species appears at 181.11 ppm in the ^{13}C NMR spectra.[124] Although NMR data also suggests that the *α*-C in **14** exhibits a carbenic character it must be also considered that the difference in chemical shifts of Mg-C resonance in **14** and the metallated N-methylindole derivative can be due to the effect of an additional N atom adjacent to this C in the case of **14**.

In order to get a better constitution of **14** we performed a theoretical study using Density Functional Theory calculations. These were performed using the Gaussian computational package G03.[128] In this series of calculations the B3LYP[129] density functionals and the 6-311G** basis set[130] were used. After each geometry optimisation, a frequency analysis was performed. The energy values quoted include the zero point energy contribution. Complex **14** was modeled as a monomer with MeBIm acting as a Mg-benzimidazolyl (A) and an N-metallocarbene (B) and found that as monomers the formation of N-metallocarbene (B) is 1.51 kcal mol^{-1} more energetically favoured than scenario (A).
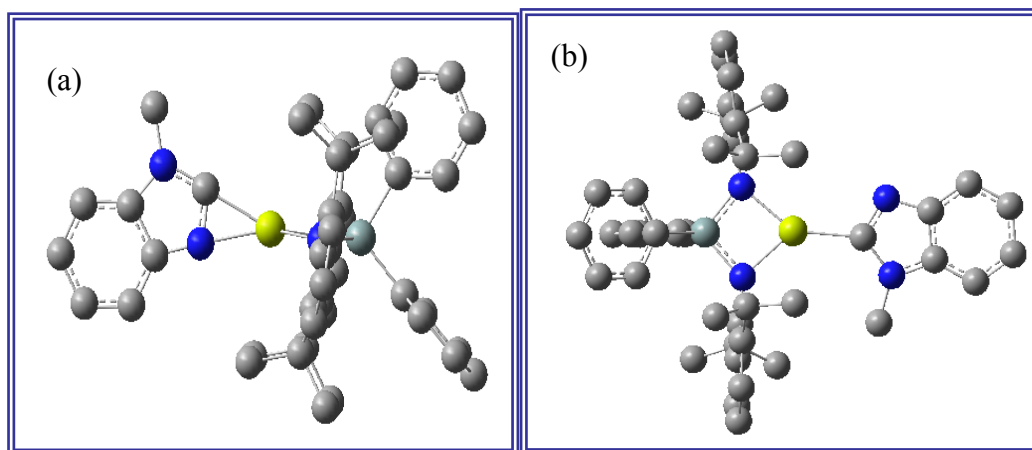
Figure 3.8: (a) MeBIm acting as a N-metallocarbene, (b) Mg-benzimidazolyl.

Table 3.2 compares the bond lengths predicted for scenario (A), the N-metallocarbene scenario (B) when modeled as a monomer and the actual bond lengths in complex **14** and as can be seen the predicted lengths for scenario (B) compare most closely to the actual lengths in complex **14**.

Bond	**14** Length (Å)	Calculated length if situation (A) (Å)	Calculated length if situation (B) (Å)
N1-C1	1.362(3)	1.336	1.356
N1-Mg	2.091(2)		2.103
C1-Mg	2.233(3)	2.129	2.161

Table 3.2: Comparison of calculated and actual bond lengths of complex **14** and modeled bond lengths when complex is a monomer for both Mg-benzimidazolyl (A) and N-metallocarbene (B).

The reaction of complex **2** with MeBIm to form a dimer was modeled by placing a Na cation 15 Å away from the anions using Mg as the origin, the resulting point energies were used to give a rough guide to the dimerisation reaction and found the reaction to have favoured exothermic energy of -71.41 kcal mol^{-1}. The structures of

the dimer modeled as a N-metallocarbene and Mg-benzimidazolyl are shown in **Figure 3.9**.
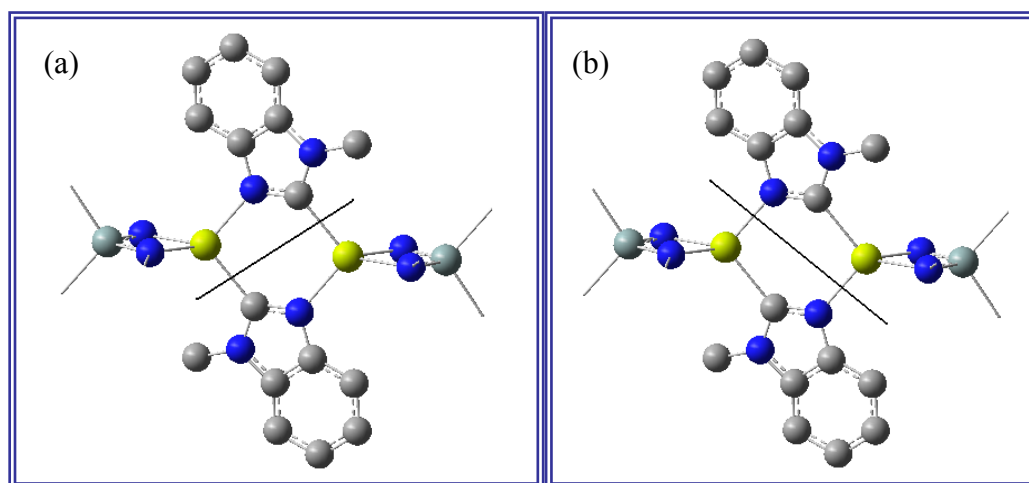
Figure 3.9: (a) MeBIm acting as a N-metallocarbene, (b) Mg-benzimidazolyl.

DFT calculations support solid-state and spectroscopic studies which suggest that the metallated MeBIm molecule displays a carbene character.

If situation (B) is occurring and complex **14** was acting as an N-metallocarbene then we predicted that it would prefer to be coordinated to a more Lewis acidic metal. Therefore, we carried out the reaction of an equivalent of **14** with the more Lewis acidic complex $ZnEt_2$ in a THF solution and allowed the reaction to stir for one hour. A colour change was observed from yellow to pale pink, unfortunately no solid material ever formed and analysis of the filtrate by ^{1}H NMR only provided broad signals which could not be assigned.

3.3.1 Magnesium-mediated benzothiazole activation

In general, the C2-deprotonation of thiazoles has been effectively carried out by magnesium based reagents such as Hauser bases[131] and "Turbo Grignard" reagents[132] which have then been intercepted with electrophiles in high yields. This methodology has also been used in large scale reactions, as shown by the 10 kg scale synthesis of arginylbenzo[d]thiazole (an intermediate to the trytapse inhibitor RWJ-56423) for which deprotonation of benzothiazole (Btz) by EtMgCl is a crucial step.[133] Thus, with these precedents in mind and encouraged by our successful

magnesiation of MeBIm we decided to investigate the reactivity of the sodium magnesiate **2** with Btz, therefore we reacted **2** with an equivalent of Btz at room temperature which resulted in an instantaneous colour change to a red solution, storage in the freezer over night resulted in the formation of complex **15** in a 28 % yield (**Scheme 3.5**).[134]
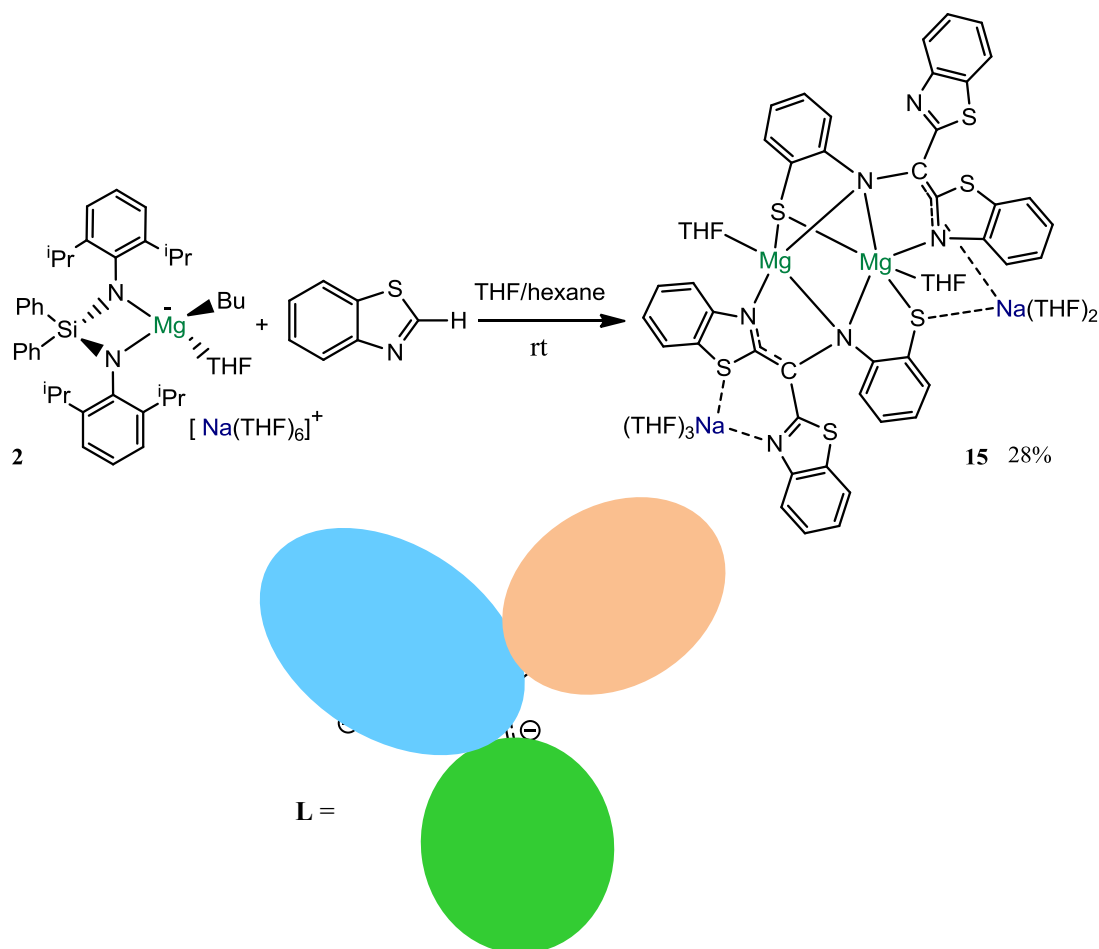
Scheme 3.5: Activation of three benzothiazole molecules to form new ligand fragment **L** in preparation of **15**.

X-ray crystallographic studies revealed the complex molecular structure of **15** (**Figure 3.10**), to feature two magnesium centres in similar chemical environments (each of them solvated by one molecule of THF) connected by the two newly generated tri-anionic fragments **L** (see **Scheme 3.5**), with two negative charges localized on a S and N atom, and a third one delocalized over the central sp^2 C and the C=N bonds of one of the neighbouring benzothiazolyl rings.
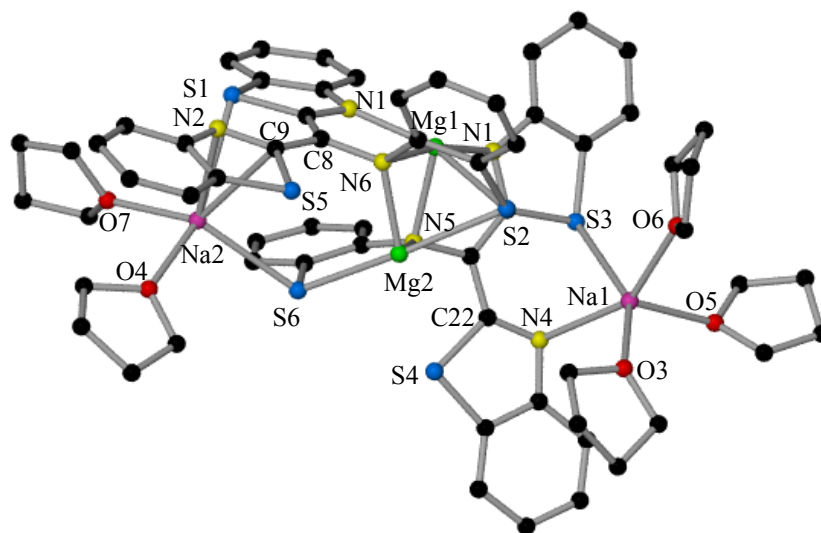
Figure 3.10: Molecular structure of **15**. Hydrogen atoms and minor disorder components on THF molecules have been omitted for clarity. Selected bond lengths (Å) and bond angles (°): *Mg1-N1 2.125(3), Mg1-N3 2.116(3), Mg1-N5 2.264(4), Mg1-N6 2.219(5), Mg1-O1 2.085(3), Mg1-S2 2.689(17), Mg2-N5 2.086(3), Mg2-N6 2.131(4), Mg2-S2 2.572(18), Mg-S6 2.459(18), Mg2-O2 2.056(3), Na1-S3 2.936(2), Na1-N4 2.453(4), Na1-O3 2.277(4), Na1-O5 2.286(4), N1-O6 2.282(4), Na2-O4 2.285(4), Na2-O7 2.266(4), Na2-N2 2.562(4), Na2-C9 2.810(4), Na2-S1 3.114(2), Na2-S6 2.724(2).*

Complex **15** is a contacted-ion pair magnesiate which is capped by two THF solvated Na atoms. The molecule is not symmetrical; Na1 is coordinated to three THF molecules and to the sulfur (S3) and nitrogen (N4) atoms of two distinct Btz rings (**Figure 3.11**). In contrast Na2 is solvated by only two THF molecules and interacts differently with the trianionic fragment **L**, by bonding to the sulfur atom (S1) of a Btz ring, by π engaging with C=N double bond of the pseudo alkyl unit of the ligand and by also interacting with the sulfur atom (S6) of one of the benzothiazolyl rings (**Figure 3.11**). Regarding coordination of the magnesium atoms, both magnesium centres exhibit an octahedral geometry but with different chemical environments. Thus, Mg1 is coordinated to an oxygen atom from a THF molecule, four nitrogen atoms (N1, N3, N5, N6) and a sulfur centre S2. Two of these four nitrogen atoms (N5, N6) and sulfur (S2) are the atoms that bear a negative charge in the trianionic ligand (**Figure 3.11**), whereas the remaining two nitrogen centers (N1 and N3) are N

atoms of the benzothiazolyl rings that are involved in the delocalization of the third negative charge (through an aza-allyl unit). Thus, the two trianionic ligand fragments **L**, by bonding to Mg1 through a combination of two different types of N (N1 and N6 for one of the ligands and N5 and N3 for the other) coordinate in chelating fashion to give rise to a five membered ring {N3C24C23N5Mg1} (**Figure 3.11**). The Mg-N bond lengths, where the N3 and N1 atoms are part of the benzothiazolyl rings that are involved in the delocalization of the negative charge through an aza-allyl unit are shorter than the Mg-N distances where N5 and N6 bear a negative charge (2.125(3), 2.116(3), 2.264(4) and 2.219(3) for N1, N3, N5 and N6 respectively). In contrast Mg2 is bonded to two oxygens (from a solvating THF molecule), two sulfur atoms (S2 and S6) and two nitrogen centres (N5 and N6), in all cases being the heteroatoms bearing a negative charge present in the benzothiazolyl ring. One trianionic ligand fragment **L** is therefore acting as a bridge between the two Mg centres which are 2.835(2) Å apart by coordinating to both Mg centres through the N5 and S2 atoms bearing a negative charge of a benzothiazolyl unit and the second trianionic fragment **L** links the two Mg centres by coordinating to both through the N6 atom. The Mg1-S2 distance (2.689(17) Å) is slightly more elongated than the Mg-S2 and Mg-S6 distance (2.572(18) and 2.459(18) Å respectively) as would be expected due to the higher coordination number of Mg1 (six) over Mg2 (five).
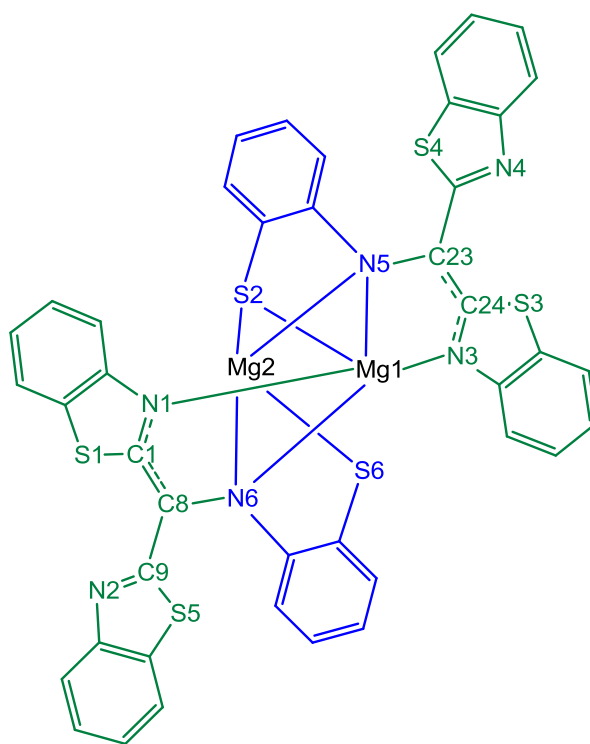
Figure 3.11: Ligand fragment formed in **15**.
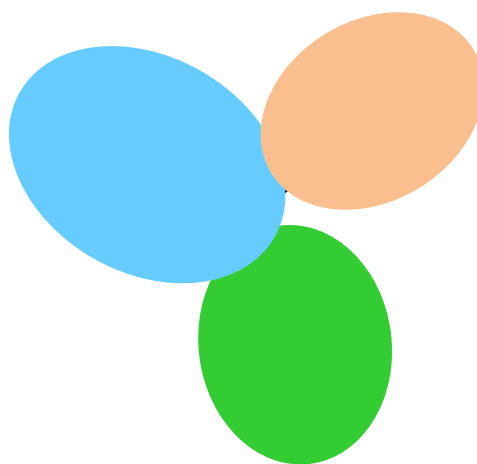
Figure 3.12: Trianionic ligand fragment **L**.

As three molecules of Btz appear to be activated to form the trianionic fragment **L** we therefore repeated the reaction with complex **2**, however this time using three equivalents of Btz and found that the yield of **15** increased substantially to 89%.

3.3.2 Proposed mechanism for benzothiazole activation: a room temperature cascade of C-H deprotonation, C-C coupling, ring opening and nucleophilic addition reaction

A closer look at the constitution of **L** shows that the activation of three Btz molecules, with one undergoing ring opening (resulting from a C-S bond cleavage) and coupling with two other benzothiazolyl units. As all three Btz molecules have been deprotonated at the C2 position this suggest that all three (two amido and one alkyl) potential basic arms of magnesiate **2** are used in forming **15**. This hypothesis was further supported by ^{1}H NMR analysis of the reaction filtrate, which confirmed the presence of bis(amine)silyl {Ph$_2$Si(NHAr*)$_2$} **1** as a major co-product. Remarkably this activation is in complete contrast to work carried out by Knochel *et al*, where Btz is magnesiated at the C2 position using (TMP)MgCl·LiCl,[132] and instead makes more parallels with work carried out by Diaconescu using d^{o}f^n metal alkyl complexes (M = Sc, Y, Lu, U) supported by 1,1'-ferrocenylene bis(amide) ligands[135] (see section **1.1.2**). Elegant mechanistic studies by Diaconescu reveal that these compounds can promote ring opening reactions of heterocycles, involving C-H activation and subsequent C-C coupling reactions, with the bis(amide) ancillary ligand playing a vital role in stabilising and trapping reaction intermediates.[135] In particular, recently she has shown that U complex [(NN^{fc})U(CH$_2$Ph)$_2$(6-Me-η^2-N,C-pyridyl)] can carry out the activation of Btz. Diaconescu proposes that Btz coordinates to uranium complex (NN^{fc})U(CH$_2$Ph)$_2$(6-Me-η^2-N,C-pyridyl) (step *i* **Scheme 3.6**), favouring a C-C coupling process to the pyridyl ligand (step *ii* **Scheme 3.6**), which brings about the dearomatisation of the Btz ring (**Scheme 3.6**), this species can then undergo a ring-opening reaction of the dearomatised heterocycle (step *iii* **Scheme 3.6**) followed by the imine functionality engaging the benzyl ligand in a migratory insertion step to yield the final product (step *iv* **Scheme 3.6**).[136] Diaconescu *et al* carry out the activation in a pentane solution at room temperature and are able to achieve moderate yields of 54%. The final product was successfully characterised by X-ray crystallographic studies; however no intermediates of the reaction were characterised.
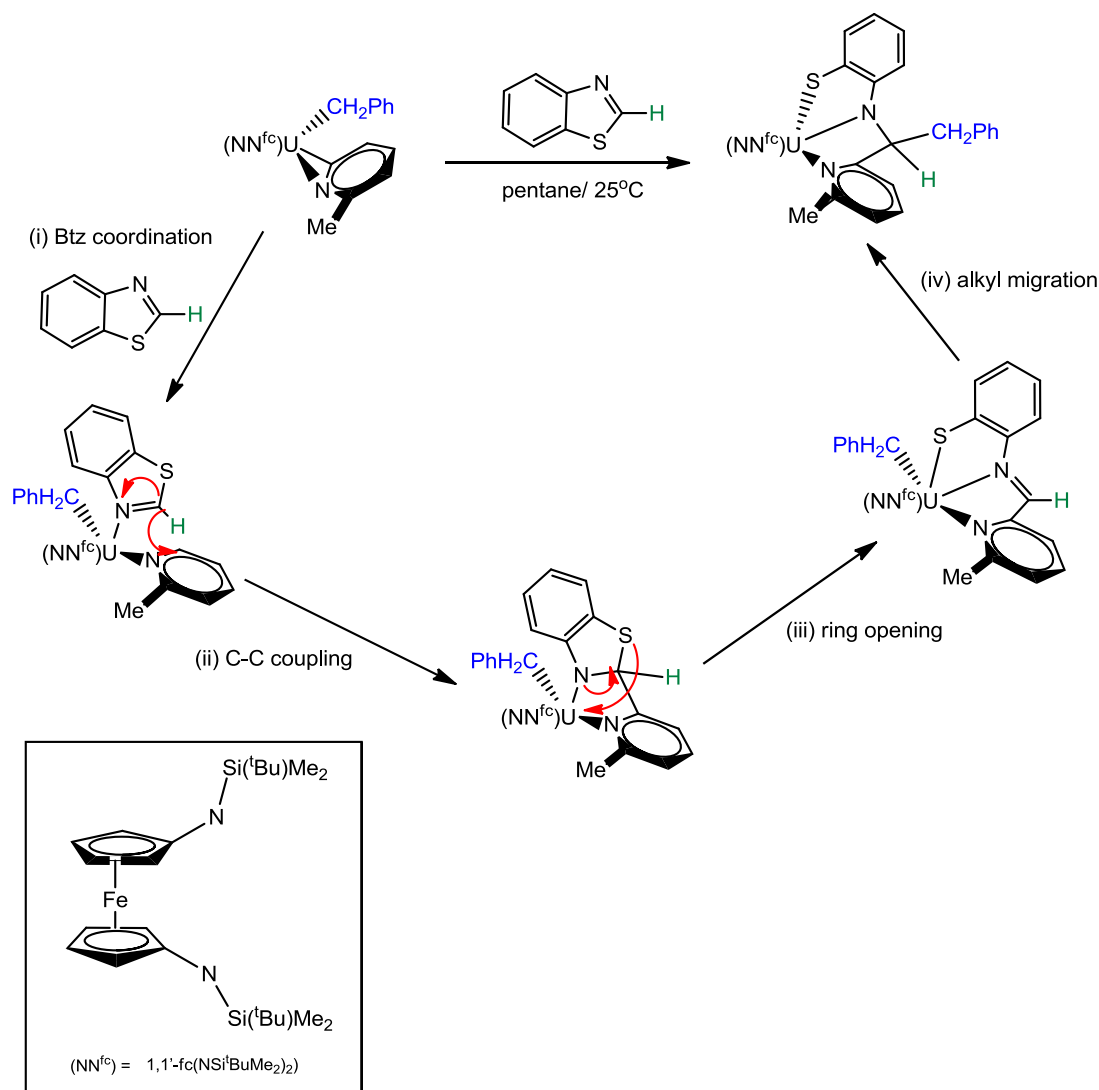
Scheme 3.6: Proposed mechanism for activation of benzothiazole by $(NN^{fc})U(CH_2Ph)_2(6\text{-}Me\text{-}\eta^2\text{-}N,C\text{-pyridyl})$.

Based on these studies and considering the similarities noted by others in certain chemistries of lanthanides and alkaline-earth metal complexes[137] a tentative mechanism to rationalise the formation of **15** can be proposed (**Scheme 3.7**). [134]
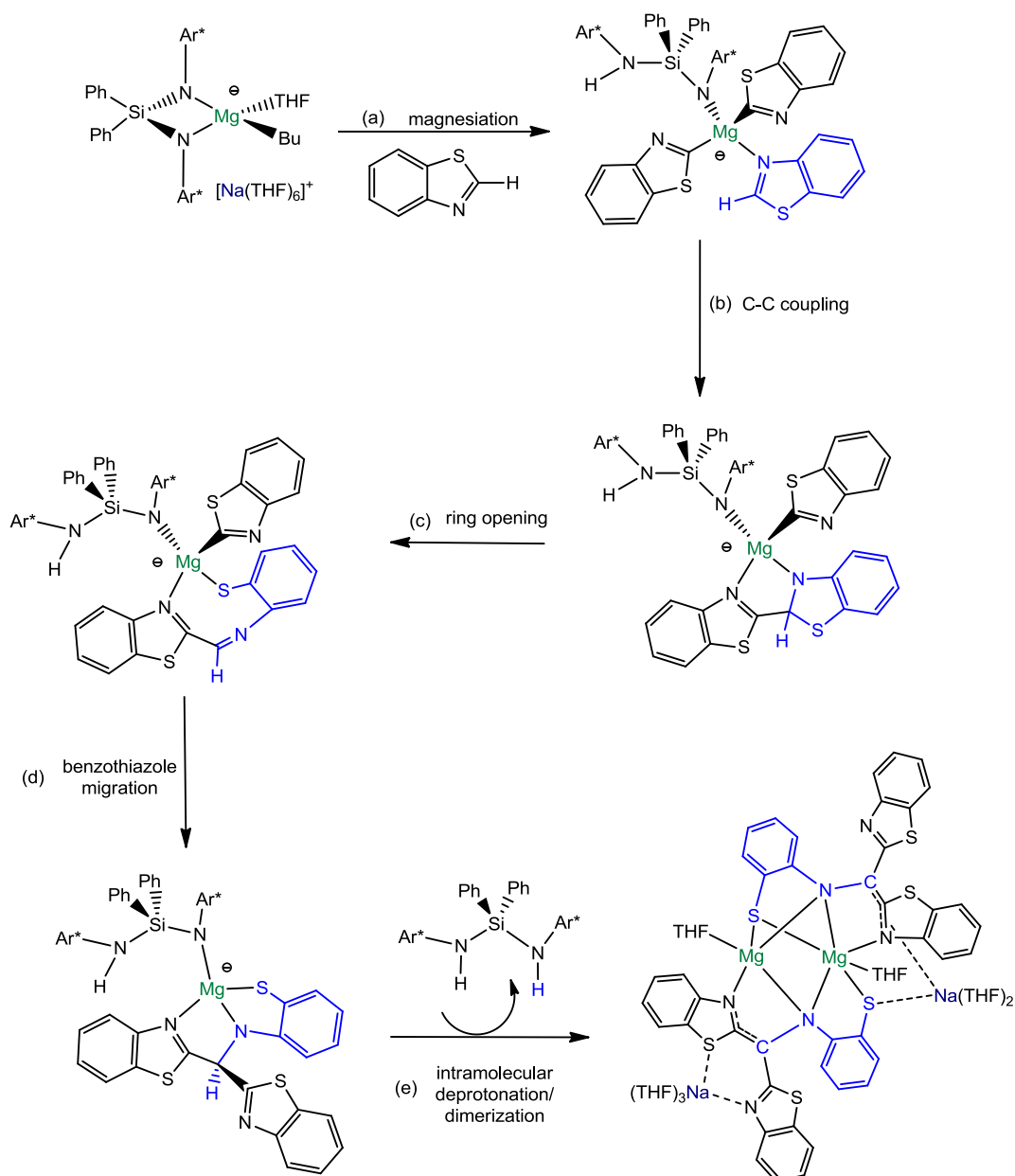
Scheme 3.7: Proposed mechanism for formation of **15**.

Thus, initially sodium magnesiate **2** mediates the deprotonation of two Btz molecules, while the third Btz may probably act as a neutral N-donor ligand to Mg (step *a*, **Scheme 3.7**). This coordination would favour the intramolecular nucleophilic attack of one benzothiazolyl unit onto the C2 position of the Btz molecule, thus bringing about dearomatisation of the latter and forming a new C-C bond (step *b*, **Scheme 3.7**). Step *a* in **Scheme 3.7** shows sodium magnesiate **2** acting as a dual alkyl/amido base, although the possibility of it acting as a bis(amido) base cannot be

ruled out. However, in this regard we found that when we reacted amido complex [{Na(THF)$_6$}$^+${(Ph$_2$Si(NAr*)$_2$)Mg(NPh$_2$)(THF)}$^-$] **7** with three equivalents of Btz, then complex **15** was not observed, instead 2,2'-dibenzothiazole could be isolated (presumably resulting from oxidation of the coupling product of a Btz molecule with a C2-magnesiated benzothiazolyl unit). These findings not only suggest that a butyl group present in **2** is crucial to promote deprotonation of the two Btz molecules shown in step *a*, but also supports the C-C coupling process proposed in step *b*. The putative intermediate formed after step *b* can then undergo ring opening of the nonaromatic ring, through C-S cleavage, to form an electrophilic C=N bond (step *c*, **Scheme 3.7**) which in turn can react with the remaining benzothiazolyl to generate a dianionic organic fragment resulting from coupling of three initial Btz molecules (step *d*, **Scheme 3.7**). Finally, this intermediate can be internally deprotonated at the remaining aliphatic sp^3 CH by the remaining basic arm of **2**, thereby generating the sodium magnesiate containing the trianionic fragment **L** (which can then dimerise to form **15**) along with the concomitant formation of bis(amine) **1** (as previously stated this was detected by ^{1}H NMR spectroscopy). Unlike the f-block imidazole activation studies, where reactions had to be thermally induced (T = 85-100°C, 2-3 days),[135] the reaction of **2** with Btz yields **15** almost instantaneously at room temperature as evidenced by ^{1}H NMR monitoring, therefore it can be considered as a genuine example of cascade chemistry. In an attempt to trap some possible reaction intermediates, the reaction was performed at 0°C (**Scheme 3.8**), producing novel sodium magnesiate **16** as an orange crystalline solid (**Figure 3.13**).[134]
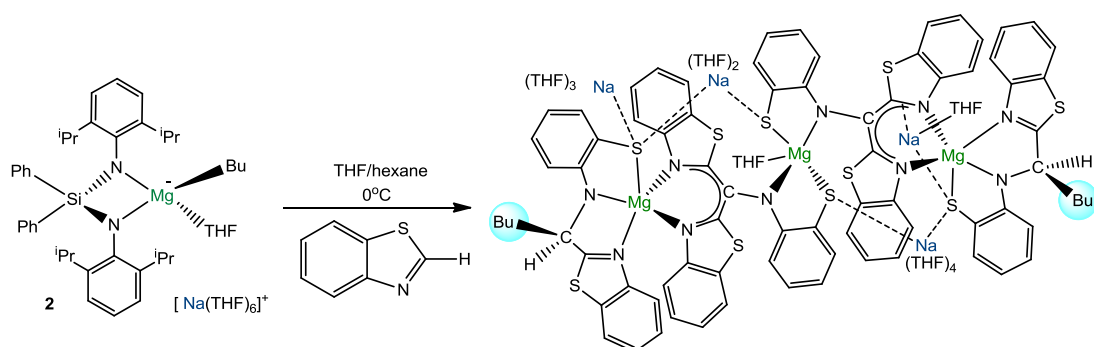
Scheme 3.8: Preparation of complex **16**.

X-ray crystallographic analysis of **16**, exhibited the molecular structure of a 4:3 Na/Mg ratio, implying it is formed through a disproportionation process. Surprisingly **16** contains two units of the same trianionic ligand fragment **L** that was present in **15**, but it coordinates in a different way. Two trianionic ligand fragments **L** now coordinate to the two terminal Mg centres through the two N atoms which are part of the benzothiazolyl rings that are involved in the delocalization of the negative charge through an aza-allyl unit, whist the third central Mg centre is chelated by the two ligand fragments **L** through the S and N atoms of the benzothiazolyl unit bearing a negative charge. The central Mg completes its coordination sphere by coordinating to a molecule of THF. Complex **16** also contains two of the newly formed dianionic ligand fragments **L*** (**Figure 3.14**), where two negative charges are localised on the S and N atoms of a benzothiazole which has undergone ring opening. Fragment **L*** has been formed by the activation of two Btz molecules which have coupled with a Bu group from the sodium magnesiate **2**. Each terminal Mg centre is coordinated to the S and N atoms bearing the negative charge on these new ligand fragments **L*** and also datively coordinates to the N atom of a distinct Btz unit in fragment **L***. There are four Na atoms present in complex **16**, compared to three Mg centres therefore as mentioned above a disproportionation process is thought to have taken place. Two of the central Na atoms are coordinated to the S atoms bearing a negative charge in both fragment **L** and **L***, one being solvated by two THF molecules and the other by four THF molecules. The two terminal Na atoms are both coordinated to the S atom bearing a negative charge in fragment **L***, one solvated by three THF molecules and the other by one THF molecule.
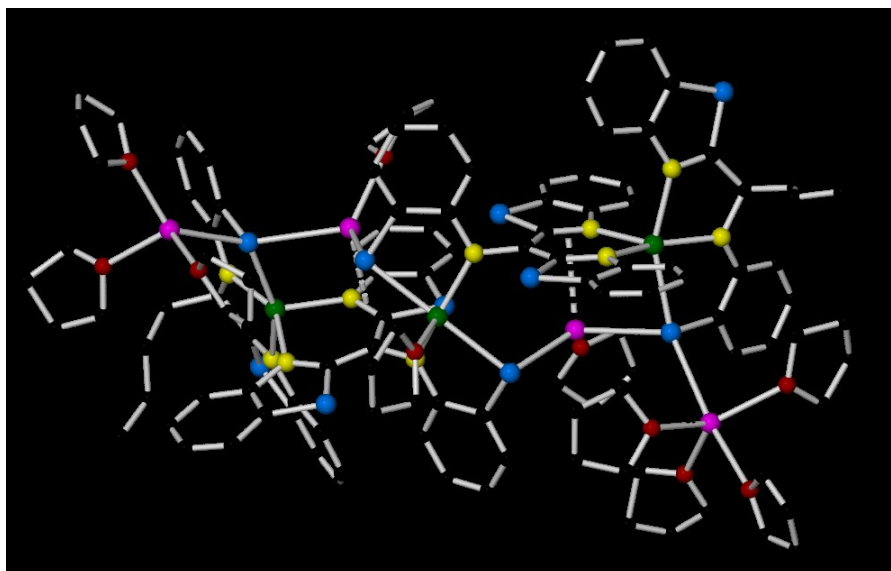
Figure 3.13: Molecular structure of **16**. Hydrogen atoms and disordered components on THF have been omitted for clarity.
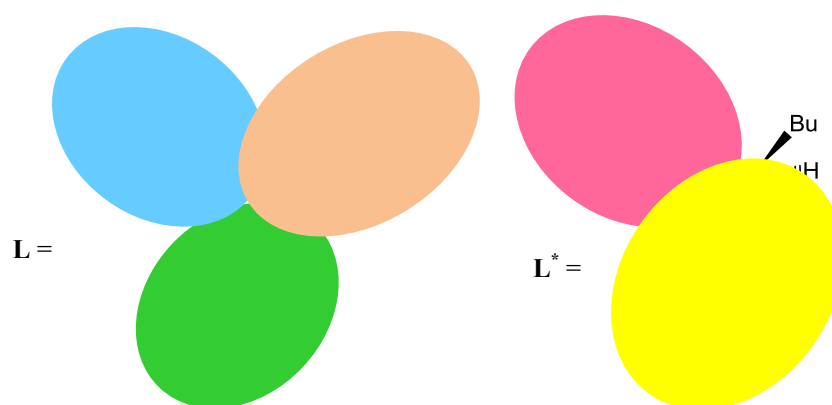
Figure 3.14: Representation of fragments **L** and **L*** resulting from the activation of Btz.

Unfortunately no geometrical parameters of complex **16** can be discussed as the structure suffered from some disorder on THF, however the connectivity is certain. Complex **16** was also analysed by ^{1}H NMR using d$_8$-THF as a solvent confirming the structure in solution, with the most indicative signals belonging to the Bu being observed at 2.12, 1.69, 1.38 and 0.94 ppm for the C*H*$_2$, C*H*$_2$, C*H*$_3$ and Mg-C*H*$_2$ respectively. These shifts are more deshielded than for the relevant shifts for the Bu group in complex **2** at 1.32, 1.04, 0.69 and -0.58 ppm.

For the formation of $\mathbf{L}^*$ only two molecules of Btz are involved. One of them is deprotonated (presumably by one of the amido arms of the $\{Ph_2SiNAr^*\}^{2-}$ ligand (**Scheme 3.9** step (*a*)) whereas the remaining Btz molecule undergoes ring-opening, retaining the H atom attached to its C2 carbon (highlighted in yellow in **Scheme 3.9**), thus implying that it is a non-deprotonated heterocyclic molecule that experiences dearomatisation with a subsequent ring-opening reaction. Furthermore, the presence of a Bu group in $\mathbf{L}^*$ suggests that deprotonation appears to be the rate determining step of this process. The formation of $\mathbf{L}^*$ can be rationalised similarly as proposed for **L (Scheme 3.7)**, where now as a result of the lower temperature, a single molecule of Btz is deprotonated (complex **2** is now acting as a mono-amido base, leaving the Bu group bonded to Mg), with a subsequent similarly fast C-C coupling (step (*b*) **Scheme 3.9**) and intramolecular ring-opening reaction (step (*c*) **Scheme 3.9**) that is then terminated by the Bu nucleophilic addition to the C=N bond (step (*d*) **Scheme 3.9**).
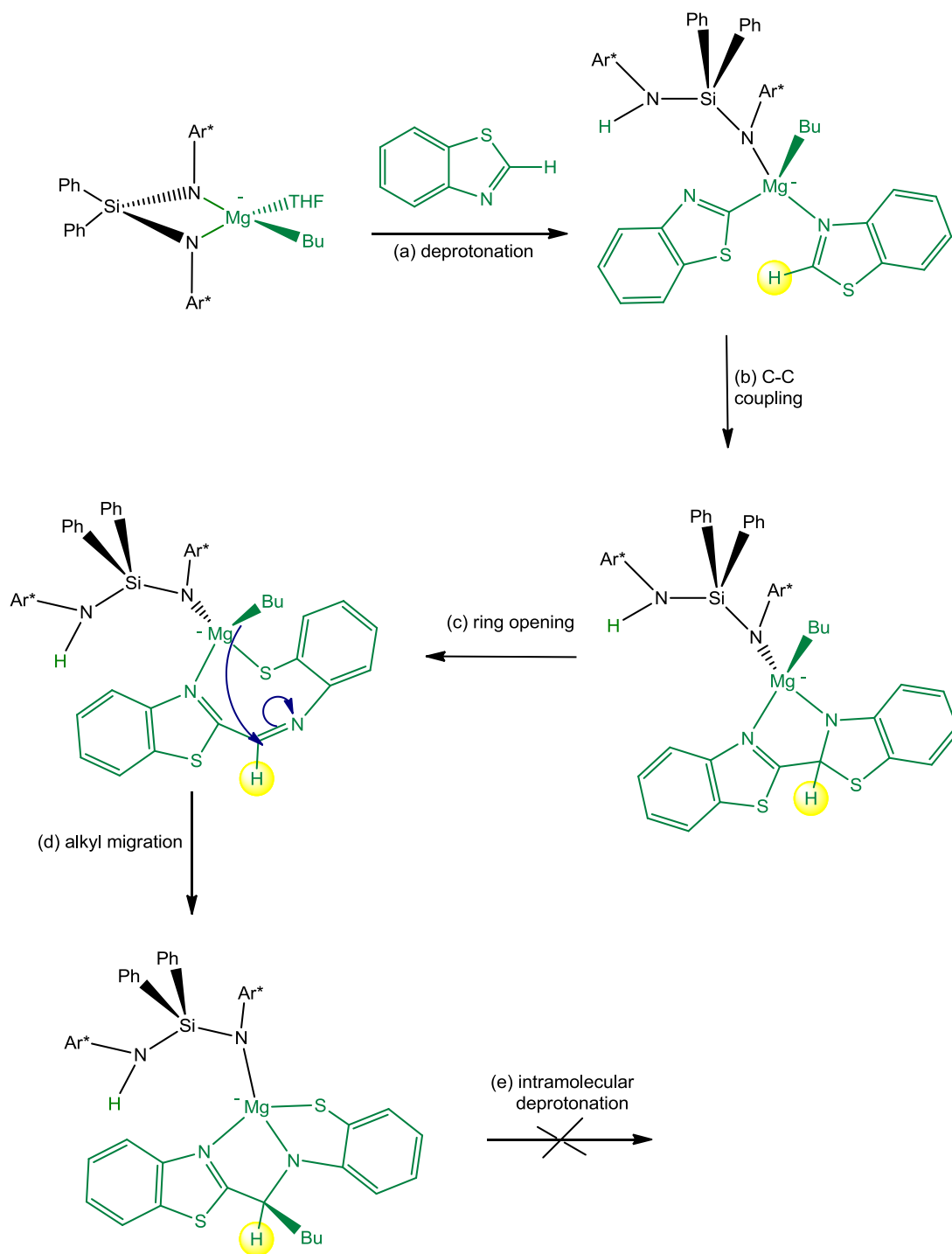
Scheme 3.9: Proposed mechanism for the formation of **L***.

In this case, the intramolecular deprotonation (step *e*, **Scheme 3.9**) does not occur, probably because it would generate a highly unstable carbanion with a negative charge localized at the *α*-position to an amido nitrogen atom.

A postulated mechanism for the formation of **16** is therefore shown in **Scheme 3.10**. The same mechanism is proposed as for the formation of ligand fragment **L** (**Scheme 3.7**), however instead of the final intramolecular deprotonation step (step *e*, **Scheme 3.7**) occurring to form ligand fragment **L**, we believe that a disproportionation reaction involving **15** and NaMg species containing **L*** takes place (step *e* **Scheme 3.10**), supporting this ^{1}H NMR analysis of the filtrate shows a complex mixture of unidentified species. This fragment then undergoes a deprotonation reaction where the proton highlighted in yellow is removed probably by the amido arm of the {Ph$_2$Si(HNAr*)(NAr*)}$^-$ ligand of the Mg complex bearing ligand fragment **L*** (step *f* **Scheme 3.10**), forming complex **16** and kicking out free bis(amine)silyl {Ph$_2$Si(NHAr*)$_2$} **1**, in addition when the filtrate was analysed by ^{1}H NMR the formation of free amine could be detected.
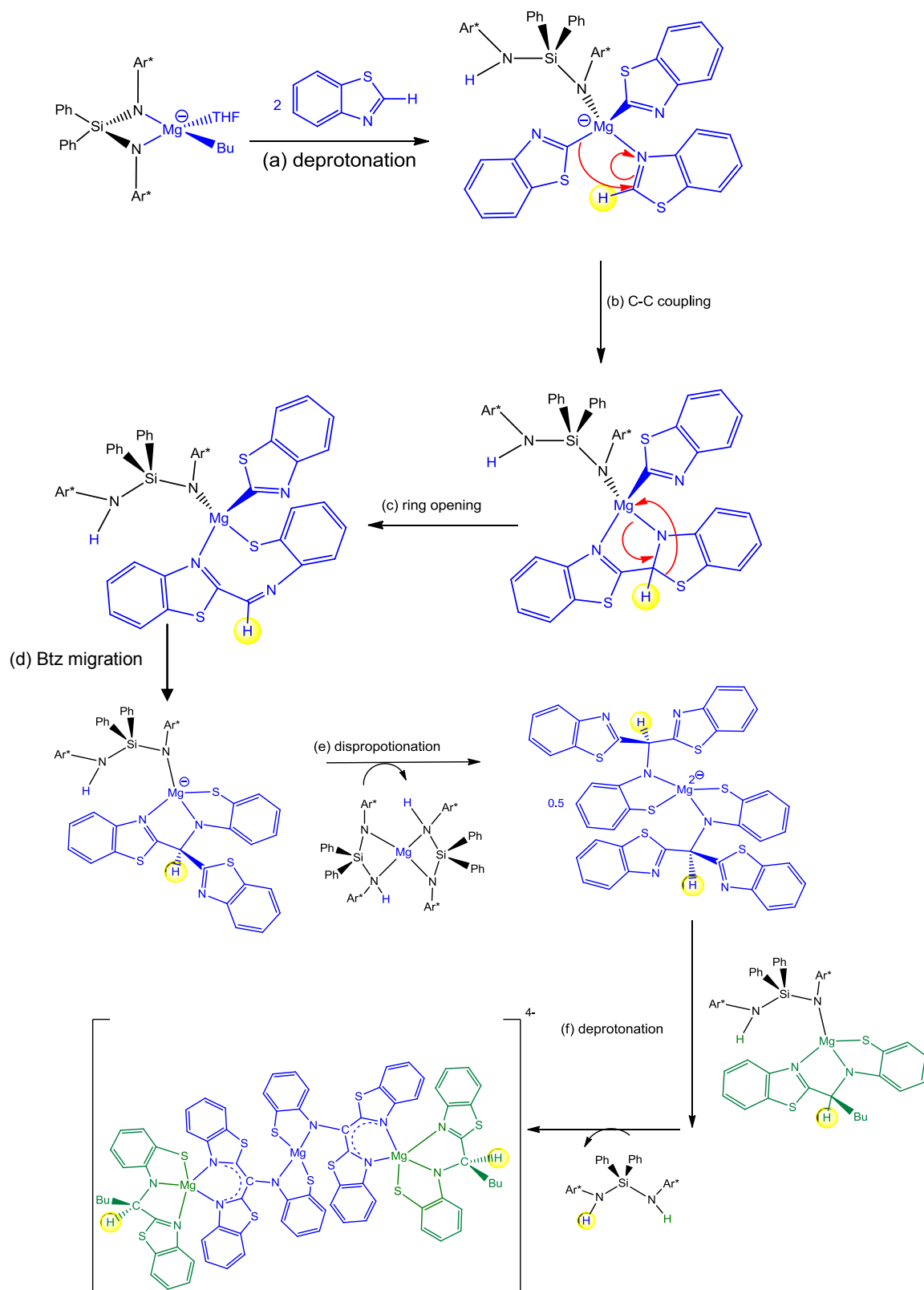
Scheme 3.10: Postulated mechanism for formation of complex **16**.

The fact that even at low temperature compounds **15** and **16** can be formed, emphasises that the formation of fragments **L** and **L**[*] are genuine examples of cascade chemistry, which once initiated are followed by unstoppable, unique sequence of fast intramolecular reactions. As mentioned earlier above this unprecedented activation of Btz using magnesiate **2** is in sharp contrast to the work carried out by Knochel *et al* where Btz can be easily metallated at the C2 position using magnesiate TMPMgCl·LiCl[132] and far more resembling of the reactivity of uranium-alkylpyridyl complex (NN[fc])U(CH$_2$Ph)$_2$(6-Me-η^2-N,C-pyridyl) towards Btz (**Scheme 3.6**) discussed previously. However, although Diaconescu discusses the important role of the ancillary ligand in stabilizing reactive intermediates, unlike our bis(amido)silyl ligand in complex **2**, it does not participate in the activation of Btz.

3.3.3 Effect of bis(amido)silyl ligand in activation of benzothiazole

In order to gain further understanding on the role played by the bulky bis(amido) ligand {Ph$_2$Si(NAr*)$_2$}$^{2-}$ in these reactions we prepared the neutral magnesium compound [(Ph$_2$Si(NAr*)$_2$)Mg(THF)$_2$] **17** by reacting equimolar amounts of bis(amine) **1** with Bu$_2$Mg in hexane as a solvent and finally adding two equivalents of THF. Compound **17** could be isolated as colourless crystals in a 41 % yield; however, NMR analysis of the filtrate revealed the reaction occurred quantitatively. Compound **17** was characterised by a combination of X-ray crystallographic studies and ^{1}H and ^{13}C multinuclear NMR spectroscopy (see Experimental Section for details).
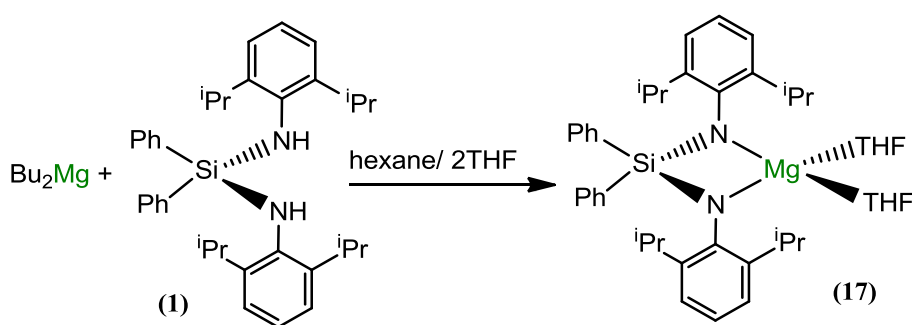
Scheme 3.11: Preparation of [(Ph$_2$Si(NAr*)$_2$)Mg(THF)$_2$] **17**.

The molecular structure of **17** displays a distorted tetrahedral Mg centre (angles range from 79.71(6)º-157.76(7)º; mean 110.92º), bonded to the chelating

bis(amido)silyl ligand and two molecules of THF. The monanionic constitution of **17** contrasts with the dimeric arrangement observed when {Me$_2$Si(HNAr*)$_2$} is reacted with Bu$_2$Mg in hexane to give [(η$_2$-Mg){μ^2-Me$_2$Si(NAr*)$_2$}$_2$] where the ligand acts now as a bridge between the two Mg centres (**Scheme 1.14**, **section 1.1.2**).
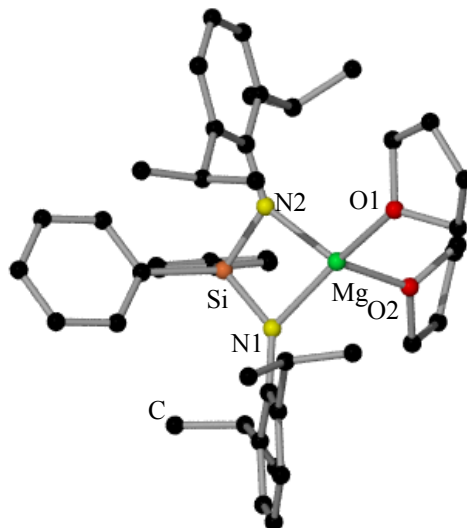
Figure 3.15: Molecular structure of **17**. Hydrogen atoms have been omitted for clarity. Selected bond lengths (Å) and bond angles (º): *Mg-N2 1.983(17), Mg-O1 2.022(16), Mg-O2 2.034(14), Mg-N1 2.0367(15), N2-Mg-O1 128.63(7), N2-Mg-O2 107.20(6), O1-Mg-O2 89.79(7), N2-Mg-N1 79.71(6), O1-Mg-N1 102.43(6), O2-Mg-N2 157.76(7).*

Isolated crystals of **17** were dissolved in THF and one molar equivalent of Btz was introduced. Similarly to the previous studies with magnesiate **2**, an instantaneous, dramatic colour change of the solution occured from colourless to deep red. Addition of hexane to this solution led to the formation of complex **18** in a modest 9% yield. NMR analysis of the solution filtrate showed the presence of **18** along with a complex mixture of other unidentified compounds.
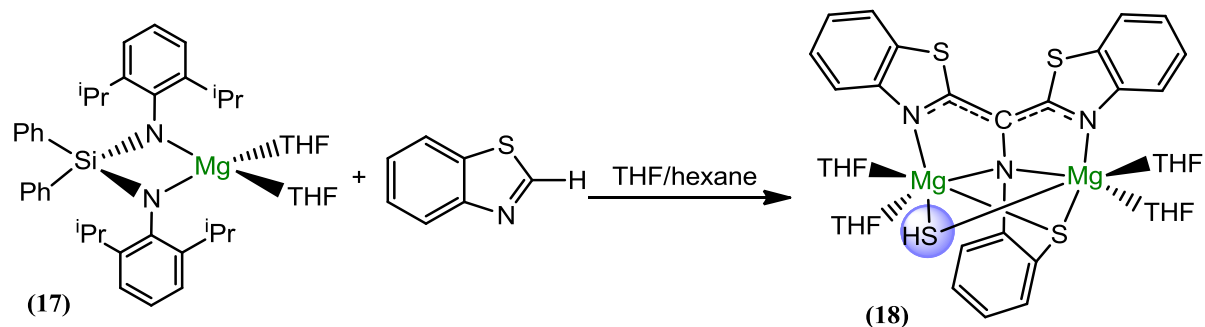
Scheme 3.12: Preparation of complex **18**.

Dimeric **18** contains the trianionic ligand fragment **L** bridging two Mg centres, thus demonstrating that even in the absence of the alkali-metal and the alkyl group, Mg ligated by the bis(amido)silyl ligand can promote the same type of Btz activation, although in a less clean and lower yielding reaction. Fragment **L** bridges the two Mg centres by coordinating to each Mg through the S and N atoms bearing a negative charge of the ring opened benzothiazole, whilst each of the N atoms which are part of the benzothiazolyl rings that are involved in the delocalization of the negative charge through a (bis)aza-allyl unit coordinate to one of the Mg centres each, in contrast to complex **16** where these N atoms chelate one Mg centre. Fragment **L** is coordinating in a similar way to complex **16**; however the benzothiazolyl rings that are involved in the delocalization of the negative charge through a (bis)aza-allyl unit can be thought to have undergone a rotation of 180º. **Figure 3.16** demonstrates the different coordination modes fragment **L** displays in complex **15**, **16** and **18** respectively.
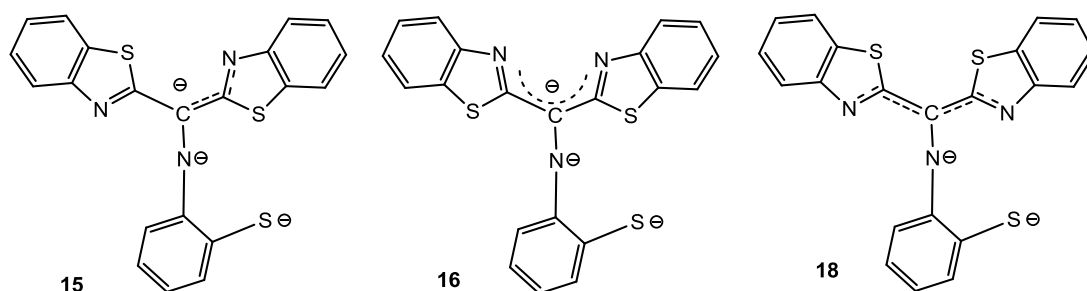
Figure 3.16: Different coordination modes of fragment **L**.

More surprisingly is the presence of a bridging SH⁻ ligand, which presumably results from the cleavage of two C-S bonds of a Btz ring.
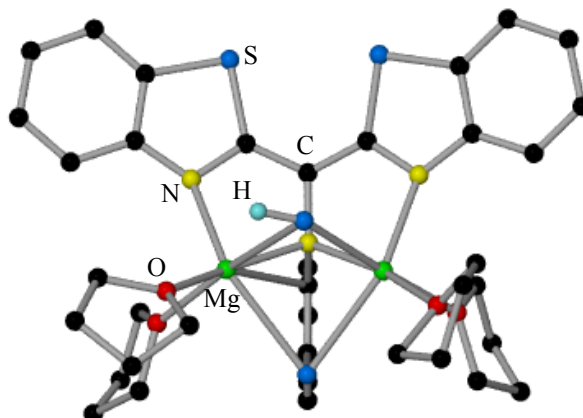
Figure 3.17: Molecular structure of **18**. Hydrogen atoms have been omitted for clarity. Structure **18** suffers high disorder.

Although S extrusion processes have been previously reported for substituted thiazoles and related thiazolium salts,[138] to our knowledge this Mg-mediated bond cleavage reaction has no precedent, though it shares some features with the recent bimetallic-induced fragmentation of THF reported by Mulvey *et al.*[139] In these studies Mulvey shows a sodium magnesiate simultaneously cleaves two C-O bonds from THF, thus generating an oxo-dianion which is trapped in the core of an inverse crown.[139] Although **18** is a minor product, and no other organometallic species could be characterised, the formation of **18** indicates that the bis(amido)silyl ligand coordinated to Mg can initiate a related cascade of reactions to that observed for sodium magnesiate **2**.[134]

3.3.4 Reaction with benzoxazole (Boz)

In the reaction of complex **2** with an equivalent of benzoxazole (Boz) in THF an immediate colour change was observed to a darker yellow and a solid crashed after stirring for thirty minutes. Unfortunately the solid proved to be insoluble and no characterisation could be obtained, however we believe that complex **2** had carried out the ring opening of benzoxazole as we have demonstrated the related Mg-alkyl complex [(^{Dipp}nacnac)Mg(Bu)(THF)] carries out the ring opening of Boz (*vide*

supra). This result is not so surprising as Boche *et al* have shown that in the reaction of Boz with organolithium reagents the equilibrium favours the formation of the ring opened complex over the ring remaining closed.[122]

3.4.1 Reaction with nitron: a stable N-heterocyclic carbene

We next endeavored to move away from the reactivity of sodium magnesiates **2** and **10** with 1,3-benzoazoles, and extend our studies to other commercially available N-heterocycles. We chose the N-heterocyclic molecule nitron, which is a zwitterionic compound whose structure consists of a cationic triazolium unit with an anionic PhN substituent. Siemeling *et al* have recently shown that rather than considering nitron as a Lewis structure it can be thought of as its NHC-tautomer (see **Scheme 3.13**), by reacting nitron with different carbene trapping reagents such as S_8 and [{Rh(μ-Cl)(CO)$_2$}$_2$]. Siemeling *et al* also carried out DFT calculations showing that in the gas phase the NHC tautomer is only 5.7 kcal mol^{-1} less stable than the zwitterion.[91]
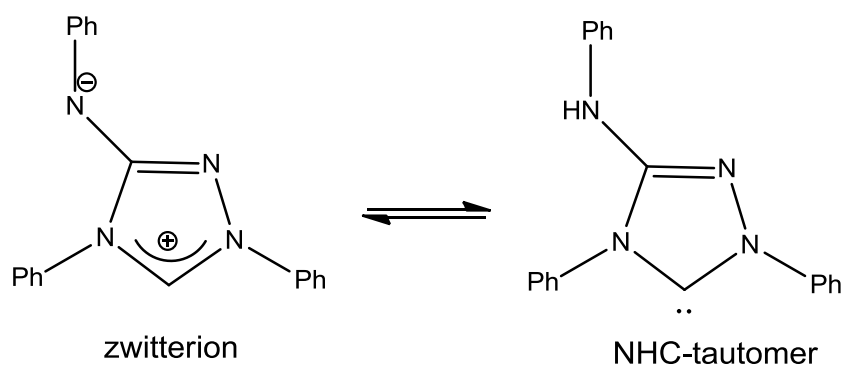
Scheme 3.13: the conventional zwitterion structure of nitron and the NHC-tautomer.

We therefore reacted complex **10** with an equivalent of nitron for one hour in a THF solution, the solution changed colour from yellow to dark green, with storage in the freezer overnight resulting in crystals of complex **19** in a 62% isolated yield (**Scheme 3.14**). Complex **19** was successfully characterised by X-ray crystallography and ^{1}H and ^{13}C NMR spectroscopy using d$_8$-THF as a solvent.
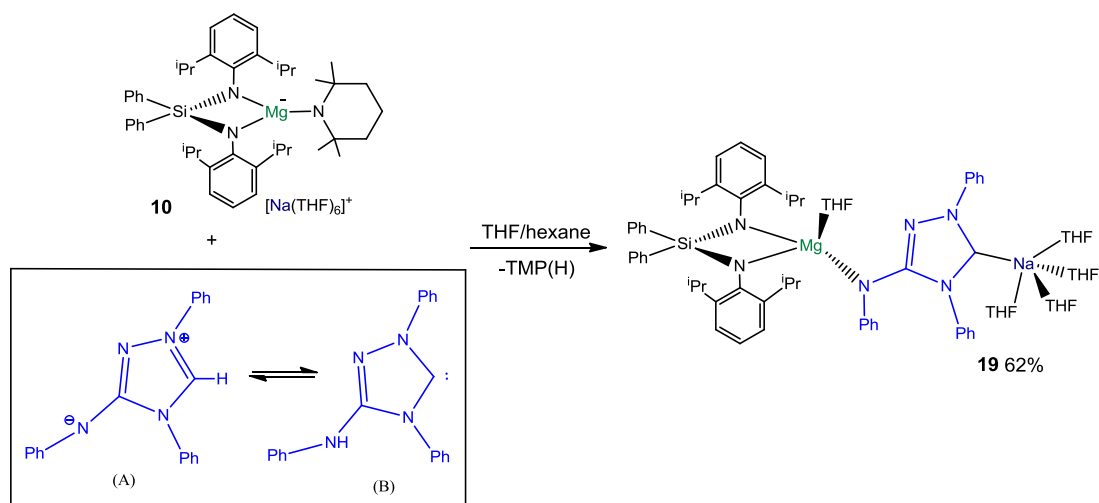
Scheme 3.14: Synthesis of complex **19**.

As discussed above nitron can be thought to exist as two tautomers, either a zwitterion (A) or a NHC (B). In this instance nitron appears to be in its NHC form (resonant form B), with the sodium magnesiate **10** carrying out the magnesiation of the NH of nitron and Na coordinating to the carbenic type carbon. X-ray crystallography revealed a contact ion pair structure, where Mg is in a distorted tetrahedral environment (angles range from 78.06(6)°-144.88(7)°; mean 108.67°). Mg is chelated by the bis(amido)silyl ligand, a molecule of THF and the NPh substituent (N6) of nitron. The Mg-N6 length (2.0866(18) Å) is comparable to other Mg$_{amide}$ bonds reported in this thesis such as in complex **7** (Mg-N3 2.021(2) Å). The N3-C38 bond length (1.315(3) Å) is significantly shorter than the N5-C38 (1.401(3) Å) as expected as N3-C38 should be a double bond while N5-C38 should be single. In addition, as would be expected if a carbene was present, the N5-C37 and N4-C37 lengths are very similar (1.345(3) and 1.374(3) Å respectively). Na completes the contact ion pair structure by coordinating to the carbene type C37 and is solvated by four molecules of THF. A search in the CSD revealed there are currently only three other reported structures where Na is coordinated to an NHC. Each of these were prepared by Hill *et al* by reacting a 1:1:2 mixture of NaHMDS, M(HMDS)$_2$ (M= Mg, Ca or Sr) and IPr (IPr = 1,3-bis(2,6-diisopropylphenyl)imidazole-2-ylidene) in toluene and in all cases are solvent separated structures where the Na cation is coordinated to IPr ligands and the anion is either Mg, Ca or Sr solvated by three HMDS ligands.[95] Only looking at the sodium magnesiate

[{Na(IPr)$_2$}$^+${Mg(HMDS)$_3$}$^-$], the Na-C distance (2.451(4) Å)[95] is much shorter than the Na-C37 length in complex **19 (**2.599(2) Å). This can be rationalised in terms of the different coordination number of Na in these compounds, in [{Na(IPr)$_2$}$^+${Mg(HMDS)$_3$}$^-$] Na is biscoordinated whereas in **19**, Na is in a pentacoordianted environment bonding to four solvating THF molecules. The smaller steric bulk of the Ph groups in complex **19** over the more sterically demanding Ar* groups in IPr will also contribute to the difference in length.
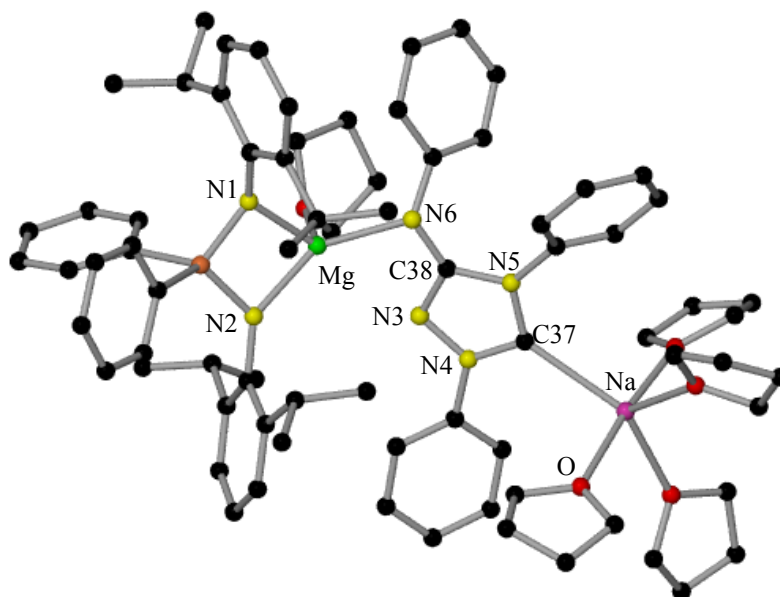
Figure 3.18: Molecular structure of **19**. Hydrogen atoms have been omitted for clarity. Selected bond lengths (Å) and bond angles (°)*:* Mg-N1 2.0333(16), Mg-N2 2.0638(15), Mg-N6 2.0866(18), Na-C37 2.599(2), N6-C38 1.534(2), N3-C38 1.315(3), N5-C38 1.401(3), N5-C37 1.374(3), C37-N4 1.345(3), N4-N3 1.391(2), N1-Mg-N2 78.06(6), N1-Mg-N6 144.88(7), N2-Mg-O1 103.92(6), N1-Mg-O1 109.12(6), N2-Mg-N6 120.26(7), N6-Mg-O1 95.79(7).

To the best of our knowledge this is the first structurally characterised compound where nitron has been metallated by a main group metal.

Complex **19** was also successfully characterised by NMR spectroscopy using d$_8$-THF as solvent. The ^{1}H NMR of nitron reveals that in solution the zwitterion form (A) is the predominant structure displaying resonance for the indicative C*H* group observed

at 9.59 ppm. Although the NHC tautomer is not observed it plays an important role for the reactivity of nitron in solution, as recently reported by Siemeling *et al*.[91] Thus, in the ^{1}H NMR spectrum of complex **19** the C*H* singlet has disappeared, and now multiplets representing all twenty-six aromatic protons from both the Ph groups and the Ar* groups are observed in the region from 8.15 to 6.03 ppm. Regarding the ^{13}C NMR the most indicative signal is at 173.38 ppm representing the carbene type carbon coordinated to Na. Resonances for the other twenty-one aromatic carbon atoms were displayed in the region from 158.72 to 115.67 ppm.

3.5.1 Reaction of 2 with quinoxaline: trapping of a radical anion

We next turned our attention to investigate the reactivity of sodium magnesiates towards six-membered ring N-heterocycles, focusing on diazines. These electron deficient heterocycles are present in many natural products[140, 141] and biologically active molecules such as Botryllazine A which is toxic towards human tumour cells.[142] Despite their important applications, their selective deprotonation using conventional homometallic bases remains a challenge, due to the enhanced acidity (in terms of pK_a values) when compared to pyridine,[143] the presence of two N atoms in the aryl ring greatly decreases the energy of the LUMO,[144] making these heterocycles more prone to nucleophilic addition than deprotonation. There is also a lack of stability of α-metallated diazines due to the repulsion between the negative charge of the carbanion generated and the lone pair of electrons on the N.

We started our studies by investigating the reaction of sodium magnesiate **2** with quinoxaline. This heterocycle has been deprotonated at the C2 position by Knochel *et al* using (TMP)$_2$Mg·2LiCl in the presence of ZnCl$_2$, which when quenched with electrophiles gives yields of up to 94%.[145] In addition, Mongin *et al* have shown that using an in situ solution of ZnCl$_2$·TMEDA and LiTMP in hexane under refluxing conditions she can carry out the metallation of quinoxaline. However no reactive intermediates were characterised, instead the reactions were quenched with I$_2$ revealing that a mixture of the 2-iodo and 2,5-diiodo complex had been formed.

In our case we found that on the addition of quinoxaline to a solution of **2** in THF, a dramatic colour change takes place, affording a deep blue solution, which on cooling

deposited blue crystals of $[\{Na(THF)_6\}_2^+\{(Ph_2Si(NAr^*)_2)Mg(Qox^\bullet)\}_2^-]$ **20**. Alkyl magnesiate **5** when reacted with quinoxaline under the same reaction conditions also resulted in the formation of complex **20**.

R= Bu **2**
R = CH$_2$SiMe$_3$ **5**
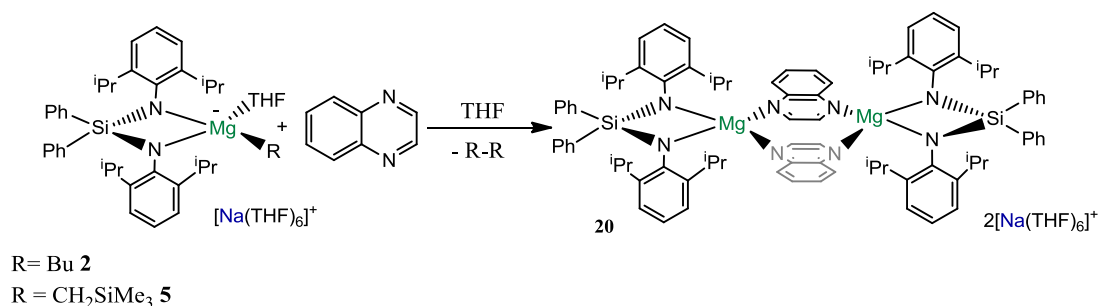
Scheme 3.15: Preparation of $[\{Na(THF)_6\}_2^+\{(Ph_2Si(NAr^*)_2)Mg(Qox^\bullet)\}_2^-]$ **20**.

X-ray crystallographic studies of **20** evidenced that remarkably in this case no metallation or nucleophilic addition reactions have taken place, instead, the formation of a quinoxalyl radical anion (Qox$^\bullet$) has occurred which is trapped within the framework of the ate complex. This can be rationalised in terms of the homoleptic cleavage of the Mg-alkyl bond of the magnesiate, allowing the transfer of one electron to the quinoxaline rings forming complex **20** along with octane or Me$_3$SiCH$_2$CH$_2$SiMe$_3$. Analysis of an aliquot of the filtrate by GC-MS when complex **2** was used did not detect the presence of octane, probably due to the high volatility of this alkane (bp = 126°C), however when complex **5** had been used as a precursor, the presence of Me$_3$SiCH$_2$CH$_2$SiMe$_3$ could be detected as a byproduct of this reaction.

Complex **20** was confirmed as a solvent separated ion pair complex, which exhibits a dimeric structure where both Na cations are solvated by six THF molecules. The dinuclear Mg dianion $[\{(Ph_2Si(NAr^*)_2)Mg(Qox^\bullet)\}_2^-]$ comprises two Mg centres which are in a distorted tetrahedral environment (angles range from 78.40(3)^o-139.50(3)^o), chelated by the bulky bis(amido)silyl ligand, and bridged by coordinating to the N atoms of two distinct quinoxalyl rings. The quinoxalyl rings sit in a perpendicular position to the bis(amido) ligand, stacking directly on top of each other (distance between quinoxalyl rings = 2.957 Å), with the carboxcyclic rings sticking out in opposite directions. The Mg-N$_{qox}$. distances, Mg-N1 (2.102(7) Å) and

Mg-N2 (2.115(7) Å) are slightly shorter to those found in related Mg complex, where Mg is coordinated to a neutral pyridine donor, [(^{Dipp}nacnac)Mg(Bu)(NC$_5$H$_5$)] (2.174(3) Å).[146] In addition, as would be expected it is more elongated in length than other Mg-N$_{amide}$ bonds such as in complexes **6** and **7** (Mg-N = 2.020(16) Å **6**, 2.021(2) Å **7**) reported earlier in this thesis.
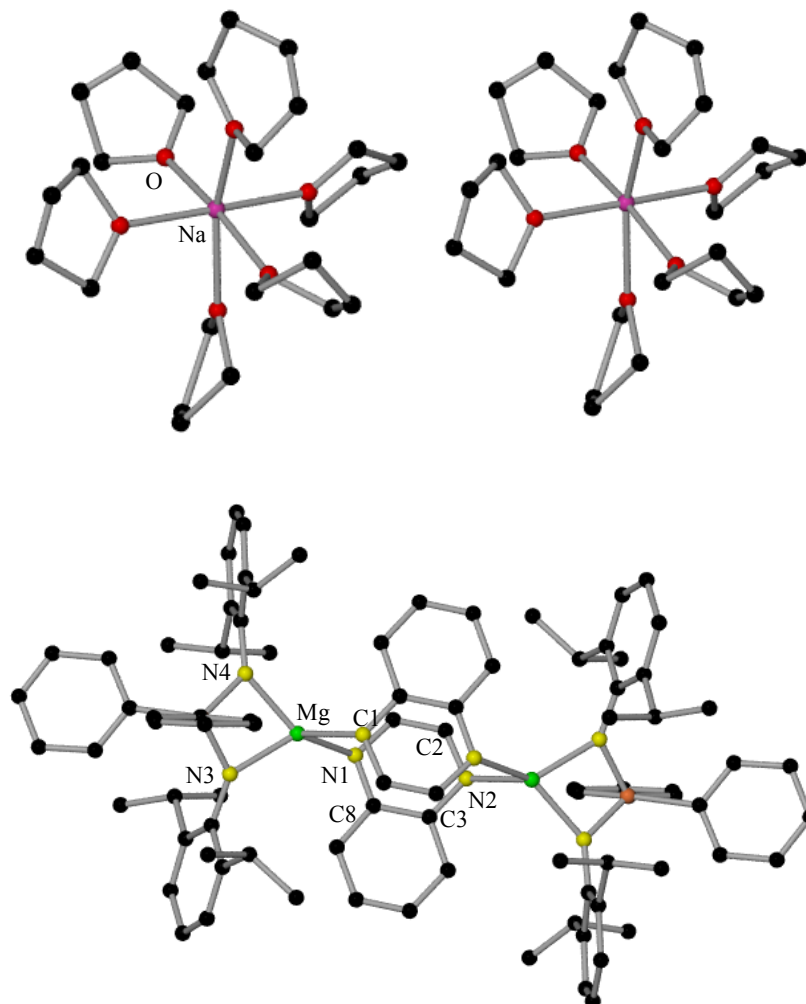
Figure 3.19: Molecular structure of **20**. Selected bond lengths (Å) and bond angles (°): Mg-N1 2.102(7), Mg-N2 2.115(7), Mg-N3 2.028(6), Mg-N4 2.042(6), N1-C1 1.344(9), N1-C8 1.393(9), N2-C3 1.361(9), N2-C2 1.348(9), N1-Mg-N4 139.5(3), N1-Mg-N3 126.1(3), N3-Mg-N4 78.4(3), N1-Mg-N2 84.1(2), N2-Mg-N4 112.9(3), N2-Mg-N3 120.0(3).

A search in the CSD found no other examples where quinoxaline has been either metallated on a carbon or coordinating through the nitrogen by Mg. There are

however examples where quinoxaline acts as a bridge between transition metals such as Cu complex [{Cu(hfac)$_2$(μ-Qox)}$_n$] (hfac = 1,1,1,5,5,5-hexafluoropentane-2,4-dione), which is a polynuclear one-dimensional chain where Cu(II) centres are linked by coordinating to the N position of quinoxaline rings acting as a bridge.[147] The C-N distances within the quinoxalyl ring in **20** (N1-C1, N1-C8, N2-C2, N2-C3, 1.344(9), 1.393(9), 1.361(9) and 1.348(9) Å respectively) are slightly elongated than the relevant distances found in free quinoxaline 1.298, 1.369, 1.308 and 1.364 Å.[148] We believe that the steric bulk provided by the bis(amido)silyl ligand must provide enough steric protection to stabilise the trapping of the radical anion, whilst the ring arrangement of the diazaaromatic rings must contribute to the overall delocalisation of the radical, and therefore stabilisation.

It is known that diazines are effective for electron transport[149] and storage[150] due to their high electron affinity[151] and they can be easily reduced by one-electron processes to form radical anions and dianions. However, structural data and computational investigations of kinetically stable species are still limited.[152] Spreading new light in this area Choua *et al* have prepared radical anion species; tricarbonylmanganese- and tricarbonylrhenium-bound quinoxaline chelates rooted within a triple decker system, which were formed from neutral substrates by chemical reduction over alkaline metals (K, Rb).[153] These systems have been characterised by X-ray crystallography, DFT calculations and EPR studies which found the radical was located in the quinoxalyl fragment.
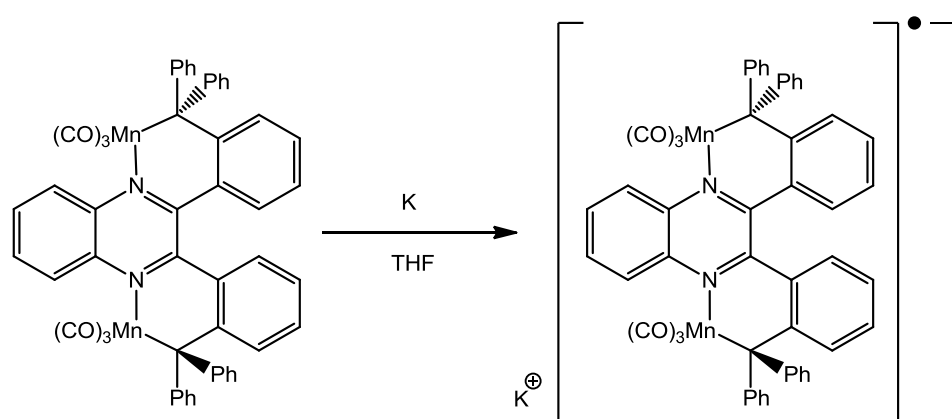
Figure 3.20: Preparation of tricarbonylmanganese-bound quinoxaline radical anion salt.

Likewise, Jackson *et al* have prepared and characterised two radical anion salts, [K(dpq)(THF)$_2$] and [K(dpq)(MeNH$_2$)$_3$] from reducing dpq, (dpq = 2,3-bis(2-pyridyl)quinoxaline) with K metal at -60°C.[154] Closely related to this work, using N containing heterocycles 2,2'- and 2,4'-bipyridine, Goicoechea *et al* have structurally defined a series of alkali metal salts of 2, 2'- and 2, 4'-bipyridyl radicals such as [K(2,2'-bipy)(en)] and [Rb$_2$(2,2'-bipy)(en)$_2$] by reacting 2,2'- and 2,4'-bipyridine with potassium or rubidium in ethylenediamine solution,[155] where the radical is delocalised in the bipyridyl rings. This radical formation of **20** by reacting complex **2** with quinoxaline is in sharp contrast to work carried out by Hill *et al* using related Mg complex [(^{Dipp}nacnac)Mg(Bu)] along with N containing heterocycle pyridine, where instead pyridine remains neutral and coordinates to Mg as a N donor.

In addition, it is noteworthy that several magnesium radical species are known, including the most utilised organomagnesium compounds, Grignard reagents (RMgX), which are thought to exist as a mixture of the following charged species in solution; Mg^{2+}, R$^\bullet$, X$^-$, R$^-$, $^\bullet$MgX, RMg$^+$. [156, 157] Fedushkin *et al* have demonstrated the ability of Grignard reagents to react as radicals in the reaction of [(dpp-bian)Na(Et$_2$O)] with ^{i}PrMgCl in ether solution to form [(dpp-bian)Mg(Et$_2$O)$_2$] (dpp-bian = 1,2-bis{(2,6-diisopropylphenyl)imino}acenaphthene). Suggesting that an intermediate formed during the reaction must undergo a disproportionation reaction with reduction of the dpp-bian radical anion to a dianion and oxidation of the ^{i}Pr carbanion to ^{i}Pr radical due to the ability of the dpp-bian ligand to accept and donate electrons.[158]
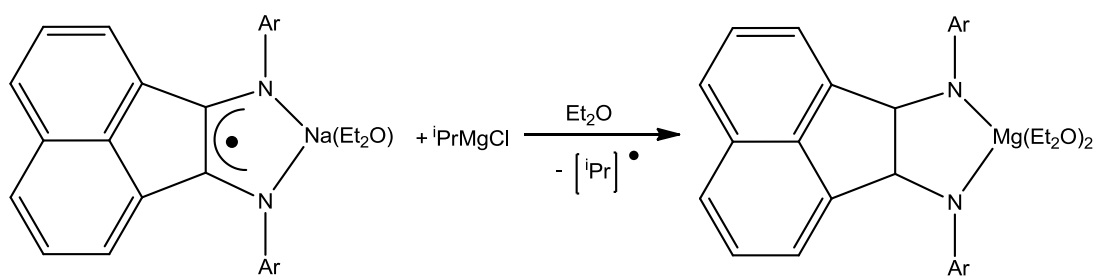
Ar = 2,6 diisopropylphenyl

Scheme 3.16: Reaction of [(dpp-bian)Na(Et$_2$O)] with ^{i}PrMgCl.

In contrast to this trapping of a radical anion by sodium magnesiate **2**, Diaconescu *et al* has shown that using an uranium complex $[(NN^{fc})_2U_2-(\mu-\eta^6,\eta^6-C_7H_8)]$ (NN^{fc} = $fc(NSi^tBuMe_2)_2$) with two equivalents of quinoxaline for ninety minutes at 85^oC led to the formation of $[((NN^{fc})U(quinoxaline))_4]$, a tetranuclear macrocycle with ferrocene diamide uranium(IV) vertices and reduced quinoxaline edges.[159] Each uranium centre in $[(NN^{fc})_2U_2-(\mu-\eta^6,\eta^6-C_7H_8)]$ has carried out a one electron reduction on two quinoxaline molecules.
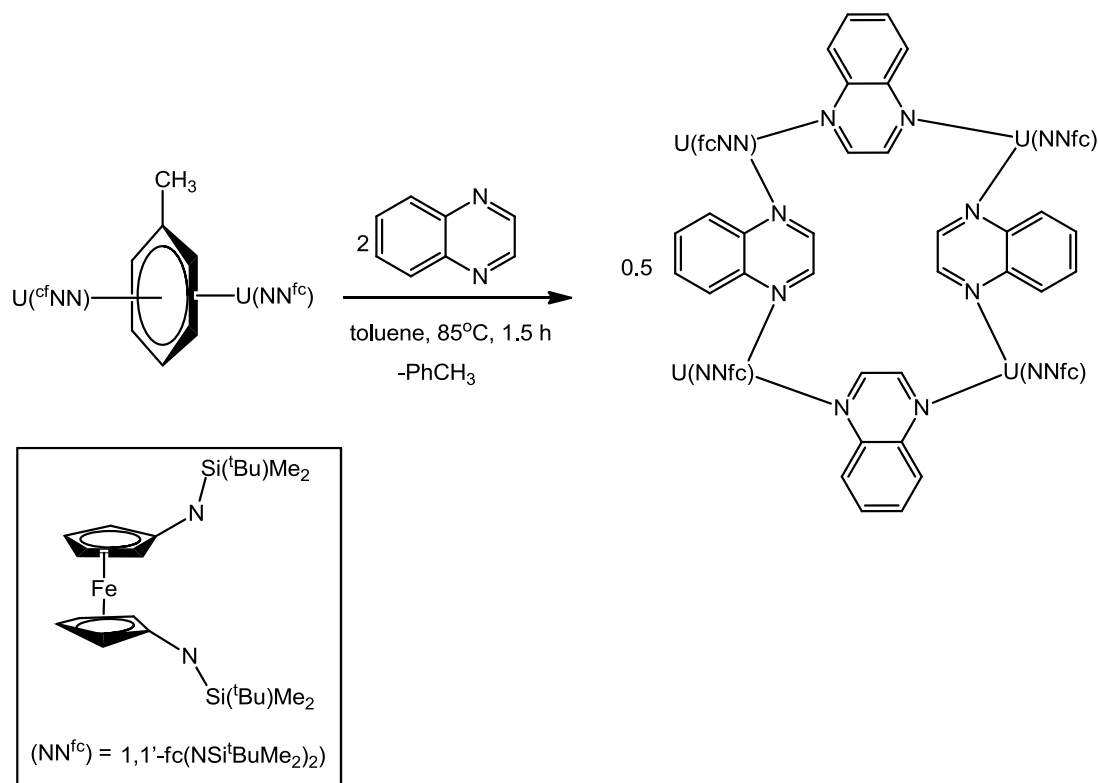
Scheme 3.17: Formation of U(*IV*) molecular quadrangle with reduced quinoxaline edges.

Furthermore Parkin *et al* have shown the remarkable C-C cleavage and dehydrogenation of quinoxaline using transition metal complex $[W(PMe_3)_4(\eta^2-CH_2PMe_2)H]$ to form $[\kappa^2-C_2-C_6H_4(NC)_2]W(PMe_3)_4]$ and $[(\eta^4-C_2N_2-QoxH)W(PMe_3)_3H_2]$, (Qox = quinoxaline), in 15% and 24 % yield respectively, using relatively harsh reaction conditions of eighteen hours and 90^oC.[160, 161] This result is impressive alone not only because of the C-C cleavage of a notoriously

difficult aromatic C-C bond, but also in producing an unprecedented example of η^4-coordination of this dinuclear aromatic compound via the heterocyclic ring.[160]
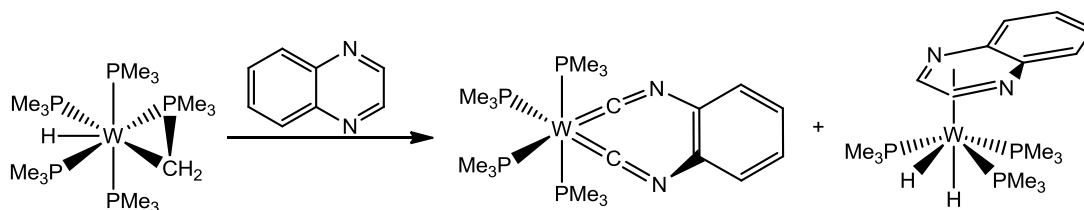
Scheme 3.18: C-C cleavage and dehydrogenation of quinoxaline using transition metal complex [W(PMe$_3$)$_4$(η^2-CH$_2$PMe$_2$)H] to form [κ^2-C$_2$-C$_6$H$_4$(NC)$_2$]W(PMe$_3$)$_4$] and [(η^4-C$_2$N$_2$-QoxH)W(PMe$_3$)$_3$H$_2$].

3.5.2 Solution Studies of complex 20

Despite the radical constitution, complex **20** could be characterised by ^{1}H and ^{13}C NMR spectroscopy using d$_8$-THF as a solvent. Although the resonance in the ^{1}H NMR spectrum are significantly broad, they can be assigned to the different fragments of the molecule. The most diagnostic resonances belonging to quinoxaline hydrogens appear at 6.88, 5.89 and 5.36 ppm; these shifts are drastically upfield in shift and much broader than for those observed in free quinoxaline starting material at 8.82, 8.07 and 7.75 ppm. Two multiplets at 4.16 and 4.03 ppm are observed which can be assigned to two different C*H* of the ^{i}Pr group of Ph$_2$SiNAr* ligand and four doublets for the C*H$_3$* of the ^{i}Pr group at 0.97, 0.88, 0.55 and 0.31 ppm, this suggest that at room temperature there is a lack of symmetry of the ^{i}Pr groups on Ar* when dissolved in d$_8$-THF.
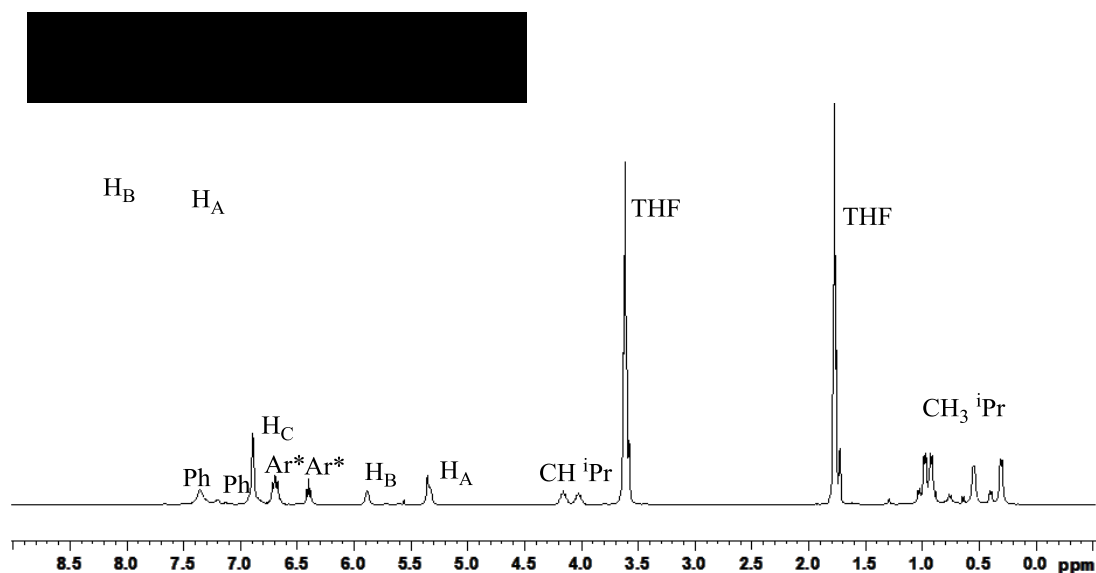
Figure 3.21: ^{1}H NMR of complex **20** in d_8-THF.

The indicative signals from the ^{13}C NMR belonging to quinoxaline are 125.98 and 124.31 ppm for the C_A and C_B respectively, which have moved upfield in shift compared to quinoxaline starting material at 146.21, 130.41 and 130.41 ppm for the C_C, C_A and C_B positions respectively. As complex **20** is a radical anion it was expected that an informative NMR spectra would be difficult to obtain, however since the protons are sitting in an orthogonal position to the orbitals where the radical can be delocalised they are less affected by the paramagnetic character of the molecule allowing the acquisition of meaningful NMR spectra (**Figure 3.22**).
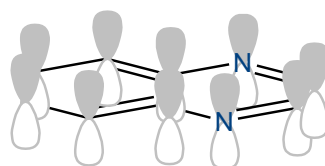
Figure 3.22: protons are sitting in an orthogonal position.

3.5.3 EPR studies and DFT Calculations

To get a better insight on the constitution of **20** we performed EPR experiments in collaboration with Prof. Eva Rentsceller at the University of Mainz, Germany

Electron paramagnetic resonance (EPR) is a technique which allows the study of materials which contain unpaired electrons, known as paramagnetic species. Such

104

species can include organic and main group radicals, as well as transition metal complexes with unpaired electrons.[162] EPR can be broadly thought of as a sister technique to NMR spectroscopy, where NMR deals with diamagnetic species (paired electrons) and EPR deals with paramagnetic species (unpaired electrons). Fundamentally EPR is the measurement of electron spin interacting with an applied external magnetic field.[162]

Magnetic susceptibility data for polycrystalline samples of complex **20** were collected in the temperature range 2-300 K in an applied magnetic field of 1 T with a SQUID magnetometer (MPMS-7, Quantum Design). Experimental susceptibility data were corrected for the underlying diamagnetism using Pascal's constants. The temperature dependent magnetic contribution of the glass holder was experimentally determined and subtracted from the measured susceptibility data. EPR spectra of **20** in THF (1 mmol/l) at $25^{o}C$ and $-169^{o}C$ were collected on a Magnettech MiniScope MS300 benchtop cw EPR spectrometer (X-band, ~9.4 GHz microwave frequency). EPR simulations were performed using EasySpin 3.1.7.

In the solid state complex **20** exhibited no paramagnetic signal over the entire temperature range of 2-300 K. It is most likely that either a disproportionation reaction of the radical is going on, or alternatively very strong antiferromagnetic coupling of the quinoxaline radicals via π-π stacking is taking place (distance between quinoxaline rings 2.957 Å). Most likely the latter situation is occurring as the single crystal data only shows one symmetry independent quinoxaline ligand in the asymmetric unit, not showing any structural indications for a disproportionation reaction taking place. Contrastingly, when crystals of **20** were dissolved in THF (1 mmol/l), in solution state a clear paramagnetic signal can be detected at both $25^{o}C$ and $-169^{o}C$. The spectra do not differ significantly from each other with the spectra measured at $-169^{o}C$ displayed in **Figure 3.23**. The signals can be satisfactorily simulated assuming an S = $^1/_2$ with an isotropic g- value close to 2.0 and a Lorenz-line-width of 1.1 mT (peak to peak). In contrast to the non-coordinated quinoxaline radicals in literature,[163] no hyperfine coupling to the nitrogen and hydrogen atoms can be observed. The paramagnetic signal observed in solution arises from dilution

of the molecules and thus dissolving the dimeric structure and thus precluding the antiferromagnetic interaction via π-π stacking.[164]
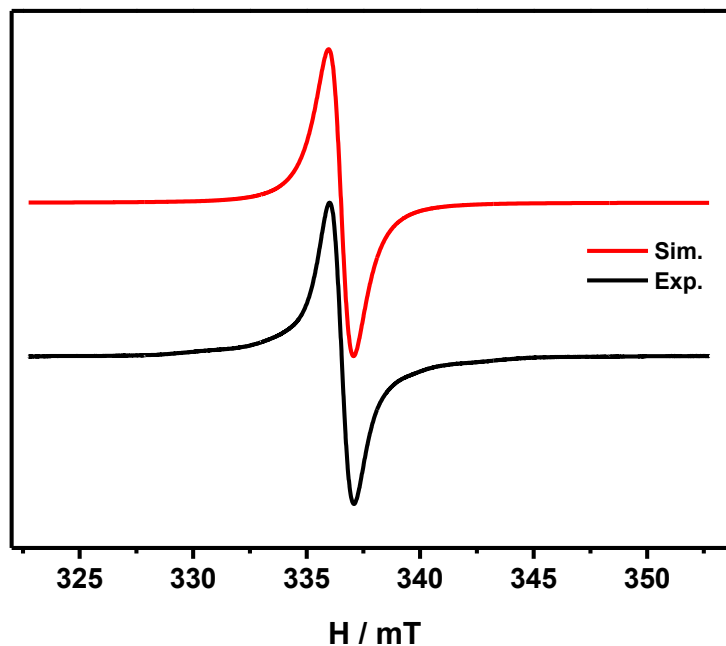
Figure 3.23: EPR spectra of **20** in THF (1 mmol/l) at -169°C.

DFT calculations were carried out to probe the electronic structure of **20**. Density Functional Theory calculations were performed using the Gaussian computational package G03.[128] In this series of calculations the B3LYP[129] density functionals and the 6-311G(d,p)[130] basis set were used. After each geometry optimisation, a frequency analysis was performed. The energy values quoted include the zero point energy contribution. Complex **20** was modeled in the singlet (I) and triplet (II) states as a dimer, the molecular models are displayed in **Figure 3.24**.

(a)

(b)
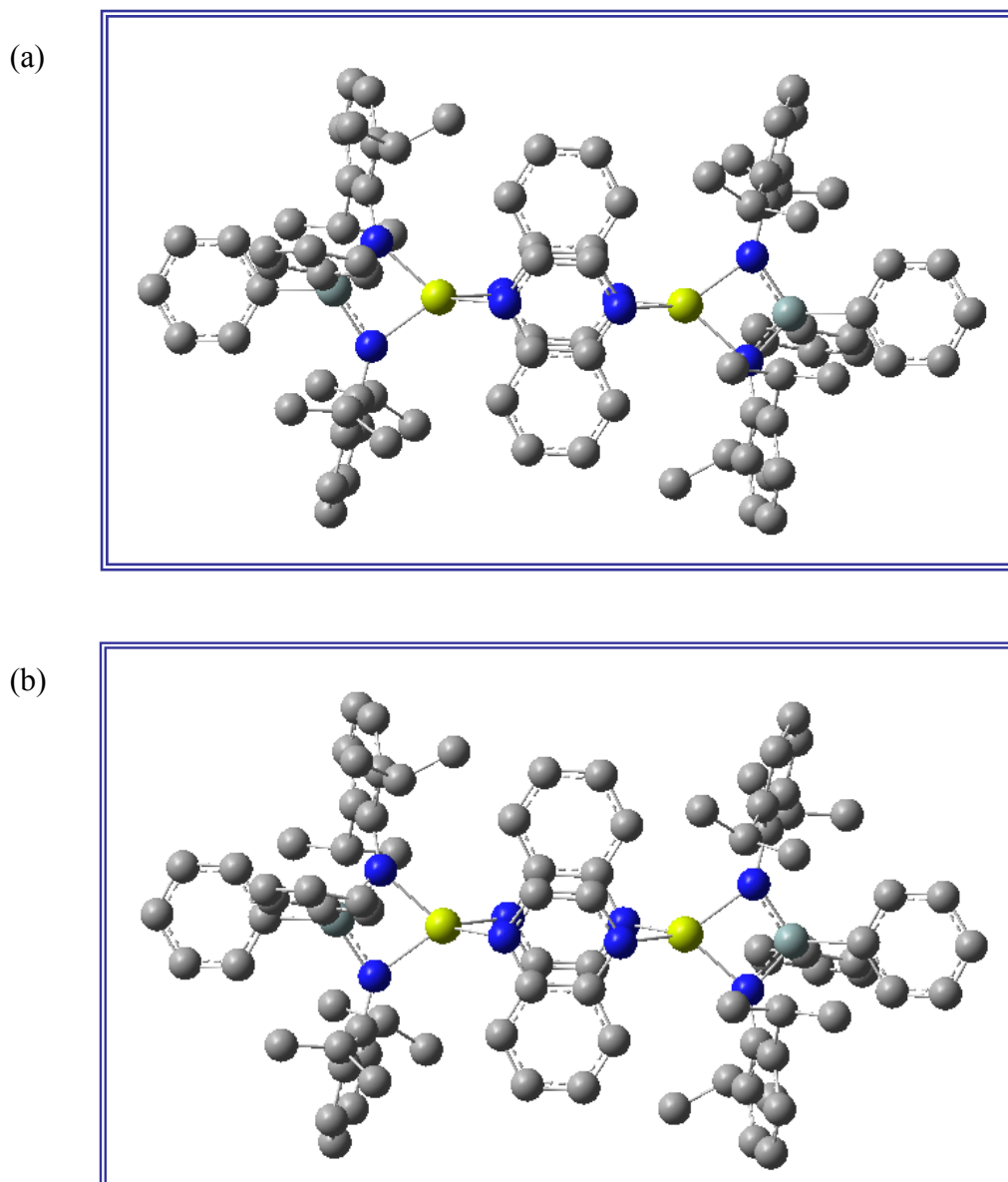
Figure 3.24: Molecular structure of complex **20** as a (a) singlet state (I) and as (b) a triplet state (II).

These studies show the singlet state to be 4.94 kcal mol^{-1} more stable than the triplet state. In the singlet state no paramagnetic signal would be detected as all electrons would be paired, therefore these findings reinforce the magnetic measurement data, which stated that in the solid state no paramagnetic behavior is present due to antiferromagnetic coupling occurring via π-π stacking of the quinoxalyl rings. Molecular structure of **20** showing the highest occupied molecular orbital (HOMO)

in the singlet state is displayed in **Figure 3.25**, as can be seen the electrons are localised in molecular orbitals of quinoxalyl rings.
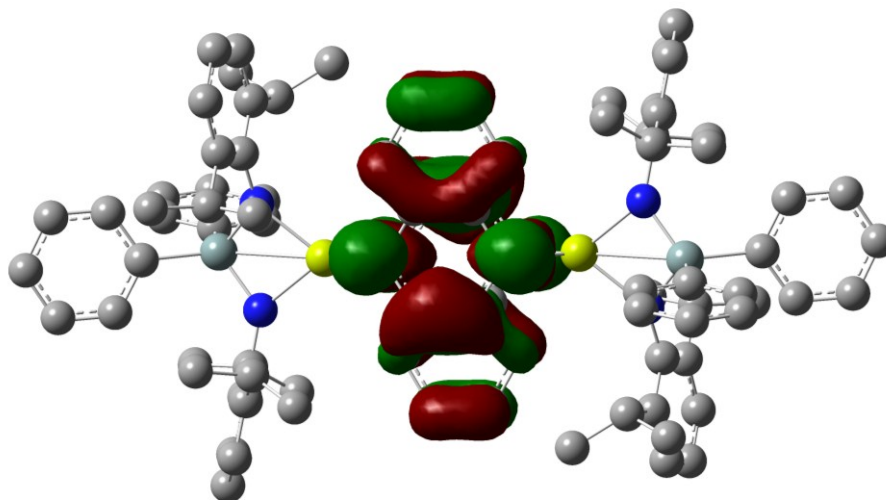
Figure 3.25: Molecular orbital diagram showing highest occupied molecular orbital (HOMO).

The calculated bond lengths within complex **20** in the singlet state compare well with the actual bond lengths of **20** (**Table 3.3**).

Bond	20 (Å)	Singlet (I) (Å)	Free quinoxaline (Å)
Mg-N quinoxaline	2.102, 2.125	2.150, 2.165	
N-C	1.361, 1.393, 1.344, 1.348	1.368, 1.389, 1.387, 1.365	1.369, 1.298, 1.308, 1.364
C-C	1.364, 1.436	1.374, 1.430	1.373, 1.391
Mg-N Amido ligand	2.028, 2.042	2.112, 2.075	

Table 3.3: Comparison of actual and calculated bond lengths (Å).

3.5.4 Reaction of complex 2 with TEMPO[•]

Since the reaction of **2** with Qox involves the homoleptic cleavage of Mg-C$_{Bu}$ bond, we then probed its reactivity with the free radical TEMPO[•] (2,2,6,6-tetramethyl-1-piperidinyloxy) (**Scheme 3.19**). TEMPO[•] is a stable nitroxide free radical which finds important uses in synthesis such as a spin label in the study of biological systems[165] and as a radical trapping agent.[166] Crystals of [(Ph$_2$Si(NAr*)$_2$)Mg(TEMPO⁻)Na(THF)$_3$] **21** crystallised in a 41% yield which were analysed by both NMR spectroscopy and X-ray crystallography, analysis of the filtrate by ^{1}H NMR revealed the reaction to be quantitative.
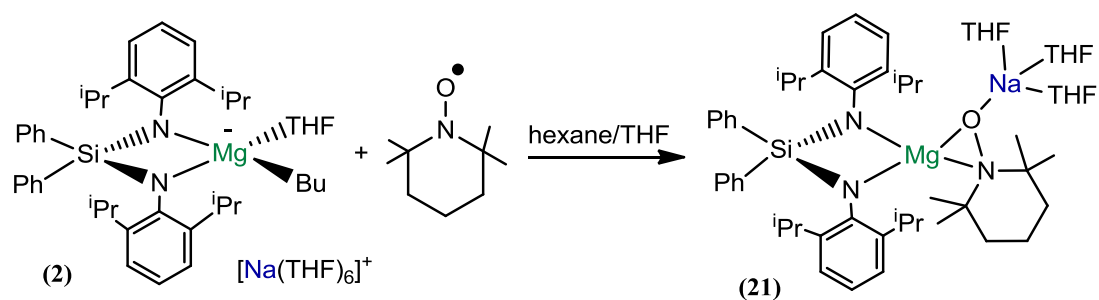
Scheme 3.19: Preparation of [(Ph$_2$Si(NAr*)$_2$)Mg(TEMPO⁻)Na(THF)$_3$] **21**.

Contrasting with the structure of sodium magnesiate **2**, complex **21** displays a contacted ion pair structure where both metals are connected by a bridging TEMPO anion. TEMPO[•] has been reduced by Mg after the Mg-C$_{Bu}$ bond of complex **2** has undergone homoleptic cleavage, to generate Bu[•] and Mg[•] that can then react with TEMPO[•]. The TEMPO anion is coordinated unsymmetrically to both metals, the Na atom coordinates to the oxygen atom and three molecules of THF. As would be expected the Na-O length of the TEMPO anion (2.236(3) Å) is shorter than the Na-O$_{THF}$ lengths (ranging from 2.270(4)-2.327(4) Å). Furthermore, the Na-O distance in **21** compares well with that reported for related zincate [(TMEDA)·Na(μ-TMP)-(μ-TEMPO)Zn(^{t}Bu)], (2.249(12) Å) prepared by Mulvey *et al* where Na is also coordinated to the oxygen of a TEMPO anion.[167] Magnesium is in a distorted tetrahedral environment (average bond angle = 113.02 Å) chelated by the bulky bis(amido)silyl ligand and completing its coordination sphere by coordinating to the nitrogen and oxygen of the TEMPO anion. The main distortion to the geometry of Mg results from the most acute angle displayed from O1-Mg-N3, TEMPO acts as a

η^2-O/N chelate to Mg (41.54(9)°). The Mg-N3 distance 2.162(3) Å in **21** is remarkably shorter than that of related structure [{Mg(HMDS)(μ-TEMPO⁻)}₂] 2.395(3) Å reported by Mulvey *et al* by reacting an equivalent of TEMPO• with HMDS(H) and half an equivalent of Bu₂Mg in hexane.[168] In complex [{Mg(HMDS)(μ-TEMPO⁻)}₂] there are two different types of TEMPO ligation: first as a η^2-O/N chelate to Mg, similar to that displayed in complex **21** but secondly as a μ_2-O bond to Mg (**Scheme 3.20**).
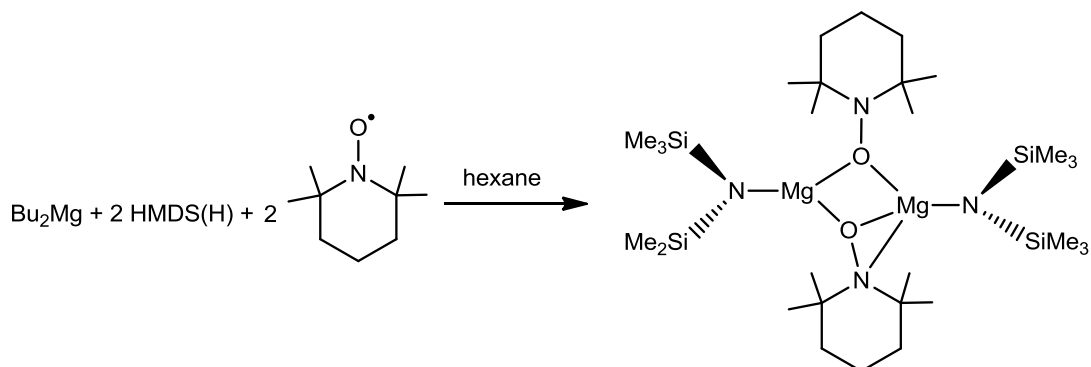
Scheme 3.20: Preparation of [{Mg(HMDS)(μ-TEMPO⁻)}₂] reported by Mulvey *et al*.

The Mg-O bond length, where TEMPO is coordinating in a η^2-O/N chelate to Mg, (1.939(2) Å) for **21** and (1.979(3) Å) for [{Mg(HMDS)(μ-TEMPO⁻)}₂] are in a similar region. These Mg-O bond lengths are also in a similar range to Mg-O bond length in [{Mg(HMDS)(μ-TEMPO⁻)}₂] (1.967(3) Å) where TEMPO is only μ_2-O bonding, showing that the bidentate coordination of TEMPO in **21** has little effect on the Mg-O bond distance.[168] In addition, the Mg-O distance in complex **21** is more elongated than the only other example in the CSD where magnesium is coordinated to the oxygen of a anionic TEMPO molecule, [(dpp-BIAN)Mg(TEMPO⁻)(THF)] (1.906(10) Å).[169] This bridging role of the TEMPO anion coordinating through two different ligating modes; μ_2-O to Na and η^2-O/N chelation to Mg is unprecedented in magnesiate chemistry with the closest structure being the previously discussed complex [{Mg(HMDS)(μ-TEMPO⁻)}₂] where the TEMPO anion coordinates in these two modes to bridge two Mg centres.
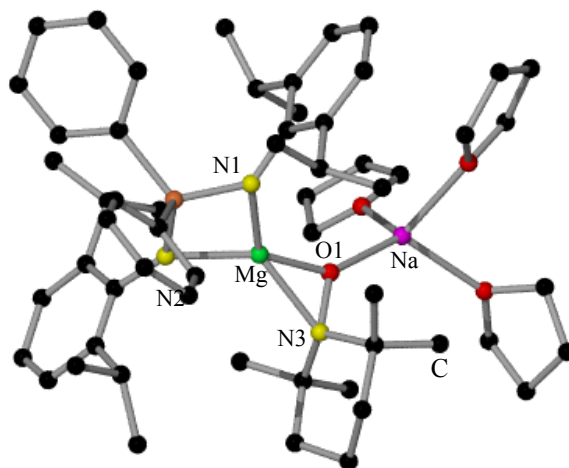
Figure 3.26: Molecular structure of **21**. Hydrogen atoms have been omitted for clarity. Selected bond lengths (Å) and bond angles (°): Mg-O1 1.939(2), Mg-N2 2.021(3), Mg-N1 2.035(3), Mg-N3 2.162(3), N3-O1 1.469(3), Na-O1 2.236(3), Na-O2 2.300(4), Na-O3 2.270(4), Na-O4 2.327(4), O1-Mg-N1 151.29(12), N2-Mg-N1 78.86(12), O1-Mg-N3 41.54(9), N2-Mg-N3 139.75(12), N1-Mg-N3 139.75(12), O1-Mg-N2 126.98(12).

Contrasting with the broad signals observed in the ^{1}H NMR of free TEMPO$^.$ in C_6D_6, the ^{1}H NMR spectra of **21** showed two sharp singlets at 1.05 and 0.97 ppm for the Me groups of the newly generated TEMPO$^-$ anion. ^{13}C NMR analysis of **21** revealed the presence of three resonances at 60.50, 42.03 and 19.38 ppm which can be assigned to the C_α, C_β and C_γ of the TEMPO anion as well as two resonances for its Me groups at 35.74 and 20.33 ppm. This data is consistent with the retention in solution of the Mg-N bond, which precludes the free rotation around the O-N bond, which would interconvert the two symmetrically unequivalent types of Me groups present in the TEMPO anion.
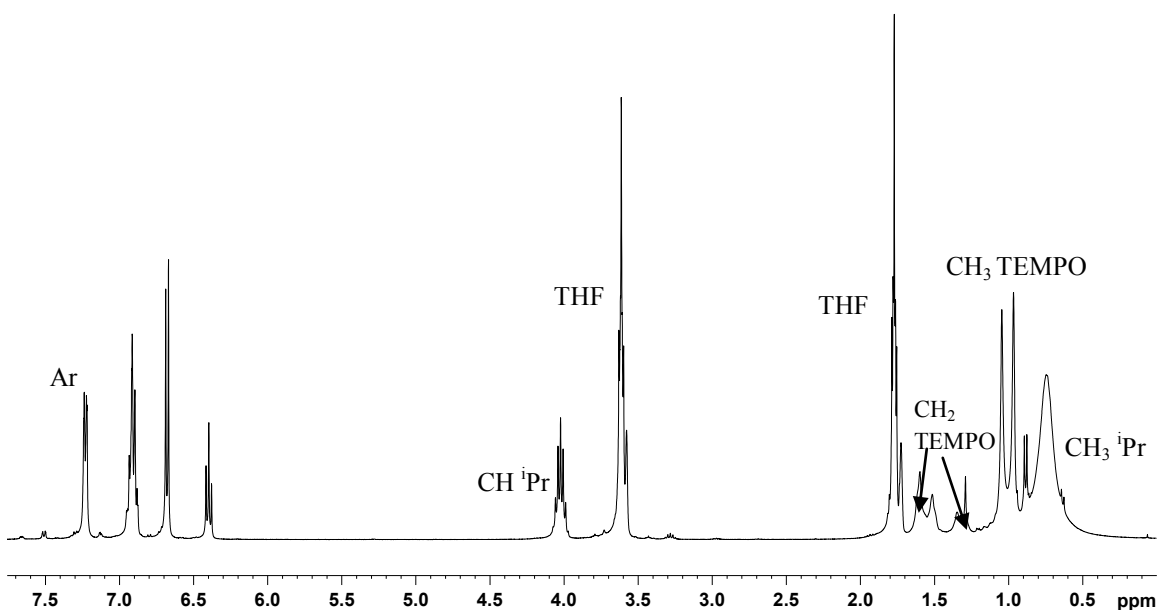
Figure 3.27: ^{1}H NMR in d_8-THF of complex **21**.

In addition to these studies, as TEMPO$^\bullet$ can be utilised as a radical trapping agent we next decided to add an equivalent of TEMPO$^\bullet$ in the reaction of complex **2** with Qox and discovered by monitoring the reaction by ^{1}H NMR that the formation of **20** is inhibited, giving rise to the formation of **21** as a major product, demonstrating that the formation of **20** could occur via a radical mechanism.

3.6.1 Conclusions

To conclude this chapter, it has been shown that the sodium magnesiate alkyl and amido bases [{Na(THF)$_6$}$^+${(Ph$_2$Si(NAr*)$_2$)Mg(Bu)(THF)}$^-$] **2** and [{Na(THF)$_6$}$^+${(Ph$_2$Si(NAr*)$_2$)Mg(TMP)}$^-$] **10** respectively, bearing the bulky bis(amido)silyl ligand have shown diverse reactivity with a series of heterocycles. In the reaction with thiophene, alkyl base **2**, the Mg-C bond was proven to be too kinetically unreactive to carry out the metallation, however the stronger amido base **10** was able to carry out magnesiation at the α position to form [{Na(THF)$_6$}$^+${(Ph$_2$Si(NAr*)$_2$)Mg(C$_4$H$_3$S)(THF)}$^-$] **13** in a good yield. The N-heterocycle MeBIm having a slightly more acidic C2 position than that of thiophene, was however successfully metallated by alkyl base **2** at the C2 position to yield complex [{Na(THF)$_5$}$_2$$^+${(Ph$_2$Si(NAr*)$_2$)Mg(MeBIm*)}$_2$$^-$] **14**. DFT calculation, NMR spectroscopic and X-ray crystallographic studies suggest that this compound can be envisaged as an N-metallocarbene species. In extending our studies to Btz

however, the initial deprotonation of the heterocycle by sodium magnesiate **2** initiates a domino of intramolecular reactions involving C-C coupling, ring opening, aryl migration and internal deprotonation to generate a new type of trianionic ligand resulting from the activation of three molecules of Btz. It is believed that the bis(amido)silyl ligand plays a major role in the activation of Btz both acting as a bis(amido) base, this was supported by results observed when Btz was reacted with the neutral magnesium complex [(Ph$_2$Si(NAr*)$_2$)Mg(THF)$_2$] **17**, with two equivalents of Btz which led to a similar Btz activation although in lower yields than the bimetallic base displayed.

Figure 3.28: Frontispiece in Angewandte

When complex **2** was reacted with nitron a contact ion pair structure **19** was formed in a good yield, where Na was coordinated to carbene type C and Mg had metallated the NH of nitron. Changing substrates to another type of N-containing heterocycle, diazines, it was found that the reaction of complex **2** with Qox yielded the trapping of a radical anion complex [{Na(THF)$_6$}$_2^+${(Ph$_2$Si(NAr*)$_2$)Mg(Qox$^\bullet$)}$_2^-$] **20**. EPR studies showed that in the solution state a paramagnetic signal could be found, however in the solid state no paramagnetic signal was detected, which was verified by DFT calculations. Complex **2** was then reacted with commercially available stable radical species TEMPO$^\bullet$ to produce crystals of [(Ph$_2$Si(NAr*)$_2$)Mg(TEMPO$^-$)Na(THF)$_3$] **21**, where TEMPO$^-$ is now an acting as a bridging anionic ligand between the metal centres proving that alkyl species **2** can participate in radical transformations. These different reactivity studies have shown the versatility of the newly prepared sodium magnesiate complexes.

Chapter 4: Isomeric and chemical consequences of the direct magnesiation of 1,3-benzazoles using β-diketiminate stabilised magnesium bases

4.1.1 Introduction

The main focus of this chapter is the synthesis and exploitation of magnesium compounds supported on a different type of highly sterically demanding ligand, β-diketiminate nacnac [{2,6-^{i}Pr$_2$C$_6$H$_3$)N(Me)C}$_2$CH].[170] In recent years β-diketiminate ligands have played an instrumental role in many key breakthroughs in magnesium chemistry. Acting as steric stabilizers, facilitating the formation of robust six-membered metallacycles, the use of these ligands has enabled the isolation of the first compounds exhibiting Mg-Mg metal-metal bonds by reduction of [MgI(OEt$_2$)(^{Dipp}nacnac)] using potassium metal.[46] In addition, the trapping of a record high nuclearity {Mg$_8$H$_{10}$}$^{6+}$ hydride cluster which shows complete hydrogen desorption at 200°C, an exceptionally low temperature for a molecular magnesium hydride complex.[45, 171] Within the context of their catalytic applications, magnesium β-diketiminate complexes have proven to be extremely active single-site initiators for the polymerisation of *rac*-lactide,[172] whereas pioneering work by Hill *et al* has shown that magnesium alkyl compounds bearing these ligands can be efficient precatalysts for intramolecular hydroamination reactions of a wide range of amino alkenes.[16] Furthermore, the extension of this chemistry to magnesiums heavier congeners calcium, strontium and barium has led to the development of novel catalytic systems for a myriad of reactions such as hydrogenation of alkenes,[173] hydrosilylation of ketones[174] and hydroamination of isocyanates,[18] carbodiimides[15] and vinylarenes[175] to name but a few. Despite the increasing interest in the synthetic applications of this important family of magnesium compounds, their potential use as metallating reagents capable of promoting direct Mg-H exchange reactions of organic molecules has not yet been investigated. This is even more surprising taking into account that magnesium reagents, in particular magnesium amides, have found employment as efficient alternatives to more traditional lithium based metallating reagents such as LiDA or LiTMP for executing deprotonation reactions of aromatic and heteroaromatic molecules as a prerequisite to tandem bond-forming approaches,[162] offering improved regioselectivities and

allowing the use of milder reaction conditions (due to a great extent to the *in situ* formation of more stable organomagnesium intermediate species).[119] Furthermore, the metallating power of these magnesium compounds can be greatly boosted by combining them with alkali-metal reagents. Major contributors to this area are Knochel's "Turbo Hauser" bases (e.g. TMPMgCl·LiCl) which in exhibiting an enhanced functional group tolerance allow access to regioselective functionalised aryl, heteroaryl and metallocenyl compounds[132] and Mulvey's heterobimetallic amide systems (e.g. [NaMg(TMP)$_2$R], R = Bu, CH$_2$SiMe$_3$) that are able to perform the direct magnesiation[176] of molecules that are usually inert towards conventional organomagnesium reagents such as benzene[73], toluene[74] or ferrocene[128] amongst many others.

As discussed in **Chapter 3**, 1,3-benzoazoles can be readily metallated at their C2 position[121] using a wide range of organometallic reagents which span from traditional homometallic bases such as organolithium and organomagnesium compounds[177] to more sophisticated 'ate' complexes such as magnesiates[178] or zincates.[179] However, in some cases complications can be encountered due to the lack of stability of the generated metallated intermediate, which depending on the reaction conditions and the organometallic source employed, can be in equilibrium with its isocyano tautomers **II**, resulting from the ring cleavage of **I** (**Scheme 4.1**). Thus, for example attempts to trap 2-lithioxazoles with electrophiles usually affords mixtures of the products of substitution at the C2 and C4 position (resulting from the reaction of the ring-open enolate form **II** with the electrophile followed by its cyclization) even when the reactions are performed at -78°C.[180]

X= O (**Boz**), S (**Btz**), NMe (**MeBlm**)
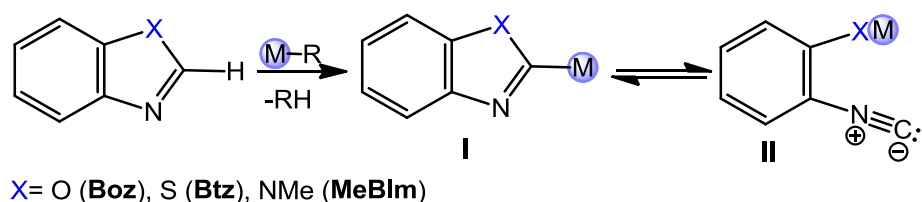
Scheme 4.1: Equilibrium between C2-metallated 1,3-azoles and their ring opened isomers.

NMR spectroscopic and X-ray crystallographic structural studies have shown that metallated thiazoles and imidazoles tend to be more stable than oxazoles, with the equilibrium depicted in **Scheme 4.1** lying mainly towards the cyclic isomer **I**.[123] In **Chapter 3** we have shown that when Mg compounds supported by the highly sterically demanding bis(amido)silyl ligand {Ph$_2$Si(NAr*)$_2$}$^{2-}$ (Ar* = 2,6-diisopropylphenyl) are employed as metallating reagents towards Btz a novel type of heterocyclic activation is promoted, where the initial magnesiation of Btz initiates an unstoppable cascade of C-C coupling, ring opening, nucleophilic addition and deprotonation reactions to generate a novel sodium magnesiate containing the trianionic ligand fragment **L** (**Scheme 4.2**).[134] Initial studies show that the bulky bis(amido) ligand rather than acting as a more steric stabiliser, plays a more active role promoting this sequence of fast intramolecular reactions.
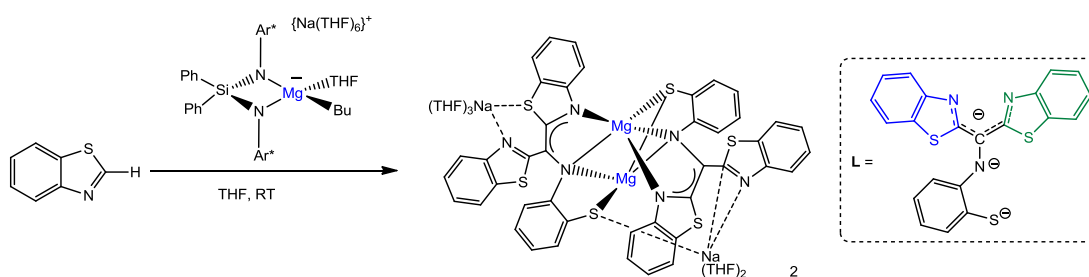
Scheme 4.2: Reactivity of Btz with [{Na(THF)$_6$}$^+${(Ph$_2$Si(NAr*)$_2$)Mg(Bu)(THF)}$^-$].

4.2.1: Synthesis of β-diketiminate magnesium bases

Firstly the synthesis of sodium magnesiates containing the β-diketiminate ligand was attempted. The reactions of one equivalent of β-diketiminate [{2,6-^{i}Pr$_2$C$_6$H$_3$)N(Me)C}$_2$CH] ^{Dipp}nacnacH with mixed metal combinations [NaMgBu$_3$] and [NaMg(TMP)$_2$Bu] were studied (**Scheme 4.3**).
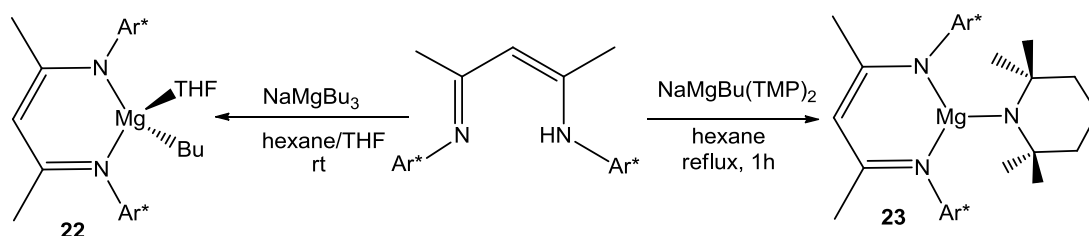
Scheme 4.3: Preparation of **22** and **23**.

Surprisingly both reactions led to the isolation of single metal magnesium complexes, allowing the isolation of [(^{Dipp}nacnac)Mg(Bu)(THF)] **22** and [(^{Dipp}nacnac)Mg(TMP)] **23** respectively. These results suggest that using this highly sterically demanding ligand with a more rigid structure than that of {Ph$_2$Si(NAr*)$_2$}$^{2-}$, the formation of the mixed-metal species (which would require the presence of two additional anionic ligands around Mg) is not favoured. As both complexes were homometallic Mg species, the reactions were repeated in the absence of BuNa and formed **22** and **23** in crystalline yields of 54% and 52% respectively (**Scheme 4.4**). In the case of **22** a solvent mixture of hexane/THF was employed, whereas for the formation of **23**, the reaction mixture had to be refluxed in hexane for one hour to ensure that the reaction went to completion. Contrasting with previous examples reported in the literature to prepare β-diketiminate magnesium amides, we found that compound **23** could not be obtained by the alternative method of treating butyl compound **22** with the amine TMP(H), even under refluxing conditions. This can be attributed to the larger steric constraints imposed by this cyclic amine in comparison with the amines employed in these previous studies (for example benzylamine, diisopropylamine or hexamethyldisilazane to name a few).[129, 181]
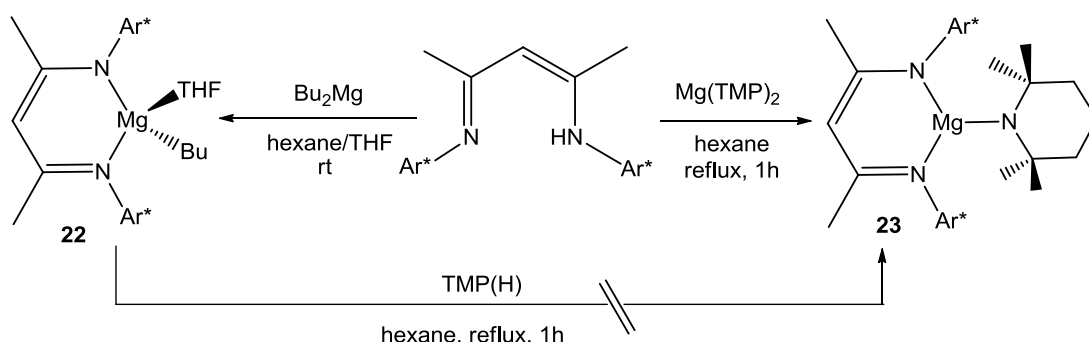
Scheme 4.4: Preparation of **22** and **23**.

The compounds were characterised in C$_6$D$_6$ solution using ^{1}H and ^{13}C NMR spectroscopy and their molecular structures determined via single crystal X-ray diffraction and the results are displayed in **Fig. 4.1** and **4.2**, respectively. Butyl complex **22** exhibits a structure similar to those previously reported for monomeric β-diketiminate magnesium alkyl species,[130] displaying a distorted tetrahedral Mg centre bonded to the chelating nacnac ligand, a terminal butyl group and a molecule

of THF. In this case the use of Lewis base THF as a co-solvent for the synthesis of **22** seems to be sufficient to avoid the formation of dimeric [(^{Dipp}nacnac)Mg(μ-η^1-Bu)]$_2$ (2.253(3) Å), formed by Roesky by reacting Bu$_2$Mg with ^{Dipp}nacnac(H) in toluene as a solvent.[182] The Mg-C(26) bond length 2.126(16) Å compares well with that of related structure found in the literature, [(^{tBu}nacnac)Mg(Bu)(THF)] (2.122(2) Å) which Chisholm *et al* prepared by refluxing MgBu$_2$ and the related β-diketiminate ^{tBu}nacnac(H) in a hexane/THF mixture.[183] In addition, it is almost identical in length to Mg-C bond in complex **2** (2.124(3) Å) reported in **Chapter 2**. Contrastingly, in monomeric TMP-complex **23**, Mg adopts a distorted trigonal planar geometry (Σ<Mg = 360º) by binding to three N atoms, two of them provided by the β-diketiminate ligand and a third one from the amide TMP. The Mg-N$_{amide}$ bond length (1.941(13) Å), lies within the range of those found for other related Mg nacnac complexes containing the also sterically hindered amides; diisopropylamide [(^{Dipp}nacnac)MgN^{i}Pr$_2$] (1.938(2) Å)[181] and hexamethyldisilazide [(^{Dipp}nacnac)MgN(SiMe$_3$)$_2$] (1.961(2) Å)[181] as well as Mg-N$_{amide}$ bond in complex **10** (1.959(4) Å), where TMP is terminally coordinated to Mg. Surprisingly, despite the numerous applications that TMP-based magnesium reagents have in organic synthesis, in particular within the area of deprotonative metallation,[53] as far as we can ascertain, **23** represents the first example of a β-diketiminate complex containing this utility amido functionality, not only of magnesium but indeed of any metal. Highlighting the large steric demands of the TMP ligand, a comparison of the bond angles around Mg denotes that those involving the nitrogen atom of this amido group [N2-Mg-N3, 134.97(6)º; N1-Mg-N3, 131.18(6)º] are considerably much more obtuse than the bite angle of the bidentate nacnac ligand [N1-Mg-N2 93.85(5)º]. In addition, it is noteworthy that TMP binds terminally to Mg since this can greatly affect the metallating ability of this compound. The importance of this terminal bonding mode has recently been highlighted by Mulvey *et al* as one of the critical aspects on the enhanced magnesiating power exhibited by Knochels "Turbo Hauser" base TMPMgCl·LiCl, since only one Mg-N bond needs to be broken to release the active base.[66]
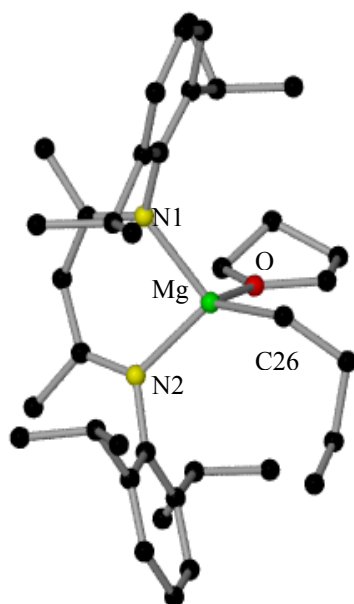
Fig 4.1: Molecular structure of **22** with hydrogen atoms omitted for clarity. Selected bond lengths (Å) and bond angles (º): *Mg1-N1 2.0657(14), Mg1-N2 2.0594(14), Mg1-O1 2.0544(12), Mg1-C26 2.1268(16), N1-Mg1-N2 92.96(5), O1-Mg1-N1 102.70(5), O1-Mg1-N2 101.10(5), N1-Mg1-C26 118.96(6), N2-Mg1-C26 126.35(7), O1-Mg1-C26 110.94(6).*
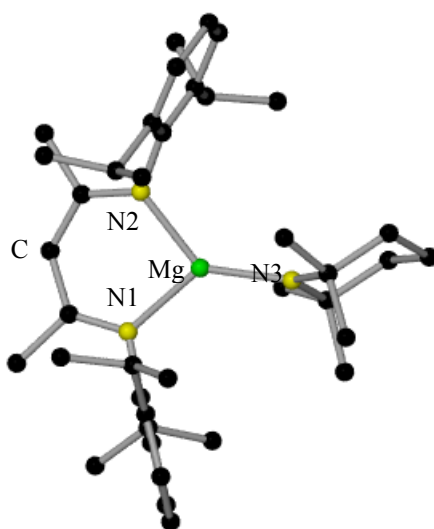
Fig 4.2: Molecular structure of **23** with hydrogen atoms omitted for clarity. Selected bond lengths (Å) and bond angles (º): *Mg1-N1 2.0451(13), Mg1-N2 2.0273(13), Mg1-N3 2.0451(13), N1-Mg1-N2 93.85(5), N2-Mg1-N3 134.97(6), N1-Mg1-N3 131.186.*

^{1}H and ^{13}C NMR spectroscopic analysis of **22** and **23** in C$_6$D$_6$ confirmed that their structures in the solid state are retained in C$_6$D$_6$ solution. Thus for the butyl derivative **22**, the ^{1}H NMR spectrum in C$_6$D$_6$ showed the relevant resonances for the ^{Dipp}nacnac ligand, along with two multiplets at 3.57 and 1.36 ppm for a molecule of THF (contrasting with the chemical shift observed for free THF in C$_6$D$_6$ appearing at 3.57 and 1.40 ppm suggesting that in solution THF is not coordinated) and four multiplets at 1.66, 1.47, 0.92, and -0.35 ppm for the Bu group (**Figure 4.3**). The CH_2 group directly bonded to Mg appears at -0.35 ppm in the ^{1}H NMR and at 4.99 ppm in the ^{13}C NMR spectrum. These chemical shifts are significantly upfield than those observed for MgBu$_2$ (at 0.07 ppm and 9.12 ppm in the ^{1}H and ^{13}C NMR respectively) but within a similar range to those obtained in sodium magnesiate **2**, -0.34 and 9.38 ppm respectively. For the amido complex **23**, the most distinct signal in the ^{1}H NMR spectrum is a singlet at 0.95 ppm (see **Figure 4.4**) which can be assigned to the α-Me groups of the TMP ligand, which appear slightly upfield than those observed for free TMP(H) at 1.06 ppm, and considerably downfield from those in sodium magnesiate complex **10** (1.40 ppm). The fact that a sole resonance is observed for the methyl groups of the TMP fragment suggest that in solution there must be free rotation about the Mg-N3 bond (even with the presence of the highly sterically demanding ^{Dipp}nacnac ligand chelated to Mg).
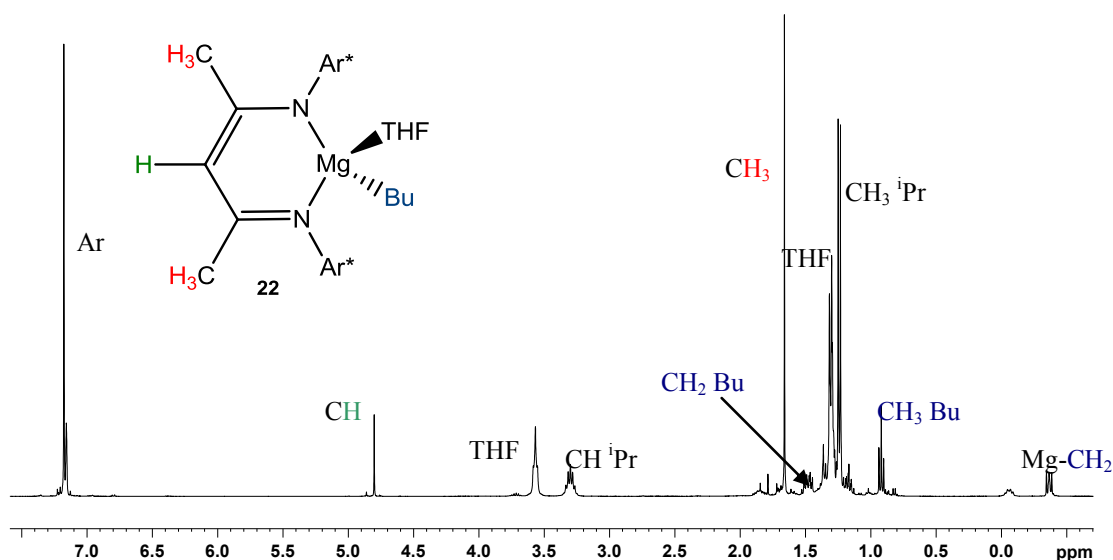
Fig 4.3:^{1}H NMR in C$_6$D$_6$ of [(^{Dipp}nacnac)Mg(Bu)(THF)] **22.**
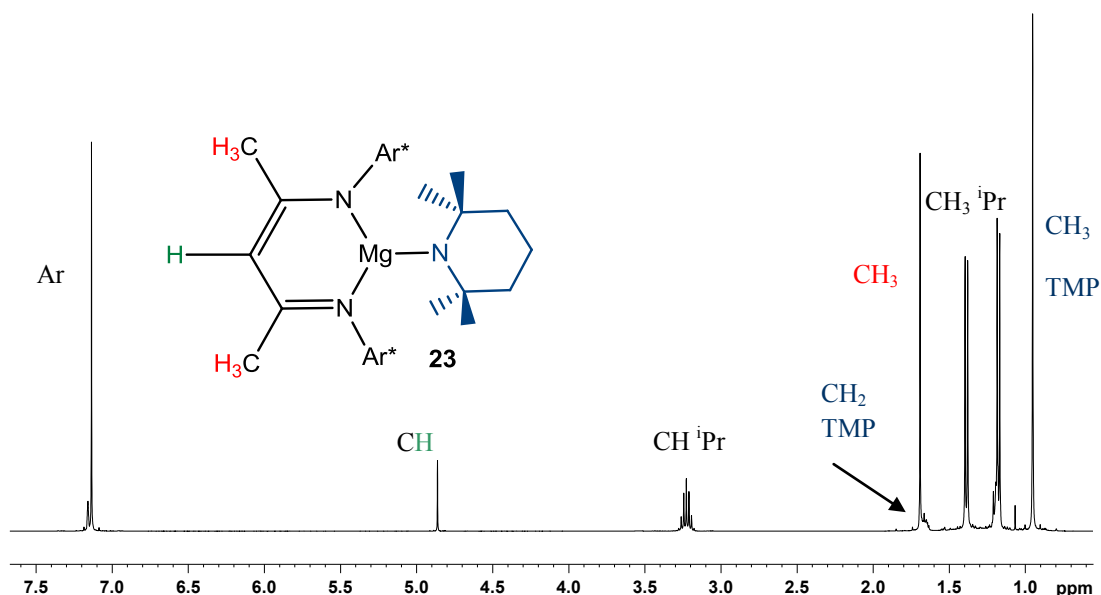
Fig 4.4: ^{1}H NMR in C_6D_6 of [(^{Dipp}nacnac)Mg(TMP)] **23**.

4.2.2 Reactivity with Benzoxazole

To probe the ability of **22** and **23** to act as bases towards 1.3-benzoazoles we first investigated their reactions with the parent benzoxazole (Boz) whose hydrogen at the C2 position is substantially more acidic, in pK_a terms (24.8, DMSO),[121] than those in benzothiazole (27.3, DMSO) or methylbenzimidazole (32.5, DMSO). The reaction of equimolar amounts of Boz and compounds **22** and **23** generated in each case a bright orange solutions which deposited a crop of yellow crystals of [(^{Dipp}nacnac)Mg{O(o-C_6H_4)NC}(THF)] **24** (**Scheme 4.5**), in a 50 and 55 % yield for **22** and **23** respectively. Complex **24** was characterised by both ^{1}H and ^{13}C NMR spectroscopy and X-ray crystallography.
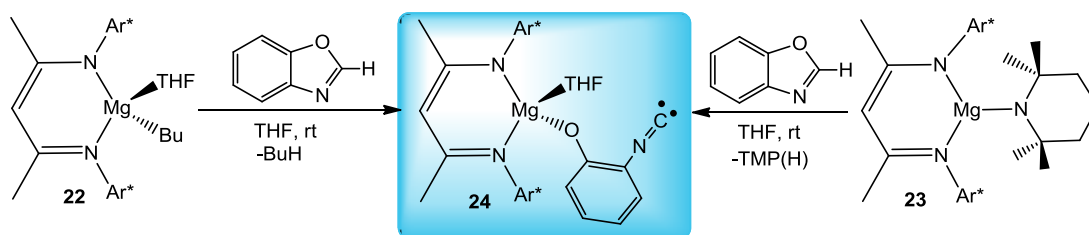
Scheme 4.5: Preparation of complex **24**.

X-ray crystallographic studies of **24** revealed the presence of an α-(isocyano)phenolate ligand, resulting from direct magnesiation of Boz by both **22**

and **23** followed by a ring opening reaction, which binds terminally to Mg through its oxygen atom (**Figure 4.5**). As a consequence of the generation of an isocyanide group the C-N bond distance (N2-C22 1.128(14) Å) is significantly shorter than that observed in the benzoxazole complex [ZnCl$_2$·(Boz$_2$)] (1.295(4) Å) which contains a molecule of Boz acting as a N-donor.[184] The β-diketiminate ligand and a molecule of THF complete the molecular structure of **24** giving Mg a distorted tetrahedral geometry overall. Although previous deprotonation studies of Boz by Mongin *et al* using the mixed metal species, LiMgBu$_3$ in THF, on the basis of NMR analysis, found that at room temperature the resulting 2-benzoxazoyl intermediate quickly isomerizes to its open α-(isocyano)phenolate form,[178] **24** is to the best of our knowledge the first ring opened intermediate to be trapped by Mg and structurally characterised. Boche *et al* have previously shown that when benzoxazole or oxazole are reacted with organolithium reagents the relevant lithiated species lies completely towards the formation of ring-opened species.[122] Thus for example attempts to trap 2-lithioxazoles with electrophiles usually afforded mixtures of the products of substitution at the C2 and C4 position, resulting from the reaction of the ring-open enolate form with the electrophile followed by its cyclization, even when the reactions are performed at -78°C.[122]
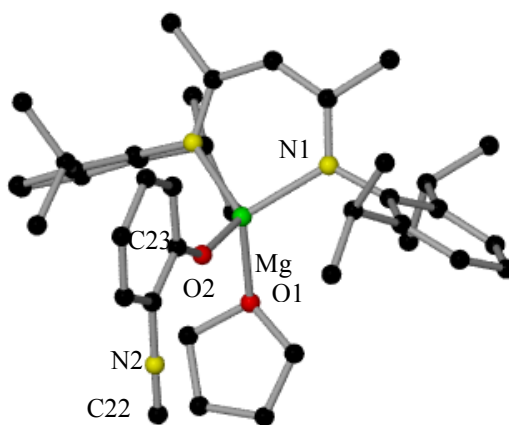
**Figure 4.5**: Molecular structure of **24** with hydrogens omitted for clarity. Selected bond lengths (Å) and bond angles (º): *Mg-O1 1.865(4), Mg-O2 2.016(4) Mg-N1, 2.033(3), O2-C23 1.462(5), N2-C22 1.128(14), O1-Mg-O2 95.43(18), O1-Mg-N1 118.79(12), O2-Mg-N1 114.89(11), N1-Mg-N1 95.58(18), O2-Mg-N1 114.88(11), O1-Mg-N1 118.79(2).*

^{1}H and ^{13}C NMR studies using deuterated THF as a solvent indicated that in solution **24** retains its solid state structure, without observing equilibration to its ring-closed isomer. As shown in **Figure 4.6** the ^{1}H NMR spectrum of **24** showed the presence of a single species in solution. The retention of the solid state structure in solution is mostly evidenced in the ^{13}C NMR by the presence of a signal at 118.02 ppm belonging to the phenolate β-C. There are also resonances at 168.90, 164.71 and 161.11 ppm, which are attributed to a quarternary *C* on the Ar* group, the phenolate α-*C* and the isocyanide *C* of the ring opened benzoxazole. These chemical shifts compare well with work published by Mongin where benzoxazole undergoes ring opening by LiMgBu$_3$ in THF at room temperature (164.5, 164.4 and 116.8 ppm for phenolate α-C, isocyanide and phenolate β-C respectively).[178]
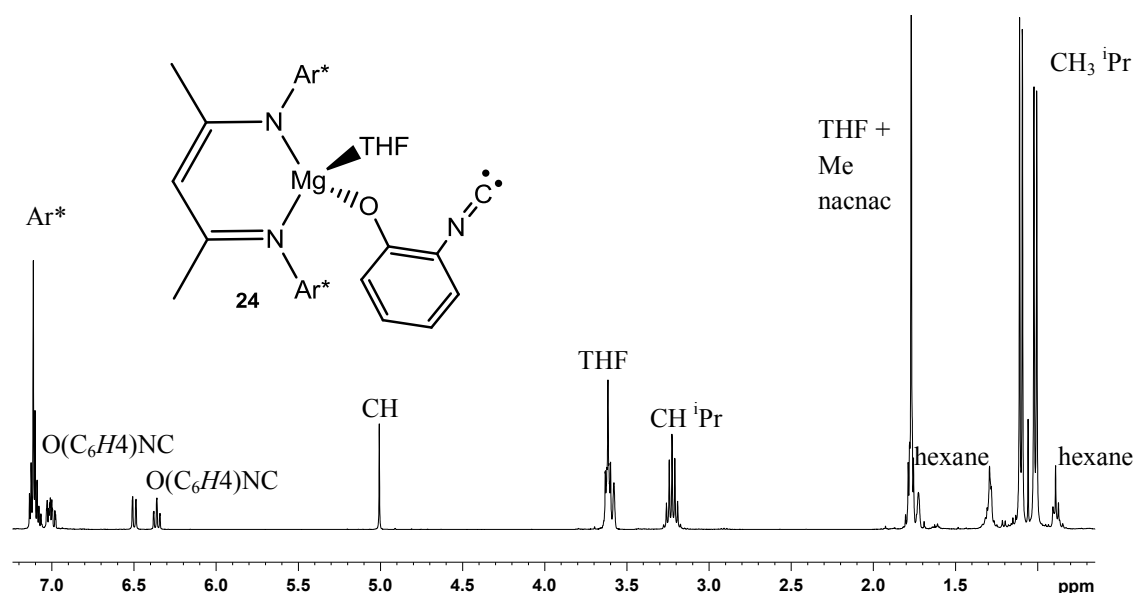
Figure 4.6: ^{1}H NMR of [(^{Dipp}nacnac)Mg{O(o-C$_6$H$_4$)NC}(THF)] **24**.

In addition, even when the spectra were recorded at low temperatures (-30°C) only complex **24** was present, suggesting that once the metalation has taken place, the cyclic intermediate, whose presence cannot be detected, rapidly undergoes complete ring opening to form acyclic **24**. As above mentioned, seminal NMR spectroscopy and X-ray crystallographic structural studies by Boche have shown that lithiated oxazoles exist in solution (even at temperatures as low as -105°C) as their acyclic isomers.[122] This can be rationalised in terms of the high oxophilic character of highly polar Li which should facilitate the cleavage of the C2-O bond. Supporting this hypothesis, the *in situ* transmetallation of these intermediates with ZnCl$_2$ leads to the formation of the relevant ring-closed zincated species (favoured by the significantly less polar and therefore more covalent character of the newly generated Zn-C bond),[122] which can then be subsequently exploited in organic transformations such as Negishi cross-coupling reactions.[122] On the view of these results, our studies suggest that magnesiated Boz behaves in a similar manner to its lithiated congener. Thus the marked affinity of Mg for coordination to an oxygen anion appears to dictate the final outcome of the reaction favouring the formation of α-(isocyano)phenolate complex **24**. Furthermore, the presence of the highly sterically demanding β-diketiminate ligand does not seem to have a measurable effect in the position of the equilibrium between the open and closed forms of this magnesiated Boz, which lies exclusively on the side

of the acyclic isomer even at lower temperatures with **24** being the only species that can be detected in solution.

4.2.3 Deprotonation of benzothiazole (Btz): magnesiation *vs* cascade activation

We next turned our attention to the sulphur congener Btz, for which the selective C2-metallation has been previously reported using magnesium-based reagents; although no structural authentification of the metallated intermediates involved have yet been forthcoming. Bearing in mind that in general magnesium amides exhibit an enhanced kinetic basicity compared to related alkyl Mg compounds,[119] we first studied the reactivity of TMP derivative **23** towards Btz. The room temperature 1:1 reaction in THF solution formed a deep red solution which deposited a crop of red crystals of [{(^{Dipp}nacnac)Mg(Btz*)}$_2$] **25** (Btz* = 2-benzothiazolyl) in an isolated yield of 43% (**Scheme 4.6**).
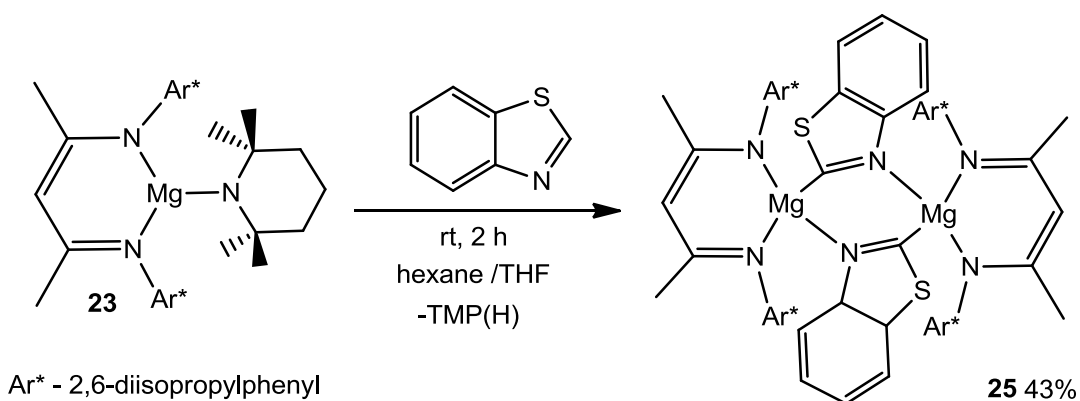
Scheme 4.6: Synthesis of complex **25**.

The centrosymmetric dimeric molecular structure of **25 (Figure 4.7)** confirmed the C2 magnesiation of Btz had taken place by featuring two {(β-diketiminate)Mg} fragments connected by two bridging benzothiazolyl (Btz*) fragments, which act as asymmetric bridges through their metallated carbon and nitrogen atoms (C7 and N3). This distinct coordination mode of the newly formed Btz* groups gives rise to the closure of a novel six-membered {MgCNMgCN} ring, which shares each Mg vertex with six membered metallacycles resulting from the chelating coordination of the nacnac ligand to Mg. The distorted tetrahedral geometry around Mg (bond angles ranging from 93.17(7) to 117.87(8)°; mean 109.56°) denotes an approximately orthogonal disposition of these fused six-membered rings. A close inspection of the

Mg-N3 (2.097(2) Å) and Mg-C7 (2.193(2) Å) bond distances in **25** shows that while the former is considerably shorter than the other Mg-N values reported for related β-diketiminate Mg compounds containing neutral nitrogen donors such as pyridine or picoline (e.g.; 2.174(3) and 2.213(4) Å),[146] the latter is slightly elongated compared to that in aryl compound [(nacnac)Mg(Ph)(OEt$_2$)] (2.139(3) Å) which also contains a *pseudo*-tetrahedral Mg bonded to an sp^2 hybridised carbon.[181] This coupled with the moderate but noticeable elongation of the N3-C7 and S-C7 bond distances and widening of the N3C7S bond angle of the Btz* rings (1.330(3), 1.743(2) Å and 110.57(15)° respectively) when compared with the values found in free benzothiazole (1.297(15), 1.722(13) Å and 116.28(9)°)[165] suggest that **25** can alternatively be described as a 3-(magnesium β-diketiminate)benzothiazol-ylidene dimer. In this regard, the structures of related lithiated and zincated thiazole compounds have been instructively described by Boche as (3-metallo-thiazol-2-ylidenes) by close comparison of the structural differences between these species and their parent thiazole molecules and those found between thiazolium salts and a thiazol-2-ylidene compound. Closely related to this work, Ruiz *et al* have recently reported the structure of a mixed Mn/Au complex where both metals are connected through a bridging thiazolyl unit coordinated asymmetrically to both metals in a similar manner to that found in **25**, by combining Mn-N and Au-C bonding. The authors interpret this compound as an N-metallated thiazo-2-ylidene carbene complex Au.[166] Consistent with this alternative description of **25**, its Mg-C distance (2.193(2) Å) is close to those witnessed in Mg-N heterocyclic carbene adducts (ranging from 2.200(2) to 2.288(5) Å)[127, 185-187] whereas its Mg-N3 bond (2.097(2) Å) is just marginally longer than the other two remaining Mg-N$_{nacnac}$ bonds present in the molecule (2.058(19) and 2.069(18) Å).
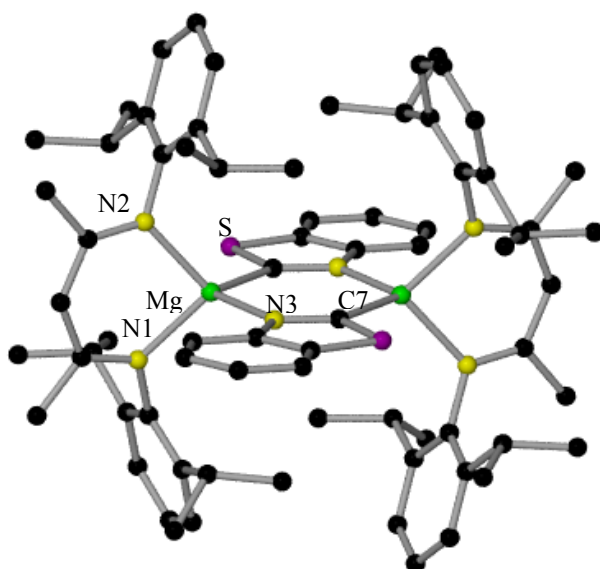
Figure 4.7: Molecular structure of **25** with hydrogens and hexane solvent molecule omitted for clarity. Selected bond lengths (Å)and angles (°): *Mg-N1 2.0587(19), Mg-N2 2.0969(18), Mg-C7 2.193(2), Mg-N3 2.097(2), N3-C7 1.330(3), C7-S 1.743(2), N3-Mg-N2 112.09(8), N3-Mg-N1 110.39(7), N10Mg-N2 93.17(7), N3-Mg-C7 106.52(8), N2-Mg-C7 116.51(8), N1-Mg-C7 117.87(8), S-C7-N3 110.57(15).*

Regarding analysis of the ^{1}H and ^{13}C NMR, spectroscopic investigations revealed that the solid state structure of **25** appears to be retained at room temperature in deuterated benzene solutions. Its ^{1}H NMR spectrum displayed four multiplets at 8.71, 7.66, 7.34 and 7.04 ppm for the hydrogens of the Btz* groups which appear slightly downfield of those present in Btz (corresponding values of 8.16, 7.50, 7.16 and 7.04 ppm). In addition, and consistent with **25** exhibiting a dimeric arrangement in solution, two separate multiplets at 4.01 and 2.54 ppm are observed for the CH's of the ^{i}Pr groups of the β-diketiminate ligand (**Figure 4.8**). The most diagnostic resonance in the ^{13}C NMR spectrum appears at 216.29 ppm for the C2 carbon of Btz* group. Showing a large downfield shift when compared with the C2 resonance observed in parent Btz (δ = 154.07 ppm), this signal is much closer to that observed for 3-(2,6-diisopropylphenyl)-4,5-dimethylthiazol-2-ylidene (δ = 254.2 ppm),[188] reflecting the moderate carbenic character of this C as previously discussed for the X-ray crystallographic studies and more importantly, characteristic of a ring-closed structure for the metallated benzothiazole groups in solution. Remarkably, both ^{1}H and [13]C

NMR spectra of **25** at room temperature displayed well-resolved sharp signals, with no resonances attributable to a ring-open α-(isocyano)phenylthiolate derivative (similar to **24**) detectable. This contrasts with previous solution studies for lithiated benzothiazole and 4,5-dimethylthiazole which show that even at lower temperatures (-35˚C) both ring opened and a ring-closed species co-exist in solution.[122] The remarkable room temperature solution stability of **25** is all the more surprising when considering that although metallated thiazoles have a much less pronounced tendency to undergo ring-opening than their parent oxazole derivatives, most of the reported synthetic procedures that involve the deprotonation of these heterocycles employing polar organolithium or organomagnesium reagents require the use of sub-ambient temperatures, suggesting that the presence of the sterically demanding β-diketiminate ligands present in **25** coupled with its rigid tricyclic dimeric structure must play an important role in conferring an enhanced stability to the newly generated $Mg-C_{Btz*}$ bonds, minimizing the competing ring-opening process. The stabilizing role of the β-diketiminate ligand is in sharp contrast with our previous studies using magnesium reagents supported on a different type of highly sterically demanding ligand, namely dianionic bis(amido)silyl ligand $\{Ph_2Si(NAr*)_2\}^{2-}$ (Ar*= 2,6-i-Pr_2-C_6H_3), where the initial deprotonation of Btz induces a cascade of reactions where the bis(silyl)amido acts itself as a base (**Scheme 4.2**) .
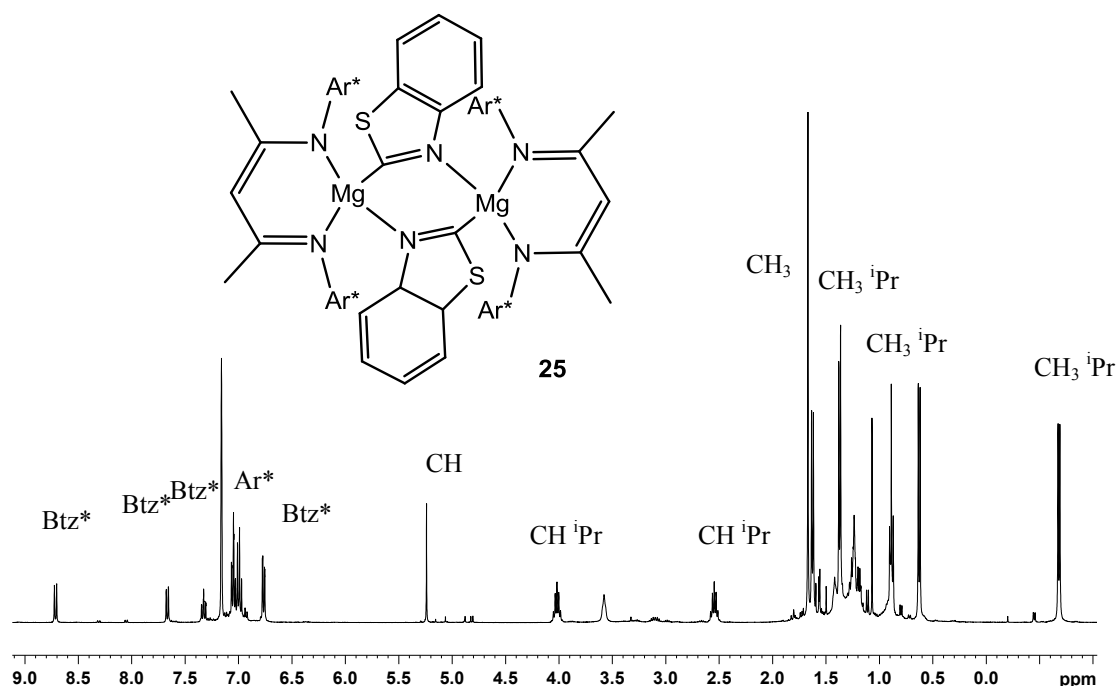
Figure 4.8: ^{1}H NMR in C_6D_6 of $[\{(^{Dipp}nacnac)Mg(Btz^*)\}_2]$ **25**.

Encouraged by the efficient and selective magnesiation ability of **23** towards Btz as well as the fact that conventional Grignard reagents can deprotonate this heterocycle at 0°C, we next decided to investigate the reactivity of the butyl magnesium β-diketiminate **22**. Thus, the addition of one molar equivalent of Btz to a solution of **22** in THF at room temperature is accompanied by a yellow to deep blue colour change. Freezer cooling of this solution afforded blue crystals of $[^{Dipp}nacnacMg\{(Btz^*)C(H)=N(2-C_6H_4-1-S)\}]$ **26** (Btz*= 2-benzothiazolyl) in an isolated yield of 23%, although when using two molar equivalents of Btz this yield increased to 58%, with ^{1}H NMR analysis of the filtrate showing the reaction is almost quantitative, **Scheme 4.7**.
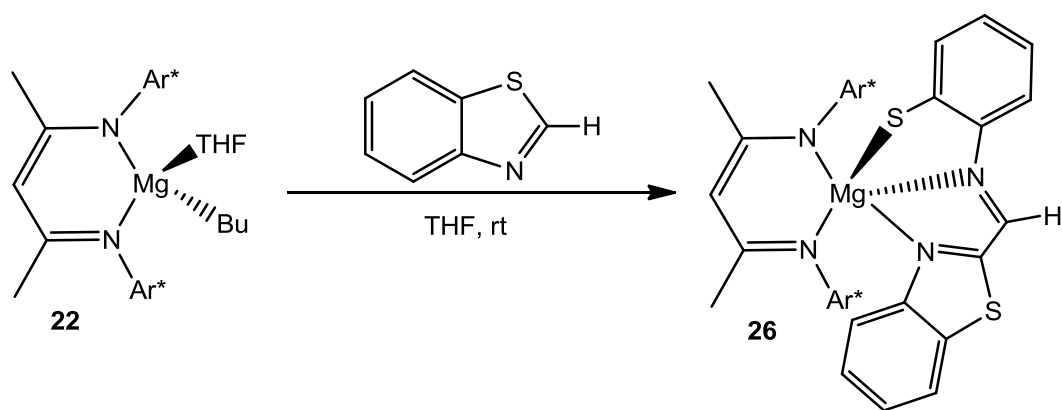
Scheme 4.7: Preparation of complex **26**.

Contrasting with the situation for **25**, X-ray crystallographic studies of **26** (**Figure 4.10**) unveiled the presence of a new monoanionic ligand **L'** (**Figure 4.9**), resulting from the activation of two molecules of Btz with a negative charge localized in one of the sulphur atoms (S1) (**Figure 4.9**).
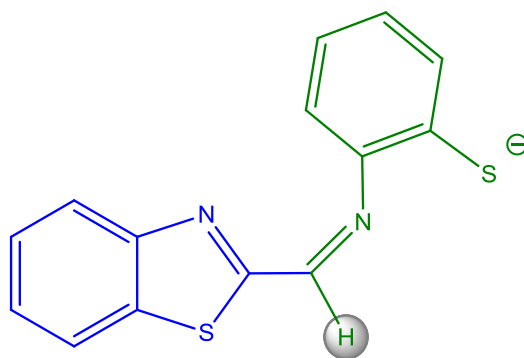
Figure 4.9: Newly formed monoanionic ligand **L'**.

From its constitution, it appears that one molecule of Btz has been deprotonated; whereas the other one retaining its hydrogen atom undergoes ring-opening (**Figure 4.10**). Coordinating to Mg in a κ^3-S, N, N fashion (involving S1, N1 and N2, (**Figure 4.10**), **L'** can be envisaged as a phenyl thiolate tethered 1,4-butadiazadiene with one of its N=C units being part of the Btz* ring. This tridentate coordination mode gives rise to the formation of two five-membered rings fused through the Mg-N1 bond (2.211(3) Å). Whereas the Mg-S distance (2.4731(14) Å) in **26** lies in the range exhibited by other magnesium thiolate complexes,[189] both Mg-N$_\text{L'}$ distances (2.211(3) and 2.346(3) Å) are significantly elongated when compared with the Mg-

N$_{Btz*}$ distance in **25** (2.097(2) Å) which can be attributed to a combination of the higher pentacoordinated environment of Mg in **26** as well as the partial amide character of the N present in **25** (*vide supra*).
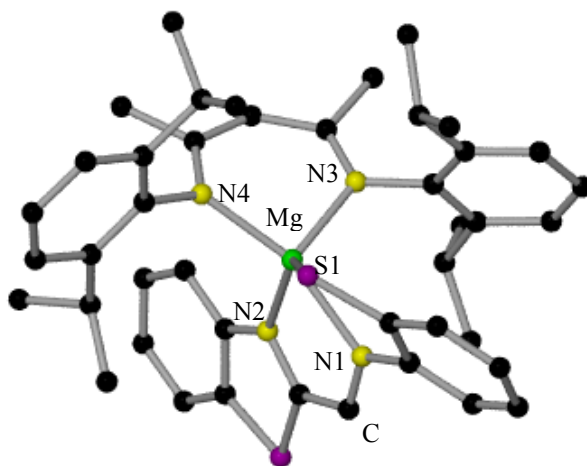
Figure 4.10: Molecular structure of **26** with hydrogens omitted for clarity. Selected bond lengths (Å) and bond angles (º): *Mg-S1 2.473(14), Mg-N2 2.346(3), Mg-N4 2.076(3), Mg-N1 2.211(3), Mg-N3 2.063(3), S1-Mg-N1 78.02(8), S1-Mg-N3 114.08(10), N1-Mg-N2 73.02(11), 153.80(13), N2-Mg-N4 99.39(12), S1-Mg-N2 142.31(9), S1-Mg-N4 96.01(10), N1-Mg-N3 113.45(14), N2-Mg-N3 99.46(12), N3-Mg-N4 92.37(13).*

All the anticipated distinct hydrogens within **L'** are accounted for and well resolved in the ^{1}H NMR spectrum of **26** in C$_6$D$_6$ solutions and they can be easily assigned by a combination of ^{1}H-^{1}H COSY and ^{1}H-^{13}C HSQC experiments (see Experimental Section for full details). Those resonances belonging to the aromatic hydrogens of Btz* 9.03, 7.28 (2H) and 6.98 ppm respectively (highlighted in blue in **Figure 4.11**), which are significantly more downfield than the aromatic hydrogens of the thiolate fragment at 7.58, 6.72, 6.35 and 6.09 ppm (highlighted in green in **Figure 4.11**). A singlet at 6.98 ppm for the C*H* group bonded to C$_\alpha$ Btz* completes the assignment of **L'**. Similarly, the ^{13}C NMR spectrum can also be assigned, with the most diagnostic signals appearing at 145.01 and 168.21 ppm for the C*H*=N and for the C$_\alpha$ carbon of the Btz* ring respectively.
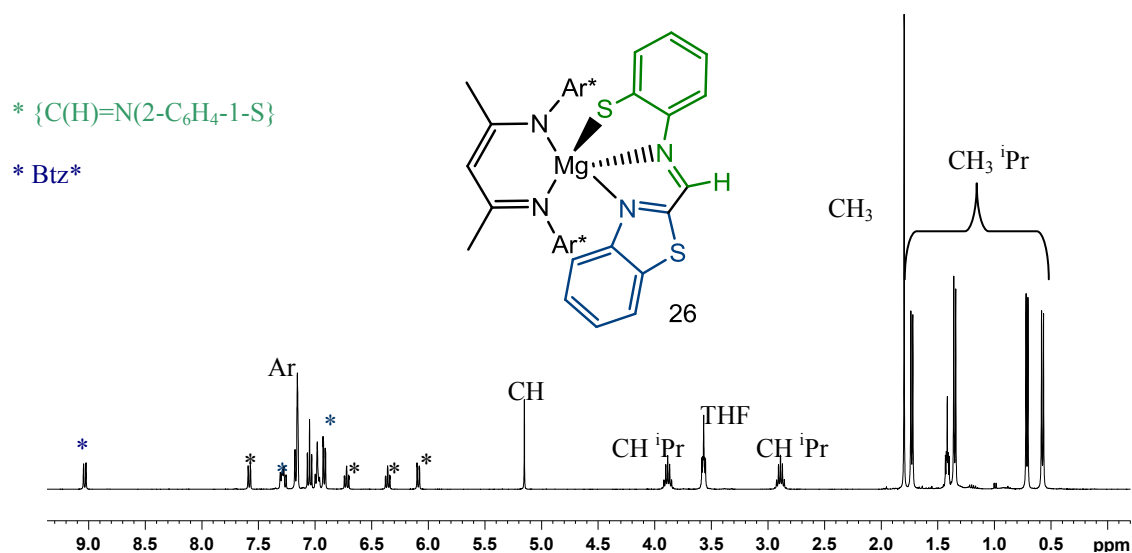
Figure 4.11: ^{1}H NMR of [(^{Dipp}nacnac)Mg{(Btz*)C(H)=N(2-C$_6$H$_4$-1-S)}] **26**.

A plausible explanation for the formation of **26** is depicted in **Scheme 4.8**. At room temperature butyl-base **22** can magnesiate Btz, though this reaction must be significantly slower than when TMP-base **23** is employed, as it involves the cleavage of a more kinetically stubborn Mg-C$_{Bu}$ bond.[119] This retardation translates into the formation of some β-diketiminate Mg-Btz* species which will coexist in the solution with some unreacted Btz molecules. This scenario switches on an alternative reaction pathway for the remaining free Btz, which can coordinate as a neutral N-donor ligand to the Mg centre (akin to the role of THF in **22**) of the benzothiazolyl species (step a, **Scheme 4.8**),[190] facilitating its intramolecular nucleophilic attack at the C2 position by the Btz* unit which generates a new C-C bond with concomitant dearomatization of the Btz molecule (step b, **Scheme 4.8**). This proposed intermediate can then undergo ring-opening of the non-aromatic ring through cleavage of its C-S bond (step c, **Scheme 4.8**) to form **26** as the final product of the reaction.

133
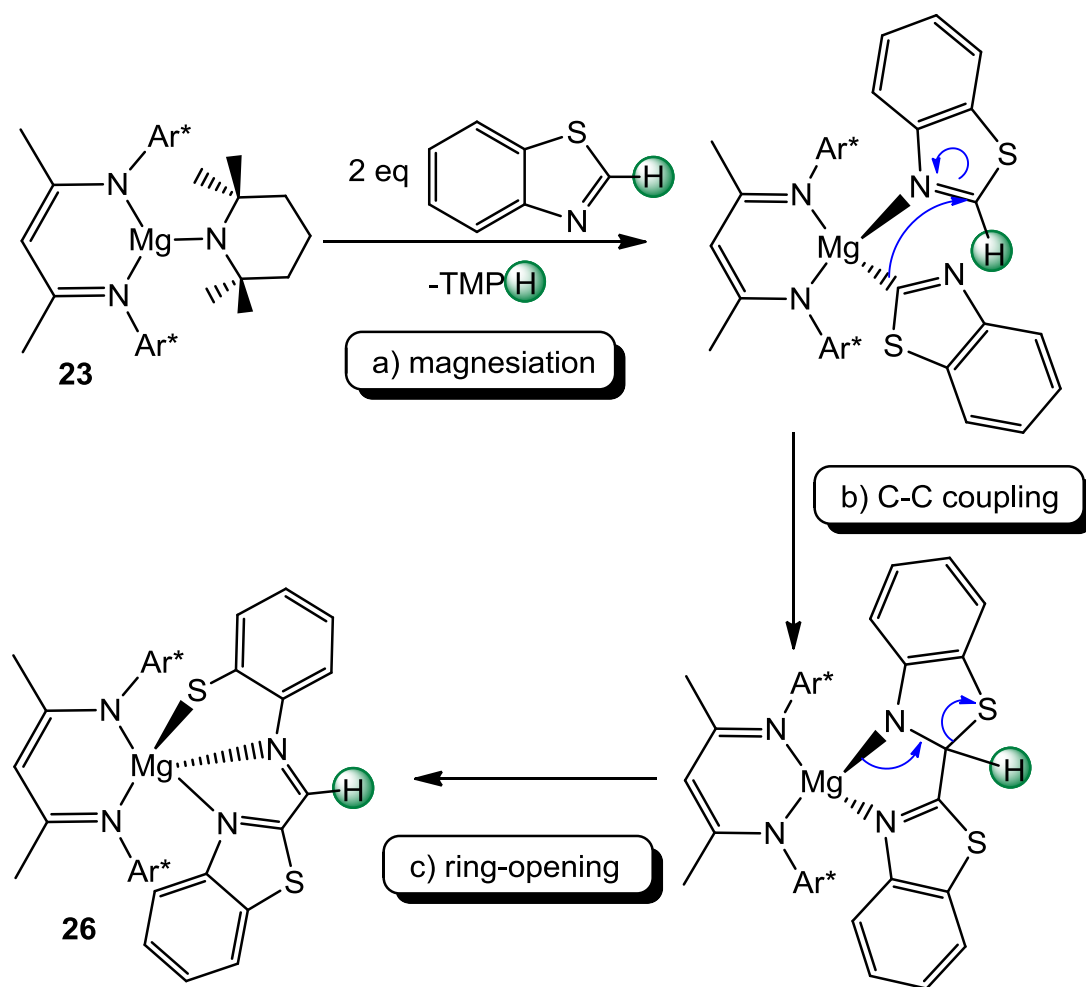
Scheme 4.8: Proposed mechanism for formation of complex **26**.

This proposed cascade process shown in **Scheme 4.8** is supported by ^{1}H NMR monitoring studies of the reaction of isolated crystals of benzothiazolyl species **25** with one molar equivalent of Btz in deuterated benzene which revealed the instantaneous formation of **26** (**Scheme 4.9**), suggesting that the reaction rate of the magnesiation step is key to enable this alternative domino of intramolecular reactions. To elaborate, using the kinetically activated TMP-base **23**, the deprotonation of Btz occurs very rapidly, and therefore the use of equimolar amounts of the starting materials leads to the isolation of the stable benzothiazolyl compound **25**.
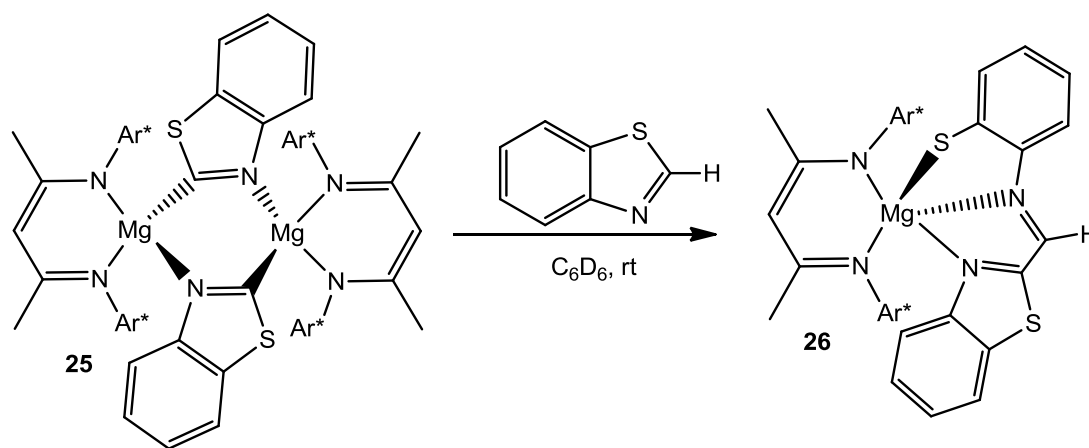
Scheme 4.9: Reaction of complex **25** with one molar equivalent of Btz in C_6D_6.

Alternatively, when an excess of Btz is employed (two molar equivalents), a situation mimicking that when equimolar amounts of butyl compound **22** and Btz are confronted arises. That is to say the presence in solution of Mg-benzothiazolyl units with free Btz can then follow the reaction pathway postulated in **Scheme 4.8**.

Furthermore, as earlier mentioned, we have recently reported the novel activation of Btz by sodium-magnesiate $[\{Na(THF)_6\}^+\{(Ph_2Si(NAr^*)_2)Mg(Bu)(THF)\}^-]$ **2** which leads to the isolation of a novel mixed-metal species containing fragment **L**. Although in this case a more complex process with more steps is involved, since **L** is made of three molecules of Btz which have been deprotonated, the initial three steps of the cascade mechanism proposed to rationalize its formation are the same as in **L'**. Thus, by using the β-diketiminate stabilised magnesium complexes **22** and **23**, new light has been shed on the constitution of the putative intermediates involved in these novel room temperature cascade activations of Btz where the initial magnesiation initiates a domino reaction of C-C coupling of the heterocyclic rings and a ring-opening reaction. In addition, these results not only provide further support for the mechanism proposed earlier but also highlight the wider generality of this type of process. Although this type of activation is unprecedented in magnesium chemistry, these results are related to the reactivity exhibited by d^0f^n metal alkyl complexes (M= Sc, Y, Lu and U) supported by a 1,1'-ferrocenylene bis(amide) ligand which can promote ring opening reactions of methyl-imidazole, involving C-H activation of the heterocycle, followed by C-C coupling reactions.[135]

Hydrolysis of **26** (prepared *in situ* by reaction of **22** with two molar equivalents of Btz) followed by oxidation with TEMPO furnished bis(benzothiazole) in a 72% yield (**Scheme 4.10**). This novel, atom efficient, synthetic route to prepare bis(benzothiazole) under mild reaction conditions, (room temperature, stoichiometric amount of Mg base, short reaction times) contrasts with previous approaches which require the use of transition metal catalysis along with longer reaction times and higher temperatures.[191] Furthermore the isolation and structural characterisation of species **25** and **26** provide essential clues that help to rationalise the formation of bis(benzothiazole). Thus, diverging from transition-metal catalysed C-C bond formation methodologies by C-H activation of 1,3-azoles,[192] here we disclose another feasible approach for the synthesis of bis(thiazoles) based on a novel sequential magnesiation, C-C coupling, ring-opening and oxidation reaction step mechanism.
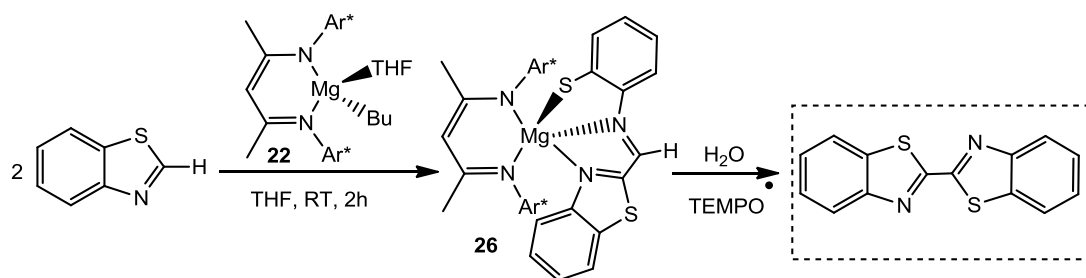
Scheme 4.10: Mg-mediated synthesis of bis(benzothiazole).

4.2.4 Deprotonation of N-methylbenzimidazole: magnesiation *vs* coordination

To conclude this systematic study, the reactions of magnesium bases **22** and **23** with methylbenzimidazole (MeBIm) were also probed. Interestingly, it should be noted that despite the limited information available on the real constitution of C2-metallated imidazoles, recent studies on d-block chemistry have revealed that the deprotonation of these heterocycles when coordinated to transition metal complexes using potassium bases followed by electrophilic quenching with methyl triflate has led to the isolation of novel NHC complexes as well as novel activation processes involving the C-N cleavage of other N-heterocyclic molecules such as imidazoles and bipyridines. [193]

Our studies show contrasting reactivities for compounds **22** and **23**, thus while the TMP-base **23** is able to promote the direct magnesiation of MeBIm at the C2 position to generate [{(^{Dipp}nacnac)Mg(MeBIm*)}$_2$] **27** (MeBIm* = N-methylbenzimidazolyl) the constitution of which has a strong resemblance to that of Btz metallation product **25**, the Bu derivative **22** is inert towards the reaction, even under refluxing conditions, leading to the isolation of MeBIm adduct [(^{Dipp}nacnac)Mg(Bu)(MeBIm)] **28**, resulting from the substitution of the THF molecule coordinated to Mg in **22** by a molecule of MeBIm (**Scheme 4.11**). Compounds **27** and **28** can be isolated as crystalline solids in 57 and 43% yields respectively and have been characterised by X-ray crystallography and NMR spectroscopic techniques.
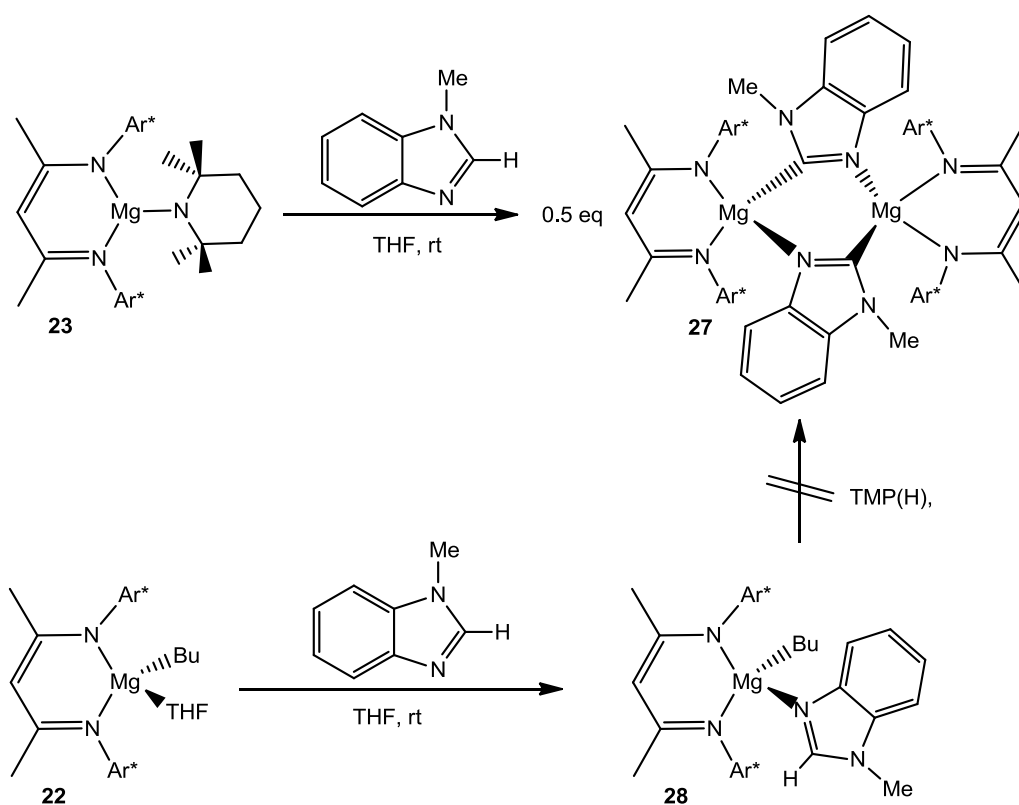
Scheme 4.11: Reactivity of MeBIm with **22** and **23**.

Structural analysis of **27** was complicated by disordered hexane solvate molecules and by generally weak diffraction intensities, however, after multiple attempts the model shown in **Figure 4.12** was obtained and this unambiguously shows the atomic connectivity and other essential structural features. Similarly to **25**, dinuclear **27** displays a centrosymmetric structure comprising two {(β-diketiminate)Mg}

fragments where the Mg atoms are doubly bridged by two anionic 2-N-methylbenzimidazolyl (MeBIm*) ligands, which coordinate asymmetrically through one of their nitrogens and the carbon that has experienced the deprotonation (N1 and C30 respectively in **Figure 4.12**), forming a {MgCNMgCN} six-membered ring. Unfortunately the intrinsic inaccuracy associated to this structure precludes a meaningful comparison of its geometrical parameters with those of **25** in order to assess the carbene character of the MeBIm* anion present in **27**. Furthermore, the relatively simple structure of **27** contrasts with the much more complex supramolecular scaffolding displayed by the product of the reaction of 1-methyl-4-*tert*-butylimidazole with methyllithium, which comprises 16 lithium atoms and 8 imidazolyl anions combined with 2 oxo and 4 alcoxy ligands anions, with the oxygen-based anions formed as a result of the partial degradation of the ethereal solvents by the organolithium reagent employed.[122]
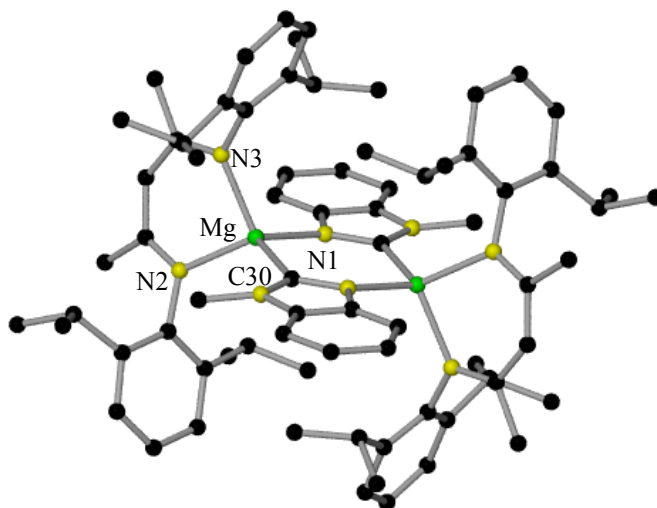
Figure 4.12: Molecular structure of **28** with hydrogen atoms omitted for clarity.

NMR studies of lithiated N-alkyl imidazoles have revealed that while 2-lithio-N-methyl imidazole stays in d8-THF solution exclusively as its ring-closed form, at temperatures as high as 60°C, at room temperature parent 2-lithio-N-methyl benzimidazole undergoes partial ring-opening. ^{1}H and ^{13}C NMR investigations of **27** in deuterated benzene solutions indicate, that similarly to **25**, its dimeric constitution is retained, without observing an equilibrium with its ring opened isomer. Thus the ^{1}H NMR spectra of **27** shows four multiplets at 8.27, 7.26, 7.11, and 6.85 ppm for the

aromatic protons of the Me-benzimidazolyl unit (at similar chemical shifts to those observed for MeBIm at 8.04, 7.22-7.16 and 6.91 ppm). The CH_3 of the Me-benzimidazolyl unit (3.75 ppm) is significantly downfield in shift from MeBIm (2.52 ppm), but in a similar region as was displayed in complex **14** (3.51 ppm). Thus the ^{13}C NMR of **27** displayed 15 well-resolved resonances in the aromatic region, 8 of which can be assigned to the β-diketiminate ligand, while the remaining 7 belong to the MeBIm* ring, including an informative signal at 192.93 ppm which can be assigned to the C2 bonded to Mg. Interestingly although this chemical shift compares well with that previously reported for the C2 of an alpha-magnesiated N-methyl indole species (181 ppm),[124] it is also close to that exhibited for the carbene C of the N-heterocyclic carbene adduct $^{n}Bu_8Mg_4 \cdot 2IPr$ (IPr= 1,3-bis-(2,6-diisopropylphenyl)imidazol-2-ylidene) (197.3 ppm),[127] hinting at a similar carbene character for **27** to that discussed for **25**. Remarkably when **27** was treated with an extra equivalent of MeBIm no reaction was observed, even when the mixture was heated under reflux for two hours which contrasts with the room temperature activation of Btz when one molar equivalent of this heterocycle is added to **25** which leads to isolation of **26** (*vide infra*).

Also diverging from the reactivity observed towards Btz, when butyl compound **22** is confronted with MeBIm the formation of the adduct [(^{Dipp}nacnac)Mg(Bu)(MeBIm)] **28** takes place. X-ray diffraction analysis shows that **28** is isostructural with precursor **22**, where now Mg is bonded to a molecule of MeBIm acting as a nitrogen donor (**Figure 4.13**). Although there are other examples in the literature containing N-alkyl imidazoles coordinated to Mg centres, the closest precedent to **28** is the pyridine (py) complex [(^{Dipp}nacnac)Mg(Bu)(py)] recently reported by Hill which in the presence of $PhSiH_3$ at 60°C promotes the dearomatization of py by a hydride transfer.[146]
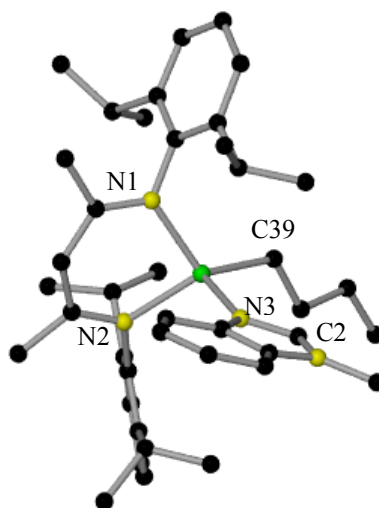
Fig 4.13: Molecular structure of **28** with hydrogens omitted for clarity. Selected bond lengths (Å) and bond angles (°): *Mg1-N1 2.078(2), Mg1-N2 2.070(2), Mg1-N3 2.144(2), Mg1-C39 2.090(3), N1-Mg1-N2 91.74(9), N2-Mg1-N3 106.48(9), N1-Mg1-N3 106.90(9), N1-Mg1-C39 120.40(6), N2-Mg1-C39 125.10(8), N3-Mg-C39 104.60(11)*

The Mg-C_{butyl} distance in **28** is slightly shorter (2.090(3) Å) than that found for **22** (2.1268(16) Å), whereas the Mg-$N_{benzimidazole}$ (2.144(2) Å) bond distance is similar to that found in the related Mg complex [(^{Dipp}nacnac)Mg(Bu)(NC$_5$H$_5$)] (2.174(3) Å) recently reported by Hill.[146] To the best of our knowledge this is the first example of a structurally defined complex where MeBIm is acting as a donor through its lone pair on the N to a Mg centre. Furthermore, a search in the CSD showed only ten hits for complexes containing MeBIm as a N-donor ligand, where the metal involved is either Zn[194] or Ln.[195] Taking into consideration the relatively high acidity of the C2-hydrogen of MeBIm (pK_a = 32.5)[121] and the close proximity of the Bu group to this H in **27** (N(3)-C(39) 3.350 Å), it is surprising that no deprotonation of the heterocycle occurs even when the mixture is left to stir at room temperature overnight or heated under reflux conditions for one hour, which illustrates the poor kinetic basicity of the Bu group in compounds **22** and **27**.

^{1}H and ^{13}C NMR spectroscopic studies confirmed that in C$_6$D$_6$ solution MeBIm remains coordinated to the Mg fragment, as evidenced by the different chemical shifts observed for the Me and C2-*H* groups of the heterocycle in **28** (at 2.63 and

7.92 ppm and 30.03 and 145.23 ppm in the ^{1}H and ^{13}C NMR spectra respectively), when compared with those observed for free MeBIm (2.52 and 8.05 ppm and 28.75 ppm and 142.78 ppm in the ^{1}H and ^{13}C NMR spectra respectively). A significant change is also observed in the ^{1}H NMR spectrum for the Mg-CH_2 group in **28** (-0.10 ppm) in comparison with that found for **22** (-0.35 ppm) which suggests the Mg-C bond in **28** is somehow less polarised.

In order to determine if the metallation of MeBIm could be carried out using only a catalytic amount of TMP(H) along with the β-diketiminate butyl species [(^{Dipp}nacnac)Mg(Bu)(THF)] **22**, the reaction of **22** with MeBIm in the presence of 10 mol % of TMP(H) was performed in a NMR tube using C$_6$D$_6$ as a solvent. After one hour the ^{1}H NMR spectrum of this solution showed the formation of aforementioned complex **27** along with unreacted TMP(H) and some unreacted complex **22**. This observation indicates that under these reaction conditions the formation of **22** is more favoured than the aminolysis reaction of **22** with TMP(H) to yield **27**. Furthermore, even when **22** was treated with TMP(H) in THF under refluxing conditions (65°C), TMP derivative **23** could not be detected which shows that the lack of reactivity of **22** towards the amine TMP(H) inhibits a possible TMP(H) catalysed deprotonation of MeBIm.

4.3.1 Conclusions

To summarise **chapter 4** two new β-diketiminate magnesium complexes [(^{Dipp}nacnac)Mg(Bu)(THF)] **22** and [(^{Dipp}nacnac)Mg(TMP)] **23**, have been synthesised and fully characterised. Exploring their reactivity towards 1,3-benzoazoles we found that while TMP derivative **23** is capable of α-deprotonating Btz and MeBIm in almost quantitative yields at room temperature, to yield complexes **25** and **27**. These represent the first examples of direct magnesiation of 1,3-benzoazoles to be structurally defined; butyl complex **22** is not kinetically reactive enough to metallate these heterocycles leading to the formation of complexes **26** and **28**. While **26** is the product of an activation process of two molecules of Btz, **28** is the product of coordination of MeBIm to the butyl precursor. Complex **26** can also be prepared by reacting benzothiazolyl species **25** with an equivalent of Btz, and this sheds new light on the mechanisms involved in the

cascade activation of Btz mediated by $[\{Na(THF)_6\}^+\{(Ph_2Si(NAr*)_2)Mg(Bu)(THF)\}^-]$ **2** described in **Chapter 3**. Furthermore hydrolysis of **26** followed by oxidation with radical TEMPO led to the isolation of bis(benzothiazole) in a 72% yield unveiling a new method to prepare this compound which contrasts with previous transition-metal catalysed methodologies.

Similarly to complex $[\{Na(THF)_5\}_2^+\{(Ph_2Si(NAr*)_2)Mg(MeBIm*)\}_2^-]$ **14**, analysis of structural and spectroscopic data suggest that benzoazolyl units in complexes **25** and **27** exhibit a marked carbenic character, which may be responsible for the formation of dimeric structures.

When the reactions of **22** and **23** with Boz were investigated complex **24** was obtained in both cases, showing that the ring-opening of benzoxazolyl anion is preferred.

Chapter 5: Hydroamination reactions of organic heterocumulenes catalysed by sodium magnesiates

5.1.1 Introduction

As mentioned before in **Chapter 1**, alkali-metal magnesiates can act as powerful nucleophiles in synthesis allowing for example the chemoselective alkylation of ketones under very mild reaction conditions.[196] Taking advantage of this feature, in **Chapter 5** we will assess the ability of sodium magnesiates to participate as catalysts in the hydroamination reactions of organic heterocumulenes RN=C=X (X=O, NR). Focusing on isocyanates (RN=C=O) and carbodiimides (RN=C=NR), the catalytic hydroamination of these unsaturated organic electrophiles is an efficient process to synthesise ureas and guanidines respectively, with both types of molecules being of great importance in organic chemistry. Ureas find a multitude of applications not only in agriculture playing a major role in the preparation of fertilisers,[197] but also in the pharmaceutical industry (i.e. for dermatological treatments)[198] and in material science as constituents of many plastics and textiles.[199] Although the stoichiometric hydroamination of some isocyanates with nucleophilic amines can be achieved, (usually harsh reaction conditions are required of high temperature and long reaction times),[200, 201] there has been very little work done carrying these reactions out catalytically using metal complexes. Thus, lanthanide(III) amides have been shown to undergo insertion reactions with isocyanates under stoichiometric conditions to form metal ureido complexes, however this has not yet been applied catalytically.[202] Contrastingly, a number of f-block,[221] and s-block complexes such as sodium naphthalene and sodium benzophenone ketyl, have been known to carry out the catalytic polymerisation of isocyanates.[203-205] An important breakthrough in this area has been the use of calcium amide complexes supported by the bulky β-diketiminate ligand nacnac, which has enabled the catalytic hydroamination of sterically demanding 1-adamantylisocyanate with diphenylamine (**Scheme 5.1**).
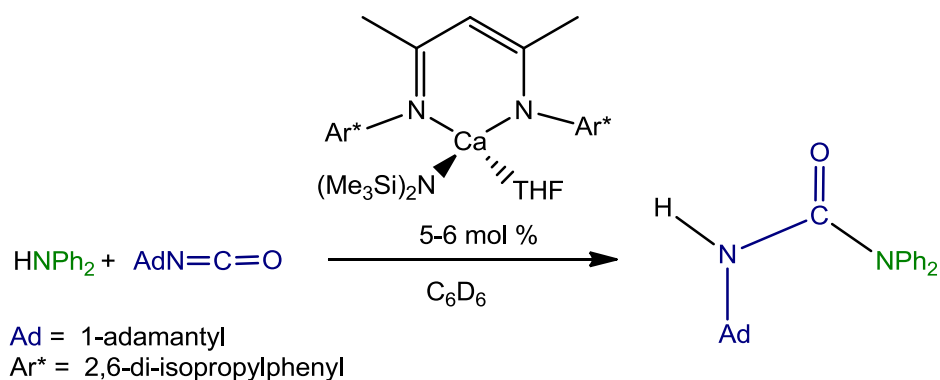
Scheme 5.1: 1-adamantylisocyanates catalysed by [{Ar*NC(Me)CHC(Me)NAr*}Ca{N(SiMe$_3$)$_2$}(THF)]].

This methodology developed by Hill *et al* allowed the synthesis of ureas derived from highly hindered isocyanates, 1-adamantyl-isocyanate and 2, 6-di-isopropylphenylisocyanate using the amine NHPh$_2$ in yields from 48-93% in temperatures ranging from 25 to 60$^{\text{o}}$C over 2-3 hours.[18] Likewise, Hill *et al* have also used heavier alkaline-earth metal amides [M{N(SiMe$_3$)$_2$}$_2$(THF)$_2$] (M = Ca, Sr and Ba) to carry out the catalytic hydroamination of carbodiimides with anilines to yield the corresponding guanidines (**Scheme 5.2**).[12]
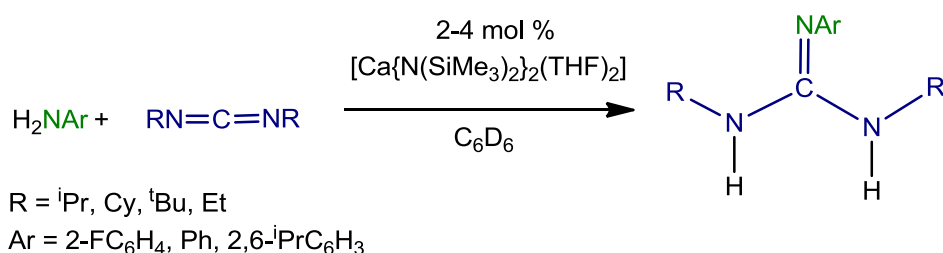
Scheme 5.2: Carbodiimides catalysed by [Ca{N(SiMe$_3$)$_2$}$_2$(THF)$_2$].

Guanidines are key ancillary ligands in preparing a variety of metal complexes.[13] They also appear as a common functional group in many biologically relevant molecules and pharmaceuticals.[14] Uncatalysed direct addition of primary amines to carbodiimides can be carried out, however high temperatures and long reaction times are often required, furthermore aromatic and secondary amines do not react even under these harsh conditions.[206] Stoichiometric studies by Chang *et al* have demonstrated that when Mg(N$^{\text{i}}$Pr$_2$)$_2$ is reacted with two equivalents of 1,3-diisopropylcarbodiimide in THF the insertion reaction occurs generating the

mononuclear guanidinate complex $[Mg\{(^iPrN)C(=N^iPr)(N^iPr_2)\}_2(THF)]$ although, a long reaction time of twelve hours is required (**Scheme 5.3**).
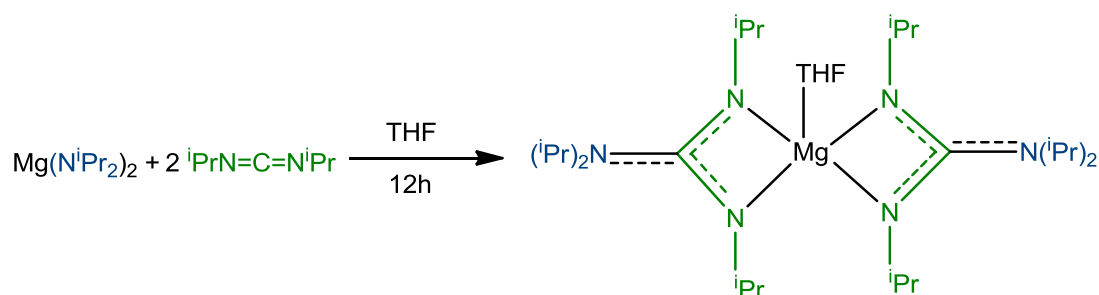
Scheme 5.3: Insertion of $Mg(N^iPr_2)_2$ into 1,3-diisopropylcarbodiimide.

A survey of the literature revealed only a handful of examples of catalytic hydroamination of carbodiimides. **Table 5.1** compares their reaction conditions as well as conversions.

Catalyst	Yield (%)	Temp (^oC)	Time (h)	Catalyst (mol %)
$[Ca\{N(SiMe_3)_2\}_2(THF)_2]$[12]	55-91	25	0.1-12	2-4
$[\{(N^iPr)C(=N^iPr)(Me_2N)\}_2Ti=N(2,6-Me_2C_6H_3)]$[207]	47-92	105	5	5
$[\{(Ar*N)C(=NAr*)(N^iPr_2)\}AlMe_2]$[208]	84-99	25	0.5-1	1
BuLi[209]	20-99	25-50	0.5-5	1.5
Bu_2Mg[209]	21-99	50	0.5-5	1.5
$ZnEt_2$[209]	41-99	25-120	0.5-16	1.5
$[\{Me_2Si(C_5Me_4)(NR')\}Ln-(CH_2SiMe_3)(THF)_n]$[210]	99	80	1-5	1.5-3

Table 5.1: General reaction conditions for various metal catalysts for the insertion reaction of carbodiimides with amines to generate the guanidines.

Transition metal complex $[\{(N^iPr)C(=N^iPr)(Me_2N)\}_2Ti=N(2,6-Me_2C_6H_3)]$ cataylses the hydroamination reaction of a series of primary aromatic amines with carbodiimides, $R^1N=C=NR^2$ (where $R^1=^iPr$ and $R^2 = ^iPr$ or Cy), however this methodology is not compatible with secondary aromatic amines since they fail to regenerate the M=N imido functionality present in the catalyst (**Scheme 5.4**).[207]
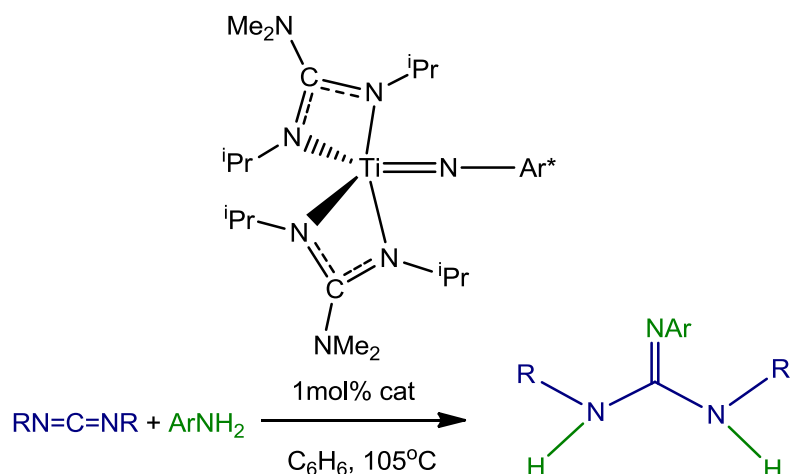
R = ^{i}Pr or Cy
Ar = $C_6F_5NH_2$, 2,6-$Me_2C_6H_3NH_2$ of p-$MeOC_6H_4NH_2$
Ar* = 2,6-$Me_2C_6H_3$

Scheme 5.4: [{(N^{i}Pr)C(=N^{i}Pr)(Me$_2$N)}$_2$Ti=N(2,6-Me$_2$C$_6$H$_3$)] as a catalyst in the hydroamination reaction of carbodiimides.

Shedding some light on the active species involved in this catalytic transformation an intermediate of the reaction of [{(N^{i}Pr)C(=N^{i}Pr)(Me$_2$N)}$_2$Ti=N(2,6-Me$_2$C$_6$H$_3$)] with ^{i}PrN=C=N^{i}Pr has been trapped and structurally characterised, showing the insertion of ^{i}PrN=C=N^{i}Pr in the Ti-arylimido bond generating a new bidentate dianionic guanidinate ligand. This titanium complex allowed the synthesis of several guanidines in good yields ranging from 47-91%, however the high reaction temperature of 105°C and relatively long reaction times of five hours were required. Similarly, Bergmann *et al* used [{(Ar*N)C(=NAr*)(N^{i}Pr$_2$)}AlMe$_2$], a guanidinate supported Al complex in a low 1 mol% load to catalyse the hydroamination of aromatic amines with several carbodiimides (**Scheme 5.5**),[208] which allows the use of mild reaction conditions (room temperature, 0.5-1 hour reaction time) affording the relevant guanidines in good yields (84-99%) although no reaction intermediates of these processes could be detected or characterised.
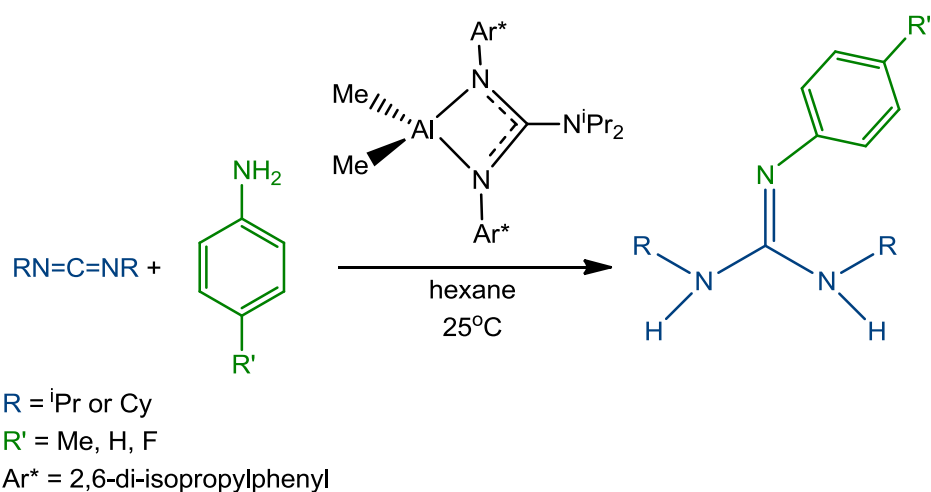
Scheme 5.5: Catalytic formation of guanidines using
$[\{(Ar^*N)C(=NAr^*)(N^iPr_2)\}AlMe_2]$ as a catalyst.

Using half sandwich rare-earth metal complex $[\{Me_2Si(\eta^5\text{-}C_5Me_4)(NR')\}Ln\text{-}(CH_2SiMe_3)(THF)_n]$ (Ln = Y, R' = Ph, ^tBu or $C_6H_2Me_2$ and n = 1 or 2), Hou *et al* have carried out the catalytic hydroamination using carbodiimides and primary anilines, heterocyclic primary amines and secondary amines,[210] although more stringent reaction conditions were required such as higher temperature of 80^oC and longer reaction times of five hours, this method allows access to a wide range of guanidines in excellent yields. More recently, Otero *et al* have shown that commercially available reagents BuLi, Bu_2Mg and $ZnEt_2$ can also catalyse the formation of guanidines by reacting several primary and secondary aromatic amines with $^iPr_2N=C=N^iPr_2$,[209] using slightly harsher reaction conditions than Bergman (0.5-5 hours and $25\text{-}120^oC$) but still achieving good yields. In this case the authors characterised the zinc guanidinate species $[Zn(Et)\{(4\text{-}tert\text{-}BuC_6H_4)N=C(N^iPr)(NH^iPr)\}]_2$ which exhibits a dimeric structure, with the guanidinate ligand acting as a bridge through one of its N atoms, however this structure was of low quality due to poor refinement.

5.2.1 Hydroamination of alkylisocyanates

Building on these precedents we decided to assess the ability of sodium magnesiate **2** as a catalyst to promote the hydroamination of isocyanates. Since **2** contains a bulky

and robust bis(amido)silyl ligand we initially thought this could facilitate as a one-site reaction catalyst. We began our studies by reacting HNPh$_2$ with an equivalent of ^{t}BuN=C=O in the presence of a catalytic amount of complex **2**. The reactions were carried out in a NMR tube using C$_6$D$_6$ and monitored by ^{1}H NMR spectroscopy (see experimental **section 6.2.5** for full details). An equivalent of HNPh$_2$ and ^{t}BuN=C=O were weighed accurately along with 10 mol% of ferrocene (used as an internal standard) before being dissolved in C$_6$D$_6$ and transferred to an NMR tube, ^{1}H and ^{13}C NMR spectra were recorded at room temperature. Catalytic amounts of **2** were added to the reaction mixture and the reaction was monitored by ^{1}H NMR spectroscopy (**Scheme 5.6**).
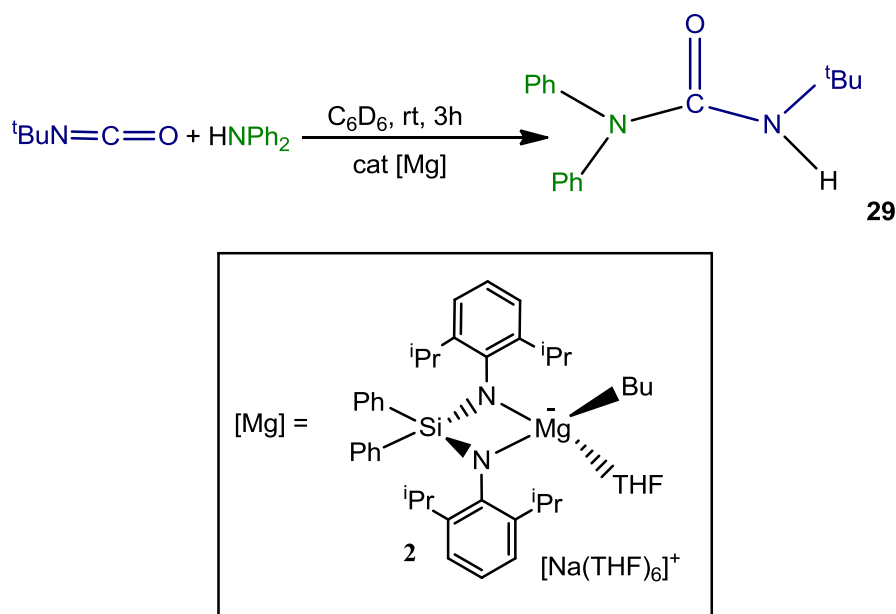
Scheme 5.6: Hydroamination reaction of ^{t}BuN=C=O with HNPh$_2$ using complex **2** as a catalyst.

As shown in **Figure 5.1 (a)** no reaction is observed between ^{t}BuN=C=O and HNPh$_2$ on their own. However, the addition of 10 mol% of sodium magnesiate **2** led to the formation of urea [(^{t}BuNH)C(=O)(NPh$_2$)] **29** in a 93 % yield (±5% error, yield as determined by integration of the ^{1}H NMR spectrum using ferrocene as an internal standard). Reaction conditions could be optimised by decreasing to 2 mol% catalyst loading of **2** which has had little effect on the overall yield, 90 %. As shown in **Figure 5.1(a)**, ^{t}BuN=C=O displays a singlet at 0.98 ppm in the ^{1}H NMR spectrum in C$_6$D$_6$ for the ^{t}Bu group, whilst the resonances belonging to HNPh$_2$ are found at 7.07,

6.85, 6.71 for the aromatic hydrogens and at 5.20 ppm for the NH group. After addition of 10 mol % of complex **2**, new resonances start to appear and a ^{1}H NMR spectrum after three hours revealed that the reaction has gone to completion (**Figure 5.1 (b)**). The signals which belonged to HNPh$_2$ and ^{t}BuN=C=O have now drastically decreased and a new set of resonances belonging to urea **29** have appeared at 7.16, 7.10 and 6.87 ppm for the Ph groups, a broad singlet at 4.35 ppm for NH, which is significantly downfield to that observed for diphenylamine (5.20 ppm) and a singlet at 1.22 ppm for the ^{t}Bu group, on the urea, which has moved upfield in shift from that found for ^{t}BuN=C=O (0.98 ppm).
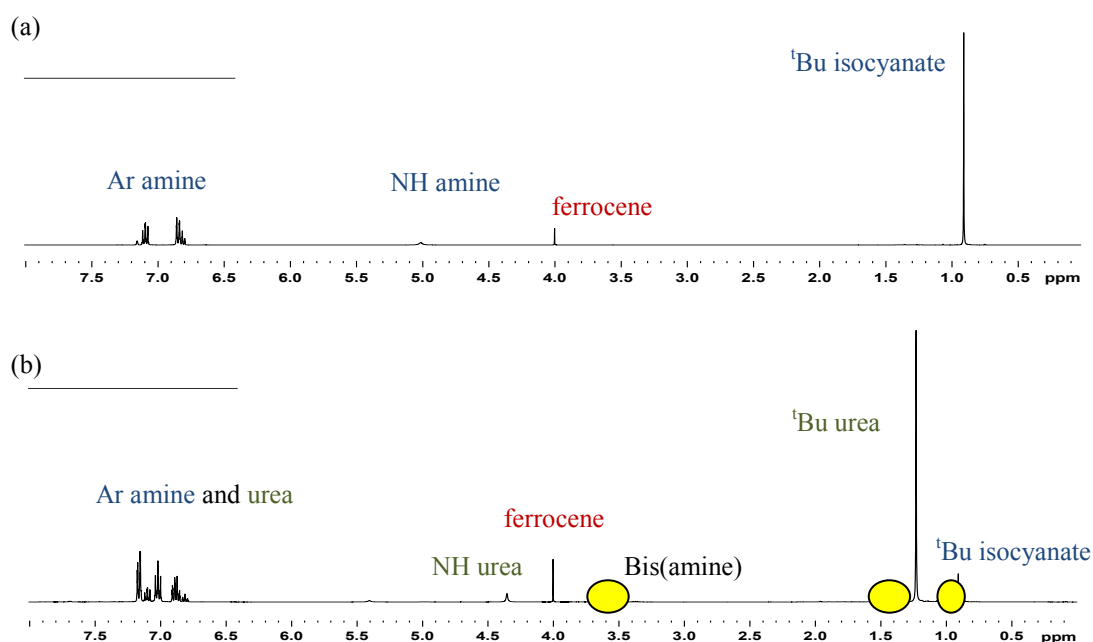
Figure 5.1: ^{1}H NMR spectra of: (a) HNPh$_2$ and ^{t}BuN=C=O, (b) addition of 10 mol % complex **2** to (a) after three hours. In both spectra ferrocene is present as an internal standard.

The urea was further characterised using ^{13}C NMR spectroscopy (see Experimental Section) and X-ray crystallographic studies (**Figure 5.2**). The most diagnostic resonance in the ^{13}C NMR spectra appears at 154.08 ppm for the NC(=O)N which is significantly downfield to the N=C=O of ^{t}BuN=C=O (122.53 ppm), reflecting the change in the hybridisation of the carbon (from sp to sp^2).
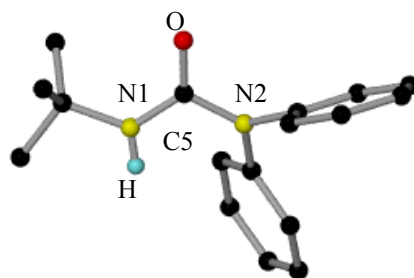
Figure 5.2: Molecular structure of **29** with hydrogens omitted for clarity. Selected bond lengths (Å) and bond angles (°): *O1-C5 1.2249(17), N1-C5 1.3451(18), N2-C5 1.4115(18), C5-N2-C6 123.53(12), C5-N2-C12 117.19(11), C6-N2-C12 118.77(11), C5-N1-C1 125.53(12), C5-N1-H1 117.3(13), C1-N1-H1 117.1(13).*

As it can be observed in **Figure 5.1(b)**, the ^{1}H NMR analysis also showed the presence of a minor product which exhibits a multiplet at 3.51 ppm and a doublet at 1.00 ppm along with several multiplets in the area of the aromatic protons. These chemical shifts are almost identical to those observed for the bis(amine) {$Ph_2Si(NHAr^*)_2$} **1**. The presence of **1** in the crude mixture was also confirmed by GC-MS analysis. These results indicate that under these reaction conditions the formation of **29** occurs accompanied by the protonation of the bis(amido)silyl ligand present in **2**. In order to gain a better understanding of the reaction and to shed light on the constitution of the active species catalysing the hydroamination reaction we studied the reaction of **2** with three equivalents of the amine $NHPh_2$ in a hexane/THF mixture, resulting in the formation of [$NaMg(NPh_2)_3(THF)_2$] **30** (**Scheme 5.7**) which constitution was confirmed by ^{1}H and ^{13}C NMR spectroscopic and X-ray crystallographic studies. This result indicates that when **2** is confronted with an excess of $HNPh_2$ it reacts not only with its Bu group but also with the two amido arms of the bis(silyl)amido ligand {$Ph_2Si(NAr^*)_2$}$^{2-}$. Complex **30** could also be prepared rationally by reacting BuNa with $Mg(CH_2SiMe_3)_2$ and three equivalents of $NHPh_2$.
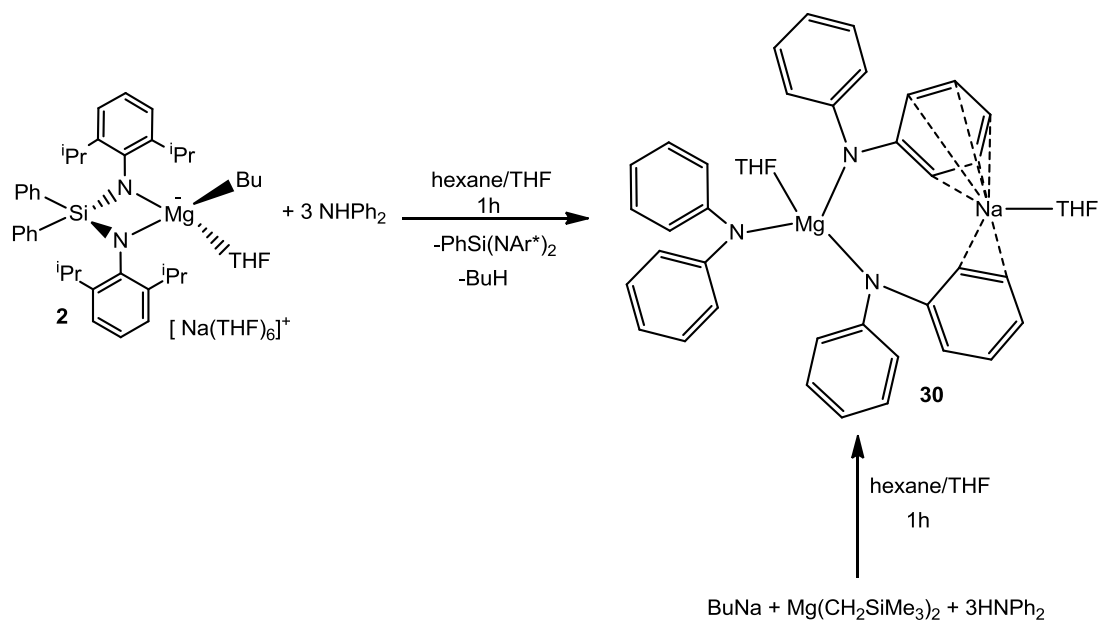
Scheme 5.7: Synthesis of [NaMg(NPh$_2$)$_3$(THF)$_2$] **30**.

X-ray crystallographic studies revealed complex **30** to be a homoleptic sodium tris(amido) magnesiate with a contacted ion pair structure where the Mg atom is bonded to three amido groups and a solvating THF molecule, whereas Na π-engages with two Ph groups each from a different NPh$_2$ ligand and a further molecule of THF within the asymmetric unit (**Figure 5.3**). The Na cation π engages with two phenyl groups, each of them from a different amido ligand. Binding in a η^5-fashion with the phenyl ring attached to N3 (Na-C distances ranging from 2.774(2) Å to 3.126(2) Å; Na-C$_{centriod}$ average distance 2.927 Å), and in a η^2-mode with the phenyl ring attached to N2 (Na-C8 2.883(2) Å, Na-C9 2.774(2) Å, mean 2.8285 Å).
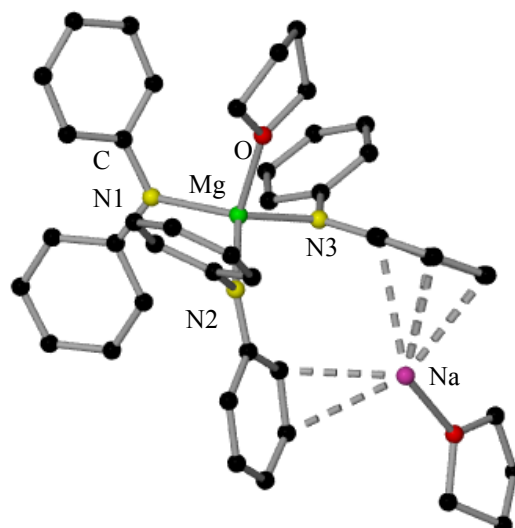
Figure 5.3: Molecular structure of [NaMg(NPh$_2$)$_3$(THF)$_2$] monomer.

Furthermore, in order to attain higher coordination, Na also interacts with the Ph group of the terminal amido group bonding to Mg {NaMg(NPh$_2$)$_3$}, forming two additional Na-C$_\pi$ bonds (Na-C23 3.010(2) Å, Na-C24 2.756(2) Å, mean 2.883 Å) giving rise to a novel polymeric chain structure (**Figure 5.4**), made up exclusively of Na-C$_{phenyl}$ π electrostatic interactions. The Mg-N bond distances display little variation in **30** (ranging from 2.0527(16) to 2.0612(17) Å) and all three N atoms of the diphenylamido groups adopt an almost trigonal planar geometry (Σ<N1 = 358.38º, N2 = 359.91º and N3 = 358.6º).
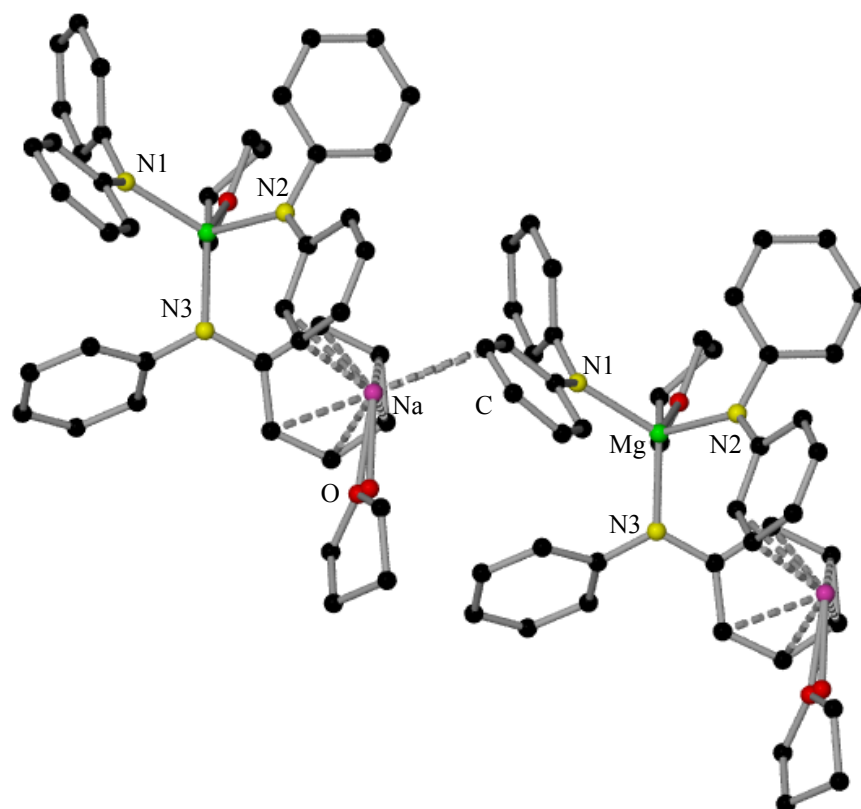
Figure 5.4: Molecular structure of **30** with hydrogens omitted for clarity. Selected bond lengths (Å) and bond angles (°):*Mg-N1 2.0527(16), Mg-N2 2.0542(17), Mg-N3 2.0612(17), Mg-1O 2.0510(14),Na-C8 2.883(2), Na-C9 2.774(2), Na-C23 3.010(2), Na-C24 2.756(2), Na-C26 3.126(2), Na-C27 2.927(2), Na-C28 2.772(2), Na-C29 2.801(2), Na-C30 3.010(2), O1-Mg-N1 105.55(6), O1-Mg-N2 109.22(7), N1-Mg-N2 111.68(7), O1-Mg-N3 95.93(6), N1-Mg-N3 122.48(7),N2-Mg-N3 110.08(7).*

The polymeric structure of **30** contrasts with those reported for other tris(amido)sodium magnesiates such as [(TMEDA)NaMg(DA)$_3$] which exhibits a discrete monomeric arrangement. Closely related to **30**, O'Hara *et al* have recently reported the structure of potassium magnesiate [(PMDETA)·K(μ-NPh$_2$)Mg(THF)(NPh$_2$)$_2$] where K also π interacts with two Ph groups of two different amido ligands but also binds to one nitrogen of an amido ligand (**Figure 5.5**).[211] Now the presence of the tridentate PMDETA ligand capping the K atom inhibits the formation of a polymeric structure.
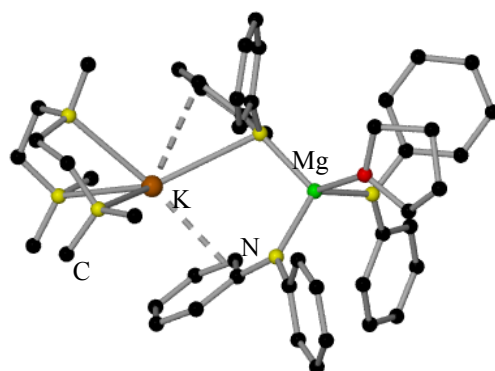
Figure 5.5: Molecular structure of [(PMDETA)·K(μ-NPh$_2$)Mg(THF)(NPh$_2$)$_2$].

Remarkably the Mg-N bond distances in this potassium magnesiate (average 2.050 Å) are very close in value to those exhibited in **30**, suggesting that these Mg-N bonds are anchoring the structure whereas the Na-C π contacts can be best described as ancillary bonds.[78]

The constitution of **30** was also confirmed by ^{1}H and ^{13}C NMR spectroscopy. The ^{1}H NMR spectrum in d$_8$-THF solution showed three multiplets at 7.42, 7.11 and 6.60 ppm which can be assigned to the Ph groups of the amido ligands as well as two multiplets at 3.61 and 1.77 ppm observed for THF molecules (**Figure 5.6**).
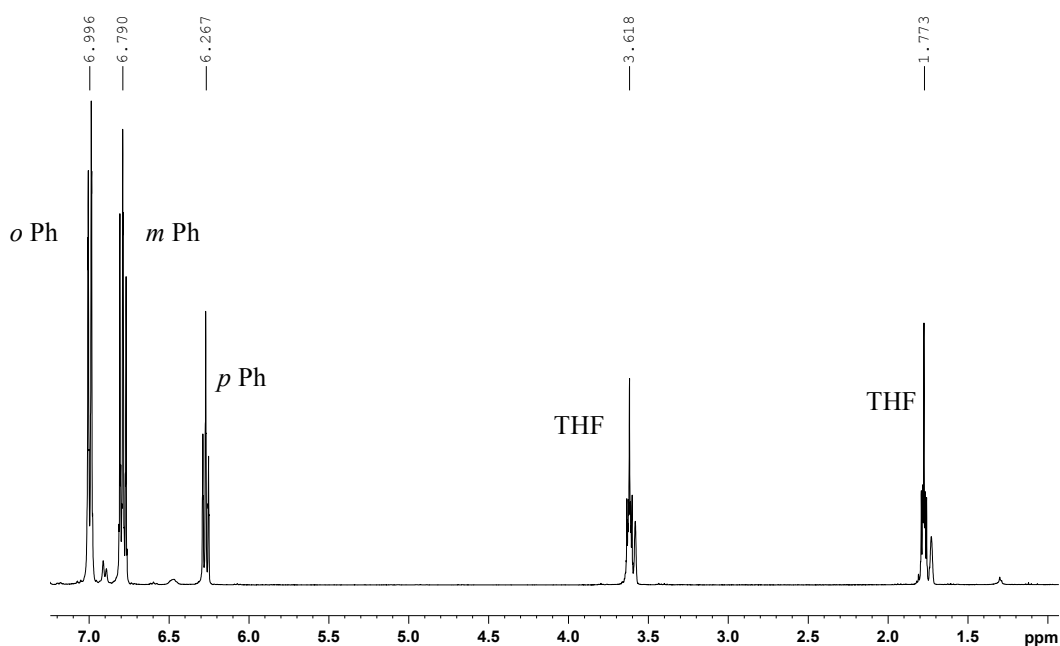
Figure 5.6: ^{1}H NMR in d$_8$-THF of complex **30**.

The formation of tris(amido) magnesiate **30** when **2** is confronted with an excess of HNPh$_2$ coupled with the detection of bis(amine) {Ph$_2$Si(NHAr*)$_2$} **1** in the reaction crude when equimolar amounts of HNPh$_2$ and ^{t}BuN=C=O are reacted in the presence of 10 mol% of **2**, suggests that under the reaction conditions employed for the catalytic study, complex **30** must be formed *in situ*. In order to assess the ability of **30** to undergo addition reactions towards isocyanates, we reacted isolated crystals of **30** with three molar equivalents of ^{t}BuN=C=O. The reaction was performed at room temperature for one hour using THF and hexane as solvent. This led to the isolation of [(THF)$_3$NaMg((^{t}BuN)C(NPh$_2$)(=O))$_3$] **31** in 62 % yield (**Scheme 5.8**).
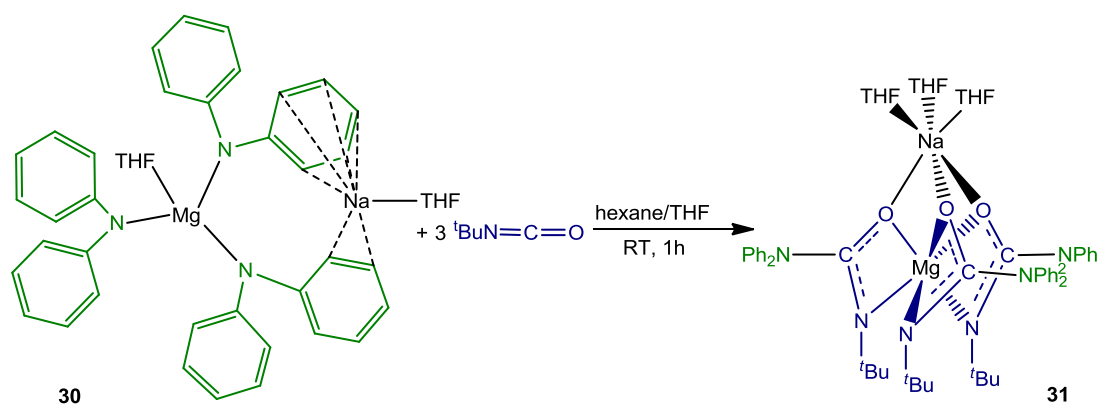
Scheme 5.8: Preparation of complex [(THF)$_3$NaMg((^{t}BuN)C(NPh$_2$)(=O))$_3$] **31**.

X-ray crystallographic studies showed the formation of a novel sodium magnesiate which contains three ureido ligands [(^{t}BuN)C(NPh$_2$)(=O)], resulting from the formal insertion of a molecule of ^{t}BuN=C=O into each of the Mg-N bonds present in the tris(amido) complex **30**, showing a remarkable activation of the three amido arms of the magnesiate towards the insertion reaction. These newly generated ureido ligands coordinate to Mg in a chelating fashion through their O and N atoms forming three four-membered {MgNCO} rings which gives rise to an octahedral geometry for Mg. The structure is completed by a sodium cation solvated by three THF molecules and also binds to the O atoms of three ureido ligands exhibiting an octahedral environment. The Na-O$_{THF}$ bond (2.377(11) Å) is shorter than the Na-O$_{ureaute}$ length 2.414(10) Å probably as a consequence of the bridging coordination of the ureido ligand to Mg and Na. The molecule has a C$_3$ symmetry axis, as shown in **Figure 5.8**, for the view through Na···Mg vector.
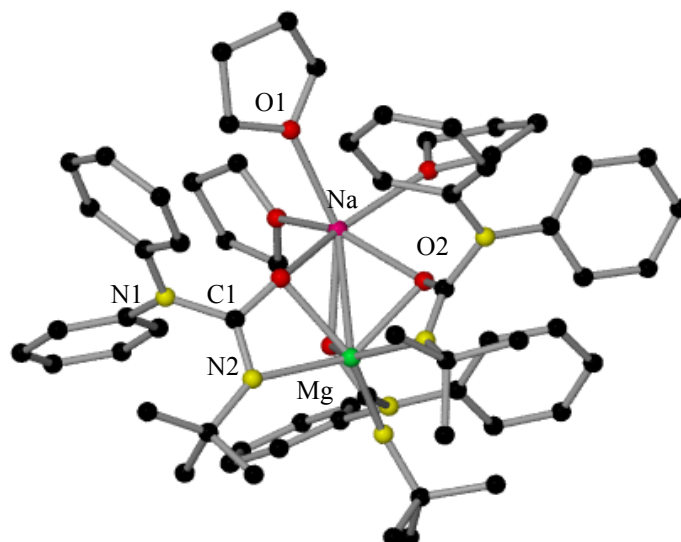
Figure 5.7: Molecular structure of **31** with hydrogen atoms omitted for clarity. Bond lengths (Å) and angles(º)*: Na-O1 2.377(11), Na-O2 2.412(10), Mg-O2 2.147(9), Mg-N2 2.168(10), O2-C1 1.277(14), N2-C1 1.296(15), C1-N1 1.446(14),C2-N1-C 1118.45(9), C3-N1-C1 116.19(9), C2-N1-C3 124.50(10), N1-C1-O2 117.00(10), N1-C1-N2 123.80(10), O2-C1-N2 119.16(10)*.
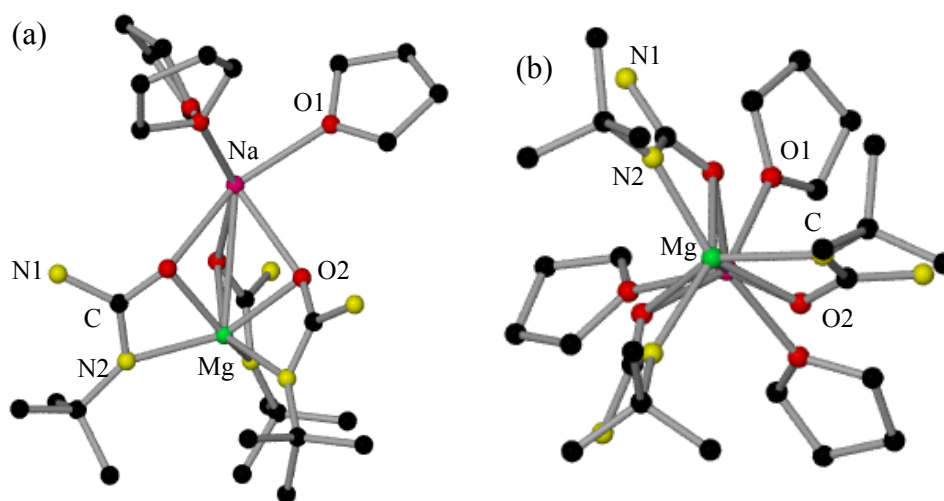
Figure 5.8: (a) Molecular structure of **31** with Ph groups and H atoms omitted for clarity and (b) alternative view of **31** across the Na···Mg vector with Ph groups and hydrogen atoms omitted for clarity.

A search in the CSD revealed that complex **31** as far as we can ascertain is the first example of a Mg compound structurally defined containing a ureido ligand. Closely

related Hill *et al* have reported the structure of the Ca species [{Ar*NC(Me)CHC(Me)NAr*}Ca{OC(NPh$_2$)N(Ad)}] (Ar* = 2,6-diisopropylphenyl, Ad = 1-adamantyl) resulting from the insertion reaction of Ad-N=C=O with the nacnac supported Ca amido complex [{Ar*NC(Me)CHC(Me)NAr*}Ca{NPh$_2$}(THF)]. Similarly to **31**, the ureido ligand coordinates in a chelating fashion through its O and one of its N atoms.[18] To the best of our knowledge these are the only two main group metal ureido complexes which have been structurally characterised, although some using lanthanide[202, 212] and transition metals[213, 214] have been reported.

Complex **31** was also characterised by ^{1}H and ^{13}C NMR spectroscopy in C$_6$D$_6$ (**Figure 5.9**). The ^{1}H NMR spectrum showed a diagnostic singlet at 1.44 ppm for the [t]Bu group of the ureido ligand which is significantly downfield in comparison for that observed for [t]BuN=C=O (0.98 ppm). Reflecting the hybridisation change experienced by the quarternary carbon of the isocyanate the ^{13}C NMR spectrum of **31** exhibits a resonance at 163.29 ppm for [[t]BuN*C*(=O)NPh$_2$] at a remarkably downfield chemical shift when compared to that of [t]BuN=*C*=O (123.61 ppm).
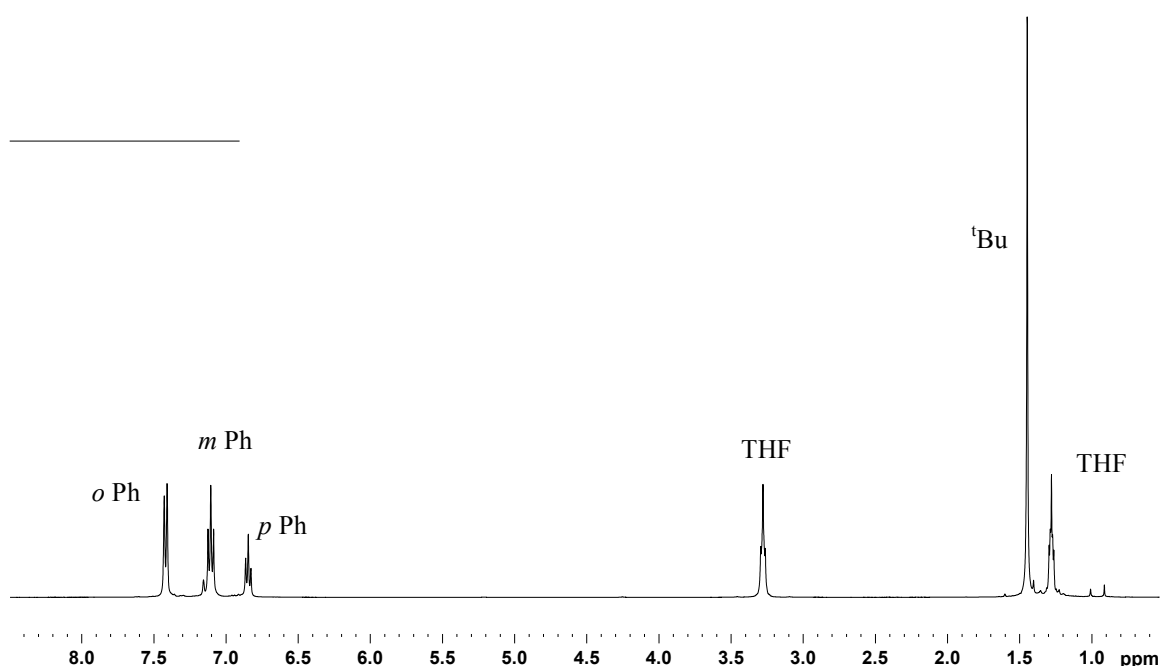
Figure 5.9: ^{1}H NMR in C$_6$D$_6$ of complex **31**.

On the view of these results, it appears that **2** in the catalytic studies is acting as a precursor of sodium magnesiate **30**, (note that since these studies are performed in C_6D_6, no THF is present in the formation of **30**) which is performing the addition reaction of the isocyanate. Furthermore, the isolation and characterisation of **31** shows that the insertion reaction occurs with an excellent atom economy since each of the three amido arms of the magnesiate can react with a molecule of $^tBuN=C=O$. Based on these studies we then decided to assess if a more simple tris(alkyl) sodium magnesiate can also promote the *in situ* formation of **30**, and therefore catalyse the hydroamination of $^tBuN=C=O$. We choose for our studies $[NaMg(CH_2SiMe_3)_3]$ **32**, a sodium magnesiate which has recently been reported by our research group.[215] This complex can easily be prepared and isolated as a crystalline solid by reacting equimolar amounts of $Na(CH_2SiMe_3)$ and $Mg(CH_2SiMe_3)_2$ using hexane as a solvent. Although in the solid state this species exhibits a complex supramolecular structure (**Figure 5.11**). ^1H DOSY NMR studies[216] suggest that when dissolved in C_6D_6 **32** displays a monomeric arrangement where Na is probably solvated by one molecule of deuterated benzene (**Figure 5.12**).
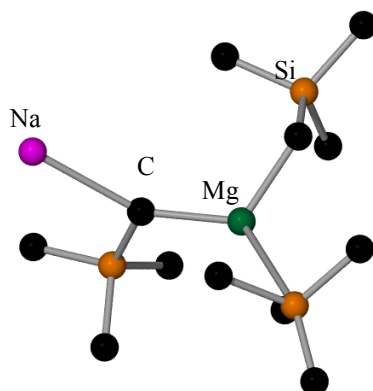
Figure 5.10: Monomer of $[NaMg(CH_2SiMe_3)_3]$ **32**.
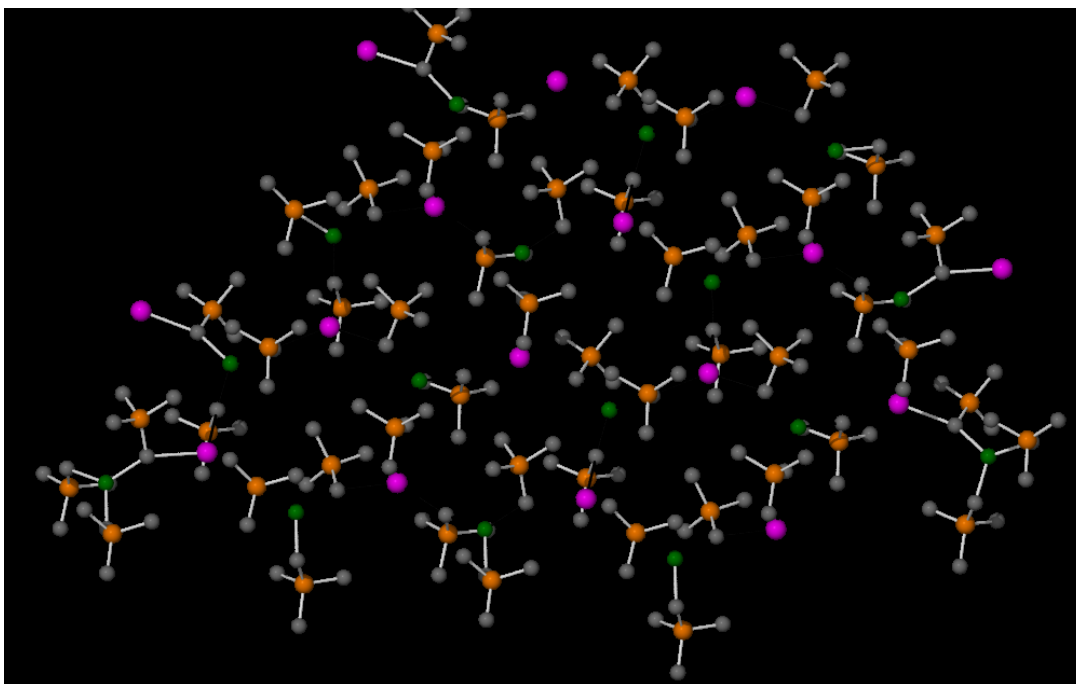
Figure 5.11: Molecular structure of trimer of [NaMg(CH$_2$SiMe$_3$)$_3$] **32**.
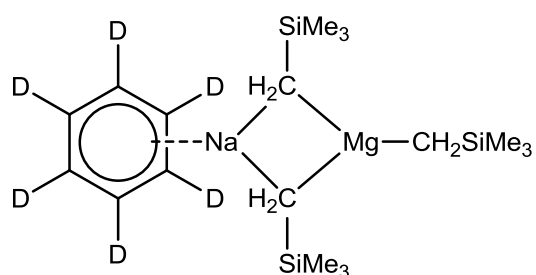
Figure 5.12: Monomeric constitution of **32** proposed on the basis of ^{1}H DOSY NMR studies.

Thus, the reaction of equimolar amounts of ^{t}BuN=C=O and NHPh$_2$ with a 2 mol % of **32** using C$_6$D$_6$ as a solvent was carried out, showing that similarly to when **2** is employed, urea **29** can be obtained in a 99% yield. Thus, building on these structural and reactivity studies the following catalytic cycle can be proposed shown in (**Scheme 5.8**) to rationalise the formation of **29** under these reaction conditions. Thus, the reaction of sodium magnesiate **32** with some of HNPh$_2$ present in solution will generate *in situ* the tris(amido) magnesiate **30**, which in turn can react with ^{t}BuN=C=O to form the insertion product **31**. It should be noted that the structure of the THF solvate of **30** and **31** are shown in **Scheme 5.8**, under the catalytic

conditions no THF is present in the reaction media, therefore structural variations of these compounds where the alkali-metal is probably solvated by deuterated C_6D_6 will be present in solution.
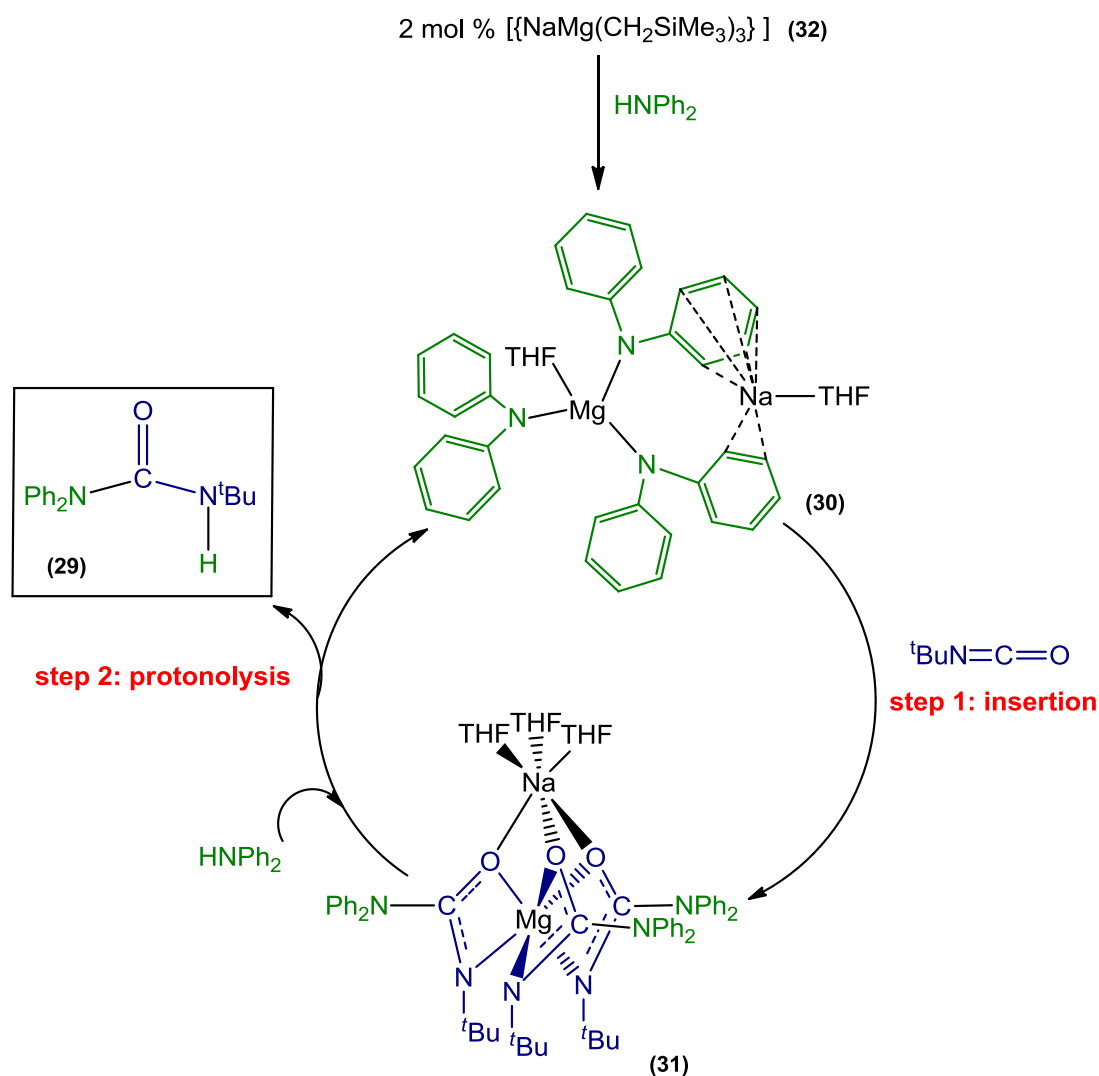
Scheme 5.8: Proposed catalytic cycle for the hydroamination of $^tBuN=C=O$ using $[NaMg(CH_2SiMe_3)_3]$ **32** as a precatalyst.

The reaction of **31** with the excess of HNPh$_2$ would then regenerate active species **30** and form the urea **29**. The keys for the success of this catalytic hydroamination reaction are the enhanced nucleophilic power of tris(amido) complex **30** when compared with tris(alkyl) precursor **32** (which minimizes the possible side reactions of alkyl addition to the isocyanate) and the ability of HNPh$_2$ to react as a protonating source for the ureido ligand to generate urea **29**.

As discussed in **section 5.1.1** Hill *et al* have used heavier congener Ca species [Ca{N(SiMe$_3$)$_2$}$_2$]$_2$ to catalyse the hydroamination of 1-adamantylisocyanate and 2,6-di-isopropylphenylisocyanate with HNPh$_2$ to form the corresponding ureas in lower yields of 86 and 62% than we achieved in forming urea **29** (99% yield). Furthermore, this Ca-mediated methodology requires elevated temperatures of 60$^{\text{o}}$C when the hindered aryl isocyanate is used. To the best of our knowledge this is the first catalytic application of a sodium magnesiate although some recent studies have shown that lithium ferrates[217] or magnesium zincates can display catalytic activity in C-C cross-coupling processes and alkylation reactions to ketones respectively. [218]

In view of these promising results, we then decided to evaluate the scope of this catalytic bimetallic approach. We first studied the reactions of $^{\text{t}}$BuN=C=O with the commercially available amines H$_2$NAr*, HNPy$_2$, HMDS(H), HNBu$_2$ and HNBz$_2$. An equimolar amount of the relevant amine and $^{\text{t}}$BuN=C=O were added to C$_6$D$_6$ and a ^{1}H NMR spectrum recorded, following the addition of 2 mol % of **32** the reaction was then monitored by ^{1}H NMR spectroscopy. The two aliphatic amines HNBu$_2$ and HNBz$_2$ proved to be nucleophilic enough to react with $^{\text{t}}$BuN=C=O without the presence of a catalyst to form the respective ureas [($^{\text{t}}$BuNH)C(=O)(NBu$_2$)] **33** and [($^{\text{t}}$BuNH)C(=O)(NBz$_2$)] **34** almost instantaneously in quantitative yields, evidencing that an increase of nucleophilic character of amine (aliphatic *vs* aromatic) allows the hydroamination to take place. In fact, it should be mentioned that the stoichiometric reaction of aliphatic amines with isocyanates has been observed although normally high reaction temperatures and long reaction times are needed.[200, 201]

The secondary amine HMDS(H) did not react at all in the presence of 2 mol % of **32**, even under refluxing conditions. This may be attributed to the much greater steric bulk of HMDS(H) when compared with HNPh$_2$. Supporting this possibility, Hill *et al* found that [{Ar*NC(Me)CH(Me)NAr*}Ca{N(SiMe$_3$)$_2$}(THF)] (Ar* = 2,6-diisopropylphenyl) did not react stoichiometrically with AdN=C=O to form an insertion intermediate, whereas when HMDS is replaced by NPh$_2$, the desired ureido complex [{Ar*NC(Me)CHC(Me)NAr*}Ca{OC(NPh$_2$)N(Ad)}] formed in almost stoichiometric yield.[18]

Aromatic amines $HNPy_2$ and H_2NAr^* yield the relevant ureas [($^tBuNH)C(=O)(NPy_2)$] **35** and [($^tBuNH)C(=O)(NHAr^*_2)$] **36** in much lower yields (17 and 34 % respectively) than when $HNPh_2$ was employed, which may be due to the decrease of nucleophilic character of the generated tris(amido) magnesiates in both reactions.

RN=C=O	Amine	urea	Catalyst (mol %)	time (h)	temp (^oC)	yield (%)
^tBu	$HNPh_2$	**29**	2	3	25	99
^tBu	$HNBu_2$	**33**	0	0	25	100
^tBu	$HNBz_2$	**34**	0	0	25	100
^tBu	$HNPy_2$	**35**	2	3	25	17[a]
^tBu	H_2NAr^*	**36**	2	3	25	34[b]
Cy	$HNBu_2$	**37**	0	0	25	100
Cy	$HNBz_2$	**38**	0	0	25	100
Cy	$HNPh_2$	**39**	2	3	25	100
Cy	$HNPy_2$	**40**	2	3	25	53[a]
Cy	H_2NAr^*	**41**	0	0	25	100
Et	H_2NAr^*	**42**	0	0	25	100
Et	$HNPh_2$	**43**	2	3	25	78
Et	$HNPy_2$	**44**	2	3	25	34[a]

Table 5.2: [$NaMg(CH_2SiMe_3)_3$] **32** catalysed hydroamination of isocyanates with amines in C_6D_6. ±5% error as yield determined by ^1H NMR spectroscopy using integration of ferrocene as an internal standard. (a) d_8-THF used as a solvent due to low solubility in C_6D_6. (b) isolated yield determined by column chromatography.

We next studied the scope of using different isocyanates along with the aforementioned amines; the NMR studies were carried out using the same methodology described above using 2 mol % of **32** as a catalyst, with ferrocene used as an internal standard for evaluating the yield. We first looked at CyN=C=O, which displayed the same reactivity with the primary amines HNBu$_2$ and HNBz$_2$ as ^{t}BuN=C=O, forming the respective ureas [(CyNH)C(=O)(NBu$_2$)] **37** and [(CyNH)C(=O)(NBz$_2$)] **38** instantaneously, without the need of the catalyst. Using 2 mol % of catalyst **32**, the hydroamination of CyN=C=O with HNPh$_2$ was carried out forming urea [(CyNH)C(=O)(NPh$_2$)] **39** in 100% yield. CyN=C=O also showed no reactivity with HMDS(H), even under refluxing conditions. Whilst the reaction between CyN=C=O and HNPy$_2$ in the presence of 2 mol % **32** yielded urea [(CyNH)C(=O)(NPy$_2$)] **40** in 53 %. In addition the hydroamination of CyN=C=O and H$_2$NAr*, surprisingly occurred without the presence of catalyst, unlike the reactivity observed for ^{t}BuN=C=O, to form the urea [(CyNH)C(=O)(NHAr*)] **41** instantaneously as evidenced by ^{1}H, ^{13}C NMR spectroscopy and GC-MS analysis. We next looked at EtN=C=O, however chose not to study the reaction with primary aliphatic amines (HNBu$_2$ and HNBz$_2$) as they had been nucleophilic enough to react with the previous isocyanates without the need of a catalyst. In addition, using the amine HMDS(H), no hydroamination reaction occurred as had also been observed for the previous isocyanates. However, the primary aniline H$_2$NAr* reacted with an equimolar amount of EtN=C=O without the presence of **32**, (similarly to CyN=C=O), to yield the urea [(EtNH)C(=O)(NHAr*)] **42**, which has been characterised by ^{1}H NMR spectroscopy and X-ray crystallography (**Figure 5.12**).
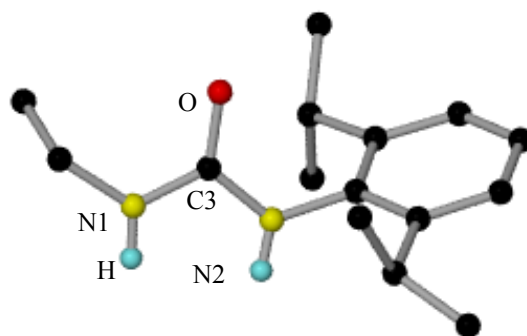
Figure 5.12: Molecular structure of urea **42**. Hydrogen atoms have been omitted for clarity. Bond Lengths (Å) and Angles (º):*O1-C3 1.240(2), N1-C3 1.347(2), N1-C1 1.453(2), N2-C3 1.362(2), N2-C4 1.429(2), C3-N2-C4, 122.96(14), C3-N4-H98 116.5(14), C4-N2-H98 119.7(14), C3-N1-C1 121.63(15), C3-N1-H99 116.8(44), C4-N1-H99 121.5(14).*

Furthermore, using the secondary aromatic amines $HNPh_2$ and $HNPy_2$ along with $EtN=C=O$ in the presence of 2 mol % **32** yielded the corresponding ureas [(EtNH)C(=O)(NPh_2)] **43** and [(EtNH)C(=O)(NPy_2)] **44** in 78 and 34% respectively. **Table 5.2** compares the different amines and isocyanates used and the reaction conditions employed.

5.2.2 Hydroamination of Arylisocyanates

We next endeavored to look at arylisocyanates, and chose pTolylN=C=O as its ^{1}H NMR spectrum displays an indicative diagnostic sharp singlet at 2.31 ppm which could facilitate the ^{1}H NMR monitoring of the reaction. Equimolar amount of pTolylN=C=O and $HNPh_2$ were added to $CDCl_3$ along with 10 mol% of ferrocene (as an internal standard) and a ^{1}H NMR spectrum was recorded (**Figure 5.13(a)**). Afterwards, 2 mol% of **32** was added and the reaction was then monitored by ^{1}H NMR spectroscopy. ^{1}H NMR spectra recorded after one hour showed the formation of a new product as evidenced by the presence of a new singlet at 2.36 ppm (**Figure 5.13(b)**). Analysis of the integration of this signal *vs* the internal standard showed a conversion of 80%. Surprisingly no attributable chemical shifts are observed for the resonances of $HNPh_2$ group. Rather than the hydroamination of pTolylN=C=O, the

trimerisation of the isocyanate has taken place resulting in (1,3,5-tris(pTolyl)-1,35-triazinane-2,4,6 trione) [{(pTolylN)C(=O)}₃] **45**.

(a)

(b)
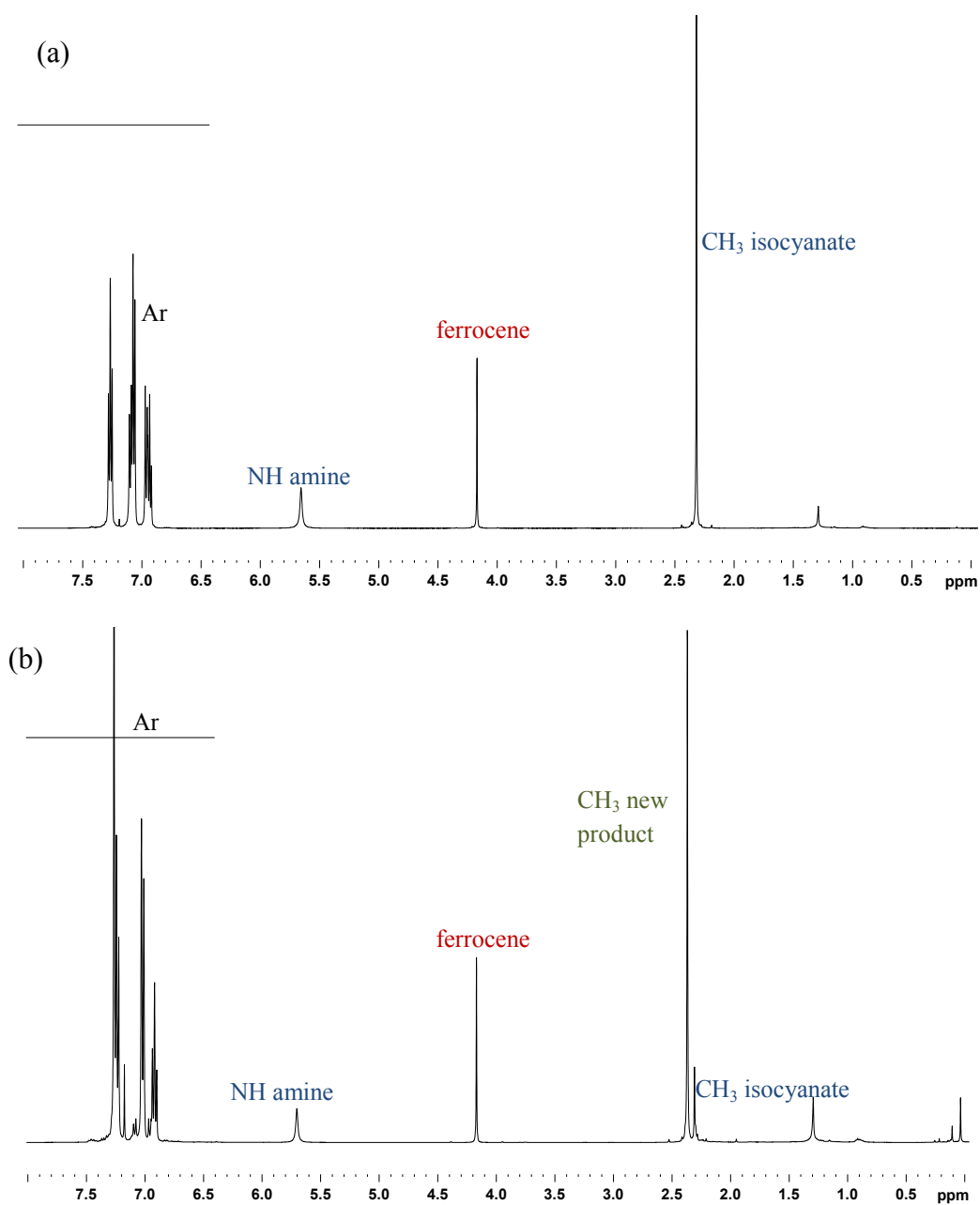
Figure 5.13: ^{1}H NMR in CDCl$_3$ (a) pTolylN=C=O and HNPh$_2$, (b) After addition of 2 mol % precatalyst **32**.

To gain further insight into the reaction taking place the stoichiometric reaction of pTolylN=C=O with complex **30** was carried out, (since building on previous results, compound **30** is formed when **32** is confronted with an excess of HNPh$_2$) resulting in compound (1,3,5-tris(pTolyl)-1,35-triazinane-2,4,6 trione) [{(pTolylN)C(=O)}₃] **45**

in a 27% yield. The trimerisation product was confirmed by ^{1}H and ^{13}C NMR spectroscopy and X-ray crystallography (**Figure 5.14**). Repeating the stoichiometric reaction now using three molar equivalents of pTolylN=C=O increased the yield of trimer to 89%.
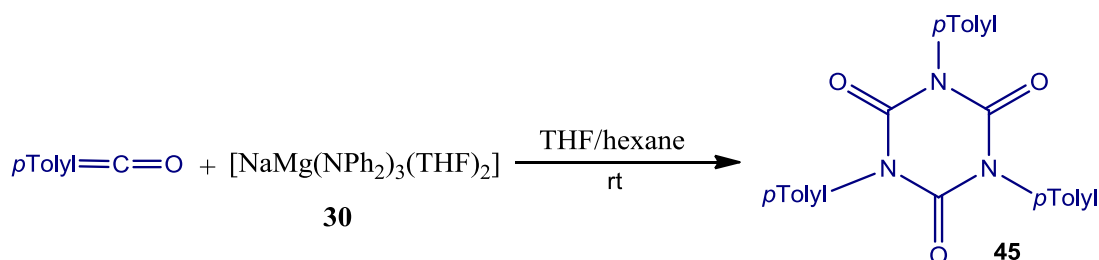
Scheme 5.9: Stoichiometric preparation of isocyanurate **45**.
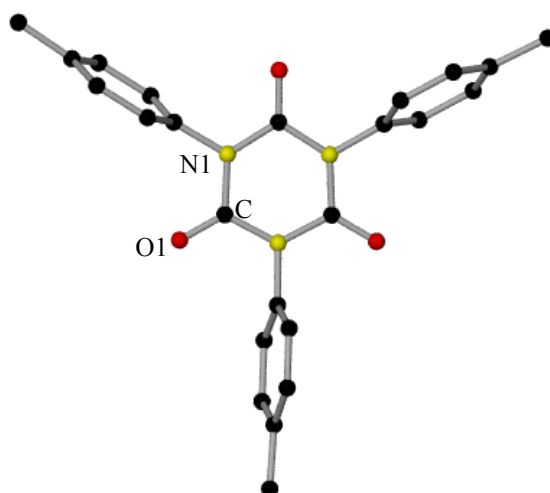
Figure 5.14: Molecular structure of urea **45**. Hydrogen atoms have been omitted for clarity.

Although catalytic trimerisation reactions of arylisocyanates have been reported in the literature, the majority of the catalysts employed are anions or neutral Lewis bases such as fluoride anions and phosphines.[213, 214] Furthermore, in many occasions these methodologies display low activity, harsh reaction conditions and poor selectivity resulting in the formation of by products.[85, 219] To overcome some of these problems rare earth metal complexes such as [{(CH$_2$SiMe$_2$)(Ar*N)$_2$}Y(SiMe$_3$)$_2$(THF)] have been shown to selectively trimerise isocyanates using a 1 mol % catalyst load at 80°C when reacted for twelve hours.[220]

Isocyanurates are important reagents as they are used to enhance the physical properties of polyurethanes, and are also employed in the preparation of copolymer resins which require water resistance and transparency.[221] Tri(aryl)isocyanurates in particular are employed as activators in the continuous anionic coplolymerisation of $\mathcal{E}$-caprolactam to nylon-6.[88] Other closely related tri(aryl)isocyanurates to **45** found in the literature include phenylisocyanurate prepared by Usanmaz by using ethyllithium in benzene to catalyse the trimerisation of phenylisocyanate.[92] Also relevant is the synthesis of 1,3,4-tris(4-isopropylphenyl)-1,3,4-triazinane-2,4,6-trione prepared by Wang *et al* in a 99% yield using a rare earth metal catalyst bearing sterically demanding bis(amido)silyl ligand to carry out the trimerisation of 4-isopropylphenylisocyanate in THF at room temperature, however the reaction took twelve hours to go to completion.[91]

In order to assess the catalytic ability of **32** in this trimerisation process we performed the reaction of *p*TolylN=C=O with **32** in the absence of HNPh$_2$. Surprisingly we found that trimer **45** can only be obtained in a modest 10% yield, indicating that alkyl magnesiate **32** shows a much lower catalytic activity in this process than related tris(amido) magnesiate **30**. Furthermore a study varying the load of **32** shows that by using a 10 mol% of **32** in the presence of HNPh$_2$**,** allowing the *in situ* formation of **30**, then the trimer **45** can be obtained in a 90% yield (**Figure 5.15**).
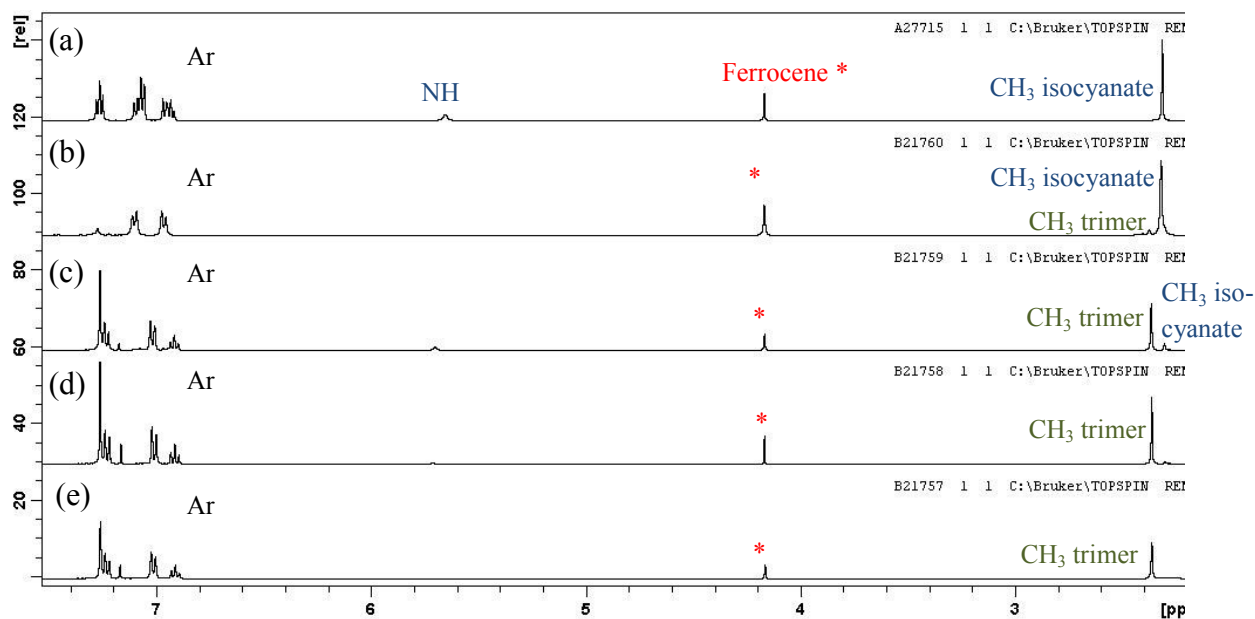
Figure 5.15: Comparison of ^{1}H NMR spectra in CDCl$_3$ of, (a) pTolylN=C=O and HNPh$_2$, (b) pTolylN=C=O and 2 mol % of **32** after 1 hour at RT, (c) pTolylN=C=O, HNPh$_2$ and 2 mol % **32** after 1 hour at RT, (d) pTolylN=C=O, HNPh$_2$ and 5 mol % **32** after 1 hour at RT, (e) pTolylN=C=O, HNPh$_2$ and 10 mol % **32** after 1 hour at RT.

Building on these results and previous mechanistic studies reported for the trimerisation of ArN=C=O mediated by lanthanide complexes,[220] the following sequence of reactions can be postulated to rationalise the formation of **45**.

Thus initially each of the amido groups in **30** can react with one molecule of pTolylN=C=O in a similar manner as already shown for the reaction with less electrophilic ^{t}BuN=C=O to form tris ureido intermediate (**I**) with a similar constitution to that described for **31**. The initial formation of this intermediate (**I**) can explain the low catalytic activity shown by alkyl species **32**, since CH$_2$SiMe$_3$ groups are much poorer nucleophiles than NPh$_2$. This is due primarily to larger steric bulk of this alkyl group as well as its lack of a lone pair of electrons. Now in the presence of a vast excess of pTolylN=C=O the amido-type nitrogen of the ureido ligand present in (**I**) can act as a nucleophile attacking the central carbon of a new isocyanate to form intermediate (**II**), this insertion step can then occur for a third time giving rise to the formation of octa-metallocycle intermediate (**III**), where now the amido

nitrogen can intramolecularly attack one of the C=O bonds leading to the formation of compound **45** and the regeneration of the tris(amido) catalyst **32** (**Scheme 5.10**).
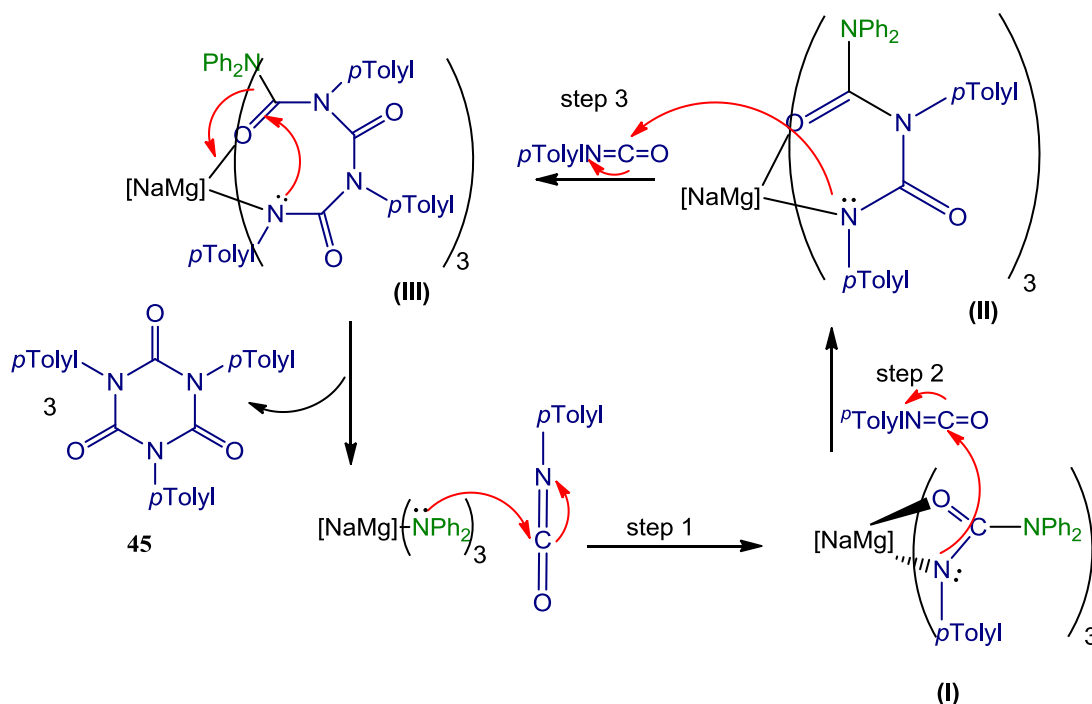
Scheme 5.10: Proposed cycle for trimerisation of *p*TolylN=C=O to yield the corresponding isocyanurate **45** catalysed by **30**.

5.3.1 Hydroamination of carbodiimides

As above mentioned, the hydroamination reactions of carbodiimides is also an important methodology in synthesis to prepare guanidines. We initiated our studies by investigating the ability of sodium-amido magnesiate $[\{Na(THF)_6\}^+\{(Ph_2Si(NAr^*)_2)Mg(NPh_2)(THF)\}^-]$ **7** to undergo insertion reactions with the aliphatic carbodiimides; dicyclohexylcarbodiimide and diisopropylcarbodiimide (**Scheme 5.11**). The reaction of equimolar amounts of **7** with CyN=C=NCy or $^iPrN=C=N^iPr$ led to the formation of $[\{Na(THF)_6\}^+\{(Ph_2Si(NAr^*)_2Mg[(CyN)C(=NCy)(NPh_2)]\}^-]$ **46** and $[\{Na(THF)_6\}^+\{(Ph_2Si(NAr^*)_2Mg[(^iPrN)C(=N^iPr)(NPh_2)]\}^-]$ **47** respectively. Complexes **46** and **47** were characterised using ^1H and ^{13}C NMR spectroscopy and the structure of **46** was determined by X-ray crystallographic studies.
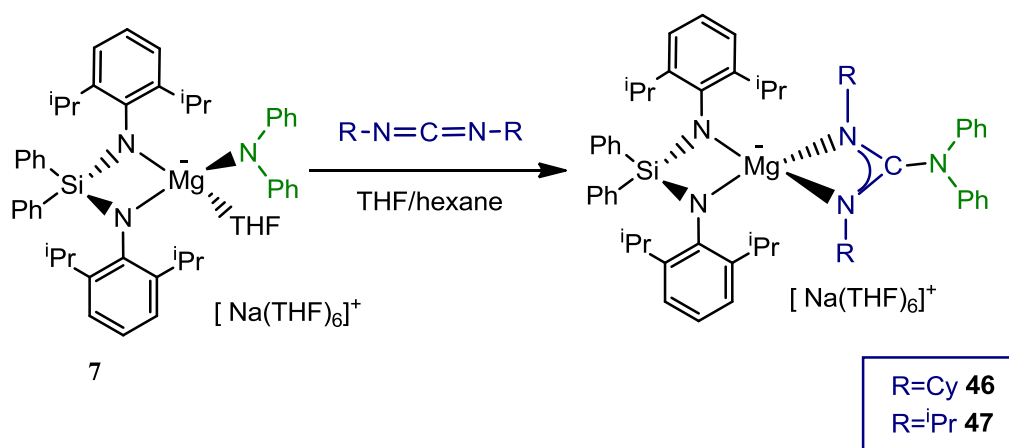
Scheme 5.11: Preparation of insertion products **46** and **47**.

The molecular structure of **46** confirmed that the organic electrophile, CyN=C=NCy has inserted into the Mg-NPh$_2$ bond of complex **7** to yield a new guanidinate ligand {(NCy)C(=NCy)(NPh$_2$)} which coordinates as a bidentate ligand to the Mg centre. Similarly to its precursor **7**, complex **46** exhibits a solvent separated ion-pair structure, containing a cationic moiety which includes a sodium atom solvated by six THF molecules. The anionic part of the molecule comprises a Mg centre in a tetrahedral environment (angles ranging from 64.33(14)º to 148.42(14)º; mean 111.65º) to four N atoms, two from the bis(amido)silyl ligand {Ph$_2$Si(NAr*)$_2$}$^{2-}$ (N1, N2) and two from the guanidinate ligand (N3, N4) (**Figure 5.12**). The Mg-N$_{guanidinate}$ ligand bond values (Mg-N3 = 2.101(4), Mg-N4 = 2.088(3) Å) are slightly elongated in comparison to those observed for the bulky bis(amido)silyl ligand (Mg-N1 = 2.077(3) , Mg-N2 = 2.020(3) Å) which can be attributed to the different charge of the two distinct N-donor ligands (monoanionic for the guanidinate *versus* dianionic for {Ph$_2$Si(NAr*)$_2$}$^{2-}$). In addition, these Mg-N$_{guanidinate}$ lengths are comparable with those found in other Mg complexes containing guanidinate ligands, as for example in the Mg(I) complex [Mg{(N^{i}Pr)C(=N^{i}Pr)(N^{i}Pr)}]$_2$, where the Mg-N$_{guanidinate}$ lengths are (Mg-N1 2.0736(10) Å).[46] The N-C distances within the guanidinate ligand in **46** are more elongated than those found in related carbodiimide Ar*N=C=NAr* (N1-C, N2-C are 1.221(2) and 1.213(2) Å respectively).[222] In addition, the C-N distances and angles within the newly generated ligand confirm that the negative charge of this ligand is delocalized across N3···C1···N4 (N3-C1 1.302(5) Å, N4-C1 1.329(5) Å) as well as the sp^2 hybridisation of C1 (sum angles about C1 = 360º).
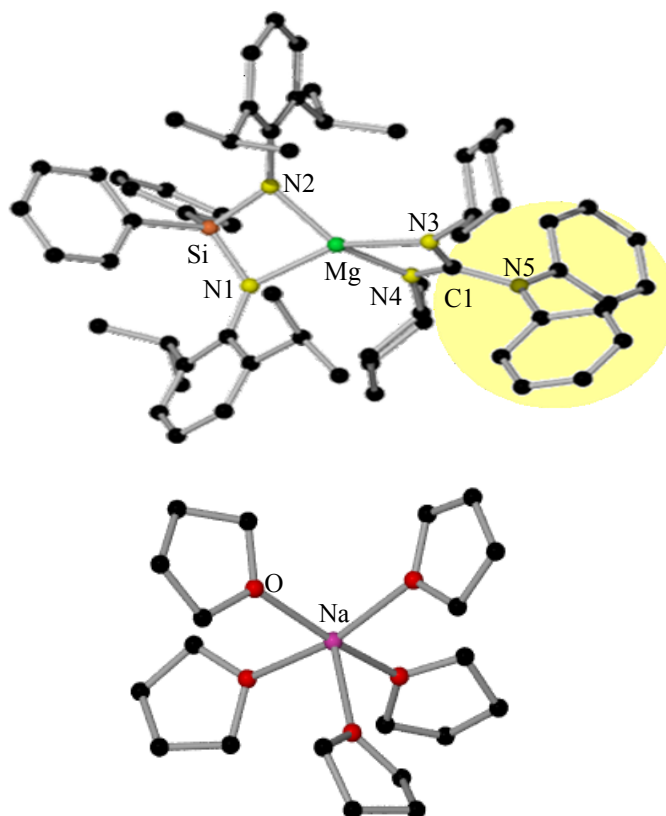
Figure 5.12: Molecular structure of **46**. Hydrogen atoms have been omitted for clarity. Bond Lengths (Å) and Angles(°)*: Mg-N2 2.020(3), Mg-N1 2.077(3), Mg-N3 2.101(4), Mg-N4 2.088(3), C1-N5 1.451(5), C1-N3 1.302(5), C1-N4 1.329(5), N2-Mg-N1 77.94(13), N1-Mg-N4 126.13(14), N4-Mg-N3 64.33(14), N3-Mg-N2 140.42(14), N2-Mg-N4 148.42(14), N1-Mg-N3 112.7(14) N3-C1-N4 116.0(3), N3-C1-N5 122.5(4), N4-C1-N5 121.5(3).*

Complexes **46** and **47** were also characterised in C_6D_6 solutions using ^{1}H and ^{13}C NMR spectroscopy. **Table 5.3** compares some selected resonances of the NMR spectra of these organometallic species with those observed for starting materials, CyN=C=NCy and [i]PrN=C=N[i]Pr.

In the ^{1}H NMR spectra of **46** and **47** there is a distinct change in the chemical shift observed for the multiplet of the C*H* unit of the [i]Pr groups present in the bidentate ligand $\{Ph_2Si(NAr^*)_2\}^{2-}$ (4.45 ppm for **46** and 4.49 ppm for **47**) in comparison with that observed in the amido precursor (3.97 ppm).

In the ^{13}C NMR spectra the most informative signal appears at 164.32 ppm for **46** and 163.86 ppm for **47** corresponding to the central carbon of the guanidinate ligand which has experienced the addition reaction, and exhibits now a sp^2 hybridisation. The change in the hybridisation of this carbon (in comparison with the sp hybridised central carbon in the organic precursors RN=C=NR (R = Cy, ^{i}Pr)) is reflected in a dramatic downfield chemical shift observed when compared with those observed in the carbodiimide (R = ^{i}Pr, 140.12 ppm, R = Cy, 139.98 ppm).

Complex	δ^{1H} (CH, ^{i}Pr,Ar*)	δ^{13C} (CH, ^{i}Pr,Ar*)	δ^{13}C NC(N)N
7	3.97	28.32	
46	4.45	27.21	164.32
47	4.49	27.87	163.86
^{i}PrN=C=N^{i}Pr			140.12
CyN=C=NCy			139.98

Table 5.3: Selected resonances observed in the ^{1}H and ^{13}C NMR spectra of complexes **7**, **46**, **47** and heterocumulenes diisopropylcarbodiimide using C$_6$D$_6$ as a solvent.

In addition for complex **46** the ^{1}H NMR spectrum showed four multiplets at 3.31, 1.76, 1.68 and 1.16 ppm which can be assigned to cyclohexyl groups. For compound **47** a multiplet corresponding to the C*H* of ^{i}Pr group of the newly formed guanidinate ligand is observed at 3.68 ppm, which can be unequivocally assigned by comparing its integration value (2H) to that observed for the C*H* of the ^{i}Pr group of {Ph$_2$Si(NAr*)$_2$}$^{2-}$ ligand at 4.48 ppm (4H).

As was mentioned above in section **5.1.1** within the context of catalytic reactions, Hill *et al* have used [Ca{N(SiMe$_3$)$_2$}$_2$(THF)$_2$] as a catalyst to carry out the hydroamination of RN=C=NR (R = ^{i}Pr, Et, Cy) with the anilines such as 2-fluoroaniline, phenylaniline and diisopropylaniline obtaining the relevant guanidines in yields ranging from 37 to 91%. Building on these precedents and with proof of concept already established for the stoichiometric hydroamination of

dicyclohexylcarbodiimide by amido complex **7**, we next decided to investigate the ability of **7** to catalyse the reaction of diphenylamine with CyN=C=NCy, using ^{1}H NMR monitoring of the reaction. Thus equimolar amounts of CyN=C=NCy and HNPh$_2$ were dissolved in C$_6$D$_6$ and 10 mol% of ferrocene (as an internal standard) and 2 mol% complex **7** were added. The ^{1}H NMR of this mixture after ten minutes showed the full conversion of **7** into the insertion product **46**, as well as unreacted CyN=C=NCy (0.9 eq) and diphenylamine (1 eq). The reaction was monitored for over 48h without any change being observed, showing that complex **7** fails to catalyse the hydroamination of HNPh$_2$ with CyN=C=NCy. A possible mechanism for a catalytic hydroamination reaction (based on previous studies reported using Ca amides as a catalyst) is shown in **Scheme 5.13**.
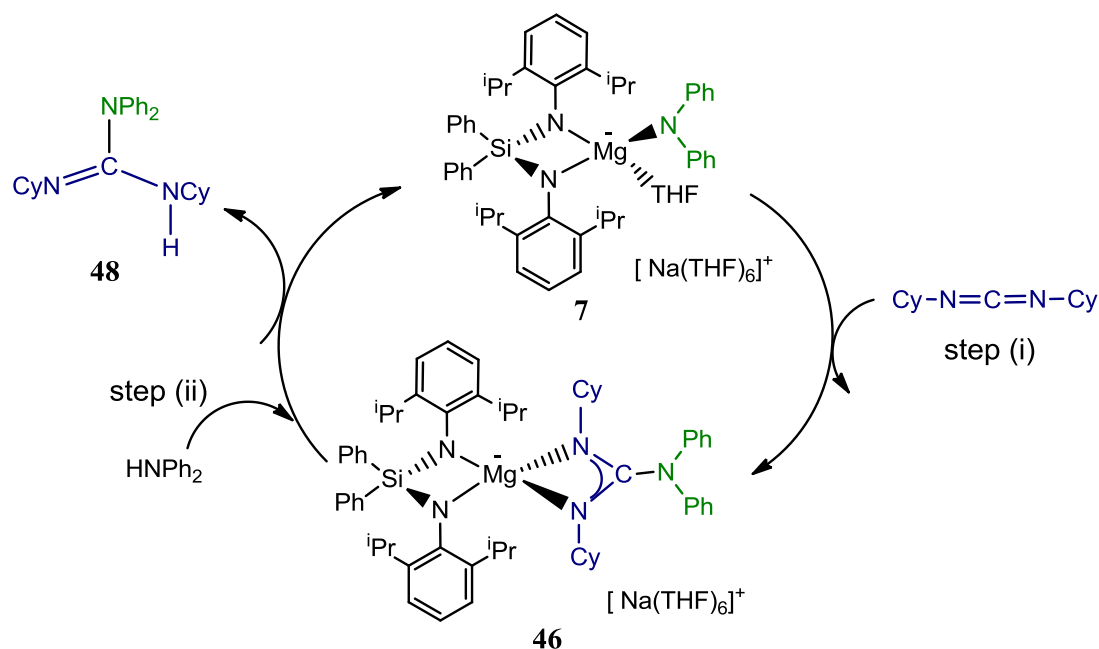
Scheme 5.13: Proposed catalytic cycle for hydroamination of dicyclohexylcarbodiimide with diphenylamine using **7** as a catalyst.

Two main steps involved in this process: (i) the insertion of the carbodiimide in the Mg-N bond and (ii) the protonation of the newly generated guanidinate ligand to yield guanidine **48** with regeneration of the active magnesium amido complex which can then react with more carbodiimide. Our experimental studies have shown that (i) can occur efficiently under stoichiometric conditions to yield complex **46**. Thus it appears that step (ii) is not favoured, which prevents the formation of the free

guanidine **48** and the regeneration of complex **7** (active species capable of reacting with the carbodiimide). This was confirmed by mixing equimolar amounts of insertion product **46** and HNPh$_2$ in C$_6$D$_6$. ^{1}H NMR monitoring of this solution over a 24 hour period showed no reaction at all.

As discussed in **section 5.1.1** guanidinate ligands are also important in organic synthesis as they are used as ancillary ligands in transition metal chemistry[13], whilst also playing a key role in pharmaceuticals and biologically active molecules.[14] There have been a handful of results in the literature using metal catalysts to carry out the hydroamination of carbodiimides with amines to form the corresponding guanidinates. Encouraged by the catalytic activity in the hydroamination reactions of isocyanates by **30**, which can be prepared *in situ* by reacting NaMg(CH$_2$SiMe$_3$)$_3$ **32** with an excess of HNPh$_2$ (*vide supra*), we decided to investigate its ability to promote the guanylation of CyN=C=NCy by HNPh$_2$ (**Scheme 5.14**).
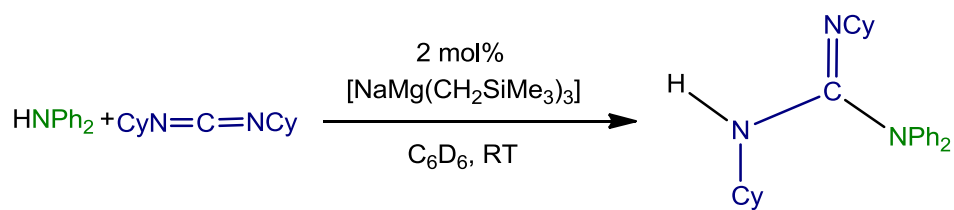
Scheme 5.14: Hydroamination of carbodiimides using catalytic amounts of [NaMg(CH$_2$SiMe$_3$)$_3$] **32**.

Thus, an equivalent of dicyclohexylcarbodiimide, HNPh$_2$ and 10 mol% of ferrocene (as an internal standard), were weighed accurately in the glove box before being dissolved in C$_6$D$_6$ and transferred to an NMR tube. A ^{1}H NMR spectrum was run before addition of 2 mol % of complex **32 (Figure 5.15(a))**. The progress of the reaction was then monitored via ^{1}H NMR spectroscopy resulting after one hour in the formation of the corresponding guanidine [(NPh$_2$)C(=NCy)(NHCy)] **48** in a 65 % yield (± 5% error as calculated from integration with ferrocene).
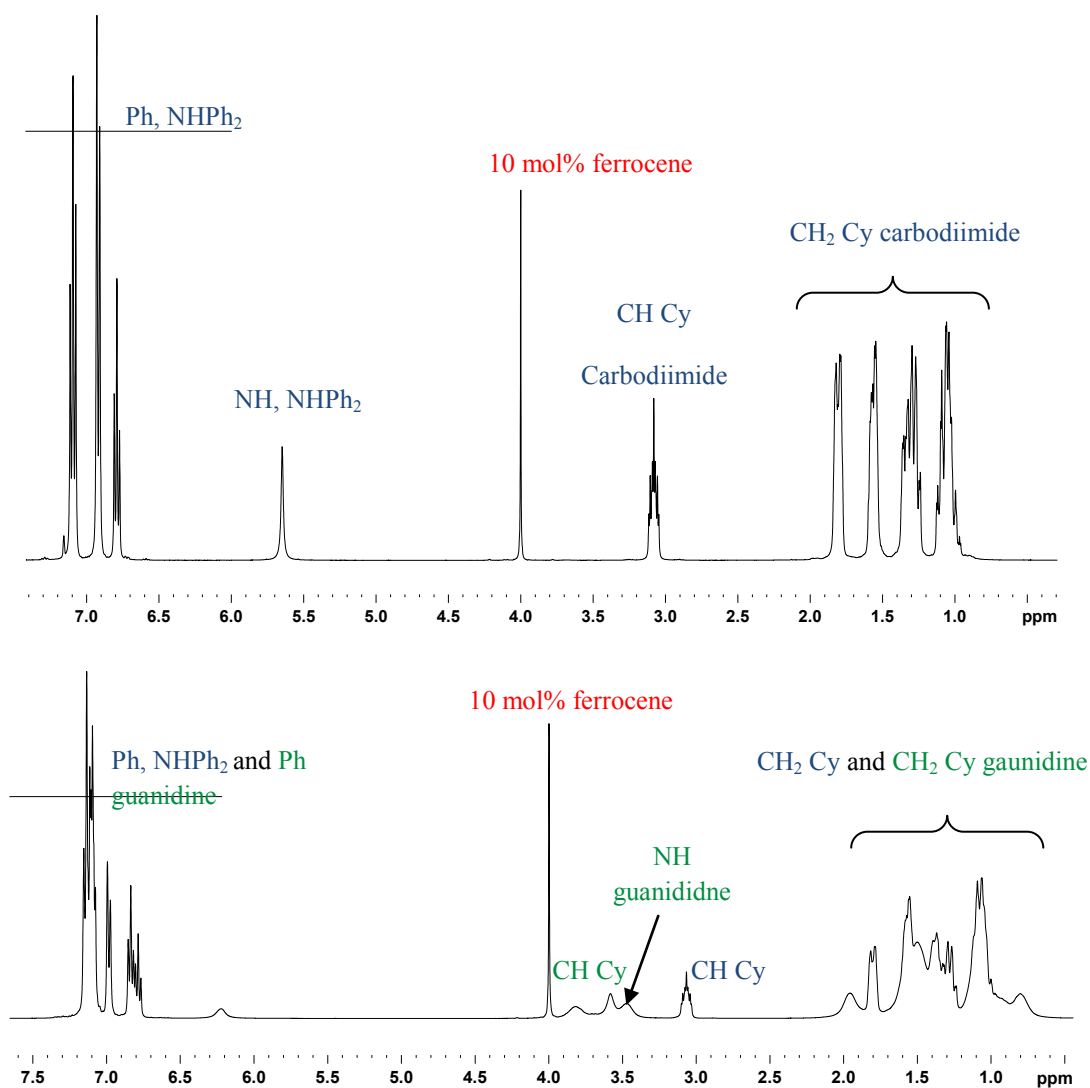
Figure 5.15: ^{1}H NMR spectra in C_6D_6 of reaction mixtures: (a) $HNPh_2$ and CyN=C=NCy with ferrocene (b) after addition of 2 mol % **32** at 25°C after 1 hour.

The reaction of $^iPrN=C=N^iPr$ with $HNPh_2$ was also studied, using the same method as described for CyN=C=NCy above. The progress of the reaction was monitored via ^{1}H NMR spectroscopy resulting in the formation of the corresponding guanidine $[(NPh_2)C(=N^iPr)(NH^iPr)]$ **49** forming in a 64 % yield after one hour, (± 5% error as calculated from integration with ferrocene), **Figure 5.16** (a) and (b) show the ^{1}H NMR of the starting materials and the ^{1}H NMR after addition of 2 mol% **32** respectively.
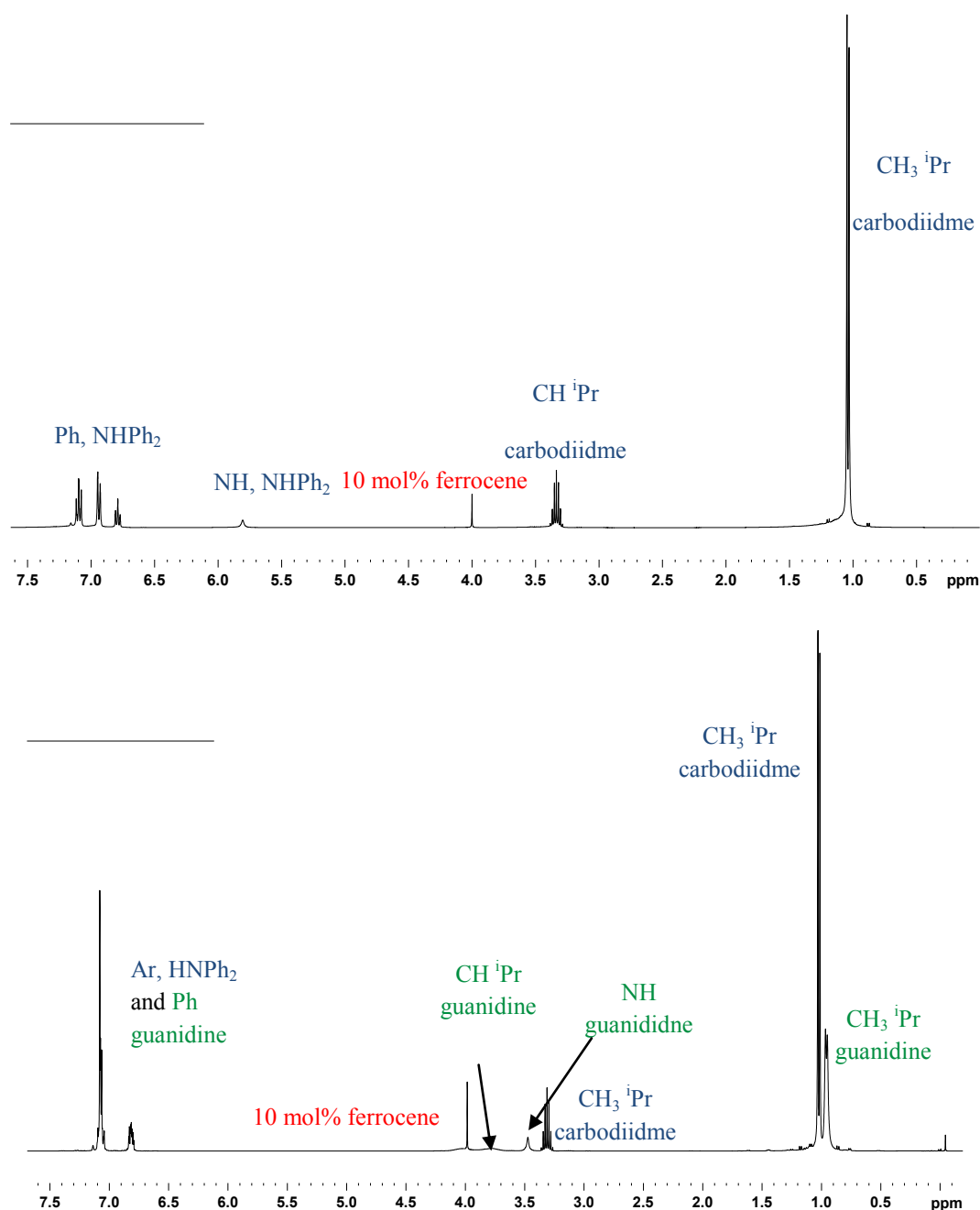
Figure 5.16: ^{1}H NMR spectra in C_6D_6 of reaction mixtures: (a) HNPh$_2$ and ^{i}PrN=C=N^{i}Pr with ferrocene (b) after addition of 2 mol % **32**.

These studies show a moderate catalytic activity for these reagents at room temperature. It should be mentioned that similar reactions carried out by Hill *et al* using heavier alkaline-earth amide [Ca{N(SiMe$_3$)$_2$(THF)$_2$] show slightly better conversions of 81 and 74 % yields for **48** and **49** respectively). Alternatively MgBu$_2$ has been shown to catalyst the hydroamination of ^{i}PrN=C=N^{i}Pr with several primary

amines although the use of refluxing conditions (using toluene as a solvent) is required to achieve greater conversions.[209]

In order to shed some light on the constitution of the intermediates involved in these reactions we therefore reacted one equivalent of CyN=C=NCy with tris(amido)magnesiate [{NaMg(NPh$_2$)$_3$(THF)$_2$]} **30** in a THF/hexane mixture which resulted in colourless crystals of complex **50** (**Scheme 5.15**) in a 24% isolated yield. This yield could be vastly increased to 72% when three molar equivalents of CyN=C=NCy were used.
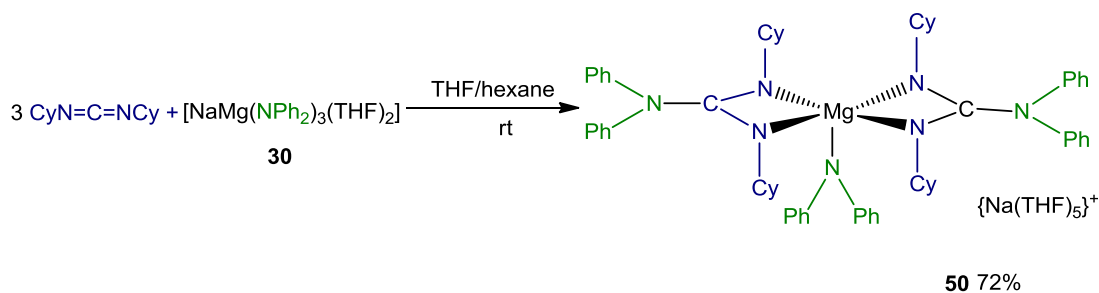
Scheme 5.15: Preparation of reactive intermediate **50**.

X-ray crystallographic analysis of **50** revealed a solvent separated structure, where the Na cation is solvated by five THF molecules. The Mg anion is pentacoordinated exhibiting a distorted square planar pyramidal geometry (angles ranging from 62.42(13) ° to 160.87(14)°; mean 105.79°), with the N atoms of the newly formed guanidinate ligands (N1, N4, N5, N2) forming the plane and the N of an unreacted amido group occupying the axial position (**Figure 5.17**). The Mg-N$_{guanidinate}$ ligand bond lengths (Mg-N1 = 2.116 (3), Mg-N2 = 1.194(3) Å and Mg-N4 = 2.178(3), Mg-N5 = 2.130(3) Å) are mostly longer than those in complex **46** (Mg-N3 = 2.101(4), Mg-N4 = 2.088(3) Å) probably due to the higher coordination number of Mg in **50**. In addition, the C-N distances and angles within the new guanidinate ligands confirm that the negative charge of this ligand is delocalized across N1···C1···N2 and N4···C1···N4 as well as the sp^2 hybridisation of C1 and C26 (Σ<C1 = 360.0° and Σ<C26 = 360.1°). Closely related to complex **50** is Ca complex [Ca{(Cy)N-C{N(SiMe$_3$)$_2$}-N(Cy)}$_2$·(Et$_2$O)] prepared by Harder *et al* by reacting two equivalents of CyN=C=NCy with [Ca{N(SiMe$_3$)$_2$}] in ether solution, where Ca is chelated by two guanidinate ligands and a molecule of ether.[164]
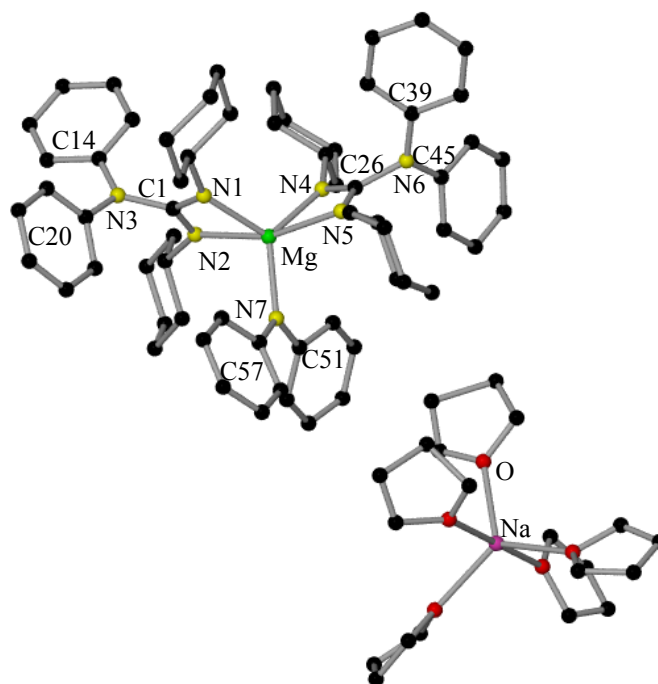
Figure 5.17: Molecular structure of **50**. Hydrogen atoms have been omitted for clarity. Bond Lengths (Å) and Angles(º):*Mg-N1 2.116(3), Mg-N2 2.194(3), Mg-N4 2.178(3), Mg-N5 2.130(3), Mg-N7 2.104(4), N4-C26 1.304(5), N5-C26 1.309(5), N6-C26 1.469(4), N1-C1 1.326(5), N2-C1 1.299(5), N3-C1 1.440(5), N1-Mg-N2 62.42(13), N1-Mg-N5 114.77(14), N1-Mg-N7 120.16(15), N1-Mg-N4 108.94(13), N2-Mg-N5 104.24(14), N2-Mg-N7 100.04(13), N2-Mg-N4 160.87(14), N4-Mg-N5 62.47(13), N4-Mg-N7 98.99(14), N5-Mg-N7 125.07(4), C14-N3-C1 117.6(3), C1-N3-C20 119.6(3), C20-N3-C14 122.6(3), C26-N6-C39 116.7(3), C26-N6-C45 117.5(3), C39-N6-C45 124.1(3), C57-N7-C51 120.1(4), C51-N7-Mg 121.9(4), C57-N7-Mg 117.9(3), N1-C1-N2 116.7(3), N2-C1-N3 122.3(3), N3-C1-N1 121.0(4), N5-C26-N6 121.7(4), N5-C26-N4 117.5(3), N6-C26-N4 120.9(4).*

This lack of activation of a third equivalent of CyN=C=NCy by [NaMg(NPh$_2$)$_3$(THF)$_2$] **30** can be due to the large steric bulk of the newly formed guanidinate ligands. These findings can help to explain the lower yields achieved in using **32** as a catalyst compared to the results seen by Hill *et al*.[12]

A postulated mechanism based on the intermediates isolated is depicted in **Scheme 5.16**. It is assumed that precatalyst **32** reacts with excess HNPh$_2$ to form complex **30**

in situ. The first step is an insertion reaction where the Mg-N$_{amide}$ bond of **30** into the carbodiimides to yield intermediate [{Na(THF)$_5$}$^+${Mg(NPh$_2$)[(NCy)C(=NCy)(NPh$_2$)]$_2$}$^-$] **50** probably through previous coordination of carbodiimide to Mg complex. Finally step 2 a protonolysis reaction occurs forming the guanidine **48** and leaving behind complex **30** to carry on the catalytic cycle.
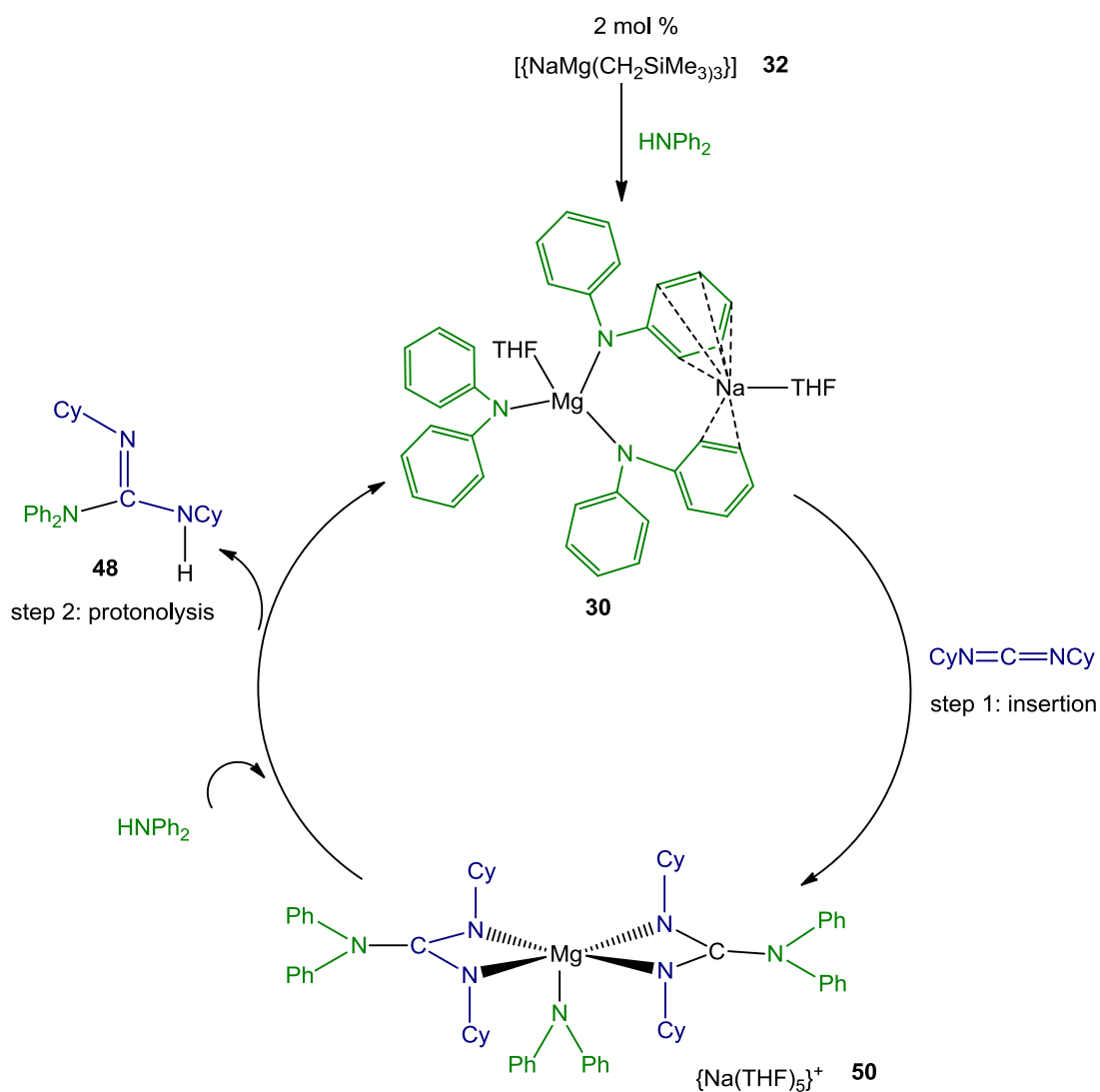
Scheme 5.16: Proposed catalytic cycle for the hydroamination of CyN=C=NCy using [{NaMg(CH$_2$SiMe$_3$)$_3$}] **32** as a precatalyst.

5.4.1 Conclusions

This chapter demonstrated the first catalytic applications of sodium magnesiates to promote the hydroamination of alkyl isocyanates and carbodiimides, under mild reaction conditions.

Through the isolation of key reaction intermediates, a greater insight into the possible mechanisms involved in these processes has been gained. Sodium magnesiate [{Na(THF)$_6$}$^+${(Ph$_2$Si(NAr*)$_2$)Mg(Bu)(THF)}$^-$] **2** can catalyse the hydroamination of ^{t}BuN=C=O by HNPh$_2$ in a 90% yield, however ^{1}H NMR monitoring of this reaction coupled with some stoichiometric studies revealed it is in fact the tris(amido)magnesiate [NaMg(NPh$_2$)$_3$] **30** which is the active species that catalyses the reaction. This complex can be efficiently prepared *in situ* using tris(alkyl)magnesiate [NaMg(CH$_2$SiMe$_3$)$_2$] **32**. Reactivity studies show that **32** can act as an efficient precatalyst for the hydroamination of several alkyl isocyanates RN=C=O (R=^{t}Bu, Cy, Et) by HNPh$_2$ in yields ranging from to 78-100%.

Remarkably **30** can also catalyse the trimerisation of *p*TolylN=C=O to form isocyanurate [{(*p*TolylN)C(=O)}$_3$] **45** under very mild reaction conditions, a reaction which has no precedents in group (II) chemistry.

The ability of complexes **32** and [{Na(THF)$_6$}$^+${(Ph$_2$Si(NAr*)$_2$)Mg(NPh$_2$)(THF)}$^-$] **7** to catalyse the hydroamination of RN=C=NR (R= Cy, ^{i}Pr) by HNPh$_2$ has also been investigated. Sterically demanding complex **7** can insert these carbodiimides in its Mg-NPh$_2$ bond under stoichiometric conditions but the large steric bulk in this compound precludes the protonation of the newly formed guanidinate ligand to regenerate **7** and allow the catalytic cycle to carry on.

On the other hand tris(alkyl) species **32** shows moderate conversions (64 and 78%) when employed as a catalyst (2 mol %) in the reactions of RN=C=NR (R = Cy, ^{i}Pr) with HNPh$_2$. This can be partially rationalised in terms of the fact that when **32** reacts with NHPh$_2$ to form tris(amido) [NaMg(NPh$_2$)$_3$] **30**, only two of its amido arms are activated towards the insertion with RN=C=NR as demonstrated by the isolation and structural characterisation of [{Na(THF)$_5$}$^+${Mg(NPh$_2$)[(NCy)C(=NCy)(NPh$_2$)]$_2$}$^-$] **50** obtained by reacting one molar equivalent of **30** with three equivalents of CyN=C=NCy.

Chapter 6: General Experimental Techniques & Procedures

6.1 General Experimental Techniques

6.1.1 Schlenk techniques

All the experimental work carried out during this project was performed using specialist standard Schlenk equipment. The Schlenk equipment provided a dry and inert atmosphere which was needed as most of the reactants and products formed were air and moisture sensitive, with some of the reagents such as ^{n}BuLi being pyrophoric in contact with air.

This special equipment consists of a Schlenk line, and Schlenk tubes, in which reactions are carried out, and a filter is occasionally used to isolate a solid product from unwanted insoluble impurities.

The line contained an inert gas/vacuum manifold, which had two separate compartments; one connected to a vacuum pump and the other connected to a supply of dry argon. All Schlenk glassware contained ground-glass joints, which were lightly greased before being connected together. This was to seal the joints securely and also prevent the glass from getting stuck together. To condense any volatile substances from being detrimental to the reaction taking place, a liquid nitrogen cooled trap was attached to the end of the Schlenk line. A pressure release bubbler is incorporated into the line to ensure there is no buildup of pressure. The Schlenk line used had five connectors which could be attached to the piece of apparatus needed. Each connector had a two way tap so that either vacuum or argon could be applied where appropriate. Air was removed from the Schlenk by applying a vacuum for fifteen minutes; the tap was then turned to allow argon in. This process was repeated a further two times to ensure a dry and inert atmosphere in the Schlenk tube. When solvents or reagents were to be added to the Schlenk tube a positive argon flow would be applied to ensure no air entered. Solvents are transferred using a syringe and needle which has been flushed with argon three times.
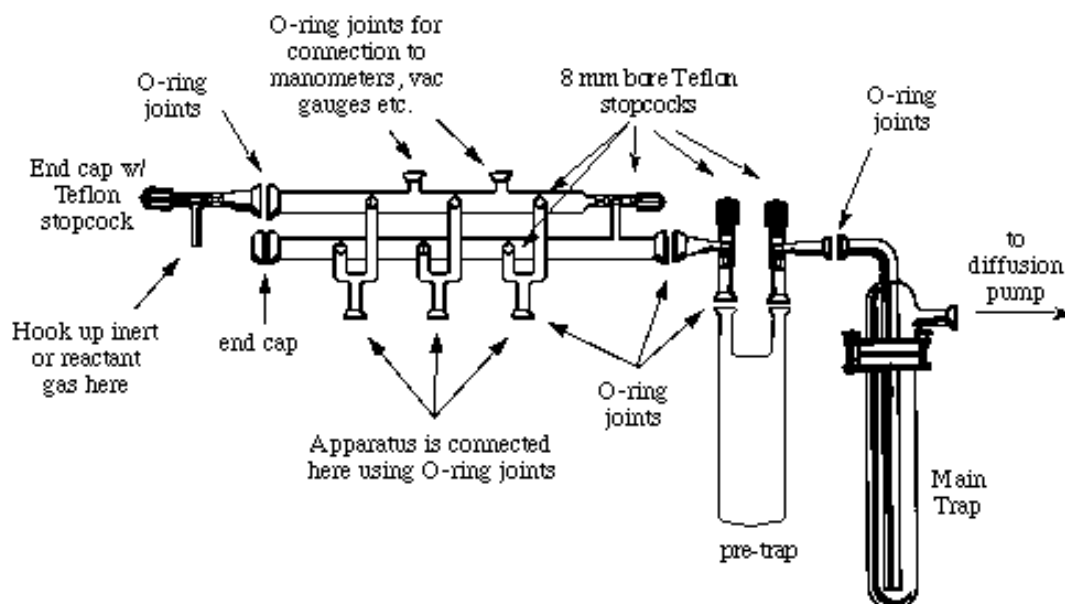
Figure 6.1 (a): Standard Schlenk line

6.1.2 Glove Box

A standard glove box was used when products which were air and moisture sensitive had to be weighed, stored and prepared for NMR.

The glove box is made of two main chambers. The larger chamber contains the large glass window and gloves and is the area where the work is carried out. The chamber is filled with dry argon. The smaller chamber is called the port; it contains an inner and outer door. The purpose of the two doors is to allow items to be placed in the large chamber without air entering. Items are placed in the port and a vacuum supplied, the port is then filled with argon. This process is carried out a further two times. The gas in the glove box is constantly circulated over a scrubber, which removes any air or moisture which may be present in the system.

Figure 6.1 (b): Glove box

6.1.3 Solvent purification

As most of the reactants and product are air and moisture sensitive all solvents were dried and de-gassed before use. All of the solvents used during this project were distilled over nitrogen, in the presence of sodium and benzophenone. Sodium when reacted with benzophenone gives a ketyl radical which is blue in colour. This is very reactive with oxygen and water to give a colourless or yellow solution. Thus these substances act as self-indicators for ensuring the removal of oxygen and water from the solvent.

6.1.4 Analytical Procedures

All ^{1}H NMR spectroscopic analysis were carried out on either a Bruker DPX400 spectrometer, which operates at 400.03 MHz. the DPX 500 which runs at 500.13 MHz or the AV400 which operates at 400.03 MHz. The ^{13}C NMR spectra were carried out on the same instruments, operating at 100.62 MHz, and all were proton decoupled.

Abbreviations of NMR patterns are as follows: s (singlet), d (doublet), t (triplet), m (multiplet), and b (broad peak).

The X-ray crystallographic data were obtained on Brucker SMART and Nonius Kappa CCD diffractometers at 150K, with graphite monochromated Mo-Kα radiation ($\lambda = 0.71073$)

General chemicals which were used all the time such as ^{n}BuLi and ^{n}Bu$_2$Mg were ordered from Sigma Aldrich and stored in the fridge. BuNa was prepared in the lab

by reacting NaO^{t}Bu and BuLi in hexane. This would then be filtered and stored in the glove box. Mg(CH$_2$SiMe$_3$)$_2$ was prepared by reacting BuLi with trimethylsilylchloride in ether. Precipitated LiCl is then filtered off. All solvent is removed by vacuum and the solid Mg(CH$_2$SiMe$_3$) sublimed, the solid is stored in the glove box.

6.1.5 NMR-Scale Experiments

In a glove box, accurately weighed ferrocene (0.018 g, 0.1 mmol), amine (1 mmol and isocyanate (1 mmol) and dissolved in deuterated solvent (2 ml) and transferred to an NMR tube. The initial concentration of reagents were measured by ^{1}H NMR spectroscopy, following which the catalyst (2-10 mol %) was added and the reaction monitored by ^{1}H NMR spectroscopy. Yields were calculated by reference to ferrocene as an internal standard.

6.2 Synthesis of products

6.2.1 Synthesis of [Ph$_2$Si(NAr*H)$_2$] 1

To an oven dried Schlenk were added diethylether (40 ml) followed by H$_2$NAr* (5.8 ml, 30 mmol). The reaction was cooled to -78°C, using an isopropanol and liquid nitrogen bath, and ^{n}BuLi added drop wise (18.75 ml, 1.6 M solution in hexane, 30 mmol). The reaction was allowed to reach room temperature then re-cooled to -78°C and Ph$_2$SiCl$_2$ added (3.15 ml, 15 mmol) drop wise. A white suspension formed that was allowed to stir over-night. The LiCl which had formed was filtered through a celite filled filter stick. The filtrate was removed by vacuum until a solid began to precipitate. The suspension was then gently heated until a clear solution was obtained which was then placed in the freezer. A large crop of colourless crystals were obtained, and isolated by filtration and stored in the glove box (yield 7.72 g, 96%).

^{1}H NMR (C$_6$D$_6$, 298 K) δ7.71 [m, 4H, Ph or Ar*], 7.12 [m, 6H, Ph or Ar*], 7.05 [m, 6H, Ph or Ar*], 3.51 [s, 2H, NH], 3.38 [m, 4H, CH, ^{i}Pr, Ar*], 1.00 [d, 24H, CH_3, ^{i}Pr, Ar*]. **^{13}C{^{1}H} NMR** (C$_6$D$_6$, 298K) δ145.26, 138.76, 136.34, [$C_{quarternay}$, Ph or Ar*],

136.02 , 135.96 , 129.89, 123.98, 123.54 [CH, Ph or Ar*], 23.4 [CH, ^{i}Pr, Ar*], 29.1 [CH_3, ^{i}Pr, Ar*].

6.2.2 Synthesis of [{Na(THF)$_6$}$^+${(Ph$_2$Si(NAr*)$_2$)Mg(Bu)(THF)}$^-$] 2

BuNa (0.32 g, 4 mmol) was suspended in a Schlenk tube in 20 ml of hexane. An equivalent of Bu$_2$Mg was added (4 ml, of a 1 M solution in heptane, 4 mmol) and the suspension stirred for a further ten minutes. Amine 1 was added (2.13 g, 4 mmol) and the reaction mixture was allowed to stir for one hour. 4 ml of THF were introduced and the mixture was heated until a solution was obtained. The Schlenk was placed in a hot water Dewar overnight. Colourless crystals which had formed were isolated and transferred to the glove box (yield 4.06 g, 89%).

^{1}**H NMR** (C$_6$D$_6$, 298 K) δ7.82 [d, 4H, Ph], 7.16 [dd, 4H, Ph], 7.10 [d, 2H, Ph], 7.05 [d, 4H, Ar*], 6.75 [t, 2H, Ar*], 3.98[s, 4H, CH, ^{i}Pr, Ar*], 3.50 [t, 28H, OCH_2, THF], 1.71 [d, 2H, CH_2, Bu], 1.59 [t, 3H, CH_3, Bu], 1.36 [m, 28H, CH_2, THF], 1.14 [m, 2H, CH_2, Bu], 1.08 [d, 24H, CH_3, ^{i}Pr, Ar*], -0.34 [t, 2H, Mg-CH_2, Bu]. ^{13}C{^{1}H} **NMR** (C$_6$D$_6$, 298K) δ152.48, 144.49, 142.34 [$C_{quarternary}$, Ph or Ar*], 135.51 [CH, Ph], 126.91 [CH, Ph] , 126.63 [CH, Ph], 123.36 [CH, Ar*], 116.30 [CH, Ar*], 68.20 [O-CH_2, THF], 33.43 [CH_2, Bu], 32.86 [CH_3, Bu], 28.14 [CH, ^{i}Pr, Ar*], 25.41 [CH_2, THF], 25.12 [CH_3, ^{i}Pr, *Ar*], 14.25 [CH_2, Bu], 9.38 [Mg-CH_2, Bu].

6.2.3 Synthesis of [{Ph$_2$Si(NHAr*)(NAr*)Na}$_2$]3

BuNa (0.08 g, 1 mmol) was suspended in a Schlenk tube in 5 ml of hexane. An equivalent of already prepared amine 1 (0.53 g, 1 mmol) was added and the suspension allowed stirring for one hour. Toluene (5 ml) was dripped in until a clear solution was obtained. A batch of crystals were isolated after storage in the freezer for 2 days and transferred to the glove box (yield = 1.16 g, 33%).

^{1}**H NMR** (C$_6$D$_6$, 298K) δ7.54 [m, 8H, Ph, or toluene], 7.11 [m, 13H, Ph or toluene], 7.00 [m, 13H, Ph or toluene or Ar*], 7.00 [m, 13H, Ph or toluene or Ar*], 6.46 [t, 2H, Ph or toluene or Ar*], 3.95 [s, 2H, NH], 3.74 [m, 4H, CH, ^{i}Pr, Ar*], 3.20 [m, 4H, CH, ^{i}Pr, Ar*], 2.11 [s, 3H, CH_3, toluene], 1.02 [d, 24H, CH_3, ^{i}Pr, Ar*], 0.93 [d,

24H, CH_3, ^{i}Pr, Ar*]. ^{13}C{^{1}H} NMR (C$_6$D$_6$, 298K) δ154.74, 142.47, 141.96, 141.64, 139.61 [$C_{quarternary}$, Ph, toluene, Ar*], 135.03, 129.16, 128.59, 127.36, 125.51, 123.43, 123.13.121.85, 113.10 [CH, Ph or toluene or Ar*], 28.76 [CH, ^{i}Pr, Ar*], 27.11 [CH, ^{i}Pr, Ar*], 23.45 [CH$_3$, ^{i}Pr, Ar*], 23.22 [CH$_3$, ^{i}Pr, Ar*], 21.12 [CH$_3$, toluene].

6.2.4 Synthesis of [{Na(THF)$_6$}$^+${(Ph$_2$Si(NAr*)$_2$)Mg(CH$_2$SiMe$_3$)(THF)}$^-$] 5

BuNa (0.24 g, 3 mmol) was suspended in a Schlenk tube in 10 ml of hexane. An equivalent of Mg(CH$_2$SiMe$_3$)$_2$ was added (0.60 g, 3 mmol) and the suspension stirred for a further 10 minutes. Amine **1** (1.60 g, 3 mmol) was then introduced and the resulting suspension was allowed to stir for one hour. 4ml of THF were introduced and the mixture was heated until a solution was obtained. The Schlenk was placed in the freezer. Colorless crystals which had formed were isolated and transferred to the glove box. Isolated crystalline yield (2.41 g, 69%).

^{1}**H NMR** (C$_6$D$_6$, 298K) δ7.89 [d, 4H, Ph], 7.11 [dd, 4H, Ph], 7.02 [d, 2H, Ph], 6.98 [d, 4H, Ar*], 6.64 [t, 2H, Ar*], 4.22 [s, 4H, CH, ^{i}Pr, Ar*], 3.47 [t, 28H, OCH_2, THF], 1.36 [m, 28H, CH_2, THF], 1.15 [d, 24H, CH_3, ^{i}Pr, Ar*], 0.34 [s, 9H, Si(CH_3)$_3$], -1.28 [s, 2H, Mg-CH_2]. ^{13}C{^{1}H} NMR (C$_6$D$_6$, 298K) δ153.91, 146.13, 143.21 [$C_{quarternary}$, Ph or Ar*], 135.11 [CH, Ph], 126.21 [CH, Ph], 126.14 [CH, Ph], 122.94 [CH, Ar*], 115.25 [CH, Ar*], 68.20 [O-CH$_2$, THF], 28.94 [CH, ^{i}Pr, Ar*], 25.41 [CH$_2$, THF], 25.26 [CH$_3$, ^{i}Pr, Ar*], 4.73 [CH$_3$, SiMe$_3$], -0.82 [Mg-CH$_2$].

6.2.5 Synthesis of [{Na(THF)$_6$}$^+${(Ph$_2$Si(NAr*)$_2$)Mg(N(SiMe$_3$)$_2$)(THF)}$^-$] 6

BuNa (0.16 g, 2 mmol) was suspended in a Schlenk tube in 10 ml of hexane. An equivalent of Mg(CH$_2$SiMe$_3$)$_2$ was added (0.40 g, 2 mmol) and the suspension stirred for 10 minutes. The already prepared amine **1** was added (1.06g, 2 mmol) and allowed the suspension to stir for one hour. HMDS(H) (0.41 ml, 2 mmol) was added and the solution allowed stirring for a further hour. THF (4 ml) was introduced and the suspension gently heated to achieve a clear solution. Crystals formed in the freezer after 24 hours. The crystals were isolated by filtration and transferred to the glove box. Isolated crystalline yield (1.77 g, 71%).

¹H NMR (d$_8$-THF, 298K) δ7.16 [d, 4H, Ph], 6.85 [dd, 4H, Ph], 6.83 [d, 2H, Ph], 6.66 [d, 4H, Ar*], 6.40 [t, 2H, Ar*], 4.04 [s, 4H, C*H*, ^{i}Pr, Ar*], 3.61 [t, 28H, OC*H$_2$*, THF], 1.77 [m, 28H, C*H$_2$*, THF], 0.76 [d, 24H, C*H$_3$*, ^{i}Pr, Ar*], -0.21 [s, 18H, C*H$_3$*, HMDS].**¹³C{¹H} NMR** (d$_8$-THF, 298 K) δ153.92, 148.21, 144.11[*C*$_{quarternary}$, Ph or Ar*], 135.82 [*C*H, Ph] , 125.87 [*C*H, Ph] ,125.83 [*C*H, Ph] 121.44 [*C*H, Ar*], 115.55 [*C*H, Ar*], 67.21 [O-*C*H$_2$, THF], 27.32 [*C*H$_2$, THF], 25.92 [*C*H, ^{i}Pr, Ar*], 6.11 [*C*H$_3$, ^{i}Pr, Ar*], 5.21 [*C*H$_3$, HMDS].

6.2.6 Synthesis of [{Na(THF)$_6$}$^+${(Ph$_2$Si(NAr*)$_2$)Mg(NPh$_2$)(THF)}$^-$] 7

BuNa (0.08 g, 1 mmol) was suspended in a Schlenk tube in 20 ml of hexane. Mg(CH$_2$SiMe$_3$)$_2$ was then added (0.20 g, 1 mmol) and allowed to stir for five minutes. The already prepared amine **1** was introduced (0.53 g, 1 mmol) and the suspension stirred for 1 hour. THF (3.5 ml) was added until a clear solution formed. Diphenylamine was added (0.16 g, 1 mmol) and the solution allowed stirring for one hour. A white suspension formed, which was carefully heated until clear. The Schlenk was left in a hot water Dewar overnight and colourless crystals were deposited. The filtrate was removed by syringe and the crystals kept under vacuum until being transferred to the glove box for isolation. Typical yield (0.86 g, 64%).

¹H NMR (C$_6$D$_6$, 298K) δ7.62–7.23 [m, 24H, Ph, NPh$_2$, Ar*], 6.67 [m, 2H, Ar*], 3.97 [s, 4H, C*H*, ^{i}Pr, Ar*], 3.42 [t, 28H, OC*H$_2$*, THF], 1.30 [m, 28H, C*H$_2$*, THF], 1.06 [d, 24H, C*H$_3$*, ^{i}Pr, Ar*]. **¹³C{¹H} NMR** (C$_6$D$_6$, 298K) δ156.24, 152.24, 146.12, 143.5, 135.4, 130.9, 127.8, 127.3, 124.2, 120.8, 118.3, 117.92 [*C*$_{quarternary}$ and *C*H, Ph, NPh$_2$ or Ar*], 68.52 [O-*C*H$_2$, THF], 28.32 [*C*H, ^{i}Pr, Ar*], 25.62 [*C*H$_3$, ^{i}Pr, Ar*], 25.12 [*C*H$_2$, THF].

6.2.7 Synthesis of [{Na(THF)$_6$}$^+${(Ph$_2$Si(NAr*)$_2$)Mg(N^{i}Pr$_2$)(THF)}$^-$] 8

BuNa (0.16 g, 2 mmol) was suspended in a Schlenk tube in 10 ml of hexane. An equivalent of Mg(CH$_2$SiMe$_3$)$_2$ was added (0.40 g, 2 mmol) and the suspension stirred for ten minutes. Added the already prepared amine **1** (1.06 g, 2 mmol) and allowed

the suspension to stir for one hour. Diisopropylamine (0.28 ml, 2 mmol) was added and allowed to stir for a further hour. 2 ml of THF was then dripped in, and the suspension gently heated until clear. The Schlenk was placed in the freezer and deposited colourless crystals after two days. The crystals were isolated by filtration and transferred to the glove box yield (0.31 g, 26%).

^{1}H NMR (C$_6$D$_6$, 298K) δ7.67 [d, 4H, Ph], 7.18 [dd, 4H, Ph], 7.19 [d, 2H, Ph], 7.09 [d, 4H, Ar*], 6.88 [t, 2H, Ar*], 4.20 [m, 4H, C*H*, ^{i}Pr, Ar*], 3.41 [t, 28H, OC*H$_2$*, THF], 3.23 [m, 2H, C*H*, N-^{i}Pr, Ar*] 1.38 [t, 28H, C*H$_2$*, THF], 1.24 [d, 12H, C*H$_3$*, N-^{i}Pr, Ar*], 1.16 [d, 24H, C*H$_3$*,^{i}Pr, Ar*]. **^{13}C{^{1}H} NMR** (C$_6$D$_6$, 298K) δ151.82, 145.86, 143.72 [*C*$_{quarternary}$, Ph or Ar*], 135.51 [*C*H, Ph], 127.81 [*C*H, Ph], 127.01 [*C*H, Ph], 123.19 [*C*H, Ar*], 117.32 [*C*H, Ar*], 68.21 [O-*C*H$_2$,THF], 49.99 [*C*H, N-^{i}Pr, Ar*], 28.21 [*C*H$_3$, N-^{i}Pr, Ar*], 28.01 [*C*H, ^{i}Pr, Ar*], 25.42 [*C*H$_2$, THF], 25.21 [*C*H$_3$, ^{i}Pr, Ar*].

6.2.8 Synthesis of [{Na(THF)$_6$}$^+${(Ph$_2$Si(NAr*)$_2$)Mg(DMP)(THF)}$^-$] 9

BuNa (0.08 g, 1mmol) was suspended in a Schlenk tube in 5 ml of hexane. An equivalent of Mg(CH$_2$SiMe$_3$)$_2$ was added (0.20 g, 1 mmol) and the suspension stirred for ten minutes. Added the already prepared amine **1** (0.53 g, 1mmol) and allowed the solution to stir for one hour. DMP(H) (0.13 ml, 1 mmol) was added and the suspension stirred for a further hour. THF (4 ml) was dripped in and the suspension gently heated until clear, removed some solvent by vacuum. Crystals formed in the freezer after twenty-four hours. The colourless crystals were isolated by filtration and transferred to the glove box yield (0.62 g, 51%).

^{1}H NMR (C$_6$D$_6$, 298K) δ7.68 [d, 4H, Ph], 7.15 [dd, 4H, Ph], 7.13 [d, 2H, Ph], 7.05 [d, 4H, Ar*], 6.88 [t, 2H, Ar*], 4.11 [m, 4H, C*H*, ^{i}Pr, Ar*], 3.35 [t, 15H, OC*H$_2$*, THF], 2.76 [m, 2H, C*H*, DMP], 1.88 [m, 2H, C*H$_2$*, DMP], 1.64 [m, 2H, C*H$_2$*, DMP], 1.34 [d, 6H, C*H$_3$*, DMP], 1.30 [t, 15H, C*H$_2$*, THF], 1.14 [C*H$_3$*, ^{i}Pr, Ar*], 0.72 [m, 2H, C*H$_2$*, DMP].**^{13}C{^{1}H} NMR** (C$_6$D$_6$, 298K) δ 153.21, 147.32, 144.10 [*C*$_{quarternary}$, Ph or Ar*], 135.89 [*C*H, Ph], 127.87 [*C*H, Ph], 127.54 [*C*H, Ph], 123.36 [*C*H, Ar*], 118.10 [*C*H, Ar*], 67.25 [O-*C*H$_2$,THF], 56.34 [*C*$_{quarternary}$, DMP], 39.08 [*C*H$_2$, DMP], 28.54

[CH, ^{i}Pr, Ar*], 28.01 [CH_2, DMP], 26.87 [CH_2, DMP], 26.35 [CH_2, THF], 26.12 [CH_3, ^{i}Pr, Ar*], 25.98 [CH_3, DMP].

6.2.9 Synthesis of [{Na(THF)$_6$}$^+${(Ph$_2$Si(NAr*)$_2$)Mg(TMP)}$^-$] 10

BuNa (0.08 g, 1 mmol) was suspended in a Schlenk tube in 5 ml of hexane. An equivalent of Mg(CH$_2$SiMe$_3$)$_2$ was added (0.20 g, 1 mmol) and the suspension stirred for ten minutes. Added the already prepared amine **1** (0.53g, 1 mmol) and allowed the solution to stir for one hour. TMP(H) (0.17 ml, 1 mmol) was added and the suspension stirred for a further hour. THF (4 ml) was dripped in and the suspension gently heated until clear, removed some solvent by vacuum. Crystals formed in the freezer after two days. The colourless crystals were isolated by filtration and transferred to the glove box (yield 1.62 g, 70%).

^{1}H NMR (C$_6$D$_6$, 298K) δ7.74 [d, 4H, Ph], 7.16 [m, 4H, Ph], 7.05 [m, 2H, Ph], 7.01 [m, 4H, Ar*], 6.70 [t, 2H, Ar*], 4.44 [m, 4H, CH, ^{i}Pr, Ar*], 3.32 [t, 24H, OCH_2, THF], 1.83 [m, 2H, CH_2, γ-TMP], 1.72 [m, 4H, CH_2, β-TMP], 1.40 [s, 12H, CH_3, TMP], 1.37 [m, 24H, CH_2, THF], 1.23 [d, 24H, CH_3, ^{i}Pr, Ar*]. **^{13}C{^{1}H} NMR** (C$_6$D$_6$, 298K) δ 152.35, 145.62, 144.02 [$C$$_{quarternary}$, Ph or Ar*], 135.86 [C$H$, Ph], 126.82 [C$H$, Ar*], 126.75 [C$H$, Ph], 122.88 [C$H$, Ar*], 116.23[C$H$, Ar*], 68.10 [O-C$H_2$,THF], 51.71 [Cα, TMP], 40.97 [$C_β$, TMP], 36.78 [CH_3, TMP], 27.14 [CH, ^{i}Pr, Ar*], 25.12 [CH_2,THF], 25.87 [CH_3, ^{i}Pr, Ar*], 20.02 [Cγ, TMP].

6.2.10 Synthesis of [{Na(THF)$_6$}$^+${(Ph$_2$Si(NAr*)(NHAr*))Mg(NHAr*)$_2$(THF)}$^-$] 11

BuNa (0.08 g, 1 mmol) was suspended in a Schlenk tube in 5 ml of hexane. An equivalent of Mg(CH$_2$SiMe$_3$)$_2$ was added (0.20 g, 1 mmol) and the suspension stirred for ten minutes. Added the already prepared amine **1** (0.53 g, 1 mmol) and allowed the solution to stir for one hour. H$_2$NAr* (0.38 ml, 2 mmol) was added and the suspension stirred for a further hour. THF (4 ml) was dripped in and the suspension gently heated until clear, removed some solvent by vacuum. Crystals formed in the

freezer after two days. The colourless crystals were isolated by filtration and transferred to the glove box (yield 0.42 g, 28%).

^{1}H NMR (C$_6$D$_6$, 298K) 7.67 [m, 4H, Ph], 7.11 [m, 6H, Ph and Ar*], 7.03 [m, 10H, Ph and Ar*], 6.54 [t, 2H, Ar*], 3.50 [m, 5H, C*H*, ^{i}Pr, Ar*], 3.50 [m, 5H, N*H*] 3.36 [m, 4H, C*H*, ^{i}Pr, Ar*], 3.26 [s, 2H, N*H*] 3.17 [m, 8H, OC*H*$_2$, THF], 1.32 [d, 24H, C*H*$_3$, ^{i}Pr, Ar*], 1.20 [t, 8H, C*H*$_2$, THF], 0.98 [d, 24H, C*H*$_3$, ^{i}Pr, Ar*]. **^{13}C{^{1}H} NMR** (C$_6$D$_6$, 298K) δ154.26, 142.62, 139.24, 135.90 [$C_{quarternary}$], 135.28 [*C*H, Ph], 132.16 [$C_{quarternary}$], 129.98 [*C*H, Ph or Ar*], 127.81 [*C*H, Ph or Ar*],123.66, 123.56, 122.94, [*C*H, Ph or Ar*], 112.49 [*C*H, Ar*], 68.09 [O*C*H$_2$, THF], 31.80 [*C*H, ^{i}Pr, Ar*], 28.30 [*C*H, ^{i}Pr, Ar*], 25.24 [*C*H$_2$, THF], 23.88, 23.69 [*C*H$_3$, ^{i}Pr, Ar*].

6.2.11 Synthesis of [{(Ph$_2$Si(NAr*)(NHAr*))Mg(NC$_4$H$_4$)$_2$(THF)Na(THF)$_2$}] 12

BuNa (0.08 g, 1 mmol) was suspended in a Schlenk tube in 5 ml of hexane. An equivalent of Mg(CH$_2$SiMe$_3$)$_2$ was added (0.20 g, 1 mmol) and the suspension stirred for 10 minutes. Added the already prepared amine **1** (0.53 g, 1 mmol) and allowed the solution to stir for one hour. Pyrrole (0.14 ml, 2 mmol) was added and the suspension stirred for a further hour. THF (4 ml) was dripped in and the suspension gently heated until clear, removed some solvent by vacuum. Crystals formed in the freezer after four days. The colourless crystals were isolated by filtration and transferred to the glove box (yield 0.41 g, 44%).

^{1}H NMR (C$_6$D$_6$, 298K) δ7.93 [d, 4H, Ph], 7.52 [s, 2H, α-C*H*, Mg-NC$_4$H$_4$], 7.22 [m, 4H, Ph], 7.15 [m, 4H, Ph and α-C*H*, Mg-NC$_4$H$_4$], 6.82 [d, 4H, Ar*], 6.65 [t, 2H, Ar*], 6.40 [s, 4H, β-C*H*$_2$, Mg-NC$_4$H$_4$], 6.36 [s, 4H, β-C*H*$_2$, Mg-NC$_4$H$_4$], 4.02 [m, 4H, C*H*, ^{i}Pr, Ar*], 3.40 [t, 24H, OC*H*$_2$, THF], 1.26 [t, 24H, C*H*$_2$, THF], 1.06 [d, 24H, C*H*$_3$, ^{i}Pr, Ar*]. **^{13}C{^{1}H} NMR** (C$_6$D$_6$, 298K) δ152.60, 144.65, 142.14, 141.95, 140.92 [$C_{quarternary}$, Ph or Ar*], 135.39 [*C*H, Ph], 127.17 [*C*H, Ph], 127.12 [α-*C*H, Mg-C$_4$H$_4$], 127.02 [*C*H, Ph], 126.76 [α-*C*H, Mg-C$_4$H$_4$], 123.13 [*C*H, Ar*], 115.67 [*C*H, Ar*], 107.79 [β-*C*H, Mg-C$_4$H$_4$], 107.45 [β-*C*H, Mg-C$_4$H$_4$], 68.46 [O-*C*H$_2$,THF], 28.54 [*C*H, ^{i}Pr, Ar*], 25.14 [*C*H$_2$, THF], 23.44 [*C*H$_3$, ^{i}Pr, Ar*].

6.2.12 Synthesis of[{Na(THF)$_6$}$^+${Ph$_2$Si(NAr*)$_2$)Mg(C$_4$H$_3$S)(THF)}$^-$] 13

Already prepared amido complex **10** (1.15 g, 1 mmol) was added to a Schlenk tube and then dissolved in THF (4 ml), to form a yellow solution. Thiophene was added (0.08 ml, 1 mmol) and the solution stirred for two hours. Hexane was added (5 ml) until the solution became slightly cloudy. The Schlenk was placed in the freezer and after a day resulted in colourless crystals. Crystals were analysed and transferred to the glove box and analysed by NMR spectroscopy. Isolated yield (0.47 g, 45%)

^{1}H NMR (C$_6$D$_6$, 298K) δ7.91 [d, 4H, Ph], 7.60 [d, 1H, C*H*, Cβ], 7.57 [d, 1H, C*H*, Cδ], 7.29 [dd, 1H, C*H*, Cγ], 7.21 [dd, 4H, Ph], 7.17 [d, 4H, Ph], 7.12 [d, 4H, Ar*], 6.81 [t, 2H, Ar*], 4.00 [m, 4H, C*H*, ^{i}Pr, Ar*], 3.43 [m, 28H, OC*H*$_2$, THF], 1.32 [m, 28H, C*H*$_2$, THF], 1.09 [m, 24H, C*H*$_3$, ^{i}Pr, Ar*]. **^{13}C{^{1}H} NMR** (C$_6$D$_6$, 298K) δ161.60 [*C*-Mg, C$_4$SH$_3$], 152.03, 144.44, 141.86 [*C*$_{quarternary}$, Ph or Ar*], 135.94 [Cβ, C$_4$SH$_3$], 135.35 [Cγ, C$_4$SH$_3$], 130.81 [Cδ, C$_4$SH$_3$], 128.63 [*C*H, Ph], 127.11 [*C*H, Ph], 127.06 [*C*H, Ph], 123.66 [*C*H, Ar*], 116.54 [*C*H, Ar*], 68.09 [O-*C*H$_2$, THF], 28.66[*C*H ,^{i}Pr, Ar*], 25.38 [*C*H$_2$, THF], 24.78 [*C*H$_3$,^{i}Pr, Ar*].

6.2.13 Synthesis of [{Na(THF)$_5$}$_2$$^+${(Ph$_2$Si(NAr*)$_2$)Mg(MeBIm*)}$_2$$^-$] 14

Isolated crystals of **2** (1.14 g, 1 mmol) were added to a Schlenk tube and dissolved in THF (3 ml) to form a pale yellow solution. 1-methylbenzimidazole was introduced (0.13 g, 1 mmol), and the reaction stirred for two hours. The solution changed to pale green in colour. Hexane (5 ml) was dripped in until a solid began to precipitate and gently heated back to solution. The Schlenk was placed in the freezer overnight resulting in yellow crystals. The solvent was then removed by syringe and the solid left under vacuum until being transferred to the glove box to be isolated. Isolated yield (0.76 g, 70%)

^{1}H NMR (d$_8$-THF, 298K) δ7.30 [d, 2H, Ph], 6.97 [m, 4H, Ph], 6.95 [m, 1H, MeBIm], 6.94 [m, 1H, MeBIm], 6.88 [d, 4H, Ar*], 6.59 [t, 2H, Ar*], 6.33 [m, 1H, MeBIm], 6.12 [t, 1H, MeBIm], 4.10 [m, 4H, C*H*, ^{i}Pr, Ar*], 3.61 [m, 20H, OC*H*$_2$, THF], 3.51 [s, 3H, C*H*$_3$, MeBIm], 1.76 [m, 20H, C*H*$_2$, THF], 0.78 [d, 24H, C*H*$_3$, ^{i}Pr, Ar*]. **^{13}C{^{1}H} NMR** (d$_8$-THF, 298K) δ194.00 [*C*-Mg], 155.90, 155.37, 148.56, 145.42, 143.43 [*C*$_{quarternary}$, Ph, Ar*) or MeBIm], 136.93 [*C*H, Ph], 127,68 [*C*H, Ph],

127.45 [CH, Ph], 123.88 [CH, Ar*], 123.10, 121.03, 120.64 [CH, MeBIm], 117.57 [CH, Ar*], 116.85 [CH, MeBIm], 69.22 [$O\text{-}CH_2$, THF], 34.66 [CH_3, MeBIm], 29.30 [CH, ^{i}Pr, Ar*], 27.39 [CH_3, ^{i}Pr, Ar*], 26.54 [CH_2, THF].

6.2.14 Synthesis of [$L_2Mg_2Na_2(THF)_5$] 15

Isolated crystals of **2** (1.14 g, 1 mmol) were dissolved in THF (5 ml) to form a pale yellow solution. Benzothiazole (Btz) was then introduced (0.3 ml, 3 mmol) and the solution stirred for thirty minutes. The solution became dark red instantaneously. Hexane (1 ml) was added, and the resulting red suspension was then gently heated until a clear solution was obtained. After twenty-four hours stored at room temperature a crop of red crystals of were obtained (yield 0.69 g, 89%).

^{1}H NMR (d$_8$THF, 298K) δ7.94 [d, 1H, CH, C_6H_4], 7.80 [d, 1H, CH, C_6H_4], 7.66 [d, 1H, CH, C_6H_4], 7.39 [d, 1H, CH, C_6H_4], 7.23-7.11 [m, 6H, CH's, C_6H_4], 6.98 [t, 2H, CH, C_6H_4], 6.87 [t, 1H, CH, C_6H_4], 6.74 [t, 2H, CH, C_6H_4], 6.74-6.33 [m, 3H,CH's, C_6H_4], 6.51 [d, 2H, CH, C_6H_4], 6.49 [t, 1H, CH, C_6H_4], 6.44 [t, 1H, CH, C_6H_4], 6.39 [d, 1H, CH, C_6H_4], 5.95 [m,2H, CH's, C_6H_4], 3.61 [m, 22H, OCH_2, THF], 1.77 [m, 22H, CH_2, THF].

Compound **15** showed limited solubility in deuterated THF which precluded the acquisition of a meaningful ^{13}C NMR spectrum. ^{1}H NMR analysis of the filtrate from this reaction showed bis(amine) **1** as the major product present in solution.

6.2.15 [$L_2L^*_2Mg_3Na_4(THF)_9$] 16

A Schlenk tube was charged with crystals of **2** (1.14 g, 1 mmol) and THF (5 ml) was added to form a pale yellow solution, which was cooled to 0°C. Benzothiazole was then added (0.1 ml, 1 mmol) and the resulting red solution was allowed to stir for ten minutes. Hexane (1 ml) was added, to form a red suspension which was then gently heated until a clear solution was obtained. After twenty-four hours at room temperature a crop of orange crystals of **16** was obtained (yield 0.58 g, 24%, note that maximum possible yield, 25%).

¹H NMR (d₈-THF, 298K**)** δ7.89 [d, 2H, C*H*, C₆H₄], 7.80 [d, 2H, C*H*, C₆H₄], 7.51-7.24 [m, 20H, C*H*'s, C₆H₄], 6.96 [m, 8H, C*H*'s, C₆H₄], 6.98 [t, 2H, C*H*, C₆H₄], 6.39 [t, 4H, C*H*, C₆H₄], 6.23 [t, 4H, C*H*, C₆H₄], 4.64 [q, 2H, C*H*C(Bu)], 3.69 [m, 44H, OC*H₂*, THF], 2.12 [m, 2H, C*H₂*, Bu],1.77 [m, 44H, C*H₂*, THF], 1.69 [m, 2H, C*H₂*, Bu], 1.38 [q, 2H, C*H₂*, Bu], 0.94 [t, 3H, C*H₃*, Bu]. Compound **15** showed limited solubility in deuterated THF which precluded the acquisition of a meaningful ¹³C NMR spectrum. ¹H NMR analysis of the filtrate from this reaction showed bis(amine) **1** as the major product present in solution.

6.2.16 Synthesis of [(Ph₂Si(NAr*)₂)Mg(THF)₂] 17

To an oven dried Schlenk tube hexane (10 ml) was added followed by Bu₂Mg (2 ml, 2 mmol). Bis(amine) **1** was added (1.06 g, 2 mmol) and the solution allowed to stir for one hour. Two equivalents of THF were introduced (0.68 ml, 4 mmol) and the resulting pale yellow solution was allowed to stir for twenty minutes at room temperature. On precipitation of a white solid, the solution was gently heated to clear and left in a hot water Dewar over night. Colourless crystals were obtained, isolated and transferred to a glove box (isolated yield 0.57 g, 41%)

¹H NMR (C₆D₆, 298K**)** δ7.76 [d, 4H, Ph], 7.20 [m, 10H, Ph or Ar*], 6.95 [m, 2H, Ar*], 3.66 [m, 4H, C*H*, ⁱPr, Ar*], 3.37 [m, 8H, OC*H₂*, THF], 1.11 [m, 8H, C*H₂*, THF], 0.98 [d, 24H, C*H₃*, ⁱPr, Ar*]. **¹³C{¹H} NMR (C₆D₆, 298K)** δ152.1, 143.9, 142.0[C_quarternary, Ph or Ar*], 135.8 [C*H*, Ph], 127.8 [C*H*, Ph], 127.8 [C*H*, Ph], 123.9 [C*H*, Ar*], 117.1 [C*H*, Ar*], 70.0 [O-C*H₂*, THF], 29.8 [C*H*, ⁱPr, Ar*], 24.5 [C*H₂*, THF], 23.6 [C*H₃*, ⁱPr, Ar*]. **¹H NMR (d₈-THF, 298K)** δ7.28 [d, 4H, Ph], 6.98 [m, 6H, Ph], 6.74 [d, 4H, Ar*], 6.45 [t, 2H, Ar*], 3.71 [m, 4H, C*H*, ⁱPr, Ar*], 3.61 [t, 8H, OC*H₂*, THF], 1.77 [t, 8H, C*H₂*, THF], 0.88 [d, 24H, C*H₃*, ⁱPr, Ar*].

6.2.17 [LMg$_2$(SH)(THF)$_4$] 18

To a solution of isolated crystals of **17** (0.70 g, 1 mmol) in THF (5 ml), two molar equivalents of benzothiazole (0.2 ml, 2 mmol) were added at 0°C affording a deep red solution. After stirring for one hour at 0°C, the solution was concentrated *in vacuo* to approximately half volume, and then placed in the refrigerator at –4°C affording a crop of red crystals of **18** along with a significant amount of a black solid which could not be dissolved in any organic solvent (isolated yield 0.04 g, 9%).

^{1}H NMR (d$_6$-DMSO, 298K**)** δ7.96 [m, 1H, C*H*, C$_6$H$_4$], 7.79 [m, 1H, C*H*, C$_6$H$_4$], 7.53 [t, 1H,C*H*, C$_6$H$_4$], 7.36 [d, 1H, C*H*, C$_6$H$_4$], 7.26-7.21 [m, 2H, C*H*'s, C$_6$H$_4$], 7.01 [d, 1H, C*H*, C$_6$H$_4$], 6.94 [m, 1H, C*H*, C$_6$H$_4$],6.24 [m, 1H, C*H*, C$_6$H$_4$], 6.17 [m, 1H, C*H*'s, C$_6$H$_4$], 6.03 [d, 1H, C*H*, C$_6$H$_4$], 5.83 [t, 1H, C*H*, C$_6$H$_4$], 3.59 [m, 16H, OC*H*$_2$, THF], 1.76 [m, 16H, C*H*$_2$, THF]. **18** showed poor solubility in deuterated solvents, even when highly polar deuterated DMSO was employed. No attributable signal for the SH group could be assigned in the ^{1}H NMR spectrum.

6.2.18 Synthesis of [(Ph$_2$Si(NAr*)$_2$)Mg(THF)(PhN(C$_2$N(NPh)$_2$)Na(THF)$_4$] 19

To an oven dried Schlenk complex 10 was added (1.15 g, 1 mmol) and dissolved in 5 ml of THF. Nitron was added (0.31 g, 1 mmol) and the solution allowed stirring for one hour, changing colour from yellow to dark green. Hexane was added 4 ml and the solution left in the freezer overnight resulting in a crop of crystals (yield 0.77 g, 62%).

^{1}H NMR (d$_8$-THF, 298K) δ8.15 [d, 1H, Ph], 8.08 [d, 1H, Ph], 7.55 [d, 2H, Ph], 7.51 [d, 1H, Ph], 7.30 [m, 4H, Ph], 7.23 [m, 5H, Ph], 7.16 [d, 2H, Ph], 7.05 [m, 2H, Ph], 6.93 [m, 3H, Ph], 6.79 [d, 4H, Ar*], 6.51 [t, 2H, Ar*], 6.29 [t, 2H, Ph], 6.03 [m, 2H. Ph], 4.31 [m, 4H, C*H*, ^{i}Pr, Ar*], 3.61 [m, 20H, OC*H*$_2$, THF], 1.77 [m, 44H, C*H*$_2$, THF], 0.88 [m, 12H, C*H*$_3$, ^{i}Pr, Ar*]. **^{13}C{^{1}H} NMR** (d$_8$-THF, 298K) δ173.38 [C-Na], 150.48, 144.12, 142.77, 142.19, 140.58, 135.48, 135.06, 129.28, 128.56, 127.88, 127.68, 125.55, 124.75, 124.57, 123.56, 123.00, 122.83, 121.75, 120.35, 118.37,

115.67 [CH, Ph and Ar*], 67.24 [O-CH_2, THF], 27.10 [CH, ^{i}Pr, Ar*], 25.44 [CH_2, THF], 22.77 [CH_3, ^{i}Pr, Ar*].

6.2.19 Synthesis of $[\{Na(THF)_6\}_2^+\{(Ph_2Si(NAr^*)_2)Mg(Qox^{\cdot})\}_2^-]$ 20

To an oven dried Schlenk **2** was added (1.14 g, 1 mmol) and dissolved in 5 ml THF. Quinoxaline was added (0.13 g, 1 mmol) and the solution allowed stirring for one hour, changing colour from yellow through to green and finally blue. Hexane was added 3 ml and the solution left at room temperature for twenty-four hours depositing a batch of blue crystals (yield 0.67 g, 55%)

^{1}H NMR (d$_8$-THF, 298K) δ7.35 [m, 8H, Ph], 6.89 [m, 16H, Ph and Hc, quinoxalyl], 6.69 [m, 8H, Ar*], 6.40 [m, 4H, Ar*], 5.89 [m, 4H, H_B, qunioxalyl], 5.36 [m, 4H, H_A, quinoxalyl], 4.16 [m, 4H, CH, ^{i}Pr, Ar*], 4.03 [m, 4H, CH, ^{i}Pr, Ar*], 3.62 [m, 44H, OCH_2, THF], 1.77 [m, 44H, CH_2, THF], 0.97 [m, 12H, CH_3, ^{i}Pr, Ar*], 0.88 [m, 12H, CH_3, ^{i}Pr, Ar*], 0.55 [m, 12H, CH_3, ^{i}Pr, Ar*], 0.31 [m, 12H, CH_3, ^{i}Pr, Ar*]. **^{13}C\{^{1}H\} NMR** (d$_8$-THF, 298K) δ154.47, 146.90, 144.93, 140.22, [$C_{quarternary}$, Ph or Ar*, or quinoxalyl], 136.77 [CH, Ph], 136.48 [CH, Ph], 127.70 [CH, Ph], 126.07 [CH, Hc quinoxalyl], 125.98 [CH, H_B quinoxalyl], 124.31 [CH, H_A quinoxalyl], 122.94 [CH, Ar*], 116.05 [CH, Ar*], 68.23 [O-CH_2, THF], 28.00 [CH, ^{i}Pr, Ar*], 27.90 [CH, ^{i}Pr, Ar*], 26.39 [CH_2, THF], 25.30, 25.28, 25.13, [CH_3, ^{i}Pr, Ar*], 23.71 [CH_3, ^{i}Pr, Ar*].

6.2.20 Synthesis of [(Ph₂Si(NAr*)₂)Mg(TEMPO)Na(THF)₃] 21

Isolated crystals of **2** were added to a Schlenk tube (1.14 g, 1 mmol) and dissolved in 5 ml of THF followed by the addition of TEMPO$^\bullet$ (0.15 g, 1 mmol) and the solution allowed stirring for one hour. The solution changed slightly deeper yellow in colour. Hexane (4 ml) was added and the Schlenk tube left in the freezer for twenty-four hours resulting in a crop of colourless crystals (yield 0.41 g, 41%).

^{1}H NMR (d$_8$-THF, 298K) δ7.23 [d, 4H, Ph], 6.91 [m, 6H, Ph], 6.68 [d, 4H, Ar*], 6.40 [t, 2H, Ar*], 4.03 [m, 4H, CH, ^{i}Pr, Ar*], 3.61 [m, 20H, OCH_2, THF], 1.77 [m, 20H, CH_2, THF], 1.55 [m, 4H, β-CH_2, TEMPO], 1.32 [m, 2H, γ-CH_2, TEMPO], 1.05 [m, 6H, CH_3, TEMPO], 0.97 [m, 6H, CH_3, TEMPO], 0.75 [m, 24H, CH_3, ^{i}Pr, Ar*].

^{13}C{^{1}H} NMR (d$_8$-THF, 298K) δ154.66, 149.41, 145.59 [$C_{quarternary}$, Ph or Ar*], 137.09 [CH, Ph], 127.34 [CH, Ph], 127.14 [CH, Ph], 123.12 [CH, Ar*], 117.25 [CH, Ar*], 69.14 [O-CH$_2$, THF], 60.50 [$C_{quarternary}$, TEMPO], 42.03 [CH$_2$, TEMPO], 35.74 [CH$_3$, TEMPO], 29.16 [CH, ^{i}Pr, Ar*], 27.33 [CH$_2$, THF], 24.66 [CH$_3$, ^{i}Pr, Ar*], 20.33 [CH$_3$, TEMPO], 19.38 [CH$_2$, TEMPO].

6.2.21 Synthesis of [(^{Dipp}nacnac)Mg(Bu)(THF)] 22

A Schlenk tube was charged with THF (10 ml) and Bu$_2$Mg (4 ml, 4 mmol) followed by ^{Dipp}nacnacH (1.66 g, 4 mmol) and the solution allowed to stir for 1 hour, resulting in a yellow solution. After twenty-four hours in the freezer a crop of colourless crystals resulted (1.23 g, 54%).

^{1}H NMR (C$_6$D$_6$, 298K) δ7.17 [s, 6H, Ar*], 4.80 [s, 1H, CH], 3.57 [m, 4H, OCH_2, THF], 3.30 [m, 4H, CH , ^{i}Pr, Ar*], 1.66 [s, 6H, CH-(CH_3)$_2$], 1.47 [m, 2H, CH_2, Bu], 1.36 [m, 2H, CH_2, Bu], 1.30 [m, 4H, CH_2, THF], 1.30 [d, 12H, CH_3, ^{i}Pr, Ar*], 1.23 [d, 12H, CH_3, ^{i}Pr, Ar*], 0.92 [t, 3H, CH_3, Bu], -0.35 [m, 2H, Mg-CH_2, Bu]. ^{13}C NMR{^{1}H} (C$_6$D$_6$, 298K) δ167.15 [C-CH$_3$], 145.28 [$C_{quarternary}$, Ar*], 141.60 [$C_{quarternary}$, Ar*], 124.33 [CH, Ar*], 122.98 [CH, Ar*], 93.83 [CH], 68.48 [OCH$_2$,THF], 31.88 [CH$_2$, THF], 31.17 [CH$_2$, Bu], 27.40 [CH, ^{i}Pr, Ar*], 24.55 [CH$_2$, Bu], 24.32 [CH$_3$, ^{i}Pr, Ar*], 23.68 [CH$_3$, ^{i}Pr, Ar*] 23.29 [C-CH$_3$], 13.90 [CH$_3$, Bu], 4.99 [Mg-CH$_2$, Bu].

6.2.22 Synthesis of [(^{Dipp}nacnac)Mg(TMP)] 23

To a Schlenk tube was added hexane (10 ml) followed by Bu$_2$Mg (4 ml, 4 mmol) and TMP(H) (1.36 ml, 8 mmol) and the solution was allowed to reflux for one hour. ^{Dipp}nacnacH (1.66 g, 4 mmol) was then added and the yellow solution refluxed for a further hour. Overnight storage in the freezer yielded a batch of colourless crystals (1.15 g, 52%).

^{1}H NMR (C$_6$D$_6$, 298K) δ7.13 [s, 6H, Ar*], 4.86 [s, 1H, CH], 3.22 [m, 4H, CH , ^{i}Pr, Ar*], 1.69 [s, 6H, CH-(CH_3)$_2$], 1.66 [m, 2H, CH_2, γ-TMP], 1.38 [d, 12H, CH_3, ^{i}Pr, Ar*], 1.18 [m, 2H, CH_2, β-TMP], 1.17 [d, 12H, CH_3, ^{i}Pr, Ar*], 0.95 [s, 12H, CH_3, TMP]. ^{13}C NMR{^{1}H} (C$_6$D$_6$, 298K) δ169.07 [C-CH$_3$], 144.14 [$C_{quarternary}$, Ar*],

141.48 [$C_{quarternary}$, Ar*], 124.96 [CH, Ar*], 123.31 [CH, Ar*], 94.65 [CH], 49.88 [$C(CH_3)_2$, TMP], 38.28 [CH_2, β-TMP], 34.81 [C($CH_3)_2$, TMP] 28.09 [CH, ^{i}Pr, Ar*], 24.10 [CH_3, ^{i}Pr, Ar*], 23.87 [CH_3, ^{i}Pr, Ar*], 23.79 [CH_2, γ-TMP], 19.00 [C-CH_3].

6.2.23 Synthesis of [(^{Dipp}nacnac)Mg{O(*o*-C$_6$H$_4$)NC}(THF)] 24

Isolated crystals of **22** (0.56 g, 1 mmol) were added to a Schlenk tube and dissolved in THF (5 ml). Benzoxazole (0.1 ml, 1 mmol) was then added and the solution allowed stirring for two hours. The solution changed from light yellow to orange in colour. Hexane (4 ml) was added and after storage in the freezer for twenty-four hours deposited red crystals (0.31 g, 55%).

^{1}H NMR (d$_8$-THF, 298K) δ7.11 [m, 6H, Ar*], 7.01 [m, 2H, {O(*o*-C$_6$H$_4$)NC}], 6.50 [d, 1H, {O(*o*-C$_6$H$_4$)NC}], 6.36 [t, 1H, {O(*o*-C$_6$H$_4$)NC}], 5.00 [s, 1H, CH], 3.61 [m, 4H, OCH_2, THF] 3.22 [m, 4H, CH, ^{i}Pr, Ar*], 1.77 [m, 4H, CH_2, THF], 1.77 [m, 6H, CH-(C$H_3)_2$], 1.10 [d, 12H, CH$_3$, ^{i}Pr, Ar*], 1.01 [d, 12H, CH$_3$, ^{i}Pr, Ar*]. **^{13}C NMR{^{1}H}** (d$_8$-THF, 298K) δ169.79 [CH, Ar* or C$_{α-pheonlate}$ or C$_{isocyanide}$], 164.71 [CH, Ar* or C$_{α-pheonlate}$ or C$_{isocyanide}$], 162.15 [CH, Ar* or C$_{α-pheonlate}$ or C$_{isocyanide}$], 144.51 [CH, Ar*], 142.38 [CH, Ar*], 129.40 [CH, {O(*o*-C$_6$H$_4$)NC}], 126.07 [CH, {O(*o*-C$_6$H$_4$)NC}], 124.96 [CH, Ar*], 123.50 [CH, Ar*], 121.09 [CH, {O(*o*-C$_6$H$_4$)NC}], 118.02 [CH, C$_{β-phenolate}$], 93.64 [CH], 27.76 [CH, ^{i}Pr, Ar*], 24.42 [CH_2,THF], 23.76 [CH_3, ^{i}Pr, Ar*], 23.64 [CH_3, ^{i}Pr, Ar*], 23.14 [CH_3].

6.2.24 Synthesis of [(^{Dipp}nacnac)Mg{O(*o*-C$_6$H$_4$)NC}(THF)] 24

Isolated crystals of **23** (0.57 g, 1 mmol) were added to a Schlenk tube and dissolved in THF (5 ml). Benzoxazole (0.1 ml, 1 mmol) was then added and the solution allowed stirring for two hours. The solution changed from light yellow to orange in colour. Hexane (4 ml) was added and after storage in the freezer for twenty-four hours deposited red crystals (0.31 g, 55%).

^{1}H NMR (d$_8$-THF, 298K) δ7.11 [m, 6H, Ar*], 7.01 [m, 2H, {O(*o*-C$_6$H$_4$)NC}], 6.50 [d, 1H, {O(*o*-C$_6$H$_4$)NC}], 6.36 [t, 1H, {O(*o*-C$_6$H$_4$)NC}], 5.00 [s, 1H, CH], 3.61 [m, 4H, OCH_2, THF] 3.22 [m, 4H, CH, ^{i}Pr, Ar*], 1.77 [m, 4H, CH_2, THF], 1.77 [m, 6H, CH-(C$H_3)_2$], 1.10 [d, 12H, CH$_3$, ^{i}Pr, Ar*], 1.01 [d, 12H, CH$_3$, ^{i}Pr, Ar*]. **^{13}C**

NMR{^{1}H} (d$_8$-THF, 298K) δ169.79 [CH, Ar* or C$_{\alpha\text{-pheonlate}}$ or C$_{\text{isocyanide}}$], 164.71 [CH, Ar* or C$_{\alpha\text{-pheonlate}}$ or C$_{\text{isocyanide}}$], 162.15 [CH, Ar* or C$_{\alpha\text{-pheonlate}}$ or C$_{\text{isocyanide}}$], 144.51 [CH, Ar*], 142.38 [CH, Ar*], 129.40 [CH, {O(o-C$_6$H$_4$)NC}], 126.07 [CH, {O(o-C$_6$H$_4$)NC}], 124.96 [CH, Ar*], 123.50 [CH, Ar*], 121.09 [CH, {O(o-C$_6$H$_4$)NC}], 118.02 [CH, C$_{\beta\text{-phenolate}}$], 93.64 [$CH$], 27.76 [$CH$, ^{i}Pr, Ar*], 24.42 [$CH_2$,THF], 23.76 [$CH_3$, ^{i}Pr, Ar*], 23.64 [$CH_3$, ^{i}Pr, Ar*], 23.14 [$CH_3$].

6.2.25 Synthesis of [{($^{\text{Dipp}}$nacnac)Mg(Btz*)}$_2$] 25

Isolated crystals of compound **23** (0.56 g, 1 mmol) were added to a Schlenk tube and dissolved in THF (5 ml). Benzothiazole was then added (0.11 ml, 1 mmol) and the solution allowed stirring for two hours. The solution turned blue instantaneously then gradually became, green and finally red in colour. Hexane (4 ml) was added and after storage in the freezer for twenty-four hours deposited red crystals (0.24 g, 43%).

^{1}H NMR (C$_6$D$_6$, 298K) δ8.71 [d, 1H, Btz*], 7.66 [d, 1H, Btz*], 7.32 [t, 1H, Btz*], 7.04 [t, 1H, Btz*], 6.98 [m, 4H, Ar*], 6.76 [d, 2H, Ar*], 5.24 [s, 1H, CH], 4.01 [m, 2H, CH, ^{i}Pr, Ar*], 2.54 [m, 2H, CH, ^{i}Pr, Ar*], 1.67 [s, 6H, CH-(CH_3)$_2$], 1.63 [d, 6H, CH_3, ^{i}Pr, Ar*], 1.42 [d, 6H, CH_3, ^{i}Pr, Ar*], 0.62 [d, 6H, CH_3, ^{i}Pr, Ar*], -0.68 [d, 6H, CH_3, ^{i}Pr, Ar*].**^{13}C NMR{^{1}H}** (C$_6$D$_6$, 298K) δ216.27 [C], 169.71, 155.24, 146.20, 142.99, 142.00 [$C_{\text{quarternary}}$, Btz* and Ar*], 125.20 [CH, Ar*], 124.86 [CH, Btz*], 124.26 [CH, Ar*], 123.73 [CH, Btz*], 123.44 [CH, Ar*], 121.22 [CH, Btz*], 120.99 [CH, Btz*], 95.43 [CH], 29.83 [CH, ^{i}Pr, Ar*], 27.27 [CH, ^{i}Pr, Ar*], 25.18 [CH_3, ^{i}Pr, Ar*], 24.93 [CH_3], 24.80 [CH_3, ^{i}Pr, Ar*], 24.12 [CH_3, ^{i}Pr, Ar*], 22.81 [CH_3, ^{i}Pr, Ar*].

6.2.26 Synthesis of [($^{\text{Dipp}}$nacnac)Mg{(Btz*)C(H)=N(2-C$_6$H$_4$-1-S)}] 26

Isolated crystals of compound **23** (0.57 g, 1 mmol) were added to a Schlenk tube and dissolved in THF (4 ml). Benzothiazole was then added (0.22 ml, 2 mmol) and the solution allowed stirring for one hour. The solution turned blue immediately. Hexane was added (3 ml) and after storage in the freezer overnight blue crystals were deposited (0.47 g, 58%).

¹H NMR (C₆D₆, 298K) δ 9.03 [d, 1H, Btz*], 7.58 [d, 1H, N(2-C₆H₄)S], 7.28 [m, 2H, Btz*], 7.18 [m, 2H, Ar*], 7.05 [m, 2H, Ar*], 6.98 [m, 2H, 1H of Btz* and 1H of C(H)=N], 6.92 [d, 2H, Ar*], 6.72 [t, 1H, N(2-C₆H₄)S], 6.35 [t, 1H, N(2-C₆H₄)S], 6.09 [d, 1H, N(2-C₆H₄)S], 5.15 [s, 1H, CH], 3.89 [m, 2H, CH, ᶦPr, Ar*], 2.89 [m, 2H, CH, ᶦPr, Ar*], 1.80 [s, 6H, CH₃], 1.73 [d, 6H, CH₃, ᶦPr, Ar*], 1.35 [d, 6H, CH₃, ᶦPr, Ar*], 0.71 [d, 6H, CH₃, ᶦPr, Ar*], 0.58 [d, 6H, CH₃, ᶦPr, Ar*]. **¹³C NMR{¹H}** (C₆D₆, 298K) δ168.21 [CHC(Me)], 164.68, 154.56, 151.40, 146.07, 145.18 [C, Ar*, N(o-C₆H₄)S and Btz*], 145.01 [CH, C(H)=N], 143.38, 141.58 [C, Ar*], 135.04 [CH, N(o-C₆H₄)S], 129.98 [CH, N(o-C₆H₄)S], 128.45, 127.26, 125.55 [CH's, Btz*], 125.01, 124.33, 122.77 [CH's, Ar*], 122.24 [CH, Btz*], 120.04, 116.59 [CH's, N(o-C₆H₄)S], 94.89 [CH], 29.04 [CH, ᶦPr, Ar*], 27.41 [CH, ᶦPr, Ar*], 25.66 [CH₃, ᶦPr, Ar*], 25.10 [CH₃, ᶦPr, Ar*], 24.89 [CH₃, ᶦPr, Ar*], 24.60 [CH₃, ᶦPr, Ar*].

6.2.27 Synthesis of [{(^DippnacnacMg(MeBIm*)}₂] 27

Compound **23** (0.56 g, 1 mmol) was dissolved in THF (5 ml). After the addition of methylbenzimidazole (0.13 g, 1 mmol) the pale yellow solution was allowed to stir for two hours resulting in a green solution. Storage for twenty-four hours in the freezer yielded colourless crystals (0.32 g, 57%).

¹H NMR (C₆D₆, 298K) δ8.27 [d, 1H, MeBIm], 7.26 [m, 1H, MeBIm], 7.11 [t, 1H, MeBIm], 7.00 [m, 2H, Ar*], 6.89 [m, 4H, Ar*], 6.85 [m, 1H, MeBIm], 5.24 [s, 1H, CH], 3.75 [s, 3H, CH₃, MeBIm], 3.57 [m, 2H, CH, ᶦPr, Ar*], 2.64 [m, 2H, CH, ᶦPr, Ar*], 1.71 [s, 6H, CH-(CH₃)₂], 1.24 [d, 6H, CH₃, ᶦPr, Ar*], 1.12 [d, 6H, CH₃, ᶦPr, Ar*], 0.65 [d, 6H, CH₃, ᶦPr, Ar*], -0.31 [d, 6H, CH₃, ᶦPr, Ar*]. **¹³C NMR{¹H}** (C₆D₆, 298K) δ192.93 [C], 169.52, 147.00, 144.75, 143.40, 141.62 [C_quarternary, MeBIm, Ar*], 124.30, 123.90 [CH, Ar*], 121.17, 120.99, 118.45, 117.91 [CH, MeBIm,], 95.89 [CH], 34.47 [CH₃, MeBIm], 28.69 [CH, ᶦPr, Ar*], 27.06 [CH, ᶦPr, Ar*], 25.39 [CH₃], 25.64 [CH₃, ᶦPr, Ar*], 24.48 [CH₃, ᶦPr, Ar*], 23.57[CH₃, ᶦPr, Ar*], 22.84 [CH₃, ᶦPr, Ar*].

6.2.28 Synthesis of [(^DippnacnacMg(Bu)(MeBIm)] 28

Isolated crystals of **22** (0.57 g, 1 mmol) were added to a Schlenk tube and dissolved in THF (5 ml). Methylbenzimidazole (0.13 g, 1 mmol) was added and the pale

yellow solution stirred for two hours. After storage in the freezer overnight, a crop of colourless crystals were produced (0.28 g, 43 %).

^{1}H NMR (C$_6$D$_6$, 298K) δ8.48 [d, 1H, MeBIm], 7.92 [s, 2H, MeBIm], 7.31 [m, 2H, MeBIm], 7.21 [m, 2H, Ar*], 7.07 [m, 2H, Ar*], 6.90 [d, 2H, Ar*], 5.21 [s, 1H, C*H*], 3.83 [m, 2H, C*H*, ^{i}Pr, Ar*], 2.95 [m, 2H, C*H*, ^{i}Pr, Ar*], 2.63 [s, 3H, C*H*$_3$, MeBIm], 1.86 [s, 6H, CH-(C*H*$_3$)$_2$], 1.69 [d, 6H, C*H*$_3$, ^{i}Pr, Ar*], 1.49 [m, 2H, C*H*$_2$, Bu], 1.42 [d, 6H, C*H*$_3$, ^{i}Pr, Ar*], 1.32 [m, 2H, C*H*$_2$, Bu], 1.06 [m, 3H, CH$_3$, Bu], 0.97 [d, 6H, C*H*$_3$, ^{i}Pr, Ar*], 0.26 [d, 6H, C*H*$_3$, ^{i}Pr, Ar*], -0.10 [m, 2H, C*H*$_2$, Bu]. **^{13}C NMR{^{1}H}** (C$_6$D$_6$, 298K) 167.59, 146.25, 142.75, 141.02, 133.95 [C$_{quarternary}$, MeBIm, Ar*], 145.23 [*C*H, MeBIm], 124.84, 109.59 [*C*H, Ar*], 124.01, 123.66, 123.26, 120.63 [*C*H, MeBIm,], 93.87 [*C*H], 33.08, 32.14 [*C*H$_2$, Bu], 30.03 [*C*H$_3$, MeBIm], 28.92 [*C*H, ^{i}Pr, Ar*], 27.19 [*C*H, ^{i}Pr, Ar*], 25.59 [*C*H$_3$, ^{i}Pr, Ar*], 24.75 [*C*H$_3$, ^{i}Pr, Ar*], 24.40 [*C*H$_3$, ^{i}Pr, Ar*], 24.02 [*C*H$_3$], 23.81 [*C*H$_3$, ^{i}Pr, Ar*], 14.43 [*C*H$_3$, Bu], 6.83 [*C*H$_2$, Mg-Bu].

6.2.29 [(^{t}BuNH)C(=O)(NPh$_2$)]   29

Reaction was carried out in an NMR tube following same method in section **6.1.5**. Yields were calculated by reference to internal standard (99 %).

^{1}H NMR (C$_6$D$_6$, 298K) δ7.14 [m, 4H, Ph], 7.02 [m, 4H, Ph], 6.88 [m, 2H, Ph], 4.37 [s, 1H, N*H*], 1.21 [s, 9H, C*H*$_3$, ^{t}Bu].**^{13}C NMR{^{1}H}** (C$_6$D$_6$, 298K) δ154.12 [*C*=O], 143.26 [C$_{quarternary}$] 128.58, 126.66 124.82 [*C*H, Ph], 50.11 [*C*(CH$_3$)$_3$], 28.35 [C(*C*H$_3$)$_3$].

6.2.30 Synthesis of [NaMg(NPh$_2$)$_3$ (THF)$_2$] 30

To an oven dried Schlenk added BuNa (0.16 g, 2 mmol) and suspended in 10 ml of hexane. Added Bu$_2$Mg (2 ml, 2 mmol) followed by HNPh$_2$ (1.01 g, 6 mmol) and allowed to stir for one hour. A white suspension formed. Added THF 4 ml until the solution was clear and placed in the freezer overnight. Colourless crystals were isolated and stored in the glove box (1.10 g, 80 %).

^{1}H NMR (d$_8$-THF, 298K) δ7.42 [d, 12H, Ph], 7.11 [dd, 12H, Ph], 6.60 [d, 6H, Ph], 3.30 [m, 24H, OC*H*$_2$, THF], 1.28 [m, 24H, C*H*$_2$, THF]. **^{13}C NMR{^{1}H}** (d$_8$-THF,

298K) δ156.50 [$C_{quarternary}$, Ar, Ph], 128.71 [CH, Ph], 120.65 [CH, Ph], 115.65 [CH, Ph].

6.2.31 Synthesis of [(THF)₃NaMg((ᵗBuN)C(NPh₂)(=O))₃] 31

Complex **29** was added to a Schlenk tube (0.69 g, 1 mmol) and dissolved in THF 4 ml. ᵗBuN=C=O was added (0.34 ml, 3 mmol) and allowed to stir for 1 hour. Hexane (1 ml) was dripped in until cloudy and Schlenk placed in the freezer overnight. Colourless crystals were isolated and stored in the glove box (0.66 g, 62 %).

¹H NMR (C_6D_6, 298K) δ7.42 [d, 4H, Ar(H), Ph], 7.10 [m, 4H, Ar(H), Ph], 3.27 [m, 4H, OCH_2, THF], 1.44 [s, 3H, CH_3, ᵗBu], 1.28 [m, n4H, CH_2, THF]. **¹³C NMR{¹H}** (C_6D_6, 298K) δ163.29 [N(ᵗBu)C(O)(NPh₂)], 146.09 [$C_{quarternary}$], 129.09, 122.04, 121.99 [CH, Ph], 67.52 [OCH_2, THF], 51.47 [C(CH₃)₃], 32.10 [C(CH_3)₃], 25.38 [CH_2, THF]

6.2.32 Synthesis of [{NaMg(CH₂SiMe₃)₃}] 32

To a suspension of Na(CH₂SiMe₃) (0.11 g, 1 mmol) in hexane (15 ml), Mg(CH₂SiMe₃) (0.2 g, 1 mmol) was added and the resulting white suspension stirred at room temperature for 1 hour. 2 ml of toluene was then introduced and the mixture was gently heated. The resulting colourless solution was allowed to stir slowly at room temperature, affording a crop of colourless crystal (0.15 g, 49%).

¹H NMR (C_6D_6, 298K) δ0.28 [s, 6H, SiCH_2], -1.71 [s, 27H, Si(CH_3)₃]. **¹³C NMR{¹H}** (C_6D_6, 298K) δ4.54 [Si(CH₃)₃], -2.16 [SiCH₂].

6.2.33 [(ᵗBuNH)C(=O)(NBu₂)]   33

Reaction was carried out in an NMR tube following same method in section **6.1.5**. Yields were calculated by reference to internal standard (100 %).

¹H NMR (C_6D_6, 298K) δ4.10 [s, 1H, NH], 3.01 [m, 2H, CH_2, Bu], 1.41 [m, 2H, CH_2, Bu], 1.37 [s, 9H, CH_3, ᵗBu], 1.17 [m, 2H, CH_2, Bu], 0.83 [m, 3H, CH_3, Bu]. **¹³C NMR{¹H}** (C_6D_6, 298K) δ156.58 [C=O], 50.25 [CH_2, Bu], 46.88 [CH_2, Bu], 31.42 [CH_2, Bu], 29.59 [C(CH₃)₃], 20.40 [C(CH_3)₃], 13.89 [CH_3, Bu].

6.2.34 [(^{t}BuNH)C(=O)(NBz$_2$)] 34

Reaction was carried out in an NMR tube following same method in section **6.1.5**. Yields were calculated by reference to internal standard (100 %)

^{1}H NMR (C$_6$D$_6$, 298K) δ7.28-7.04 [m, 10H, Ph], 4.28 [s, 4H, CH_2, Bz], 4.14 [s, 1H, NH], 1.25 [s, 9H, CH_3, ^{t}Bu]. **^{13}C NMR{^{1}H}** (C$_6$D$_6$, 298K) δ157.37 [C=O], 141.02, 138.9, 128.4, 126.9 [CH, Ph], 53.25 [CH$_2$, Bz], 50.47 [C(CH$_3$)$_3$], 20.40 [C(CH$_3$)$_3$].

6.2.35 [(^{t}BuNH)C(=O)(NPy$_2$)]   35

Reaction was carried out in an NMR tube following same method in section **6.1.5**. Yields were calculated by reference to internal standard (17 %).

^{1}H NMR (d$_8$-THF, 298K) δ9.97 [s, 2H, NH], 8.33 [m, 4H, Py], 7.50 [m, 4H, Py], 7.00 [m, 2H, Py], 1.40 [s, 9, CH_3, ^{t}Bu].

6.2.36 [(^{t}BuNH)C(=O)(NHAr*)]   36

Reaction was carried out in an NMR tube following same method in section **6.1.5**. Yields were calculated by reference to internal standard (37 %).

^{1}H NMR (C$_6$D$_6$, 298K) δ7.13 [m, 2H, Ph, Ar*], 7.08 [m, 1H, Ph, Ar*], 4.10 [br s, 2H, NH], 3.56 [m, 2H, CH, ^{i}Pr, Ar*], 1.21 [d, 12H, CH_3, ^{i}Pr, Ar*], 1.13 [s, 9H, CH_3, ^{t}Bu].

6.2.37 [(CyNH)C(=O)(NBu$_2$)]   37

Reaction was carried out in an NMR tube following same method in section **6.1.5**. Yields were calculated by reference to internal standard (100 %).

^{1}H NMR (C$_6$D$_6$, 298K) δ4.58 [s, 1H, NH], 3.90 [m, 1H, CH, Cy], 3.12 [m, 2H, CH_2, Bu], 2.01 [m, 2H, CH_2, Cy], 1.59 [m, 2H, CH_2, Bu], 1.46 [m, 4H, CH_2, Cy], 1.21 [m, 2H, CH_2, Bu], 1.20 [m, 2H, CH_2, Cy] 1.10 [m, 2H, CH_2, Cy], 0.84 [m, 3H, CH_3, Bu]. **^{13}C NMR{^{1}H}** (C$_6$D$_6$, 298K) δ156.77 [C=O], 53.14 [CH, Cy], 49.50 [CH$_2$, Cy], 46.85 [CH$_2$, Bu], 34.56 [CH$_2$, Cy], 31.25 [CH$_2$, Bu], 26.01 [CH$_2$, Cy], 25.52 [CH$_2$, Cy], 20.36 [CH$_2$, Bu], 14.07 [CH$_3$, Bu].

6.2.38 [(CyNH)C(=O)(NBz$_2$)] 38

Reaction was carried out in an NMR tube following same method in section **6.1.5**. Yields were calculated by reference to internal standard (100 %).

^{1}H NMR (C$_6$D$_6$, 298K) δ 7.12-7.05 [m, 10H, Bz], 4.33 [s, 4H, CH_2, Bz], 4.28 [s, 1H, NH], 3.99 [m, 1H, CH, Cy], 1.84 [m, 2H, CH_2, Cy], 1.35 [m, 2H, CH_2, Cy], 1.13 [m, 4H, CH_2, Cy], 0.88 [m, 2H, CH_2, Cy]. **^{13}C NMR{^{1}H}** (C$_6$D$_6$, 298K) δ157.59 [C=O], 138.85, 128.68, 127.31, 127,30 [CH, Bz], 50.50 [CH, Cy], 49.7 [CH$_2$, Bz], 33.69 [CH$_2$, Cy], 25.80 [CH$_2$, Cy], 24.95 [CH$_2$, Cy].

6.2.39 [(CyNH)C(=O)(NPh$_2$)] 39

Reaction was carried out in an NMR tube following same method in section **6.1.5**. Yields were calculated by reference to internal standard (100 %).

^{1}H NMR (C$_6$D$_6$, 298K) δ7.17 [m, 4H, Ph], 7.06 [m, 4H, Ph], 6.91 [m, 2H, Ph], 4.36 [s, 1H, NH], 3.80 [m, 1H, CH, Cy], 1.78 [d, 2H, CH_2, Cy], 1.38 [d, 4H, CH_2, Cy]. 1.10 [d, 4H, CH_2, Cy], 0.76 [d, 2H, CH_2, Cy].**^{13}C NMR{^{1}H}** (C$_6$D$_6$, 298K) δ 154.83 [C=O], 144.18 [$C_{quarternary}$] 129.23, 125.23 123.54 [CH, Ph], 49.29 [CH, Cy], 33.28, 25.59, 24.94 [CH$_2$, Cy].

6.2.40 [(CyNH)C(=O)(NPy$_2$)] 40

Reaction was carried out in an NMR tube following same method in section **6.1.5**. Yields were calculated by reference to internal standard (53 %).

^{1}H NMR (d$_8$-THF, 298K) δ9.78 [s, 1H, NH], 8.35, [m, 2H, Py], 7.60 [m, 2H, Py], 7.05 [m, 2H, Py], 6.78 [m, 4H, Py], 4.60 [m, 1H, CH, Cy], 2.33 [m, 2H, CH_2, Cy], 1.80 [m, 2H, CH_2, Cy], 1.62 [m, 2H, CH_2, Cy], 1.34 [m, 4H, CH_2, Cy].

6.2.41 [(CyNH)C(=O)(NHAr*)] 41

Reaction was carried out in an NMR tube following same method in section **6.1.5**. Yields were calculated by reference to internal standard (100 %).

^{1}H NMR (CDCl$_3$, 298K) δ7.34 [t, 1H, Ph, Ar*], 7.05 [d, 2H, Ph, Ar*], 5.55 [s, 1H, NH], 3.68 [m, 1H, CH, Cy], 3.30 [m, 2H, CH, ^{i}Pr, Ar*], 1.86 [m, 2H, CH_2, Cy], 1.60

[m, 4H, C*H*₂, Cy], 1.34 [m, 2H, C*H*₂, Cy], 1.19 [m, 12H, C*H*₃, ⁱPr, Ar*], 0.94 [m, 2H, C*H*₂, Cy]. **¹³C NMR{¹H}** (CDCl₃, 298K) δ159.91 [*C*=O], 148.13, 130.91, 124.15 [*C*H, Ph], 53.29 [*C*H, Cy], 48.78 [*C*H, ⁱPr, Ar*], 34.77, 33.80, 28.15, 25.03 [*C*H₂, Cy], 23.83 [*C*H₃, ⁱPr, Ar*].

6.2.42 [(EtNH)C(=O)(NHAr*)] 42

Reaction was carried out in an NMR tube following same method in section **6.1.5**. Yields were calculated by reference to internal standard (100 %).

¹H NMR (CDCl₃, 298K) δ7.22-7.16 [m, 3H, Ph], 6.24 [s, 1H, N*H*], 3.27-3.16 [m, 4H, C*H*₂, Et and C*H*, ⁱPr, Ar*], 1.25-1.07 [m, 15H, C*H*₃, Et and C*H*₃, ⁱPr, Ar*]. **¹³C NMR{¹H}** (CDCl₃, 298K) δ157.70 [*C*=O], 148.04, 128.82, 124.05 [*C*H, Ph], 34.98 [*C*H₂, Et], 28.70 [*C*H, ⁱPr, Ar*], 23.70 [*C*H₃, ⁱPr, Ar*], 14.92 [*C*H₃, Et].

6.2.43 [(EtNH)C(=O)(NPh₂)] 43

Reaction was carried out in an NMR tube following same method in section **6.1.5**. Yields were calculated by reference to internal standard (78 %).

¹H NMR (C₆D₆, 298K) δ7.10 [m, 4H, Ph], 6.93 [m, 4H, Ph], 6.81 [m, 2H, Ph], 5.62 [s, 1H, N*H*], 3.68 [m, 2H, C*H*₂, Et], 1.02 [m, 3H, C*H*₃, Et]. **¹³C NMR{¹H}** (C₆D₆, 298K) δ 155.36 [C=O], 142.95 [*C*quarternary] 128.70, 120.12, 117.27 [*C*H, Ph], 37.23 [*C*H₂, Et], 12.34 [*C*H₃, Et].

6.2.44 [(EtNH)C(=O)(NPy₂)] 44

Reaction was carried out in an NMR tube following same method in section **6.1.5**. Yields were calculated by reference to internal standard (34 %).

¹H NMR (d₈-THF, 298K) δ δ9.58 [s, 1H, N*H*], 8.39, [m, 2H, Py], 7.64 [m, 2H, Py], 7.09 [m, 2H, Py], 6.78 [m, 4H, Py], 3.66 [m, 2H, C*H*₂, Et], 1.21 [m, 3H, C*H*₃, Et].

6.2.45 Synthesis of [{(*p*TolylN)C(=O)}₃] 45

Complex **30** (0.69 g, 1 mmol) was added to a Schlenk tube and dissolved in THF (4 ml), pTolylN=C=O (0.38m l, 3 mmol) was then added and the reaction allowed stirring for 1 hour. Hexane was added 1 mol and the Schlenk stored in the freezer for

24 hours resulting in colourless crystals which were isolated and stored in the glove box (0.35 g, 89%).

¹H NMR (C_6D_6, 298K) δ7.16 [m, 8H, Ph], 6.94 [m, 4H, Ph], 2.00 [s, 9H, C*H*₃,]. **¹³C NMR{¹H}** (C_6D_6, 298K) δ148.70 [*C*=O], 138.83, 132.09, 129.75, 128.54 [*C*H, Ph], 20.75 [*C*H₃].

6.2.46 Synthesis of [{Na(THF)₆}⁺{(Ph₂Si(NAr*)₂Mg[(CyN)C(=NCy)(NPh₂)]}⁻] 46

BuNa (0.08g, 1mmol) was suspended in a Schlenk tube in hexane (10 ml). Bu₂Mg was then added (1ml, 1M solution in heptane, 1mmol) and allowed to stir for 5 minutes. The already prepared ligand **1** was added (0.53g, 1mmol) and the suspension stirred for 1 hour. THF (4 ml) was introduced until a clear solution formed. Diphenylamine was added (0.16 g, 1mmol) and the solution stirred for a further hour, to form a white suspension. The solution was gently heated until clear. Dicyclohexylcarbodiimide (0.20 g, 1mmol) was added and the solution allowed to stir overnight, to form a suspension. Heated to a clear solution and placed the Schlenk in the freezer. Colourless crystals formed overnight. The crystals were isolated and transferred to the glove box. Isolated yield (0.72 g, 55%)

¹H NMR (C_6D_6, 298K) δ8.03 [d, 4H, Ph or NPh₂], 7.37 [d, 4H, Ph or NPh₂], 7.20 [m, 4H, Ph or NPh₂], 7.13 [m, 4H, Ph or NPh₂], 7.05 [d, 4H, Ar*], 7.01 [m, 2H, Ph or NPh₂], 6.90 [m, 2H, Ph or NPh₂], 6.63 [m, 2H, Ar*], 4.45[m, 4H, CH, ^iPr, Ar*], 3.37 [m, 24H, OC*H*₂, THF], 3.31 [m, 2H, C*H*₂, Cy], 1.39[m, 24H, C*H*₂, THF], 1.76 [d, 8H, C*H*₂, Cy], 1.68 [d, 8H, C*H*₂, Cy], 1.39 [d, 24H, C*H*₃, ^iPr, Ar*], 1.16 [d, 4H, C*H*₂, Cy]. **¹³C NMR{¹H}** (C_6D_6, 298K) δ164.32 [N*C*(N)N], 154.7, 147.1, 146.3, 143.8, [*C*quarternary, Ph or NPh₂ or Ar*], 143.6, 135.3, 129.8, 128.8, 126.6, 123.3, 122.2, 114.3, [*C*H, Ph or NPH₂ or Ar*], 67.21 [*C*H₂, THF], 54.72 [*C*H, Cy], 36.87 [*C*H₂, Cy], 34.21 [*C*H₂, Cy], 27.21 [*C*H, ^iPr, Ar*], 25.62 [*C*H₃, ^iPr, Ar*], 25.12 [*C*H₂, THF], 24.23 [*C*H₂, Cy].

6.2.47 Synthesis of [{Na(THF)₆}⁺{(Ph₂Si(NAr*)₂Mg[(^iPrN)C(=N^iPr)(NPh₂)]}⁻] 47

BuNa (0.08g, 1mmol) was suspended in a Schlenk tube in hexane (5 ml). Bu₂Mg was then added (1ml, 1M solution in heptane, 1mmol) and allowed to stir for 5 minutes.

The already prepared ligand **1** was added (0.53g, 1mmol) and the suspension stirred for 1 hour. THF (4 ml) was introduced until a clear solution formed. Diphenylamine was added (0.16g, 1mmol) and the solution stirred for a further hour, to form a white suspension which was gently heated until a clear solution was obtained. Diisopropylcarbodiimide (0.15 g, 1mmol) was added and the reaction mixture allowed to stir overnight, to form a white suspension which was heated to give a clear solution. Colourless crystals were formed on slow cooling of the solution. Crystals were isolated and stored in the glove box. Isolated yield (0.38 g, 29%)

^{1}H NMR (C$_6$D$_6$, 298K) δ8.08 [m, 4H, Ph or NPh$_2$], 7.35 [m, 4H, Ph or NPh$_2$], 7.20 [m, 4H, Ph or NPh$_2$], 7.13 [m, 4H, Ph or NPh$_2$], 7.05 [m, 4H, Ar*], 7.01 [m, 2H, Ph or NPh$_2$], 6.90 [m, 2H, Ph or NPh$_2$], 6.63 [m, 2H, Ar*], 4.13 [m, 4H, C*H*, ^{i}Pr, Ar*], 3.68 [m, 2H, C*H* , N^{i}Pr, Ar*], 3.32[t, 24H, OC*H*$_2$, THF], 1.45[m, 24H, C*H*$_2$, THF], 1.45[d, 24H, C*H*$_3$, ^{i}Pr, Ar*], 1.12 [d, 12H, C*H*$_3$, N^{i}Pr, Ar*]. **^{13}C{^{1}H} NMR** (C$_6$D$_6$, 298K) δ163.86 [*C*$_{quarternary}$, NCN], 153.92, 146.7, 146.1, 144.2, 135.4, 134.7, [*C*$_{quarternary}$, Ph and Ar*], 129.7, 129.2 127.4, 127.3, 126.45, 124.34 123.9, 123.6, 123.2, 114.52 [*C*H, Ph, NPh$_2$, Ar*], 67.89 [*C*H$_2$, THF], 27.87 [*C*H, ^{i}Pr, Ar*], 26.23 [*C*H, N^{i}Pr, Ar*], 26.12 [*C*H$_3$, ^{i}Pr, Ar*], 25.12 [*C*H$_2$, THF], 24.56 [*C*H$_3$, N^{i}Pr].

6.2.48 [(NPh$_2$)C(=NCy)(NHCy)]48

Reaction was carried out in an NMR tube following same method in section **6.1.5**. Yields were calculated by reference to internal standard (64 %).

^{1}H NMR (C$_6$D$_6$, 298K) δ7.12 [m, 8H, Ph], 6.78 [m, 2H, Ph], 3.82 [m, 1H, C*H*, Cy], 3.58 [m, 1H, N*H*], 1.96 [m, 2H, C*H*$_2$, Cy] 1.48, 1.08 [m, 4H, C*H*$_2$, Cy], 0.80 [m, 4H, C*H*$_2$, Cy]. **^{13}C NMR{^{1}H}** (C$_6$D$_6$, 298K) δ145.80 [*C*=O], 143.06 [*C*$_{quarternary}$, Ph], 128.68, 121.83, 117.21 [*C*H, Ph], 67.41 [*C*H, Cy], 34.49, 32.35, 24.98, 24.51 [*C*H$_2$, Cy].

6.2.49 [(NPh$_2$)C(=N^{i}Pr)(NH^{i}Pr)] 49

Reaction was carried out in an NMR tube following same method in section **6.1.5**. Yields were calculated by reference to internal standard (78 %).

¹H NMR (C₆D₆, 298K) δ7.09 [m, 8H, Ph], 6.83 [m, 2H, Ph], 3.85-3.72 [b, 1H, C*H*, ^iPr], 3.48 [s, 1H, N*H*], 0.97 [d, 6H, C*H₃*, ^iPr]. **¹³C NMR{¹H}** (C₆D₆, 298K) δ154.75 [*C*=O], 144.87 [*C*quarternary, Ph], 129.45, 122.59, 120.95 [*C*H, Ph], 48.75 [*C*H, ^iPr], 24.74 [*C*H₃, ^iPr].

6.2.50 [{Na(THF)₅}⁺{Mg(NPh₂)[(NCy)C(=NCy)(NPh₂)]₂}⁻] 50

Complex **30** was added to a Schlenk tube (0.69 g, 1 mmol) and dissolved in THF 4 ml. CyN=C=NCy was added (0.60 g, 3 mmol) and allowed to stir for 1 hour. Hexane was dripped in until cloudy 1 ml and Schlenk placed in the freezer overnight. Colourless crystals were isolated and stored in the glove box (1.08 g, 78 %).

¹H NMR (C₆D₆, 298K) δ7.40 [d, 8H, Ph], 7.31 [d, 4H, Ph], 7.22 [m, 8H, Ph], 7.11 [m, 4H, Ph], 7.00 [m, 2H, Ph], 6.84 [m, 4H, Ph], 3.59 [m, 20H, OC*H₂*], 3.12 [m, 4H, C*H*, Cy], 1.85 [m, 8H, C*H₂*, Cy], 1.41 [m, 16H, C*H₂*, Cy], 1.41 [m, 20H, C*H₂*, THF] 1.17 [m, 16H, C*H₂*, Cy]. **¹³C NMR{¹H}** (C₆D₆, 298K) δ163.29, 155.11, 144.98, 129.19, 128.47, 120.99, 119.66, 116.28 [*C*H, Ph], 67.15 [O*C*H₂, THF], 54.21 [*C*H. Cy], 54.05 [*C*H₂, Cy], 36.53 [*C*H₂, Cy], 36.09 [*C*H₂, Cy], 25.79 [*C*H₂, Cy], 25.57 [*C*H₂,Cy], 24.82 [*C*H₂, Cy].

Overview, Conclusions and Future Work

The use of highly sterically demanding ligands such as β-diketiminates, NHC or bis(amides), has been instrumental for recent landmarks in synthesis. Some examples are the isolation of the first stable species containing Mg-Mg metal bonds or development of several Ca and Ba species which can effectively catalyse hydroamination reactions of unsaturated organic molecules. On the other hand, recent advances in magnesium chemistry have shown that combining Mg with a more polar metal such as Li or Na can greatly enhance the reactivity of the Mg centre. Bringing these two fundamentally different areas of research together, the main objective of this PhD programme was to design a new series of mixed metal systems supported by sterically demanding ligands, and study these new reagents within the context of deprotonative metallation and their applications as catalysts for hydroamination reactions of organic electrophiles. To reach this target, a combination of different analytical techniques have been employed, including X-ray crystallography, multinuclear NMR spectroscopy, DFT calculation and EPR studies.

A new generation of sodium magnesiates has been prepared bearing the sterically demanding dianionic bis(amido)silyl ligand $\{Ph_2Si(NAr*)_2\}^{2-}$ which is bonded to Mg through the N atoms. Thus the reaction of $NaMgBu_3$ with bis(amine) $[Ph_2Si(NAr^*H)_2]$ **1** allows the isolation of butyl species $[\{Na(THF)_6\}^+\{(Ph_2Si(NAr*)_2)Mg(Bu)(THF)\}^-]$ **2**. A similar approach led to the isolation of $[\{Na(THF)_6\}^+\{(Ph_2Si(NAr*)_2)Mg(CH_2SiMe_3)(THF)\}^-]$ **5**. Complex **5** can be used as a precursor to prepare new amido derivatives **6-10** by reacting it with one molar equivalent of several amines $[\{Na(THF)_6\}^+\{Ph_2Si(NAr*)_2Mg(NR_2)(THF)_x\}^-]$ (NR$_2$ = HMDS, x =1, **6**; NPh$_2$, x = 1, **7**; DA, x = 1, **8**; DMP, x = 1, **9**, TMP, x=0, **10**). When primary aniline (H$_2$NAr*) is used a new structural motif was observed for $[\{Na(THF)_6\}^+\{(Ph_2Si(NAr*)(NHAr*))Mg(NHAr*)_2(THF)\}^-]$ **11**, still a solvent separated structure but now the bis(amido)silyl ligand has been protonated at one of its amido arms and is now acting in a monodentate fashion coordinating to Mg which completes its coordination by bonding to two NHAr* amido groups and a molecule

of THF. Likewise, the aromatic amine pyrrole also demonstrates the partial protonation of the bis(amido)silyl ligand but for the first time we observed a contact ion pair structure [{(Ph$_2$Si(NAr*)(NHAr*))Mg(NC$_4$H$_4$)$_2$(THF)Na(THF)$_2$}] **12** as Na is π engaged with the aromatic ring of two pryrrolyl anions.

In order to assess the metallating ability of these new sodium magnesiates towards heterocyclic molecules, thiophene was investigated. We found that while alkyl base **2** is not active enough to promote the magnesiation of this heterocycle, TMP derivative **10** can selectively deprotonate thiophene at its C2 position at room temperature and in almost quantitative yields. Contrastingly both complexes **2** and **10** can promote the magnesiation of MeBIm to yield dimer [{Na(THF)$_5$}$_2^+${(Ph$_2$Si(NAr*)$_2$)Mg(MeBIm*)}$_2^-$] **14**. Structural and spectroscopic analysis of **14** coupled with DFT calculations suggest that the C atom in the benzimidazolyl anion displays a markedly carbenic character, which translates in a partial negative charge on the adjacent nitrogen, which may explain the formation of the dimeric arrangement of **14**, which is maintained in solution.

Extending the study to the heterocycle benzothiazole, using the alkyl magnesiate **2** an unprecedented activation of the N-heterocycle takes place in a cascade reaction involving initial magnesiation of Btz followed by, C-C coupling, ring opening and intramolecular deprotonation to form complex [L$_2$Mg$_2$Na$_2$(THF)$_5$] **15**. This reaction is a genuine example of cascade chemistry, verified when the reaction was carried out at 0°C, activation of benzothiaozle still occured to yield complex [L$_2$L$^*_2$Mg$_3$Na$_4$(THF)$_9$] **16**. This activation is in sharp contrast to the straight forward magnesiation at the C2 position exhibited by Knochels "turbo grignard" reagent [TMPMgCl·LiCl]. The sterically demading bis(amido)silyl ligand appears to play a key role in this activation being directly involved in the metallation of two benzothiazole molecules. Supporting this proposal the reaction of neutral bis(amido)silyl magnesium complex [(Ph$_2$Si(NAr*)$_2$)Mg(THF)$_2$] **17** was also able to successfully activate benzothiaozle to yield [LMg$_2$(SH)(THF)$_4$] **18**, however in a less clean and lower yielding reaction that the sodium magnesate. Building on these initial results which show that these novel sodium magnesiates have proved to be

efficient magnesiating reagents, as well as able to promote novel activation reactions, further work in this area should look to extend the scope of substrates, for example substituted imidazoles could be used such as methylimidazole, vinylimidazole and *tert*butoxycarbonylimidazole. Likewise, oxazoles and benzoxazole could be reacted, oxygen containing heterocycles have been known to undergo ring opening when reacted with conventional orgaolithium reagents even in cryogenic conditions which suggest that they may undergo cascade activation more easily than benzothiazole.

In changing heterocycle to the diazine quinoxaline with complex **2**, it was possible to prepare and structurally characterise the trapping of a radical anion in the form of dimer $[\{Na(THF)_6\}_2^+\{(Ph_2Si(NAr^*)_2)Mg(Qox^\bullet)\}_2^-]$ **20**. The presence of a radical in solution was confirmed by EPR studies. This is in contrast to work carried out by Knochel using $TMP_2Mg\cdot2LiCl$ in the presence of $ZnCl_2$, where quinoxaline is metallated at the C position next to the N atom. It is presumed that the ligand plays a key role here in stabilising the radical anion. Further investigations in this area could look at using other diazine substrates with complex **2** as a base to see if metallation occurs or would lead to the isolation of new species. Furthermore, the reactivity that these radical species can exhibit when confronted with other organic molecules such as RN=C=O or PhN=NPh should also be explored which may lead to novel coupling reactions. Substrates such as pyrazine, pyrimidine and pyridazine have been shown to undergo selective metallation using mixed metal systems such as $[Li(TMP)Zn(^tBu)_2]$, $TMP_2Mg_2\cdot LiCl$ in the presence of $ZnCl_2$ and $CdCl_2\cdot TMEDA$ in the presence of LiTMP, by our own group and others. As nitrogen containing heterocycles are important building blocks in many pharmaceuticals and other biologically active molecules and a key tool in incorporating these substrates into larger systems is metallation reactions, further investigations would be worthwhile extending the scope of N containing heterocycles used such as pyridines, pyrazoles and triazoles. Precedents have been set in the literature for these substrates to undergo metallation using mixed metal systems such as $[Li(TMP)Zn(^tBu)_2]$ and $TMPMg\cdot LiCl$. Whilst Hill *et al* have shown that pyridine undergoes dearomatisation using a β-diketiminate Mg-Bu complex.In addition to bis(amido)silyl ligands the synthesis of sodium magnesiate compounds bearing β-diketiminate ligands was also

attempted. However these studies led to the isolation of homometallic alkyl and amido magnesium complexes [(^{Dipp}nacnac)Mg(Bu)(THF)] **22** and [(^{Dipp}nacnac)Mg(TMP)] **23** respectively bearing ^{Dipp}nacnac ligands. Due to the successful magnesiation of N-heterocycles by magnesiates **2** and **10**, we decided to assess the metallating ability of **22** and **23** towards 1,3-benzoazoles. Both complexes **22** and **23** when reacted with benzoxazole, which has the most acidic C2 position of the N-heterocycles studied, underwent ring opening, to produce complex [(^{Dipp}nacnac)Mg{O(o-C$_6$H$_4$)NC}(THF)] **24**, which to the best of our knowledge is the first iso(cyano)phenolate Mg intermediate to be structurally characterised. In moving to benzothiazole, amido base **23** can selectively deprotonate Btz to give dimer [{(^{Dipp}nacnac)Mg(Btz*)}$_2$] **25** with a structure that has a strong resemblance to that described for the MeBIm metallation product by **2**. Exhibiting a similar dimeric motif, structural and spectroscopic analysis suggests that the C2 of the benzothiazolyl anion has a marked carbenic character. Contrastingly, butyl complex **22** promotes a different type of reaction involving magnesiation, C-C coupling and ring opening to form complex [(^{Dipp}nacnac)Mg{(Btz*)C(H)=N(2-C$_6$H$_4$-1-S)}] **26**. Studies using MeBIm show that the alkyl derivative **22** was not reactive enough to deprotonate the heterocycle forming [(^{Dipp}nacnac)Mg(Bu)(MeBIm)] **28** where MeBIm acts as a N donor to Mg. However the more kinetically reactive Mg-TMP complex **23** could carry out the deprotonation at the C2 position to yield [{(^{Dipp}nacnac)Mg(MeBIm*)}$_2$] **27** which is isostructural to **25**.

This work shows the promise of these Mg reagents not only towards N-heterocycle activation but also towards the development of their applications in synthesis. Further work in this exciting area may involve the sequential reactions of complexes **22** and **23** with different 1,3-benzoazoles to assess if this will allow entry to a library of heterocoupled 1,3-bis(benzoazoles) as well as extend these studies to substituted 1,3-azoles to be able to assess the functional group tolerance of this methodology. Another important line of work that should be studied is the use of these Mg-β-diketiminate reagents towards other N-heterocyclic molecules such as pyridines, diazines and indoles to name a few.

In the final chapter the study of hydroamination reactions of heterocumulenes; isocyanates and carbodiimides was studied. Hydroamination reactions of these electrophiles have been carried out successfully using lanthanide, transition metal and main group catalysts. However to the best of our knowledge no precedents exist in mixed-metal chemistry. Initial studies using complex **2** as a catalyst showed that the bis(amido)silyl ligand did not play a part in these hydroamination reactions and in fact the active species in the reaction was tris(amido) $[NaMg(NPh_2)_3(THF)_2]$ **30**. Thus the tris(alkyl) magnesiate $[NaMg(CH_2SiMe_3)_3]$ **32** was an excellent precursor of **30** and were successfully able to carry out the hydroamination of three different alkyl isocyanates with a series of different amines to form the corresponding ureas, also the hydroamination of carbodiimides with $HNPh_2$ to yield the respective guanidines. Studies showed that nucleophilic aliphatic amines underwent hydroamination with isocyanates without the need for a catalyst, and out of the aromatic amines the most nucleophilic gave the highest yielding ureas as would be expected. When aryl isocyanates were used along with 2 mol % **32**, it was found that the trimerisation of the isocyanates occurred instead of the hydroamination, although there are many precedents in the literature for the trimerisation of aryl isocyanates as far as we are aware, no previous examples of magnesium catalyst were known. Further investigation could look to extend the scope of amines, isocyanates and carbodiimides used in these hydroamination reactions. Other electrophiles such as vinylarenes, and amino alkenes, which have both shown promise for undergoing hydroamination reactions by Ca catalysts could also be studied. Finally the reactivity of sulfur containing electrophiles could also be looked at such as thiocyanates.

In extension to this work, further investigations using the sodium magnesiate **2** could be used in preparing a Mg hydride cluster, as Hill *et al* had carried out using a sterically demanding NHC ligand coordinated to a Mg-HMDS complex to form a Mg_4 hydride cluster. Likewise, the record breaking magnesium hydride cluster containing $\{Mg_8H_{10}\}^{6+}$ fragment using a modified β-diketiminate ligand para-phenylene which can be employed as a double based nacnac diketiminate prepared by Harder *et al*. These hydride clusters have potential important applications in hydrogen storage and as this is considered by many to be the potential fuel of the future, the need to study these complexes is of extreme importance. Initial studies

reacting complex **2** with PhSiH$_3$ unfortunately failed to form a hydride cluster. However, for future investigation this could be a worthwhile area of study. By changing reaction conditions and source of hydride, complex **2** supported by a bulky bis(amido)silyl ligand for support could possibly be successful in forming a high Mg hydride cluster, alternatively other amido bases such as HMDS derivative **6** may prove to work.

During the course of this PhD programme a sodium zincate bearing a bulky bis(amido)silyl ligand [{Na(THF)$_6$}$^+${(Ph$_2$Si(NAr*)$_2$)ZnEt}$^-$] **51** was prepared, by reacting BuNa with Et$_2$Zn and equivalent of amine **1** in a hexane/THF mixture. Zincates are known to be less reactive than magnesiates, however displaying greater selectivity and functional group tolerance. Initial reactivity studies using complex **51** with heterocycles thiophene, oxazole and imidazole showed no reaction was taking place. Further investigations could however look to prepare new amido sodium zincates bearing sterically demanding ligands, and use these reagents to carry out zincations of heterocycles; with work throughout this thesis demonstrating the greater metallating ability of M-N bonds over M-C bonds. Alkali-metal zincates have also been shown to carry out metal-halogen exchange reactions by our own group and groups around the world such as Kondo *et al*. In addition, alkali-metal zincates are efficient reagents for 1,4-conjugate addition and 1,2 addition reactions to aldehydes and ketones. Further investigations could use complex **51** as well as newly prepared sodium zincates coordinated to bulky ligands to possibly carry out these synthetic reactions.

In summary, a series of new sodium magnesiates have been prepared brearing a sterically demanding bis(amido)silyl ligand. These newly prepared bases have proven to be versatile reagents in synthesis carrying out selective magnesiations of heterocycles, the unprecedented activation of benzothiaozle in a cascade reaction involving metallation, C-C coupling, ring opening and intramolecular deprotonation, also the trapping of a radical anion. The sterically demading ligand has played a key role in stabilising the product formed. Likewise, an alkyl and amido magnesium complex bearing β-diketimainte ligands have been prepared and used to carry out the metallation of N-heterocycles, clearly indicating the greater reactivity of the Mg-N

bond over the Mg-C bond. Finally the hydroamination of isocyantes and carbodiimides has been carried out catalytically using a sodium magnesiate, whilst the trimerisation of arylisocyanates can also be accomplished. This thesis has demonstrated that novel chemistry can be carried out using mixed-metal systems coordinated to sterically demanding ligands. Given that most of mixed metal chemistry has not yet been explored, a systematic approach covering the periodic table (main group, transition metal, lanthanide) will be important in determining its full potential, this along with the vast choice of sterically demanding ligands available means that this area of research could provide numerous interesting and unique results.

References

[1]   C. Jones, *Coord. Chem. Rev.* **2010**, *254*, 1273.
[2]   D. Bourissou, O. Guerret, F. P. Gabbai, G. Bertrand, *Chem. Rev.* **2000**, *100*, 39.
[3]   L. Bourget-Merle, M. F. Lappert, J. R. Severn, *Chem. Rev.* **2002**, *102*, 3031.
[4]   P. J. Bailey, S. Pace, *Coord. Chem. Rev.* **2001**, *214*, 91.
[5]   A. W. Hofmann, *Chem. Ber.* **1872**, *5*, 704.
[6]   V. Meyer, *Chem. Ber.* **1894**, *27*, 510.
[7]   W. K. Kim, M. J. Fevola, L. M. Liable-Sands, A. L. Rheingold, H. H. Theopald, *Organometallics.* **1998**, *17*, 4541.
[8]   C. Cui, H. W. Roesky, H. G. Schmidt, M. Noltemeyer, H. Hou, F. Cimpoesu, *Angew. Chem. Int. Ed.* **2000**, *39*, 4274.
[9]   A. P. Dove, V. C. Gibson, C. L. Marshall, A. J. P. White, D. J. Williams, *Chem. Commun.* **2011**, 283.
[10]   L. F. Sanchez-Barba, D. L. Hughes, S. M. Humphrey, M. Bochmann, *Organometallics.* **2005**, *24*, 3792.
[11]   R. Jiao, M. Xue, Z. Shen, Y. n. Zhang, Y. Yao, Q. Shen, *Eur. J. Inorg. Chem.* **2010**, 2523.
[12]   J. R. Lachs, A. G. M. Barrett, M. R. Crimmin, G. Kociok-Kohn, M. S. Hill, M. F. Mahon, P. A. Procopiou, *Eur. J. Inorg. Chem.* **2008**, 4173.
[13]   P. J. Bailey, S. Pace, *Coord. Chem. Rev.* **2003**, *240*, 157.
[14]   A. Mori, B. D. Cohen, A. Lowenthal, Plenum Press, New York, **1985**.
[15]   A. G. M. Barrett, M. R. Crimmin, M. S. Hill, P. B. Hitchcock, P. A. Procopiou, *Dalton Trans.* **2008**, 4474.
[16]   M. R. Crimmin, M. Arrowsmith, A. G. M. Barrett, I. J. Casely, M. S. Hill, P. A. Procopiou, *J. Am. Chem. Soc.* **2009**, *131*, 9670.
[17]   M. R. Crimmin, A. G. M. Barrett, M. S. Hill, P. B. Hitchcock, P. A. Procopiou, *Organometallics.* **2008**, *27*, 497.
[18]   A. G. M. Barrett, T. C. Boorman, M. R. Crimmin, M. S. Hill, G. Kociok-Kohn, P. A. Procopiou, *Chem. Commun.* **2008**, 5206.
[19]   W. Wang, R. Quillan, P. Wei, H. Wang, X. J. Yang, Y. Xie, R. B. King, P. V. R. Schleyer, H. F. Schaefer, G. H. Robinson, *J. Am. Chem. Soc.* **2005**, *127*, 11944.
[20]   I. Resa, E. Carmona, E. Gutierrez-Puebla, A. Monge, *Science.* **2004**, *305*, 1136.
[21]   A. Grirrane, I. Resa, A. Rodriguez, E. Carmona, E. Alvarez, E. Gutierrez-Puebla, A. Monge, A. Galindo, D. Del Rio, R. A. Andersen, *J. Am. Chem. Soc.* **2007**, *129*, 693.
[22]   T. Li, S. Schulz, P. W. Roesky, *Chem. Soc. Rev.* **2012**, *41*, 3759.
[23]   Y. Tsai, D. Lu, Y. Lin, J. Hwang, J. Yu, *Chem. Commun.* **2007**, 4125.
[24]   A. Luhl, H. Pada Nayek, S. Blechert, P. W. Roesky, *Chem. Commun.* **2011**, *47*, 8280.
[25]   M. J. Monreal, S. Khan, P. L. Diaconescu, *Angew. Chem. Int. Ed.* **2009**, *48*, 8352.
[26]   P. L. Diaconescu, *Acc. Chem. Res.* **2010**, *43*, 1352.
[27]   C. T. Carver, M. J. Monreal, P. L. Diaconescu, *Organometallics.* **2008**, *27*, 363.
[28]   C. T. Carver, P. L. Diaconescu, *J. Am. Chem. Soc.* **2008**, *130*, 7558.
[29]   C. T. Carver, D. Benitez, K. L. Miller, B. N. Williams, E. Tkatchouk, W. A. Goddard, P. L. Diaconescu, *J. Am. Chem. Soc.* **2009**, *131*, 10269.
[30]   P. L. Arnold, A. J. Blake, C. Wilson, J. B. Love, *Inorg. Chem.* **2004**, *43*, 8206.
[31]   P. L. Arnold, G. M. Jones, S. O. Odoh, G. S. Schreckenbach, N. Magnani, J. B. Love, *Nat. Chem.* **2012**, *4*, 221.
[32]   E. A. B. Kantchev, C. J. O'Brien, M. G. Organ, *Angew. Chem. Int. Ed.* **2007**, *46*, 2768.
[33]   N. Marion, S. P. Nolan, *Acc. Chem. Res.* **2008**, *41*, 1440.

[34]   C. J. O'Brien, E. A. B. Kantchev, C. Valente, N. Hadei, G. A. Chass, A. Lough, A. C. Hopkinson, M. G. Organ, *Chem. Eur. J.* **2006**, *12*, 4743.

[35]   C. Valente, S. Calimsiz, K. H. Hoi, D. Mallik, M. Sayah, M. G. Organ, *Angew. Chem. Int. Ed.* **2012**, *51*, 3314.

[36]   C. J. O'Brien, E. A. B. Kantchev, G. A. Chass, N. Hadei, A. C. Hopkinson, M. G. Organ, D. H. Setiadi, T. H. Tang, D. C. Fang, *Tetrahedron.* **2005**, *61*, 1991.

[37]   M. Perez-Rodriguez, A. A. Braga, M. Garcia-Melchor, M. H. Perez-Temprano, J. A. Casares, G. Ujaque, A. R. de Lara, R. Alvarez, F. Maseras, P. Espinet, *J. Am. Chem. Soc.* **2009**, *131*, 3650.

[38]   A. J. Arduengo, R. L. Harlow, M. Kline, *J. Am. Chem. Soc.* **1991**, *113*, 361.

[39]   A. Alexakis, *Angew. Chem. Int. Ed.* **2010**, *49*, 3346.

[40]   S. J. Bonyhady, D. Collis, G. Frenking, N. Holzmann, C. Jones, A. Stasch, *Nat. Chem.* **2010**, *2*, 865.

[41]   Y. Wang, Y. Xie, P. Wei, R. B. King, H. F. Schaefer, P. R. Schleyer, G. H. Robinson, *Science.* **2008**, *321*, 1069.

[42]   H. Braunschweig, R. D. Dewhurst, K. Hammond, J. Mies, K. Radacki, A. Vargas, *Science.* **2012**, 1420.

[43]   T. Nguyen, A. D. Sutton, M. Brynda, J. C. Fettinger, G. J. Long, P. P. Power, *Science.* **2005**, *310*, 844.

[44]   M. S. Hill, M. Arrowsmith, D. J. MacDougall, M. F. Mahon, *Angew. Chem. Int. Ed.* **2009**, *48*, 4013.

[45]   S. Harder, J. Spielmann, J. Intemann, *Angew. Chem. Int. Ed.* **2011**, *50*, 4156.

[46]   S. P. Green, C. Jones, A. Stasch, *Science.* **2007**, *318*, 1754.

[47]   C. Pi, Y. Wan, H. Gu, C. Wu, W. Wang, L. Zheng, Z. Weng, X. Chen, L. Wu, *Organometallics.* **2009**, *28*, 5281.

[48]   V. Snieckus, *Chem. Rev.* **1990**, *90*, 879.

[49]   R. E. Mulvey, F. Mongin, M. Uchiyama, Y. Kondo, *Angew. Chem.* **2007**, *117*, 380.

[50]   R. E. Mulvey, *Acc. Chem. Res.* **2009**, *42*, 743.

[51]   M. Schlosser, *Angew. Chem.* **2005**, *117*, 380.

[52]   P. Knochel, F. Kopp, *Handbook of Functionalized Organometallics, Vol. 1*, Wiley-VCH, Weinheim, **2005**.

[53]   B. Haag, M. Mosrin, H. Ila, V. Malakhov, P. Knochel, *Angew. Chem. Int. Ed.* **2011**, *50*, 9794.

[54]   *Chemfiles* **2007**, *7*, 3.

[55]   V. Grignard, *Compt. Rend. Acad. Sci. Paris.* **1900**, *130*, 1322.

[56]   R. Abegg, *Chem. Ber.* **1905**, *38*, 4112.

[57]   D. Seyferth, *Organometallics.* **2009**, *28*, 1598.

[58]   T. Imamoto, S. Sakamoto, K. Yamaguchi, *Org. Lett.* **2001**, *3*, 1793.

[59]   P. Knochel, F. M. Piller, A. Metzger, M. A. Schade, B. Haag, A. Gavryushin, *Chem. Eur. J.* **2009**, *15*, 7192.

[60]   P. E. Eaton, C. H. Lee, Y. Xiong, *J. Am. Chem. Soc.* **1989**, *111*, 8016.

[61]   C. R. Hauser, H. Walker, *J. Am. Chem. Soc.* **1947**, *69*, 295.

[62]   L. Meunier, *C. R. Hebd. Seances Acad. Sci.* **1903**, *136*, 758.

[63]   W. Schlecker, A. Huth, E. Ottow, J. Mulzer, *Synthesis* **1995**, 1225.

[64]   T. Ooi, Y. Uematsu, K. Maruoka, *J. Org. Chem.* **2003**, *68*, 4576.

[65]   R. Sanchez, G. Vest, W. Scott, P. S. Engel, *J. Org. Chem.* **1989**, *54*, 4026.

[66]   R. E. Mulvey, P. Garcia-Alvarez, D. Graham, E. Hevia, A. R. Kennedy, J. Klett, C. T. O'Hara, S. Weatherstone, *Angew. Chem. Int. Ed.* **2008**, *47*, 8079.

[67]   R. E. Mulvey, D. R. Armstrong, P. Garcia-Alvarez, A. R. Kennedy, J. P. Parkinson, *Angew. Chem. Int. Ed.* **2010**, *49*, 3185.

[68]   R. E. Mulvey, *Acc. Chem. Res.* **2009**, *42*, 743.
[69]   J. Wanklyn, *A. Ann.* **1858**, *108*, 67.
[70]   G. Wittig, F. J. Meyer, G. Lange, *Liebigs Ann. Chem.* **1951**, *571*, 167.
[71]   E. Hevia, D. V. Graham, A. R. Kennedy, R. E. Mulvey, *Organometallics.* **2006**, *25*, 2396.
[72]   M. Schlosser, *Organometallics in Synthesis*, 2nd ed., Wiley, New York, **2002**.
[73]   E. Hevia, D. J. Gallagher, A. R. Kennedy, R. E. Mulvey, C. T. O'Hara, C. Talmard, *Chem. Commun.* **2004**, 2422.
[74]   P. C. Andrikopoulos, D. R. Armstrong, D. V. Graham, E. Hevia, A. R. Kennedy, R. E. Mulvey, C. T. O'Hara, C. Talmard, *Angew. Chem. Int. Ed.* **2005**, *44*, 3459.
[75]   R. E. Mulvey, *Organometallics.* **2005**, *25*, 1060.
[76]   R. E. Mulvey, W. Clegg, B. Conway, P. Garcia-Alvarez, A. R. Kennedy, L. Russo, T. Tuttle, *Chem. Eur. J.* **2009**, *15*, 10702.
[77]   R. E. Mulvey, D. R. Armstrong, A. R. Kennedy, R. B. Rowlings, *Angew. Chem. Int. Ed.* **1999**, *38*, 131.
[78]   R. E. Mulvey, *Chem. Commun.* **2001**, 1049.
[79]   D. V. Graham, E. Hevia, A. R. Kennedy, R. E. Mulvey, C. T. O'Hara, C. Talmard, *Chem. Commun.* **2005**, 417.
[80]   V. L. Blair, A. R. Kennedy, J. Klett, R. E. Mulvey, *Chem. Commun.* **2008**, 5426.
[81]   V. L. Blair, A. R. Kennedy, R. E. Mulvey, C. T. O'Hara, *Chem. Eur. J.* **2010**, *16*, 8600.
[82]   W. Clegg, K. W. Henderson, A. R. Kennedy, R. E. Mulvey, C. T. O'Hara, R. B. Rowlings, D. M. Tooke, *Angew. Chem. Int. Ed.* **2001**, *40*, 3902.
[83]   M. Hatano, T. Matsumura, K. Ishihara, *Org. Lett.* **2005**, *7*, 573.
[84]   P. Murugavel, P. Palanisami, R. Butcher, *J. Organomet. Chem.* **2003**, *675*, 65.
[85]   M. Cheng, X. Pu, N.-B. Wong, M. Li, A. Tian, *New. J. Chem.* **2008**, *32*, 1060.
[86]   M. S. Hill, P. B. Hitchcock, *Organometallics.* **2002**, *21*, 3258.
[87]   X. Zhu, J. Fan, Y. Wu, S. Wang, L. Zhang, G. Yang, Y. Wei, C. Yin, H. Zhu, S. Wu, H. Zhang, *Organometallics* **2009**, *28*, 3882.
[88]   A. Xia, M. J. Heeg, C. H. Winter, *Organometallics.* **2002**, *21*, 4718.
[89]   E. Hevia, A. R. Kennedy, R. E. Mulvey, S. Weatherstone, *Angew. Chem. Int. Ed.* **2004**, *43*, 1709.
[90]   C. N. Ayala, M. H. Chisholm, J. C. Gallucci, C. Kremper, *Dalton. Trans.* **2004**, 9239.
[91]   R. Chinchilla, C. Najera, M. Yus, *Chem. Rev.* **2004**, *104*, 2667.
[92]   T. Sakamoto, Y. Kondo, H. Yamanaka, *Heterocycles* **1988**, *27*, 2225.
[93]   H. Gilman, D. A. Shirley, *J. Am. Chem. Soc.* **1949**, *71*, 1870.
[94]   H. W. Gschwend, H. R. Rodriguez, *Org. React.* **1979**, *26*, 1.
[95]   J. Clayden, in *Tetrahedron Organic Chemistry Series., Vol. 23*, Pergamon, Oxford, **2002**.
[96]   R. E. Mulvey, S. D. Robertson, A. R. Kennedy, *Dalton. Trans.* **2010**, *39*, 9091.
[97]   in *Chemical and Engineering News., Vol. 89*, **2011**, p. 12.
[98]   R. E. Mulvey, A. R. Kennedy, J. Klett, V. L. Blair, *Chem. Commun.* **2008**, 5426.
[99]   M. Shilai, Y. Kondo, T. Sakamoto, *J. Chem. Soc. Perkin Trans 1.* **2001**, 442.
[100] A. R. Kennedy, J. Klett, C. T. O'Hara, R. E. Mulvey, G. M. Robertson, *Eur. J. Inorg. Chem.* **2009**, 5029.
[101] R. Campbell, B. Conway, G. S. Fairweather, P. Garcia-Alvarez, A. R. Kennedy, J. Klett, R. E. Mulvey, C. T. O'Hara, G. M. Robertson, *Dalton. Trans.* **2010**, *39*, 511.
[102] M. Vestergren, B. Gustafsson, O. Davidsson, M. Hakansson, *Angew. Chem. Int. Ed.* **2000**, *39*, 3435.
[103] T. T. Nguyen, F. Chevallier, V. Jouikov, F. Mongin, *Tetrahedron Lett.* **2009**, *50*, 6787.
[104] A. R. Kennedy, R. E. Mulvey, R. B. Rowlings, *J. Am. Chem. Soc.* **1998**, *120*, 7816.

[105]   M. Gartner, R. Fischer, L. J., H. Gorls, D. Walther, M. Westerhausen, *Inorg. Chem.* **2007**, *46*, 5118.

[106]   D. Graham, E. Hevia, A. R. Kennedy, R. E. Mulvey, C. T. O'Hara, C. Talmard, *Chem. Commun.* **2006**, 417.

[107]   Y. Zhao, C. Mao, Y. Li, P. Zhang, Z. Huang, F. Bi, R. Huang, Q. Wang, *J. Agric. Food Chem.* **2008**, *56*, 7326.

[108]   K. L. Baumann, D. E. Butler, C. F. Deering, K. E. Mennen, A. Millar, T. A. Nanninga, C. W. Palmer, B. D. Roth, *Tetrahedron Lett.* **1992**, *33*, 2283.

[109]   M. Mathis, W. Harsha, T. W. Hanks, *Chem. Mater.* **1998**, *10*, 3568.

[110]   F. G. Bordwell, G. E. Drucker, H. E. Fried, *J. Org. Chem.* **1981**, *46*, 632.

[111]   F. G. Bordwell, J. C. Branca, D. L. Hughes, M. M. Olmstead, *J. Org. Chem.* **1980**, *45*, 3305.

[112]   B. Conway, E. Hevia, A. R. Kennedy, R. E. Mulvey, S. Weatherstone, *Dalton. Trans.* **2005**, 1532.

[113]   J. A. Garden, A. R. Kennedy, R. E. Mulvey, S. D. Robertson, *Dalton Trans.* **2011**, *40*, 11945.

[114]   A. R. Katritzky, C. W. Rees, E. F. Scriven*, Vol. 11*, Pergamon, Oxford, **1999**.

[115]   M. Yoshikawa, T. Morikawa, H. Matsuda, G. Tanate, O. Muraoka, *Med. Chem.* **2002**, *10*, 1547.

[116]   L. S. Jeong, S. A. Choe, P. Gunaga, H. O. Kim, H. W. Lee, K. W. Lee, D. K. Tosh, A. Patel, Z.-G. Gao, K. A. Jacobson, H. R. Moon, *J. Med. Chem.* **2007**, *50*, 3159.

[117]   L. W. Ye, C. Y. Sun, C. Y. Li, Y. Tong, *J. Org. Chem.* **2007**, *72*, 1335.

[118]   J. Noh, Y. Jeong, E. Ito, M. Hara, *J. Phys. Chem. C.* **2007**, *111*, 2691.

[119]   K. W. Henderson, W. J. Kerr, *Chem. Eur. J.* **2001**, *7*, 3431.

[120]   R. Chinchilla, C. Najera, M. Yus, *Chem. Rev.* **2004**, *104*, 2667.

[121]   K. Shen, Y. Fu, J. N. Liu, Q. X. Guo, *Tetrahedron.* **2007**, *63*, 1568.

[122]   C. Hilf, F. Bosold, K. Harms, M. Marsch, G. Boche, *Chem. Ber.* **1997**, *130*, 1213.

[123]   C. Hilf, F. Bosold, K. Harms, J. C. W. Lohrenz, M. Marsch, M. Schimeczek, G. Boche, *Chem. Ber. Recueil.* **1997**, *130*, 1201.

[124]   B. Conway, E. Hevia, A. R. Kennedy, R. E. Mulvey, *Chem. Commun.* **2007**, 2864.

[125]   Y. Tang, L. N. Zakharov, A. L. Rheingold, R. A. Kemp, *Organometallics.* **2005**, *24*, 836.

[126]   M. A. Huertos, J. Perez, L. Riera, A. Menendez-Velazquez, *J. Am. Chem. Soc.* **2008**, *130*, 13530.

[127]   R. E. Mulvey, S. D. Robertson, A. R. Kennedy, *Dalton Trans.* **2010**, *39*, 9091.

[128]   K. W. Henderson, A. R. Kennedy, R. E. Mulvey, C. T. O'Hara, R. B. Rowlings, *Chem. Commun.* **2001**, 1678.

[129]   A. G. M. Barrett, I. T. Casely, M. R. Crimmin, M. S. Hill, J. R. Lachs, M. F. Mahon, P. A. Procopiou, *Inorg. Chem.* **2009**, *48*, 4445.

[130]   V. C. Gibson, J. A. Segal, A. J. P. White, D. J. Williams, *J. Am. Chem. Soc.* **2000**, *122*, 7120.

[131]   M. Shilai, Y. Kondo, S. Sakamoto, *J. Chem. Soc. Perkin Trans. 1.* **2001**, 442.

[132]   A. Krasovskiy, V. Krasovskaya, P. Knochel, *Angew. Chem. Int. Ed.* **2006**, *45*, 2958.

[133]   B. D. Kenney, M. Breslav, R. Chang, R. Glaser, B. D. Harris, C. A. Maryanorr, M. J., A. Roessler, B. Segmuller, J. Villani, F. J. , *J. Org. Chem.* **2007**, *75*, 9798.

[134]   V. L. Blair, W. Clegg, A. R. Kennedy, Z. Livingstone, L. Russo, E. Hevia, *Angew. Chem. Int. Ed.* **2011**, *50*, 9857.

[135]   P. L. Diaconescu, *Acc. Chem. Res.* **2010**, *43*, 1352.

[136]   S. Duhovic, M. J. Monreal, P. L. Diaconescu, *Inorg. Chem.* **2010**, *49*, 7165.

[137]   A. G. M. Barrett, M. R. Crimmin, M. S. Hill, P. A. Procopiou, *Proc. R. Soc. London Ser. A.* **2010**, *466*, 927.

[138]	M. Alajarin, J. Cabrera, A. Pastor, P. Sanchez-Andrada, D. Bauista, *J. Org. Chem.* **2006**, *71*, 5328.

[139]	R. E. Mulvey, V. L. Blair, W. Clegg, A. R. Kennedy, J. Klett, L. Russo, *Nat. Chem.* **2010**, *2*, 588.

[140]	T. Eicher, S. Hauptmann, A. Speicher, 2nd. ed., Wiley. , Weinheim, **2003**.

[141]	A. R. Katritzky, 1st ed., Pergammon, New York, **1985**.

[142]	F. Buron, N. Ple, A. Turck, G. Queguiner, *J. Org. Chem.* **2005**, *70*, 2616.

[143]	F. Chevallier, F. Mongin, *Chem. Soc. Rev.* **2008**, *37*, 595.

[144]	G. Queguiner, F. Marsais, V. Snieckus, J. Epsztajin, *Adv. Heterocycl. Chem.* **1991**, *52*, 187.

[145]	Z. Dong, G. C. Clososki, S. H. Wunderlich, A. Usinn, J. Li, P. Knochel, *Chem. Eur. J.* **2009**, *15*, 457.

[146]	M. S. Hill, D. J. MacDougall, M. F. Mahon, *Dalton. Trans.* **2010**, *39*, 11129.

[147]	T. Kogane, N. Koyama, T. Ishida, T. Nogami, *Plolyhedron.* **2007**, *26*, 1811.

[148]	S. Ranganathan, S. Mahapatra, T. S. Thakur, D. G. R., *Acta. Cryst. E.* **2010**, *66*, 2789.

[149]	M. B. Casu, P. Imperia, S. Schrader, B. Schulz, M. Jandke, P. Strohriegl, *Synth. Met.* **2001**, *121*, 1673.

[150]	Y. Nakagawa, T. Nishiyama, H. Kamisuki, G. Harada, S. Kaneko, M. Kurosaki, T. Nobuta, M. Mitani*, Vol. 6 678 150 B2* (Ed.: N. T. Corp), US, **2004**.

[151]	U. Lottermoser, P. Rademacher, M. Mazik, K. Kowski, *Eur. J. Org. Chem.* **2005**, 522.

[152]	H. Bock, A. John, C. Naether, K. Ruppert, *Helv. Chim. Acta.* **1994**, *77*, 1505.

[153]	S. Choua, J.-P. Djukic, J. Dallery, A. Bieber, R. Welter, J.-P. Gisselbrecht, P. Turek, L. Ricard, *Inorg. Chem.* **2009**, *48*, 149.

[154]	A. S. Ichimura, L. P. Szajek, Q. Xie, X. R. Huang, S. Z. Huang, M. J. Wagner, J. L. Dye, J. E. Jackson, *J. Phys. Chem. B.* **1998**, *102*, 11029.

[155]	E. Gore-Randall, M. Irwin, M. S. Denning, J. M. Goicoechea, *Inorg. Chem.* **2009**, *48*, 8304.

[156]	W. V. Evans, R. Pearson, *J. Am. Chem. Soc.* **1942**, *64*, 2865.

[157]	A. M. Henriques, A. G. H. Barbosa, *J. Phys. Chem. A.* **2011**, *115*, 12259.

[158]	I. L. Fedushkin, A. A. Skatove, M. Hummert, H. Schumann, *Eur. J. Inorg. Chem.* **2005**, 1601.

[159]	M. J. Monreal, S. I. Khan, J. L. Kiplinger, P. L. Diaconescu, *Chem. Commun.* **2011**, *27*, 9119.

[160]	A. Satler, G. Parkin, *Nature.* **2010**, *463*, 523.

[161]	G. P. Miscione, M. A. Carvajal, A. Bottoni, *Organometallics.* **2011**, *30*, 4924.

[162]	Y. Kondo, A. Yoshida, T. Sakamoto, *J. Chem. Soc. Perkin Trans 1.* **1996**, 2331.

[163]	B. Srinivas, C.-C. Chang, C.-H. Chen, M. Y. Chiang, I.-T. Chen, Y. Wang, G.-H. Lee, *J. Chem. Soc. Dalton. Trans.* **1997**, 957.

[164]	F. Feil, S. Harder, *Eur. J. Inorg. Chem.* **2005**, 4438.

[165]	A. A. A. Abdalsalam, M. T. M. A-Dajani, N. Mohamed, M. Hemamalini, H.-K. Fun, *Acta. Cryst. Sect. E.* **2011**, *67*, o2342.

[166]	J. Ruiz, B. F. Perandones, *Chem. Commun.* **2009**, 2741.

[167]	D. R. Armstrong, L. Balloch, J. J. Crawford, B. J. Fleming, L. M. Hogg, A. R. Kennedy, J. Klett, R. E. Mulvey, C. T. O'Hara, A. A. Orr, S. D. Robertson, *Chem. Commun.* **2012**, *48*, 1541.

[168]	G. C. Forbes, A. R. Kennedy, R. E. Mulvey, P. J. A. Rodger, *Chem. Commun.* **2001**, 1400.

[169]	L. Fedushkin, A. G. Morzov, V. A. Chudakova, G. K. Fukin, V. K. Cherkasol, *Eur. J. Inorg. Chem.* **2009**, 4995.

[170] M. Stender, R. J. Wright, B. E. Eichler, J. Prust, M. M. Olmstead, H. W. Roesky, P. P. Power, *J. Chem. Soc. Dalton. Trans.* **2001**, 3465.

[171] E. Hevia, R. E. Mulvey, *Angew. Chem. Int. Ed.* **2011**.

[172] F. Drouin, T. J. J. Whitehorne, F. Schaper, *Dalton. Trans.* **2011**, *40*, 1396.

[173] J. Spielmann, F. Buch, S. Harder, *Angew. Chem. Int. Ed.* **2008**, *47*, 9434.

[174] J. Spielmann, S. Harder, *Eur. J. Inorg. Chem.* **2008**, 1480.

[175] C. Brinkmann, A. G. M. Barrett, M. S. Hill, P. A. Procopiou, *J. Am. Chem. Soc.* **201**, *134*, 2193.

[176] R. E. Mulvey, *Angew. Chem. Int. Ed.* **2007**, *46*, 3802.

[177] S. E. Whitney, B. Rickborn, *J. Org. Chem.* **1991**, *56*, 3058.

[178] O. Bayh, H. Awad, F. Mongin, C. Hoarau, L. Bischoff, F. Trecourt, G. Queguiner, F. Marsais, F. Blanco, B. Abarca, R. Ballesteros, *J. Org. Chem.* **2005**, *70*, 5190.

[179] S. H. Wunderlich, P. Knochel, *Angew. Chem. Int. Ed.* **2007**, *46*, 7685.

[180] J. C. Hodges, W. C. Patt, C. J. Connolly, *J. Org. Chem.* **1991**, *56*, 449.

[181] A. P. Dove, V. C. Gibson, P. Hormnirum, E. L. Marshall, J. A. Segal, A. J. P. White, D. J. Williams, *Dalton. Trans.* **2003**, 3088.

[182] H. Hao, H. W. Roesky, Y. Ding, C. Cui, M. Schromann, H.-G. Schmidt, M. Noltemeyer, B. Zemya, *J. Fluorine. Chem.* **2002**, *115*, 143.

[183] C. N. Ayala, M. H. Chsholm, J. C. Gallucci, C. Krempner, *Dalton. Trans.* **2009**, 9237.

[184] R. C. Jones, M. W. Chojnacka, J. Wilson Quail, M. G. Gardiner, A. Decken, B. F. Yales, R. A. Gossage, *Dalton Trans.* **2011**, *40*, 1594.

[185] J. I. Arduengo, R. V. Dias, F. Davidson, R. L. Harlow, *J. Organomet. Chem.* **1993**, *462*, 13.

[186] D. Zhang, H. Kawaguchi, *Organometallics.* **2006**, *25*, 5506.

[187] P. L. Arnold, I. J. Casely, Z. R. Turner, R. Bellabarba, R. B. Tooze, *Dalton. Trans.* **2009**, 7236.

[188] J. I. Arduengo, J. R. Goerlich, W. J. Marshall, *Liebigs Ann./Recuil.* **1997**, 365.

[189] W. Teng, U. Englich, K. Rhuhlanndt-Senge, *Inorg. Chem.* **2000**, *39*, 3875.

[190] P. Jutzi, H. J. Hoffmann, D. J. Brauer, C. Kruger, *Angew. Chem. Int. Ed.* **1973**, *12*, 1002.

[191] M. Zhu, K. Fujita, R. Yamaguchi, *Chem. Commun.* **2011**, *47*, 12876.

[192] H. Do, O. Daugulis, *J. Am. Chem. Soc.* **2009**, *131*, 17052.

[193] M. A. Huertos, J. Pe'rez, L. Riera, *J. Am. Chem. Soc.* **2008**, *130*, 13530.

[194] E. C. Escudero-Adan, A. Benet-Buchholz, A. W. Kleij, *Dalton. Trans.* **2008**, 734.

[195] K. L. Miller, C. T. Carver, B. N. Williams, P. L. Diaconescu, *Organometallics.* **2010**, *29*, 2272.

[196] H. Yorimitsu, K. Oshima, (Ed.: Patai), Wiley, Chichester, **2008**.

[197] B. Chambers, P. Dampney, *Proceeding-International Fertiliser Society.* **2009**, *657*, 1.

[198] P. Rani, H. Veesam, *International Journal of Pharmacy* **2012**, 179.

[199] T. G. Sadikogiv, C. Shikin, C. G. Gulerguv, E. B. Gamze, *Journal of Scientific and Industrial Research* **2003**, *62*, 462.

[200] R. Lantzsch, D. Arlt, *Synthesis* **1977**, 756.

[201] I.-H. Kim, H.-J. Tsai, K. Nishi, T. Kasagami, C. Morisseau, B. D. Hammock, *J. Med. Chem.* **2007**, *50*, 5217.

[202] L. Mao, Q. Shen, M. Xue, *Organometallics.* **1997**, *16*, 3711.

[203] V. E. Shashoua, W. Sweeny, R. F. Tietz, *J. Am. Chem. Soc.* **1960**, *82*, 866.

[204] J.-H. A. Shin, Y. Nath, S.-Y. Park, M. S. Rahman, S. Samal, J.-S. Lee, *J. Am. Chem. Soc.* **2005**, *127*, 4132.

[205] N. Fukuwatari, H. Sugimoto, S. Inoue, *Macromol. Rapid. Commun.* **1996**, *17*, 1.

[206] E. W. Thomas, E. E. Nishizawa, D. C. Zimmermann, D. J. Williams, *J. Med. Chem.* **1989**, *32*, 228.

[207] T.-G. Ong, G. P. A. Yap, D. S. Richeson, *J. Am. Chem. Soc.* **2003**, *125*, 8100.

[208] J. Koller, R. G. Bergman, *Organometallics.* **2010**, *29*, 5946.

[209] C. Alonso-Moreno, F. Carrillo-Hermosilla, A. Garces, A. Otero, I. Lopez-Solera, A. M. Rodriguez, A. Antinolo, *Organometallics.* **2010**, *29*, 2789.

[210] W.-X. Zhang, M. Nishiura, Z. Hou, *Chem. Eur. J.* **2007**, *13*, 4037.

[211] B. J. Fleming, P. Garcia-Alvarez, E. Keating, A. R. Kennedy, C. T. O'Hara, *Inorganica. Chim. Acta.* **2012**, *384*, 154.

[212] R. Pothiraja, A. P. Milanov, D. Barreca, A. Gasparotto, H.-W. Becker, M. Winter, R. A. Fischer, A. Devi, *Chem. Commun.* **2009**, 1978.

[213] D. C. Leitch, L. L. Schafer, *Organometallics.* **2010**, *29*, 5162.

[214] D. C. Leitch, J. D. Beard, R. K. Thomson, V. A. Wright, B. O. Patrick, L. L. Schafer, *Eur. J. Inorg. Chem.* **2009**, 2691.

[215] S. E. Baillie, W. Clegg, P. Garcia-Alvarez, E. Hevia, A. R. Kennedy, J. Klett, L. Russo, *Chem. Commun.* **2011**, *47*, 388.

[216] D. Li, I. Keresztes, R. Hopson, P. G. Williard, *Acc. Chem. Res.* **2009**, *42*, 270.

[217] B. D. Sherry, A. Furstner, *Acc. Chem. Res.* **2008**, *41*, 1500.

[218] C. Stude, B. Breit, *Angew. Chem. Int. Ed.* **2009**, *47*, 5457.

[219] A. P. Murray, M. J. Miller, *J. Org. Chem.* **2003**, *68*, 191.

[220] Y. Wu, S. Wang, X. Zhu, G. Yang, Y. Wei, L. Zhang, H. Song, *Inorg. Chem.* **2008**, *47*, 5503.

[221] J. Tang, T. Mohan, J. G. Verkade, *J. Org. Chem.* **1994**, *59*, 4931.

[222] M. Findlater, N. J. Hill, A. H. Cowley, *Dalton Trans.* **2008**, 4419.

Appendix I

Compound	2	3
Formula weight	1141.96	1174.83
Crystal System, space group	monoclinic, P12$_1$/c1	Monoclinic, P21/c
a [Å]	14.0302(5)	13.9586(16)
b [Å]	27.3605(10)	15.763(3)
c [Å]	18.6211(6)	16.1002(19)
α [°]	90	90
β [°]	105.777(4)	92.495(12)
γ [°]	90	90
Cell volume [Å^3]	6878.9(4)	3539.2(9)
Z	4	2
T, K	150(2)	123(2)
Reflections collected	25457	16278
Independent reflections	12014	6776
R$_{int}$	R$_{int}$ = 0.0431	0.0605
Final R indicies [F^2>2σ]	R1 = 0.0574, wR2 = 0.1443	R1 = 0.0666, wR2 = 0.1779
R indices (all data)	R1 = 0.1196, wR2 = 0.1576	R1 = 0.1408, wR2 = 0.1932
Goodness-of-fit on F^2	0.868	0.888
θ range for data collection°	3.0 to 25.0	3.78 to 26.00

Compound	4	5
Formula weight	1106.39	1172.07
Crystal System, space group	monoclinic, P 21/c	monoclinic, P12/n1
a [Å]	19.3846(7)	32.8478(10)
b [Å]	13.8329(5)	11.4901(2)
c [Å]	25.6393(9)	37.3125(9)
α [º]	90	90
β [º]	101.017(3)	92.870(2)
γ [º]	90	90
Cell volume [Å^3]	6748.4(4)	14065.0(6)
Z	4	8
T, K	123	150(2)
Reflections collected	97559	101369
Independent reflections	13259	24724
R$_{int}$	0.0413	0.0657
Final R indicies [F^2>2σ]	R1 = 0.0673, wR2 = 0.1956	R1 = 0.0717, wR2 = 0.1791
R indices (all data)	R1 = 0.0979, wR2 = 0.2092	R1 = 0.1385, wR2 = 0.2020
Goodness-of-fit on F^2	1.092	1.032
θ range for data collection°	3.05 to 26.00	3.0 to 25.0

Compound	6	7
Formula weight	1245.24	1253.06
Crystal System, space group	Monoclinic, P 21/c	Monoclinic, P 21/c
a [Å]	24.4061(5)	10.5577(4)
b [Å]	16.2527(3)	25.9803(8)
c [Å]	18.9071(3)	27.0467(8)
α [º]	90	90
β [º]	98.198(2)	98.352(3)
γ [º]	90	90
Cell volume [Å^3]	7423.1(2)	7340.0(4)
Z	4	4
T, K	123(2)	123(2)
Reflections collected	55165	47874
Independent reflections	17031	14393
R$_{int}$	0.0372	0.0830
Final R indicies [F^2>2σ]	R1 = 0.0492, wR2 = 0.1207	R1 = 0.0511, wR2 = 0.0791
R indices (all data)	R1 = 0.0872, wR2 = 0.1303	R1 = 0.1391, wR2 = 0.0925
Goodness-of-fit on F^2	0.957	0.818
θ range for data collection°	2.81 to 27.50	2.76 to 26.00

Compound	9	10
Formula weight	1204.06	1151.98
Crystal System, space group	Monoclinic, P 2/n	orthorhombic, Pca2$_1$
a [Å]	32.5960(17)	20.9222(6)
b [Å]	11.1823(6)	13.3693(4)
c [Å]	38.568(2)	24.8200(8)
α [º]	90	90
β [º]	93.116(5)	90
γ [º]	90	90
Cell volume [Å^3]	14037.2(13)	6942.5(4)
Z	8	4
T, K	123(2)	150(2)
Reflections collected	67450	18829
Independent reflections	27552	11344
R$_{int}$	0.0808	0.0321
Final R indicies [F^2>2σ]	R1 = 0.1331, wR2 = 0.3018	R1 = 0.0750, wR2 = 0.1922
R indices (all data)	R1 = 0.2275, wR2 = 0.3662	R1 = 0.1049, wR2 = 0.2249
Goodness-of-fit on F^2	1.035	1.027
θ range for data collection°	2.77 to 26.00	2.5 to 26.7

Compound	11	12
Formula weight	1509.74	929.61
Crystal System, space group	monoclinic, P 21/n	monoclinic, P 21/n
a [Å]	11.0261(7)	10.4287(6)
b [Å]	18.0103(11)	38.3533(18)
c [Å]	44.259(2)	14.3444(7)
α [º]	90	90
β [º]	94.473(6)	104.314(5)
γ [º]	90	90
Cell volume [Å^3]	8762.3(9)	5559.3(5)
Z	4	4
T, K	123	123(2)
Reflections collected	38363	39077
Independent reflections	17297	13477
R_{int}	0.1028	0.0410
Final R indicies [F^2>2σ]	R1 = 0.1028 wR2 = 0.3128	R1 = 0.0665, wR2 = 0.1553
R indices (all data)	R1 = 0.1134 wR2 = 0.3645	R1 = 0.0968, wR2 = 0.1707
Goodness-of-fit on F^2	1.049	1.043
θ range for data collection°	2.12 to 25	3.16 to 28.89

Compound	14	15
Formula weight	2143.60	844.72
Crystal System, space group	monoclinic, P12$_1$/c1	Orthorhombic,P b c a
a [Å]	19.3321(10)	18.1842(5)
b [Å]	17.1557(8)	20.5204(5)
c [Å]	19.9580(11)	21.8073(6)
α [º]	90	90
β [º]	113.694(6)	90
γ [º]	90	90
Cell volume [Å^3]	6061.2(5)	8137.3(4)
Z	2	8
T, K	150(2)	123(2)
Reflections collected	41345	56921
Independent reflections	12833	8846
R$_{int}$	0.0921	0.0776
Final R indicies [F^2>2σ]	R1 = 0.0533, wR2 = 0.1084	R1 = 0.0457, wR2 = 0.1050
R indices (all data)	R1 = 0.1726, wR2 = 0.1275	R1 = 0.0973, wR2 = 0.1134
Goodness-of-fit on F^2	0.753	0.832
θ range for data collection°	3.1 to 28.5	3.08 to 27.00

Compound	16	17
Formula weight	2433.96	701.34
Crystal System, space group	monoclinic, $P12_1/n1$	monoclinic, $P12_1/n1$
a [Å]	23.638(2)	10.4936(4)
b [Å]	22.9428(12)	18.6355(4)
c [Å]	25.3173(18)	11.4103(3)
α [º]	90	90
β [º]	110.588(9)	116.925(4)
γ [º]	90	90
Cell volume [Å^3]	12853.4(17)	1989.45(12)
Z	4	2
T, K	150(2)	123(2)
Reflections collected	53979	9299
Independent reflections	26210	6556
R_{int}	0.1124	0.0183
Final R indicies [$F^2 > 2\sigma$]	R1 = 0.1238, wR2 = 0.3071	R1 = 0.0337, wR2 = 0.0700
R indices (all data)	R1 = 0.2963, wR2 = 0.3777	R1 = 0.0428, wR2 = 0.0718
Goodness-of-fit on F^2	0.936	0.942
θ range for data collection°	3.0 to 28.5	3.09 to 30.95

Compound	18	19
Formula weight	1547.31	1252.00
Crystal System, space group	monoclinic, P12$_1$/n1	monoclinic, P2$_1$/c
a [Å]	23.9542(16)	14.387(2)
b [Å]	13.5142(10)	26.968(5)
c [Å]	27.924(3)	19.216(3)
α [º]	90	90
β [º]	111.317(9)	103.614(2)
γ [º]	90	90
Cell volume [Å^3]	8421.1(12)	7246(2)
Z	4	4
T, K	423(2)	150(2)
Reflections collected	64381	70829
Independent reflections	16510	17125
R$_{int}$	0.0759	0.0789
Final R indicies [F^2>2σ]	R1 = 0.0897, wR2 = 0.2534	R1 = 0.0665, wR2 = 0.1734
R indices (all data)	R1 = 0.1204, wR2 = 0.2832	R1 = 0.0914, wR2 = 0.1914
Goodness-of-fit on F^2	1.070	1.054
θ range for data collection°	3.52 to 26.00	1.5 to 27.3

Compound	20	21
Formula weight	2430.00	1003.25
Crystal System, space group	monoclinic, P2$_1$/n	Orthorhombic, Pna21
a [Å]	12.601(7)	24.4651(11)
b [Å]	15.449(8)	10.8289(4)
c [Å]	34.612(19)	22.8846(10)
α [º]	90	90
β [º]	92.851(8)	90
γ [º]	90	90
Cell volume [Å^3]	6730(6)	6062.8(4)
Z	2	4
T, K	120(2)	123(2)
Reflections collected	29380	21243
Independent reflections	8121	11240
R$_{int}$	0.1625	0.0416
Final R indicies [F^2>2σ]	R1 = 0.0957, wR2 = 0.2585	R1 = 0.0664, wR2 = 0.1478
R indices (all data)	R1 = 0.1887, wR2 = 0.3258	R1 = 0.0916, wR2 = 0.1648
Goodness-of-fit on F^2	1.023	1.039
θ range for data collection°	1.7 to 21.3	2.72 to 28.00

Compound	22	23
Formula weight	571.16	582.19
Crystal System, space group	Triclinic, P-1	Monoclinic, p21/n
a [Å]	9.1792(4)	9.0121(2)
b [Å]	12.1190(4)	20.1333(5)
c [Å]	15.8077(6)	19.8758(4)
α [º]	85.527(3)	90
β [º]	77.912(3)	91.504(2)
γ [º]	87.404(3)	90
Cell volume [Å^3]	1713.51(11)	3605.09(14)
Z	2	4
T, K	123(2)	120(2)
Reflections collected	20725	20209
Independent reflections	8803	7869
R$_{int}$	0.0499	0.0299
Final R indicies [F^2>2σ]	R1 = 0.0513, wR2 = 0.1110	R1 = 0.0478, wR2 = 0.1115
R indices (all data)	R1 = 0.0998, wR2 = 0.1216	R1 = 0.0673, wR2 = 0.1216
Goodness-of-fit on F^2	0.902	1.054
θ range for data collection°	2.79 to 29.00	3.03 to 27.00

Compound	24	25
Formula weight	633.17	619.21
Crystal System, space group	rhombohedral, R3m	triclinic, P2$_1$/n
a [Å]	32.394(6)	13.5757(17)
b [Å]	32.394(6)	14.4034(18)
c [Å]	11.017(2)	18.932(2)
α [º]	90	90
β [º]	90	92.2137(13)
γ [º]	120	90
Cell volume [Å^3]	10012(3)	3699.1(8)
Z	9	4
T, K	150(2)	150(2)
Reflections collected	20087	26382
Independent reflections	3237	6415
R$_{int}$	0.0534	0.0865
Final R indicies [F^2>2σ]	R1 = 0.0927, wR2 = 0.2341	R1 = 0.0830, wR2 = 0.1985
R indices (all data)	R1 = 0.0938, wR2 = 0.2372	R1 = 0.0910, wR2 = 0.2099
Goodness-of-fit on F^2	1.192	1.157
θ range for data collection°	3.5 to 22.5	3.4 to 24.2

Compound	26	27
Formula weight	801.43	652.77
Crystal System, space group	monoclinic, P2$_1$/n	monoclinic, P2$_1$/n
a [Å]	18.964(5)	14.0179(4)
b [Å]	12.505(3)	13.5976(3)
c [Å]	38.624(10)	21.7756(6)
α [°]	90	90
β [°]	96.385(3)	96.842(3)
γ [°]	90	90
Cell volume [Å^3]	9103(4)	4121.08(19)
Z	8	4
T, K	120(2)	123(2)
Reflections collected	69167	21743
Independent reflections	16016	8094
R$_{int}$	0.0683	0.0378
Final R indicies [F^2>2σ]	R1 = 0.0747, wR2 = 0.1794	R1 = 0.0661, wR2 = 0.1987
R indices (all data)	R1 = 0.1027, wR2 = 0.1958	R1 = 0.1040, wR2 = 0.2133
Goodness-of-fit on F^2	1.039	0.975
θ range for data collection°	1.1 to 24.2	2.93 to 26.00

Compound	28	29
Formula weight	1232.38	268.35
Crystal System, space group	Orthorhombic, P21/n	Triclinic, P1
a [Å]	12.703(3)	6.0329(5)
b [Å]	21.654(5)	7.7817(7)
c [Å]	13.282(3)	9.0003(7)
α [º]	90	115.116(8)
β [º]	90.01(2)	101.212(7)
γ [º]	90	99.162(7)
Cell volume [Å^3]	3653.5(15)	361.11(5)
Z	2	1
T, K	123(2)	123(2)
Reflections collected	9900	3468
Independent reflections	5404	2806
R$_{int}$	0.1131	0.0087
Final R indicies [F^2>2σ]	R1 = 0.0995, wR2 = 0.1517	R1 = 0.0307, wR2 = 0.0750
R indices (all data)	R1 = 0.2566, wR2 = 0.2344	R1 = 0.0321, wR2 = 0.0761
Goodness-of-fit on F^2	1.026	1.026
θ range for data collection°	3.07 to 24.99	3.58 to 29.42

Compound	30	31
Formula weight	696.20	1065.64
Crystal System, space group	monoclinic, P21/c	triclinic, R3
a [Å]	9.4286(3)	20.8559(6)
b [Å]	39.1553(19)	20.8559(6)
c [Å]	10.2035(3)	11.8574(4)
α [º]	90	90
β [º]	97.029(3)	90
γ [º]	90	120
Cell volume [Å^3]	3738.6(2)	4466.6(2)
Z	4	3
T, K	123	123
Reflections collected	8155	5988
Independent reflections	6036	2994
R$_{int}$	0.997	0.91
Final R indicies [F^2>2σ]	R1 = 0.0546 wR2 = 0.1201	R1 = 0.0344 wR2 = 0.0870
Goodness-of-fit on F^2	1.027	1.077

Compound	42	45
Formula weight	248.36	399.44
Crystal System, space group	Monoclinic, P 21/c	Hexagonal, R3c
a [Å]	8.5300(4)	12.6655(19)
b [Å]	20.4534(7)	12.6655(19)
c [Å]	9.1786(4)	26.761(5)
α [°]	90	90
β [°]	113.992(5)	90
γ [°]	90	120
Cell volume [Å^3]	1463.01(11)	3717.7(11)
Z	4	6
T, K	123(2)	123(2)
Reflections collected	7237	2894
Independent reflections	2910	1477
R$_{int}$	0.0329	0.0234
Final R indicies [F^2>2σ]	R1 = 0.0548, wR2 = 0.1470	R1 = 0.0511, wR2 = 0.1362
R indices (all data)	R1 = 0.0689, wR2 = 0.1568	R1 = 0.0610, wR2 = 0.1443
Goodness-of-fit on F^2	1.081	1.028
θ range for data collection°	4.32 to 73.13	3.57 to 29.40

Compound	46	50
Formula weight	1315.18	1397.21
Crystal System, space group	Orthorhombic, Pbc2$_1$	triclinic, P$\bar{1}$
a [Å]	13.3087(2)	13.997(3)
b [Å]	27.8790(5)	14.578(4)
c [Å]	41.4630(7)	20.366(5)
α [º]	90	84.145(3)
β [º]	90	81.076(3)
γ [º]	90	79.487(2)
Cell volume [Å^3]	15384.2(4)	4024.8(17)
Z	8	2
T, K	123(2)	150(2)
Reflections collected	72062	22604
Independent reflections	30714	9650
R$_{int}$	0.0589	0.0730
Final R indicies [F^2>2σ]	R1 = 0.0658, wR2 = 0.1505	R1 = 0.0910, wR2 = 0.2517
R indices (all data)	R1 = 0.0949, wR2 = 0.1603	R1 = 0.1309, wR2 = 0.2767
Goodness-of-fit on F^2	1.028	1.070
θ range for data collection°	3.24 to 28.19	3.4 to 21.3